Sulfur Oxygenase Reductases -
A Structural and Biochemical Perspective

vom Fachbereich Biologie
der Technischen Universität Darmstadt zur
Erlangung des akademischen Grades eines
Doctor rerum naturalium
genehmigte

Dissertation

vorgelegt von

Dipl. Biol. Andreas Veith
aus Seeheim-Jugenheim

1. Referent: Dr. habil. Arnulf Kletzin
2. Referent: Prof. Dr. Felicitas Pfeifer

Eingereicht am 21.07.2011
Tag der mündlichen Prüfung: 16.09.2011

Darmstadt 2011
D 17

"Trying to determine the structure of a protein by UV spectroscopy was like trying to determine the structure of a piano by listening to the sound it made while being dropped down a flight of stairs."

-- Francis Crick

Die vorliegende Arbeit wurde als Promotionsarbeit am Institut für Mikrobiologie und Genetik des Fachbereichs Biologie der Technischen Universität Darmstadt unter Leitung von Herrn Dr. Arnulf Kletzin in der Abteilung von Frau Prof. Felicitas Pfeifer im Zeitraum von Mai 2007 bis Juli 2011 angefertigt. Ein Teil der vorliegenden Arbeit wurde in Portugal am Instituto de Tecnologia Químicia e Biológica, Universidade Nova de Lisboa (ITQB/UNL), Oeiras, Portugal in der Arbeitsgruppe von Dr. Carlos Frazão, Dr. Cláudio M. Gomes und Prof. Miguel Teixeira im Rahmen einer Kooperation durchgeführt.

Ehrenwörtliche Erklärung

Ich erkläre hiermit ehrenwörtlich, dass ich die vorliegende Arbeit selbstständig angefertigt habe. Sämtliche aus fremden Quellen direkt oder indirekt übernommenen Gedanken sind als solche kenntlich gemacht.
Die Arbeit wurde bisher keiner anderen Prüfungsbehörde vorgelegt und noch nicht veröffentlicht.

Darmstadt, den 21.07.2011

Andreas Veith

Acknowledgements

First and foremost I would like to thank my supervisor Dr. Arnulf Kletzin for giving me the opportunity to step into the fascinating world of proteins. I was in the lucky position to receive great support, encouragement and to find a door that was always open for questions and discussions.

Special thanks go to Prof. Felicitas Pfeifer for taking the position of the co-advisor and for her extensive support throughout my work. And many thanks for making Darmstadt an outpost for the intriguing Archaea.

I would like to express my deepest gratitude for Dr. Carlos Frazão (ITQB, Oeiras, Portugal), my supervisor of the crystallographic part of the thesis. He never got tired to teach crystallography to a raw beginner and to discuss results over and over again, even beyond my visits at ITQB. Putting much work into all SOR projects, he managed it to determine the *Hn*SOR structure.

Thanks to all members of the Molecular Xtallography group at ITQB, especially Catarina, Joana, Ana, Mario, José, Miguel, Matteo, Bruno and Przemek for their help and for sharing various wild-pig or Fado experiences. You made me feel extremely comfortable from the first day on! Specials thanks go to Tiago Bandeiras for his great passion for science (and Benfica) and many lunch-time discussions (Zé Varunca). I also would like to thank Ricardo Coelho for having a helping hand in growing and fishing crystals and also for taking care of the *Hn*SOR, when I was absent.

I would like to thank Prof. Miguel Teixeira (ITQB) for providing the EPR data. Dr. Cláudio M. Gomes (ITQB) and his entire group are gratefully acknowledged for the time at their lab. Special thanks go to Hugo Botelho for his great help during my short stay.

Claudia Rittmeyer (Goethe-Universität, Frankfurt, Germany) is acknowledged for performing the TXRF measurements.

Ok, this might take a while, but it cannot be missed out: a huge thank you goes to all former and present colleagues from the Kletzin & Pfeifer Lab, especially Ina Schmidt, Larissa Marschaus, Stella Tavlaridou, Regina Frommherz, Dennis Petrasch, Michael Forth, Matti Eckert, "Cpt." Fabian Müller, Bastian Naß and Gerald Losensky. Jonas Protze is acknowledged for providing mutant and biochemical data during his "Forschungspraktikum" and for keeping the ÄKTA running. Katrin Faist and Gaby Liebing (who will do the "back-scratching" now?) are especially acknowledged for their excellent assistance. Special thanks go to Renate Fröhlich, who shared the lab with me the past few years and always guaranteed a "fresh" start to the day. Thanks also to Nam-Suk Polin, Cordula Bernhardt and Giuseppe Vetrano for making work a bit easier. Thanks to all of you for providing such an amazing working atmosphere and for sharing those great experiences in- and outside the lab.

I would also like to thank all present and former colleagues from the third floor (AG Heider, AG Simon and AG Göringer). Tamara Heß is especially acknowledged for her great help all these years.

Thanks go to Tim Urich for always finding time to discuss some new facts about the “tiny and lovely” SOR.

Mark Günzel and Till Albrecht are gratefully acknowledged for the correction of this work.

Thanks to Andreas “Flash” Klingl for the great “heavy metal” interaction. The Mühlhiasl prophesized it!

A very special thank you goes to Dr. Sabrina Fröls for personal care, encouragement, discussions and unlimited helpfulness throughout practical courses, diploma and PhD thesis.

Jens Riede is thankfully acknowledged for his friendship and for his help to think outside the “microbiology box”.

Thanks to Gabi, Thomas, Heinz, Anni and Kurt for their continuous support all these years. This would have never been possible without you!!!

And more than thousand thanks to Nadine for her special support and her surpassing patience especially at the end of this work.

Publications

Parts of the present work and of other projects during the time of this thesis have already been published or have been submitted for publication.

Veith, A., Klingl, A., Zolghadr, B., Lauber, K., Mentele, R., Lottspeich, F., Rachel, R., Albers, S. V. and Kletzin, A. (2009) *Acidianus, Sulfolobus* and *Metallosphaera* surface layers: structure, composition and gene expression. *Mol Microbiol* **73**: 58-72.

Botelho, H. M., Leal, S. S., **Veith, A**., Prosinecki, V., Bauer, C., Fröhlich, R., Kletzin, A. and Gomes, C. M. (2010) Role of a novel disulfide bridge within the all-beta fold of soluble Rieske proteins. *J Biol Inorg Chem* **15**: 271-281.

[1]**Veith, A.**, Urich, T., Seyfarth, K., Protze, J., Frazão, C. and Kletzin, A. (2011) Substrate pathways and mechanisms of inhibition in the sulfur oxygenase reductase of *Acidianus ambivalens*. *Front Microbio* **2:**37. doi: 0.3389/fmicb.2011.00037

[2]**Veith, A**., Botelho, H. M., Gomes, C. M. and Kletzin, A. (2011) The Sulfur Oxygenase Reductase from the Mesophilic Bacterium *Halothiobacillus neapolitanus* is a Highly Active Thermozyme. *Submitted June 2011*

Veith, A., Coelho, R., Kletzin, A. and Frazão, C. (2011) Cloning, expression, purification, crystallization and preliminary crystallographic studies of the sulfur oxygenase reductase of *Halothiobacillus neapolitanus* DSM 15147. *In preparation*

[1]The tetramer channel mutants Del L, Del K, $F_{141}A$, $F_{133}A$ and $F_{133}A/F_{141}A$ were originally constructed by Kerstin Seyfarth. The active site pore mutants $M_{296}V$, $M_{297}A$, $MM_{296/297}TT$ and $MM_{296/297}VT$ were constructed by Jonas Protze under my supervision in the course of this work. Mutants of the trimer channel and of the zinc-binding site were generated in the course of this work. The structural datasets of *Aa*SOR complexed with iodoacetamide, zinc acetate or *p*-chloromercuribenzoic acid were initially obtained by Tim Urich and refined by Carlos Frazão (ITQB).

[2]All Far UV / CD spectroscopy experiments were performed under the guidance of Hugo Botelho (ITQB) in the group of Cláudio M. Gomes (ITQB) in the course of this work. All other experiments were carried out in Darmstadt in the course of this work.

Summary 1

1. Introduction 3
1.1. Elemental sulfur 3
1.2. Microbial sulfur oxidation 4
1.2.1. Bacterial sulfur oxidation pathways 4
1.2.2. Archaeal sulfur oxidation pathways 7
1.2.3. Sulfur oxidation pathway of *Acidianus ambivalens* 8
1.3. The sulfur oxygenase reductase 10
1.4. Goals of this study 18

2. Materials and Methods 20
2.1. Materials 20
2.1.1. Chemicals 20
2.1.2. Microorganisms 21
2.1.3. Plasmids 21
2.1.4. Enzymes and kits 21
2.1.5. Synthetic oligonucleotides 22
2.1.6. Molecular weight standards 23
2.1.7. Media 23
2.1.8. Buffers and solutions 24
2.2. Microbiological Methods 25
2.2.1. Growth of Halothiobacillus neapolitanus DSM 15147 25
2.3. Molecular Biological Methods 25
2.3.1. Genomic DNA extraction from *Halothiobacillus neapolitanus* DSM 15147 25
2.3.2. Amplification of *Halothiobacillus neapolitanus* and *Aquifex aeolicus sor* genes 26
2.3.3. Preparation of SOR amplification products and of the pASK-SOR.05 vector 27
2.3.4. DNA ligation and analysis of transformants 27
2.3.5. Site directed-mutagenesis and analysis of transformants 28
2.3.6. Agarose gel electrophoresis 29
2.3.7. Heterologous gene expression in *E. coli* 29
2.3.8. Constructs for heterologous gene expression 29
2.4. Biochemical methods 30
2.4.1. Purification of recombinant SOR from *E. coli* 30
2.4.2. Unfolding and refolding of recombinant SOR from inclusion bodies 31
2.5. Analytic procedures 32
2.5.1. SOR activity assay 32
2.5.2. Inhibitor studies 33
2.5.3. Protein quantification 34
2.5.4. Iron quantification 34
2.5.5. SDS–PAGE 35
2.5.6. BN–PAGE 36
2.5.7. In-gel enyzme activity assay 37
2.6. Spectroscopic Methods 37
2.6.1. UV/Visible spectroscopy 37
2.6.2. CD spectroscopy 37
2.6.3. EPR spectroscopy 38
2.6.4. DLS analysis 38

2.6.5. TXRF analysis 39
2.7. Sequence Analysis 39
2.7.1. Phylogenetic analysis 39
2.7.2. Homology modeling 40
2.8. Crystallization 40
2.8.1. Crystallization of SOR-wt, SOR mutants and SOR derivatives 41
2.8.2. X-Ray diffraction data collection 41
2.8.3. Data processing and refinement of SOR models 42
2.8.4. Model analysis 43

Abbreviations 44

3. Sulfur pathway and zinc inhibition of the *A. ambivalens* SOR 47
3.1. Introduction 47
3.2. Results 48
3.2.1. Polysulfide can serve as SOR substrate 48
3.2.2. Properties of the SOR mutants 49
3.2.3. Mutations at the tetramer channel 50
3.2.4. Mutations at the trimer channel 52
3.2.5. Mutations at the active site pore 54
3.2.6. Zinc-mediated inhibition of the SOR 55
3.3. Discussion 60
3.3.1. Polysulfide is a SOR substrate 60
3.3.2. Fourfold symmetry axis pores restrict SOR enzyme activity 61
3.3.3. Mutagenesis at the threefold symmetry axis elevates SOR activity 61
3.3.4. The integrity of the active site pore is important 62
3.3.5. Inhibition mechanism of Zinc 63

4. Active site and reaction mechanism of the *A. ambivalens* SOR 64
4.1. Introduction 64
4.2. Results 66
4.2.1. Crystallization of recombinant *Aa*SOR 66
4.2.2. Properties of active site mutants 69
4.2.3. Crystallization of the *Aa*SOR mutants $E_{87}A$ and $E_{87}D$ 72
4.2.4. Generation of metal-substituted SOR derivatives 74
4.2.5. Characterization of metal derivatives of the *Aa*SOR 75
4.2.6. Crystallization of the Co-SOR 81
4.3. Discussion 87
4.3.1. Different *Acidianus* SOR structures represent different stages of catalysis 87
4.3.2. A hydrogen bond network is present at the active site 88
4.3.3. Redox change of the metal center is not strictly required for SOR catalysis 89
4.3.4. Co-derivatized SOR is highly similar to the Fe-containing wild-type enzyme 91

5. Characterization of the *Halothiobacillus neapolitanus* SOR 93
5.1. Introduction 93
5.2. Results 94
5.2.1. Generation of a pASK_HnSOR plasmid 94
5.2.2. Overproduction and purification of recombinant *Hn*SOR 95
5.2.3. Biochemical characterization of the recombinant *Hn*SOR 96

5.2.4. Structural properties of the recombinant *Hn*SOR 100
5.2.5. Crystallization of the recombinant *Hn*SOR and data collection 102
5.2.6. Analysis of the *Hn*SOR structure 105
5.3. Discussion 112
5.3.1. *Hn*SOR exhibits a broad temperature and pH range 112
5.3.2. Architecture of different SORs is highly similar 115
5.3.3. Two different channels in the outer shell of the *Hn*SOR 116
5.3.4. Entrance and exit channels of the catalytic center 117
5.3.5. Active site architecture 118

6. General Discussion 120
6.2. Phylogenetic origin of the SOR 121
6.3. General properties of the *Hn*SOR and its relevance for the SOR protein family 122
6.4. Transport of sulfur substrate into the microbial cell 123
6.5. The sulfur substrate pathway 124
6.6. The active site of the SOR 127
6.6.1. Temperature-induced persulfuration of the cysteine 127
6.6.2. Hydrogen bond network and the metal's redox state 128
6.7. Catalytic mechanism of the SOR 130
6.8. Conclusions and perspectives 132

Literature 134

Appendix 146

Summary

Sulfur oxygenase reductases (SORs) catalyze the oxygen-dependent disproportionation reaction of elemental sulfur with sulfite, thiosulfate and sulfide as products. The SOR is the initial sulfur-oxidizing enzyme in the hyperthermophilic and chemolithoautotrophic archaeon *Acidianus ambivalens*. Although the enzyme is biochemically and structurally well characterized, details on the reaction mechanism are still unknown. Here, structure-function relationships of the SOR are analyzed using site-directed mutagenesis, metal substitution, spectroscopic methods and X-ray crystallography. In addition, the first characterization of a SOR from a mesophilic microorganism is presented.

It was hypothesized that the initial SOR substrate is a linear sulfur species and not α-S_8. An in-gel enzyme activity assay was performed with the *Acidianus ambivalens* SOR (*Aa*SOR), demonstrating enzyme activity with the linear polysulfide. The outer shell of the spherical and hollow enzyme harbors two different channel types at the rotational fourfold and threefold symmetry axes. They allow the entrance of the sulfur substrate and the exit of reaction products, respectively. Both pores were enlarged via site-directed mutagenesis, resulting in an up to fourfold elevated enzyme activity and causing a change of the proposed 1:1 stoichiometry of oxidized and reduced products. A small hydrophobic pore allows access to the active site, which resides in a small pocket separated from the inner hollow. The pore was enlarged using site-directed mutagenesis, but expansion led to a significant decrease of enzyme activity. Zn^{2+}, a strong SOR-inhibitor, was previously localized in a blind-ending channel that opens near the active site entry pore and which is far from the catalytic center itself. Zn coordination was analyzed using previously obtained crystallographic data, indicating that two histidines are involved. Alanine mutants of both histidines tripled the K_i values for Zn^{2+} in comparison to the wild type enzyme. It was concluded that both histidines are essential for zinc ligation.

The active site comprises a cysteine persulfide and a mononuclear iron center coordinated by two histidines and one glutamate. Diffraction data from a newly crystallized *Aa*SOR were analyzed, showing the cysteine in an unmodified form. The results pointed to a heat-induced auto-sulfuration process that converts C_{31} into a cysteine persulfide. An H-bond network was hypothesized to be centered around the catalytic site. Several amino acids, expected to be interacting with essential active site residues, were mutated. Most of the

variants had moderately diminished activities. The substitution of a single glutamate (E_{87}), located in H-bond distance to one of the iron-binding histidines, almost abolished enzyme activity. An aspartate variant ($E_{87}D$) with slightly lowered catalytic activity was crystallized. Analyses of the diffraction data showed nearly identical H-bond distances between the histidine and the aspartate, indicating the importance of an interaction between both residues. Previous EPR experiments demonstrated a redox change of the active site iron from Fe^{3+} to Fe^{2+} upon incubation with sulfur at high temperatures. Inclusion bodies of *Aa*SOR were refolded in presence of different non-iron metals to investigate, whether such a redox change is essential for catalysis. Refolded SORs with Fe, Co, Mn or Ni incorporated were biochemically active. EPR spectra of Co- and Mn-containing SORs showed signals for Co^{2+} and Mn^{2+} species, respectively. The signal intensities decreased slightly when the enzyme was incubated with sulfur at high temperature while the metal remained in the same oxidation state, suggesting that small changes occur near the metal center during catalysis. The Co-containing protein was crystallized. Diffraction data did not point to significant structural rearrangements around the metal center.

Only a small number of SOR mutants featured a crucial impact on enzyme activity. Therefore, a naturally occurring SOR variant from the mesophilic bacterium *Halothiobacillus neapolitanus* was analyzed. In this study, the first biochemical and structural characterization of a SOR derived from a mesophilic microorganism is presented (*Hn*SOR). After gene expression in *E. coli*, the soluble enzyme (*Hn*SOR) was purified and biochemically characterized. The optimal enzyme activity was at pH 8.4 and 80°C. The temperature range of activity covered nearly 90°C. CD spectroscopy showed that *Hn*SOR and *Aa*SOR are similarly folded. Hydrodynamic diameters of both proteins were calculated from Dynamic Light Scattering and were nearly identical. The *Hn*SOR structure was determined at 2.9 Å resolution and compared to the *Aa*SOR. Both are structurally similar icosatetrameric proteins. Based on these observations, the sulfur pathway route identified for the *Aa*SOR was applied to the *Hn*SOR. An additional active site exit pore was found, which was so far not identified in the *Aa*SOR but which seems to be present at closer inspection. The active site cavity resembled the situation in the *Aa*SOR including a cysteine persulfide, which was modified without additional heat treatment. The mononuclear iron center is coordinated by three amino acids (H_{88}, H_{92} and E_{116}) and water molecules in a slightly distorted octahedral geometry. The second coordination sphere does not consist of the E_{87}-homologous residue E_{89} but of a tyrosine at position 118 (Y_{118}).

1. Introduction

1.1. Elemental sulfur

Sulfur is the 16th most abundant element in the earth's crust and very versatile with respect to the number of sulfur allotropes. The most common form in nature is the orthorhombic and cyclic α-S_8 sulfur with a characteristic crown-like shape. At temperatures above 95.6°C, orthorhombic α-S_8 sulfur is converted into monoclinic ß-S_8 sulfur, which is only stable at higher temperatures. Sulfur is almost insoluble in water at 25°C (5 µg/l; Boulegue, 1978) but the solubility increases up to 25-fold at 80°C (Kamyshny, 2009). Thus the availability of sulfur is clearly elevated at the growth temperature of (hyper-) thermophilic sulfur-oxidizing microorganisms, while this is not the case for mesophilic representatives. Therefore, many microorganisms have to activate sulfur prior to oxidation to make it available. Elemental sulfur can either be activated through S_8 ring opening by nucleophilic attack, thereby forming polysulfanes, or by the reduction to polysulfide. There is a general agreement that highly reactive linear sulfur molecules like polysulfide are the initial substrates for sulfur-oxidizing enzymes rather than the octameric sulfur (Rohwerder and Sand, 2007; Franz *et al.*, 2007).

Elemental S^0 is stable under aerobic and anaerobic conditions. It is also stable under acidic conditions but it disproportionates to thiosulfate and sulfide in the presence of hydroxyl ions according to equation 1.1 (McCampbell Hamilton, 1991).

Eq. 1.1 $\frac{1}{2} S_8 + 4\ OH^- \rightarrow S_2O_3^{2-} + 2\ HS^- + H_2O$

It should be noted that this reaction occurs at a pH of 11.5 and at ambient temperatures. At higher temperatures of 80°C, sulfur disproportionation begins to start at a pH of 7.6 due to the increased chemical reactivity of sulfur.
In addition, polysulfide is formed from S^0 and sulfide at neutral and alkaline pH. It is stable under anaerobic conditions and in aqueous solutions. It is hydrolyzed under aerobic conditions and at acidic pH to elemental sulfur and sulfide (Eq. 1.2; Schauder and Kröger, 1993).

Eq. 1.2 $nS^0 + HS^- \rightarrow S_{n+1}^{2-} + H^+$

1.2. Microbial sulfur oxidation

Biological sulfur oxidation is one of the most important energy-yielding processes in volcanic or similar extreme environments (Friedrich *et al.*, 2005). A broad range of taxonomically and physiologically diverse sulfur-metabolizing bacteria and archaea utilize various inorganic sulfur compounds (ISCs) that occur naturally in oxidation states between -2 and +6 (Ghosh and Dam, 2009; Friedrich *et al.*, 2005). Sulfide (HS^-), metal sulfides such as pyrite (FeS_2), polysulfides (S_n-SH^-), elemental sulfur (S^0), sulfite (HSO_3^-), thiosulfate ($S_2O_3^{2-}$), sulfate (SO_4^{2-}) and polythionates (*e.g.* tetrathionate $S_4O_6^{2-}$) can all serve as substrates. Chemolithotrophic bacteria and archaea use ISCs for feeding electrons into the respiratory chain, while phototrophic bacteria mainly use ISCs to transfer electrons for CO_2 fixation.

1.2.1. Bacterial sulfur oxidation pathways

Oxidation of elemental sulfur in Archaea is restricted to members of the *Sulfolobales* of the Crenarchaeota, while many different lithotrophic bacteria are known to oxidize sulfur. Chemolithotrophic sulfur-oxidizing bacteria comprise *Acidiphilium, Acidithiobacillus, Aquifex, Beggiatoa, Desulfocapsa, Halothiobacillus, Magnetospirillum, Paracoccus, Sulfobacillus, Starkeya, Tetrathiobacter, Thiobacillus and Thiomicrospira* (Friedrich *et al.*, 2001). They mainly grow at moderate or at elevated temperatures around 45 - 50°C with the exception of the hyperthermophile *Aquifex* with growth temperatures around 90°C. Neutrophiles can be found as well as alkaliphiles or acidophiles. The high physiological divergence of these prokaryotes is also reflected by the fact that various sulfur compounds such as sulfide, various metal sulfides, polysulfide, elemental sulfur, sulfite, thiosulfate and polythionates like tetrathionate can be metabolized. Consequently, several different systems are utilized in sulfur metabolism.

Paracoccus pantotrophus is one of the best-studied members of neutrophilic sulfur-oxidizing bacteria. It oxidizes thiosulfate to sulfate via a SOX (**S**ulfur **Ox**idation) multi-enzyme complex (Figure 1.1; Rother *et al.*, 2001; Friedrich *et al.*, 2005; Friedrich *et al.*, 2008). This enzyme system was demonstrated to oxidize thiosulfate, sulfite, sulfide and elemental sulfur, while cytochrome c is used as an electron acceptor. The *sox* gene cluster comprises 15 genes, which encode four periplasmic proteins that interact with each other.

SoxXA catalyzes the oxidative transfer of thiosulfate and/or other ISCs to the thiol group of a conserved cysteine in SoxYZ. The substrate is oxidized while covalently attached to SoxYZ and the sulfone sulfur is cleaved off by the hydrolase SoxB, yielding sulfate. The outer sulfur atom of the cysteine persulfide in SoxYZ is then oxidized to cysteine-S-sulfate by $Sox(CD)_2$ and is finally hydrolyzed by SoxB to regenerate SoxYZ.

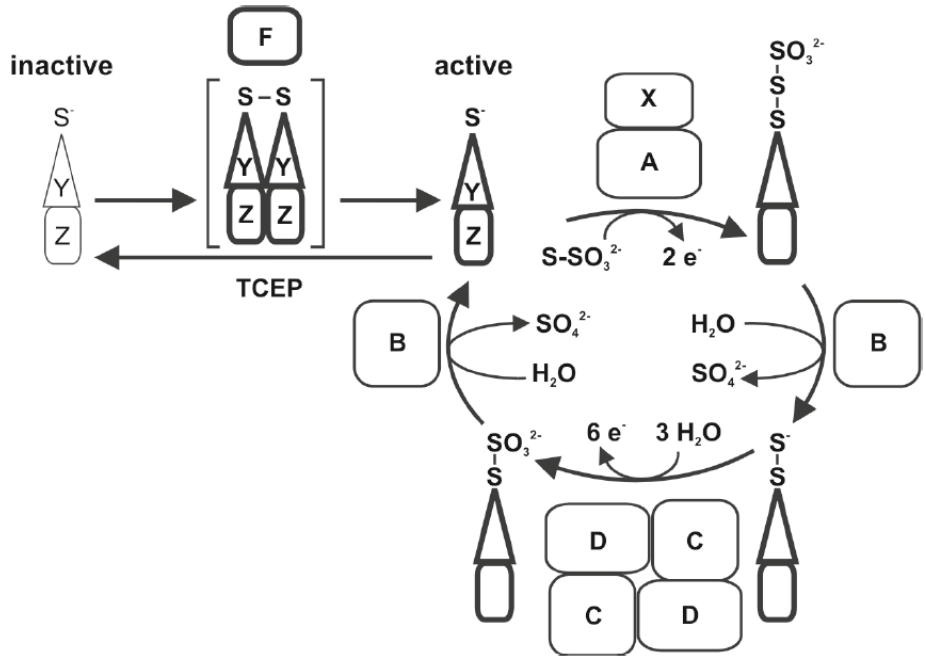

Figure 1.1 Schematic representation of the reaction cycle of thiosulfate oxidation by the Sox enzyme system of *Paracoccus pantotrophus* (from Friedrich *et al.*, 2008).

In contrast, the SOX multienzyme-complex is absent in most bacteria that grow at acidic conditions (pH 1 - 3) like *Acidithiobacillus* or *Acidiphilium*. Instead, a periplasmic sulfur dioxygenase (SDO) is proposed to be responsible for the initial oxidation step of elemental sulfur to sulfite, although the enzyme has not yet been purified (Figure 1.2; Rohwerder and Sand, 2007). Sulfite is oxidized to sulfate by a sulfite:acceptor oxidoreductase (SAOR). In addition, a sulfide:quinone oxidoreductase (SQR) and a thiosulfate:quinone oxidoreductase (TQO) were proposed to be involved in the sulfur oxidation pathway of *Acidithiobacillus ferrooxidans* (Wakai *et al.*, 2004; Brasseur *et al.*, 2004) catalyzing the oxidation of the respective sulfur compounds coupled to the reduction of quinones, which are in turn involved in electron transfer.

Tetrathionate can be degraded by a tetrathionate hydrolase (TTH) to sulfate and thiosulfate. The enzyme was characterized for *Acidithiobacillus ferrooxidans* (Kanao *et al.*, 2007; Beard *et al.*, 2011) and *Acidithiobacillus caldus (*Bugaytsova and Lindstrom, 2004; Rzhepishevska *et al.*, 2007).

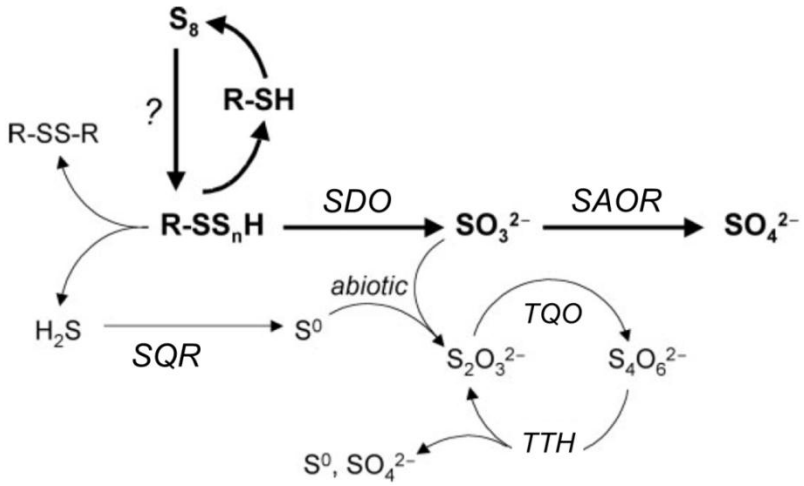

Figure 1.2 Hypothetical model of sulfur oxidation in acidophilic proteobacteria (from Rohwerder and Sand, 2007). SDO = sulfur dioxygenase; SAOR = sulfite:acceptor oxidoreductase; SQR = sulfide:quinone oxidoreductase; TQO = thiosulfate:quinone oxidoreductase; TTH = tetrathionate hydrolase.

Transcriptomic and proteomic data of *Acidithiobacillus ferrooxidans* also suggested that a heterodisulfide reductase (Hdr) might be involved in sulfur oxidation, even though biochemical evidence is missing. Hdr catalyzes the reversible reduction of the disulfide bond in heterodisulfide coupled with electron transfer in methanogenic archaea and sulfate-reducing bacteria and archaea. It was hypothesized that the cytoplasmic Hdr works in the reverse way by oxidation of the disulfide intermediates originating from S^0 oxidation and delivering electrons to the quinone pool (Quatrini *et al.*, 2009). It is still not known, whether the SDO pathway is valid for all acidophilic Gram-negative bacteria but is likely that more than one enzymatic system is present in most species (Rohwerder and Sand, 2007). This is supported by recent results on the closely related bacterium *Acidithiobacillus caldus*. Genome and proteome data revealed an incomplete SOX system (with SoxCD missing), one gene encoding a sulfur oxygenase reductase (SOR) and two putative orthologs of Hdr. During growth on S^0, *sox* and *hdr* genes are up-regulated indicating that they are involved in sulfur utilization (Mangold *et al.*, 2011). The potential use of Hdr and/or SOR in the *Acidithiobacillus caldus* sulfur oxidation pathway remains to be resolved. It was speculated that they might be used under different growth conditions or for different sulfur substrates.

The anoxygenic phototrophic sulfur bacteria can be divided into green sulfur, purple sulfur and purple non-sulfur bacteria and include genera such as *Allochromatium, Chlorobaculum*, *Ectothiorodospira*, *Rhodobacter* and *Rhodospirillum*, which oxidize reduced inorganic sulfur compounds mainly for photosynthetic CO_2 fixation and growth under anaerobic conditions (Sakurai *et al.*, 2010; Ghosh and Dam, 2009).

This group is mainly mesophilic but some members also inhabit extreme environments like acidic hot springs and saline soda lakes (Madigan, 2003). Sulfur globules containing elemental sulfur are formed as an intermediate during oxidation of sulfur compounds and are stored intra- or extracellularly. It had been demonstrated for *Allochromatium vinosum*, a purple sulfur bacterium of the Chromatiaceae family, that the formation of sulfur globules is a result of an incomplete SOX complex, which lacks the sulfur dehydrogenase SoxCD (Hensen *et al.*, 2006; Grimm *et al.*, 2008). During the oxidation of thiosulfate to sulfate, the sulfane sulfur at SoxY cannot be directly oxidized and is probably transferred to internal sulfur globules. These are in turn degraded and oxidized by a reversely working dissimilatory sulfite reductase (DsrAB), which is encoded by the first two genes of a 15 gene *dsr* cluster (Pott and Dahl, 1998; Dahl *et al.*, 2005; Frijgaard and Dahl, 2009). Clusters of *sox* and *dsr* genes have also been identified in other sulfur-storing bacteria, suggesting that these mechanisms of sulfur oxidation are evolutionary highly conserved.

1.2.2. Archaeal sulfur oxidation pathways

Utilization of elemental sulfur and inorganic sulfur compounds for energy conservation is a common feature of hyperthermophilic archaea. Solfataras, hydrothermal vents, hot springs and other hot and sulfur-rich environments are typical habitats of these microorganisms (Figure 1.3) and provide a high variety of sulfur substrates as major energy sources. The majority of isolates are anaerobic sulfur-reducing species while most aerobic sulfur-oxidizing archaea belong to the order *Sulfolobales*.

Figure 1.3 (**A**) Fumarole at Lagoa das Furnas on São Miguel, Azores, Portugal (Photo: A. Kletzin). (**B**) Thin section electron micrograph of *Acidianus ambivalens* (Photo: W. Zillig).

1.2.3. Sulfur oxidation pathway of *Acidianus ambivalens*

Acidianus ambivalens is a facultatively anaerobic and sulfur-dependent crenarchaeon belonging to the *Sulfolobales* (Figure 1.3; Zillig *et al.*, 1985; Zillig *et al.*, 1986; Fuchs *et al.*, 1996). The optimal growth conditions of the chemolithotrophic organism are 80°C and pH 2.5. *Acidianus ambivalens* has since been established as a model-organism for sulfur metabolism. When grown aerobically, elemental sulfur is oxidized to sulfuric acid in several steps that involve cytoplasmic and membrane-bound proteins (Figure 1.4).

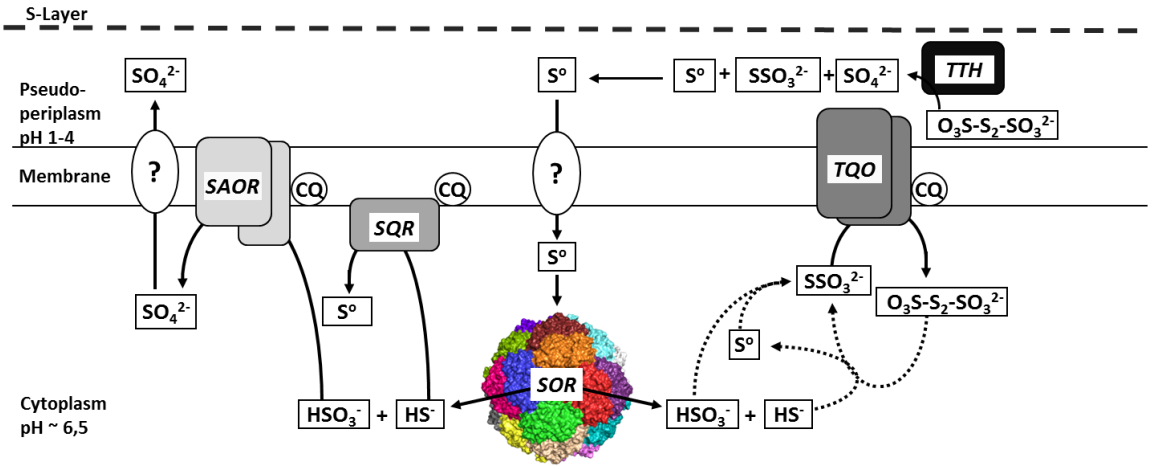

Figure 1.4 Hypothetical model of the sulfur oxidation pathway in *A. ambivalens* with localization of the corresponding enzymes (adapted from Kletzin, 2008). *SAOR* = sulfite:acceptor oxidoreductase; SQR = sulfide:quinone oxidoreductase; *SOR* = sulfur oxygenase reductase; *TQO* = thiosulfate:quinone oxidoreductase; *TTH* = tetrathionate hydrolase; *CQ* = caldariella quinone. *straight arrows*, enzymatic reactions; *dotted arrows*, non-enzymatic reactions.

The initial enzyme of the S^0 oxidation pathway is the cytoplasmic sulfur oxygenase reductase (SOR). Therefore, sulfur has to be transferred from the medium across the cytoplasmic membrane into the cell but it is still unclear how this transport is achieved. The SOR catalyzes an oxygen-dependent disproportionation reaction of sulfur to sulfite, thiosulfate and hydrogen sulfide. No energy conservation occurs during SOR catalysis but the reaction products formed are substrates for downstream enzymes. Thiosulfate is oxidized to tetrathionate by a membrane protein termed thiosulfate:quinone oxidoredutase (TQO; Müller *et al.*, 2004). Sulfite is oxidized to sulfate by a sulfite:acceptor oxidoreductase (SAOR; Zimmermann *et al.*, 1999), which has not yet been isolated.

The third enzyme is a membrane-bound sulfide:quinone oxidoreductase (SQR), whose 3D structure was recently resolved (Brito *et al.*, 2009) and which catalyzes the oxidation of hydrogen sulfide to elemental sulfur. The three enzymes couple substrate oxidation to energy conservation by delivering electrons to the quinone-pool of the membrane. Furthermore, tetrathionate is decomposed to sulfate, thiosulfate and elemental sulfur by an extracellular tetrathionate hydrolase in tetrathionate-grown cells (TTH; Protze *et al.*, 2011). The enzyme is probably attached to the cytoplasmic membrane or to the proteinaceous surface layer, the sole cell wall component of *A. ambivalens* (Veith *et al.*, 2009). The *Acidianus* TTH is biochemically and phylogenetically similar to the *Acidithiobacillus* TTH (Bugaytsova and Lindström, 2004). Both enzymes are located outside the cell and have optimal activities at acidic pH values (Protze *et al.*, 2011).

1.3. The sulfur oxygenase reductase

The SOR represents the initial enzyme in the sulfur oxidation pathway of *Acidianus ambivalens* and is the best-studied enzyme among all other proteins involved. The first SOR was described from *Acidianus brierleyi* (formerly *Sulfolobus brierleyi*; Emmel *et al.*, 1986) and characterized as a sulfur oxygenase (Table 1.1). Reductase activity had not been reported but the enzyme was comparable to the SORs described and purified from *A. ambivalens* (Kletzin, 1994) and *Acidianus tengchongensis* (formerly *Acidianus* sp. strain S5; He *et al.*, 2000 and Sun *et al.*, 2003). More recently, SORs and *sor*-encoding genes have also been reported from Bacteria such as *Aquifex aeolicus* (Table 1.1; Pelletier *et al.*, 2008), *Acidithiobacillus* sp. strain SM-1 (Chen *et al.*, 2007), *Acidithiobacillus caldus* (Mangold *et al.*, 2011) and "*Acidithiobacillus caldus"*-like strains (Janosch *et al.*, 2009). The *sor* gene is usually present in prokaryotes that can be found in solfataras, hot springs and metal mines and are therefore also present among microbial bioleaching communities. The bioleaching process describes the extraction of metals from their mineral source (ores) by naturally occurring microorganisms (Brandl, 2001). Up to date, *sor* genes were also found in the Archaea *Acidianus hospitalis*, *Sulfolobus tokodaii*, *Sulfolobus metallicus*, *Picrophilus torridus*, *Ferroplasma acidarmanus* and in the Bacteria *Halothiobacillus neapolitanus*, *Acidithiobacillus ferrivorans*, *Desulfomicrobium baculatum*, *Sulfobacillus acidophilus* and *Sulfobacillus thermosulfidooxidans* (two ORFs; Figure 1.5).

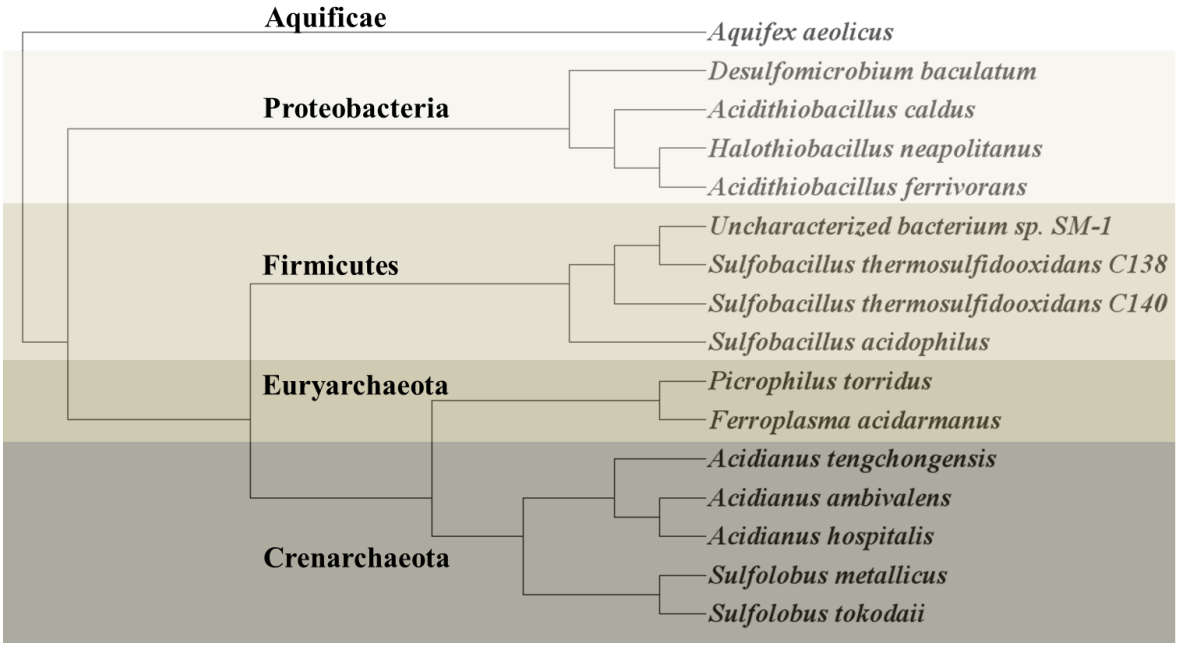

Figure 1.5 Tree representation of the phylogenetic relationship of SOR proteins with the corresponding host organism. The microbial phyla are indicated by grey boxes.

The SOR catalyzes the simultaneous oxidation and reduction of elemental sulfur S^0 to sulfite, thiosulfate and hydrogen sulfide. The *A. ambivalens* enzyme has its optimal activity at 85°C and at a pH between 7.0 - 7.4 (Kletzin, 1989). It is still not clear whether thiosulfate is formed by non-enzymatic sulfite condensation with excess S^0 or whether it is a primary reaction product. The SOR is only active under aerobic conditions but not under H_2 or N_2 atmosphere (Kletzin, 1989) and does not require external cofactors. A moderate incorporation of ^{18}O from O_2 into sulfite had been demonstrated with the sulfur oxygenase of *A. brierleyi* (Emmel *et al.*, 1986).

The determination of the reaction stoichiometry is not trivial as H_2S is highly volatile and quick evaporation results in understoichiometric amount of reduced products. Zinc acetate has been used to precipitate (hydrogen) sulfide in the activity assay resulting in an approximate 1:1 stoichiometry of reduced and oxidized products (Kletzin, 1989):

Eq. 1.3 $4\ S^0 + O_2 + 4\ H_2O \rightarrow 2\ HS^- + 2\ HSO_3^- + 4\ H^+$ (sum)

The overall reaction can be formally split into two partial reactions: a sulfur oxygenase reaction (Eq. 1.4) and a sulfur disproportionation reaction (Eq. 1.5):

Eq. 1.4 $S^0 + H_2O + O_2 \rightarrow HSO_3^- + H^+$

Eq. 1.5 $3\ S^0 + 3\ H_2O \rightarrow 2\ HS^- + HSO_3^- + 3\ H^+$

It was proposed that thiosulfate is formed non-enzymatically from sulfite and S^0 (Kletzin, 1989). The K_m values for sulfur, determined separately for the oxygenase and the reductase reaction of the *A. ambivalens* SOR, were 23 mM and 13 mM, respectively, calculated on the basis of S^0, not S_8. The k_{cat} values were 2.2 s^{-1} and 0.1 s^{-1} (oxygenase and reductase, respectively; Urich *et al.*, 2004).

Localization of the SOR in *Acidianus tengchongensis* was investigated by electron microscopy using SOR-specific antibodies labeled with immunogold particles (Chen *et al.*, 2005). It showed that the enzyme is present in the cytoplasm and that it is also attached to the cytoplasmic membrane. Enzyme particles of purified *Acidianus ambivalens* SOR had a spherical shape with a diameter of 15 nm when analyzed with electron microscopy (Kletzin, 1989; Urich *et al.*, 2004; Figure 1.6).

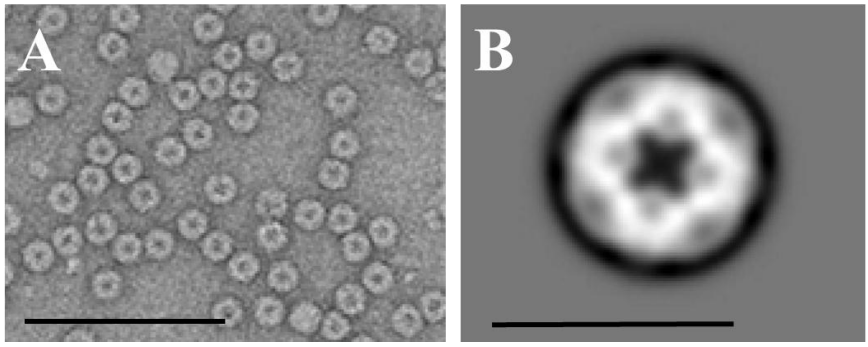

Figure 1.6 Electron micrographs of negatively stained SOR and image reconstruction. (**A**) Micrographs of native *A. ambivalens* SOR-wt; the bar represents 100 nm; (**B**) Results of single particle averaging of SOR particles; the bar represents 15 nm. Photos: R. Rachel (Regensburg); from Urich *et al.*, 2004.

Up to date, 3D structures of three archaeal SORs were resolved (*A. ambivalens*, Urich *et al.*, 2006; *A. tengchongensis*, Li *et al.*, 2008; *S. tokodaii*, unpublished data, http://pfwww.kek.jp/acr2006pdf/part_b/pf06b222.pdf; July 2011). However, the coordinates of the *S. tokodaii* enzyme are not presently available. X-ray crystallographic analysis indicated that the protein consists of 24 identical subunits assembling to a hollow and spherical complex with a 432 point group symmetry (Janner, 2008a; Janner 2008b) and an external diameter of approximately 15 nm (Figure 1.7).

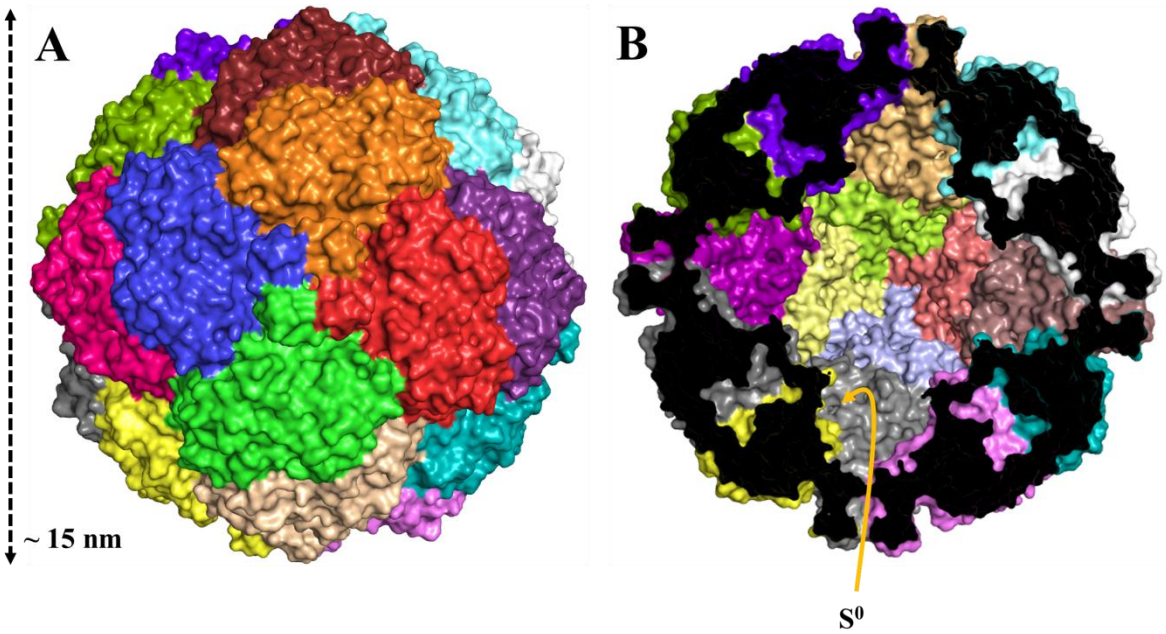

Figure 1.7 (**A**) Surface representation of the SOR holoenzyme with subunit coloring centered at the fourfold symmetry axis; the particle size is depicted by the dashed black arrow. (**B**) Representation of the protein structure and the inner surface of the holoenzyme sliced at the center of the fourfold symmetry axes; the putative entry site of the sulfur substrate to the inner cavity is indicated by the orange arrow.

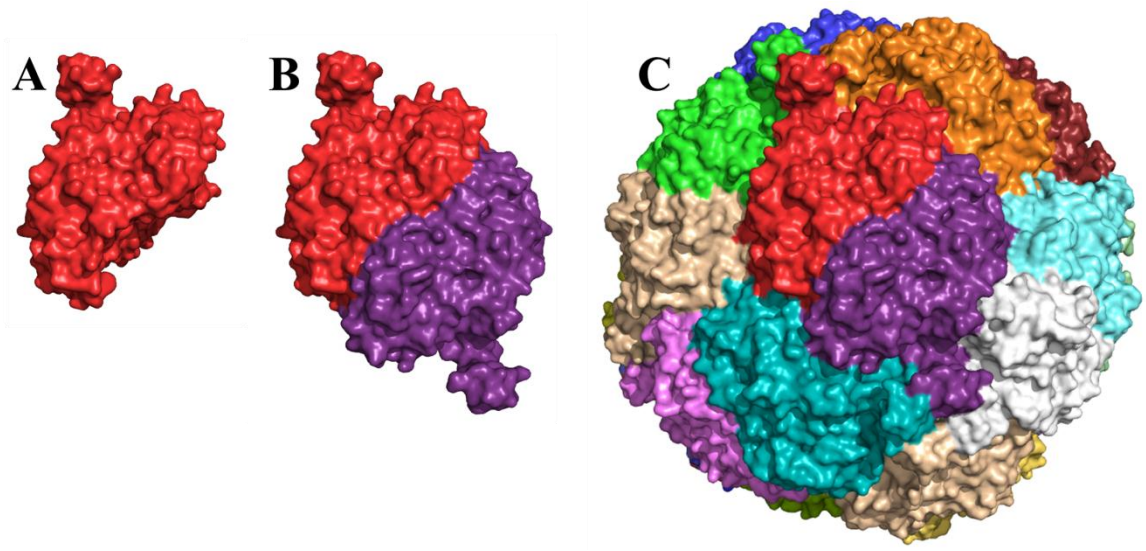

Figure 1.8 Surface representation of SOR holoenzyme. (**A**) SOR monomer; (**B**) SOR dimer; (**C**) SOR icosatetramer.

The *A. ambivalens* holoenzyme has a molecular mass of 840 kDa (native, Table 1.1) and is assembled from homodimers (Figure 1.8) as shown by reversible denaturation experiments (Urich *et al.*, 2004). The inner cavity can be accessed through chimney-like structures that open to a hydrophobic channel at the fourfold-symmetry axes of the protein. The active site of the SOR resides inside a pocket in the interior of each subunit (Figure 1.9).

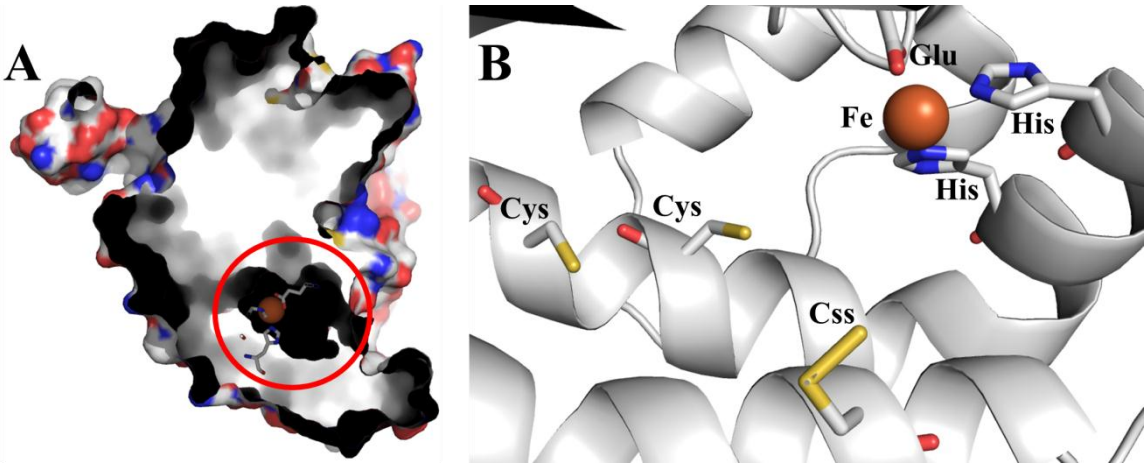

Figure 1.9 (**A**) Surface representation of a single *A. ambivalens* SOR monomer with atom coloring (red - oxygen; blue - nitrogen; yellow - sulfur; grey - carbon) and the active site pocket encircled in red. (**B**) Ribbon and stick representation of the active site of the *A. ambivalens* SOR with the iron center (depicted as orange sphere) and the corresponding iron ligands and the three conserved cysteine residues.

Each active site pocket is well separated from each other with a minimal distance between the Fe atoms of 37 Å, making a direct interaction most unlikely. The pocket is accessible through a narrow pore from the inner cavity.

The active site contains three conserved cysteine residues that are present in all SOR sequences so far (Urich *et al.*, 2005b; Chen *et al.*, 2005; Chen *et al.*, 2009; Figure 1.10). Site-directed mutagenesis showed that only one of these cysteines is essential for catalysis (C_{31} in *A. ambivalens* numbering) and that it cannot be replaced for an alanine without loss of activity. The side chains of the other two cysteines face the lumen of the active site pocket. They are positioned in an α-helix and form a C-X-X-C sequence motif. Substitution of C_{101} and C_{104} (*A. ambivalens* numbering) into alanines resulted in 30 % residual activity in a double mutant, thus showing that these cysteines are not essential for the enzyme activity (Urich *et al.*, 2005b). The active site also comprises a mononuclear non-heme iron center that was predicted by EPR spectroscopy. The iron center is in the high-spin Fe^{3+} state, which is reduced to Fe^{2+} after incubation with sulfur at high temperatures (Urich *et al.*, 2004). It has an unusual low reduction potential of E_0' = - 268 mV, which may be a result of hydrogen-bonding interactions near the metal site. The reduction potential is low enough to explain the reductase activity of the SOR (E_0' = - 270 mV for H_2S/S^0; Thauer *et al.*, 1977), but it is more than 300 mV lower than for other enzymes that contain mononuclear non-heme iron centers (Kletzin, 2008; Urich, 2005c). The metal is coordinated by a common structural motif, the 2-His-1-carboxylate facial triad. Among mononuclear non-heme iron enzymes, iron is ligated in the active site by the imidazole groups of two histidines and by the carboxylate group of an aspartate or glutamate (Figure 1.9), while water or solvent molecules complete the metal coordination (Hegg and Que, 1997; Costas *et al.*, 2004; Bruijnincx *et al.*, 2008). Substitution of any of the iron-ligating amino acids into an alanine showed a highly reduced enzyme activity resulting from low iron occupancy below 1 % (Urich *et al.*, 2005b).

Following page:

Figure 1.10 Multiple alignment of SOR sequences available in public databases with details from the *Acidianus ambivalens* 3D structure. Black arrows represent α-helices, white cylinders ß-strands. Accession numbers as follows: CAA39952.1(*Acidianus ambivalens*); AAK58572.1 (*Acidianus tengchongensis*); AEE93024.1 (*Acidianus hospitalis*); NP_377053.1 (*Sulfolobus tokodaii*); ABN04222.1 (*Sulfolobus metallicus*); ZP_05571354.1 (*Ferroplasma acidarmanus*); YP_023579.1 (*Picrophilus torridus*); ABF20541.1 (Uncharacterized bacterium described as *Acidithiobacillus sp*. SM-1); YP_003157691.1 (*Desulfomicrobium baculatum*); YP_003263105.1 (*Halothiobacillus neapolitanus*); ZP_05293375.1 (*Acidithiobacillus caldus*); ZP_08488838.1 (*Acidithiobacillus ferrivorans*); NP_213322.1 (*Aquifex aeolicus*). *Sulfobacillus acidophilus* and both *Sulfobacillus thermosulfidooxidans* SOR sequences were obtained from the corresponding genome sequences available at JGI (http://www.jgi.doe.gov; *S. acidophilus*, 4084280.fsa; *S. thermosulfidooxidans*, 4084278.fsa). Abbreviations: AP, active site pore; Css, cysteine persulfide; C, active site cysteines; Fe, iron-coordinating residues; 3, trimer channel pore-forming residues; Zn, 2-His motif around the zinc-coordinating His_{277}.

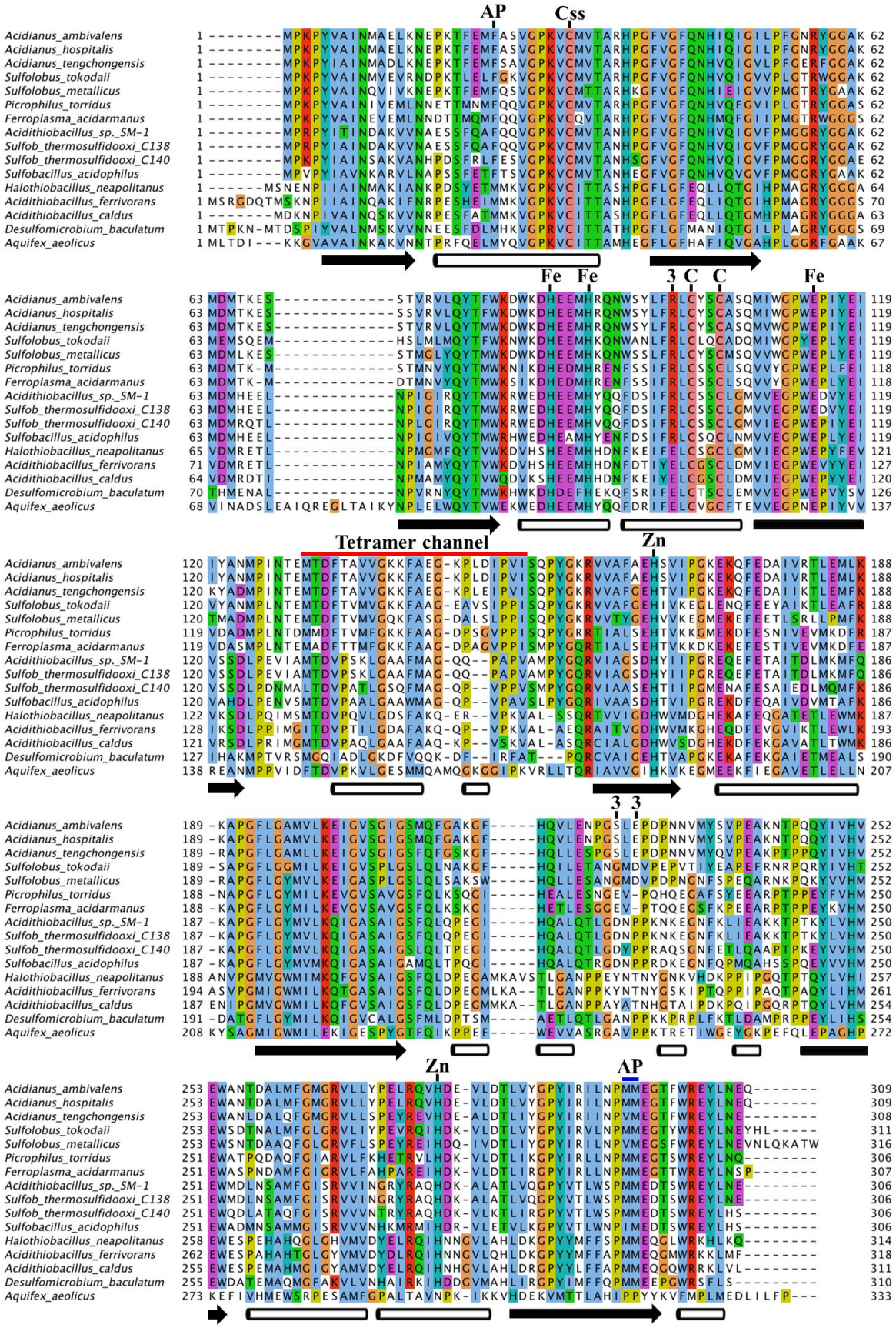
AP
Css
Fe
Fe
3
C
C
Fe
Tetramer channel
Zn
3
3
Zn
AP
Acidianus_ambivalens
Acidianus_hospitalis
Acidianus_tengchongensis
Sulfolobus_tokodaii
Sulfolobus_metallicus
Picrophilus_torridus
Ferroplasma_acidarmanus
Acidithiobacillus_sp._SM-1
Sulfob_thermosulfidooxi_C138
Sulfob_thermosulfidooxi_C140
Sulfobacillus_acidophilus
Halothiobacillus_neapolitanus
Acidithiobacillus_ferrivorans
Acidithiobacillus_caldus
Desulfomicrobium_baculatum
Aquifex_aeolicus

It was concluded from the structural and the mutational analysis that the iron center and C_{31} constitute the core of the active site of *A. ambivalens* SOR. Additional electron density at the γ-sulfur atom of C_{31} was detected in the *A. ambivalens* structure, suggesting a persulfide moiety at the respective amino acid residue. It was concluded that sulfur binds covalently to the modified cysteine (Css_{31}) and that a linear sulfur chain ($R\text{-}S_n\text{-}SH$) becomes aligned to the metal site (Urich, 2005c; Kletzin 2008). The SOR reaction most likely starts with a hydrolytic release of hydrogen sulfide from the sulfur chain, forming a sulfenic acid intermediate ($R\text{-}S_n\text{-}SOH$) that is highly reactive (Figure 1.11). The following events are rather speculative. Dioxygen activation in mononuclear non-heme iron enzymes can either be mediated by the metal center, which has to be in the reduced state (Fe^{2+}) or by the substrate that has to be activated by the metal center (Pau *et al.,* 2007). As a consequence, iron would have to undergo a redox change in both cases but it has recently been shown that dioxygen can also be activated in non-heme monooxygenases without a change in the redox state of the corresponding metal (Emerson *et al.*, 2008).

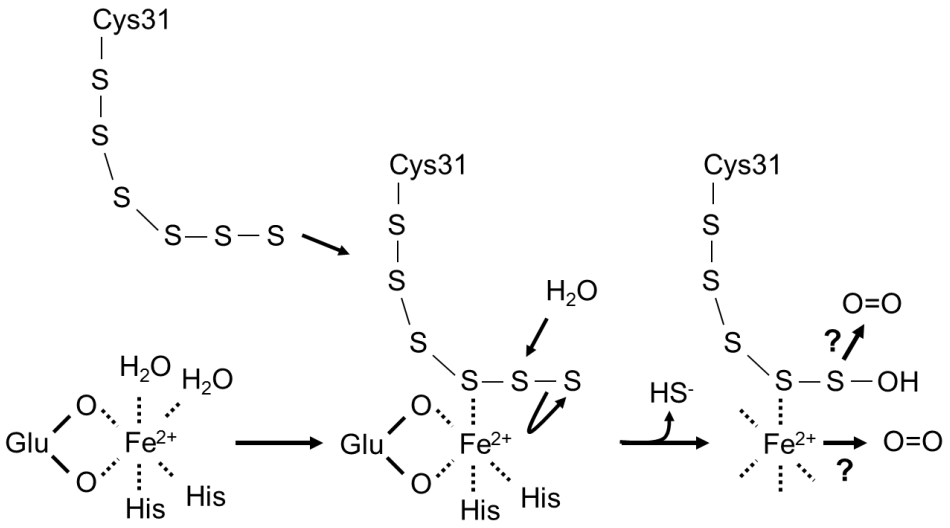

Figure 1.11 Hypothetical SOR reaction mechanism with both possibilities of dioxygen activation.

Table 1.1 Biochemical properties of the SOR enzymes and the sulfur oxygenase; n.r., not reported.

Species	*A. ambivalens*	*A. ambivalens*	*A. tengchongensis*	*A. brierleyi*	*Acidithiobacillus* sp. strain SM-1	*Acidithiobacillus caldus*-like strains S1 & S2	*Aquifex aeolicus*
Source	Native	*E. coli*	*E. coli*	Native	*E. coli*	Native	*E. coli*
Molecular mass subunit	[b]35,187 Da	[b]36,311 Da	[b]35,172 Da	[a]35,000 Da	[b]34,491 Da	[b]34,829 Da	[b]37,674 Da
Molecular mass (Holoenzyme)	[c]844,488 Da	[c]871,464 Da	n.r.	550,000 Da	n.r	n.r.	[cd]602,000 Da
pH_{opt}/ pH range	7.0 - 7.4 / 4 - 8	n.r.	5 / 3.5 - 9.0	7.0 / n.r.	7.5 / n.r.	n.r.	n.r. / 5.5 - 8.0
T_{opt}/ T_{range}	85°C / 50 - 108°C	n.r.	70°C / 50 - >90°C	65°C / 50 - >80°C	75 - 80°C / n.r.	65°C / 30 - > 65°C	80°C / 20 - 90°C
Specific oxygenase activity	10.6 U/mg	2.8 U/mg	753 U/mg	0.9 U/mg	3.76 U/mg	n.r.	78.8 U/mg
Specific reductase activity	2.6 U/mg	0.66 u/mg	45.2 U/mg	n.r.	n.r.	n.r.	3.05 U/mg
Reference	Kletzin, 1989	Urich *et al.*, 2004	Sun *et al.*, 2003	Emmel *et al.*, 1986	Chen *et al.*, 2007	Janosch *et al.*, 2009	Pelletier *et al.*, 2008

[a] apparent mass in SDS gels. [b]calculated from sequence. [c] excluding iron. [d] considered as a 16mer.

1.4. Goals of this study

The sulfur oxygenase reductase represents the best-studied enzyme involved in the sulfur oxidation pathway of the crenarchaeon *Acidianus ambivalens*. The protein has been biochemically and structurally characterized but detailed knowledge of the SOR reaction mechanism is still missing. The interpretation of the present crystallographic data gave first hints to the pathway of the sulfur substrate, even though no biochemical data were available to support the hypothesis. The first goal was to identify the different steps of the sulfur pathway by analyzing the impact of mutations at the suspected entry and exit sites of the enzyme. The knowledge was also limited for the events occurring during catalysis at the active site. It had been demonstrated that the active site pocket of the SOR comprises conserved cysteine residues and a mononuclear iron center, which becomes reduced upon incubation with sulfur at elevated temperatures. The change of the iron's redox state suggested that it is involved in dioxygen activation although it was not clear, whether O_2 is rather activated by the metal or by the sulfur substrate. To address this question, SOR derivatives containing non-iron transition metals were generated and analyzed via EPR spectroscopy in order to investigate if a redox change of the metal is required during catalysis.

The redox potential of the Fe center had been previously determined and it was unusually low for mononuclear non-heme iron proteins. It had been shown by site-directed mutagenesis that certain members of the second coordination sphere of the SOR play a crucial role with respect to the enzyme activity (Seyfarth, 2006). These mutants were reproduced in this work and prepared for crystallization in order to investigate changes within the catalytic center that resulted from the amino acid substitutions. Additionally, further putative members of the hypothesized hydrogen bond network were analyzed using site-directed mutagenesis. Various SOR mutants of the *A. ambivalens* SOR were generated, while only few had a major impact in regard to enzyme activity. Consequently, the attention was focused on other naturally occurring SOR variants. At the beginning of this work, only SOR proteins from (hyper-) thermophilic prokaryotes were known. Several genome sequences of mesophilic and moderately thermophilic sulfur-oxidizing bacteria became available and indicated the presence of *sor* genes in these organisms. The *sor* gene of the mesophilic sulfur-oxidizing bacterium *Halothiobacillus neapolitanus* was chosen for further studies.

The results are summarized in the following chapters 3 - 6.

Chapter 3 concentrates on the characterization of the suspected sulfur substrate and products pathways in the *A. ambivalens* SOR. The putative entry and exit pores were modified by site-directed mutagenesis and the constructed mutant proteins biochemically analyzed. Additionally, the mechanism of zinc inhibition of the SOR was investigated using biochemical and structural data and discussed in context of the sulfur substrate pathway.

Chapter 4 addresses the question, whether the hydrogen bond network at the active site center of the SOR influences activity. Amino acids potentially involved in this network were substituted via site-directed mutagenesis and the corresponding mutants were biochemically and structurally characterized. Furthermore, the redox change of the metal center was investigated using metal-substituted SOR proteins. Those SOR-derivatives were analyzed for metal content, enzyme activity and the redox state was monitored via EPR spectroscopy. In addition, the sulfurization at the essential active site cysteine was examined by crystallization of the *A. ambivalens* SOR-wt.

Chapter 5 focuses on studies of the *H. neapolitanus* SOR. The corresponding *sor* gene was heterologously expressed and the purified recombinant protein was biochemically and structurally characterized. It was eventually compared to the available 3D structure of the *Acidianus ambivalens* SOR to add new details to the knowledge on the SOR protein family.

All data are summarized in **Chapter 6**, discussing the available data on SOR proteins in the biochemical and structural context in order to establish a general reaction mechanism and to describe general properties valid for all SOR proteins.

2. Materials and Methods

2.1. Materials

2.1.1. Chemicals

Chemicals and materials that were used but not listed below were purchased from Merck KG, Darmstadt, Germany; Carl Roth, Karlsruhe, Germany and Laborservice, Griesheim, Germany.

2-mercaptoethanol	Roth, Karlsruhe, Germany
2-propanol	LS, Griesheim, Germany
6-amino caproic acid	Roth, Karlsruhe, Germany
6 x loading dye	Fermentas, St. Leon-Roth, Germany
Acrylamide (30:0.8)	Roth, Karlsruhe, Germany
Agarose (Seakem ME)	BMA, Walkersville, USA
Ampicillin	Roche Diagnostics, Mannheim, Germany
Ammonium persulfate (APS)	Roth, Karlsruhe, Germany
Anhydrotetracycline (AHT)	IBA, Göttingen, Germany
Bromcresol purple	Merck, Darmstadt, Germany
Chloramphenicol	Roth, Karlsruhe, Germany
Cobalt(II) sulfate (heptahydrate)	Merck, Darmstadt Germany
Coomassie Brilliant Blue G250	Serva, Heidelberg, Germany
Coomassie Brilliant blue, colloidal	Roth, Karlsruhe, Germany
Copper(II) sulfate (pentahydrate)	Merck, Darmstadt, Germany
D-desthiobiotin	IBA, Göttingen, Germany
dNTPs	Roth, Karlsruhe, Germany
Ethanol	Roth, Karlsruhe, Germany
Ethidiumbromide	Roth, Karlsruhe, Germany
Ethylendiamine tetraacetic acid (EDTA)	LS, Griesheim, Germany
Formalin (37 % formaldeyhde)	LS, Griesheim, Germany
Fuchsine	Merck, Darmstadt, Germany
Gallium(III) nitrate (monohydrate)	Alfa Aesar, Karlsruhe, Germany
Glycerol	Roth, Karlsruhe, Germany
Iron(II) chloride (tetrahydrate)	Sigma-Aldrich, Buchs, Switzerland
Hydroxy-azophenyl benzoic acid (HABA)	Acros Organics, Geel, Belgium
Magnesium(II) sulfate (heptahydrate)	Merck, Darmstadt, Germany
Manganese(II) chloride (tetrahydrate)	Merck, Darmstadt, Germany
Methanol	LS, Griesheim, Germany
Nickel(II) sulfate (hexahydrate)	Sigma, St. Louis, USA
Ruthenium(III) chloride (monohydrate)	Merck, Darmstadt, Germany
Sodium dodecyl sulfate (SDS)	Roth, Karlsruhe, Germany
Strep-Tactin Gravity Flow Column	IBA, Göttingen, Germany
Strep-Tactin Superflow Column	IBA, Göttingen, Germany
Strep-Tactin Sepharose	IBA, Göttingen, Germany
Sulfur, elemental	AppliChem, Darmstadt, Germany
Tetramethylethylendiamine (TEMED)	Roth, Karlsruhe, Germany
TPTZ (2,4,6-Tri-(2-pyridyl-1,3,5-triazine)	Acros Organics, Geel, Belgium
Tris-(hydroxymethyl)-aminomethan	Roth, Karlsruhe, Germany
Tryptone	BD, Le Pont de Claix, France
TTC (2,3,5-triphenyltetrazolium chloride)	Merck, Darmstadt, Germany
Tween 20	Roth, Karlsruhe, Germany
Urea	Roth, Karlsruhe, Germany
Vanadyl(IV) sulfate	Merck, Darmstadt, Germany
Yeast extract	BD, Le Pont de Claix, France

2.1.2. Microorganisms

Halothiobacillus neapolitanus DSM 15147	DSMZ, Braunschweig, Germany
Acidianus ambivalens DSM 3772	DSMZ, Braunschweig, Germany
Escherichia coli TOP10'	Stratagene (Agilent Technologies), Waldbronn, Germany
Escherichia coli BL21-CodonPlus (DE3)-RIL	Stratagene (Agilent Technologies), Waldbronn, Germany

2.1.3. Plasmids

pASK-SOR.05	Urich *et al.*, 2004
pASK_HnSOR	this work
pASK_AqSOR	this work
pETSOR	Pelletier *et al.*, 2008

2.1.4. Enzymes and kits

Restriction Endonucleases	Fermentas, St. Leon-Rot, Germany NEB, Frankfurt, Germany
Taq Polymerase	Invitrogen, Darmstadt, Germany
Pfu Polymerase	Fermentas, St. Leon-Rot, Germany
Pfu Ultra High-Fidelity Polymerase	Agilent Technologies, Waldbronn, Germany
T4 DNA Ligase	NEB, Frankfurt, Germany
Antarctic Phosphatase	NEB, Frankfurt, Germany
E.Z.N.A. Plasmid Miniprep Kit I	Omega Bio-Tek, Norcross, USA
QIAprep Spin Miniprep Kit	Qiagen, Hilden, Germany
GenElute PCR Clean-Up Kit	Sigma-Aldrich, St. Louis, USA
BCA Protein Assay Kit	Novagen, Darmstadt, Germany

2.1.5. Synthetic oligonucleotides

All synthetic oligonucleotides were purchased from Biomers, Ulm, Germany. Primers were resuspended in HPLC-grade water and stored at -20°C. The corresponding reverse-complimentary oligonucleotides for the Quikchange method (Stratagene, now Agilent Technologies, Waldbronn, Germany) are not shown.

Table 2.1: Synthetic oligonucleotides. Substituted nucleotides are shown in lower case letters (R= A or G and Y= T or C). Inserted or removed restriction sites are underlined. Bold letters indicate an exchange in the amino acid sequence of the corresponding mutant.

Oligo-nucleotide Name	**Sequence**	
M_{22}C fwd	5'-AAAACTTTcGAA**tgc**TTTGCCTCAGTA-3'	Addition of *Bsp*119I site
M_{22}L fwd	5'-AAAACTTTcGAA**ttg**TTTGCCTCAGTA-3'	Addition of *Bsp*119I site
T_{34}S fwd	5'-GGTCTGCATGG**Tct**CAGCAAGGCATCCGGG-3'	Addition of *Eco31*I site
M_{89}A fwd	5'-TGGAA**g**GACCATGAAGAA**gcG**CACAGGCAAAAC-3'	Addition of *Eco*47I site
R_{91}A fwd	5'-GGAAAGAtCATGAAGAAATGCAC**gcg**CAAAACTGG-3'	Addition of *Dpn*I site
R_{99}A fwd	5'-GGAGTTACTTATTC**gcg**CTATGCTATTCATGCGC-3'	Addition of *Bsh*1236I site
R_{99}IL fwd	5'-AACTGGAGcTACTTATTC**mtc**CTATGCTATTCATG-3'	Addition of *Alu*I site
M_{130}A fwd	5'-ATAAACACTGAA**gcG**ACCGACTTCAC-3'	Addition of *Bsh*1285I site
H_{166}A fwd	5'-GCCTTTGCAGAG**gcg**TCAGTAATTCC-3'	Loss of *Bsp*1286I site
S_{205}A fwd	5'-GGAAATAGGAGTT**gCC**GGAATTGGAAGC-3'	Loss of *Kpn*2Isite
S_{226}A fwd	5'-AACCCTGGA**gCA**CTTGAGCCcGATCCAAAT-3'	Addition of *Psu*I site
S_{226}IL fwd	5'-AACCCTGGA**mtA**CTTGAGCCcGATCCAAAT-3'	Addition of *Psu*I site
S_{226}T fwd	5'-AACCCTGGA**aCA**CTTGAGCCcGATCCAAAT-3'	Addition of *Psu*I site
E_{228}A fwd	5'-CCTGGATCACTT**GcG**CCcGATCCAAATAAT-3'	Loss of *Psu*I site
H_{277}A fwd	5'-TAAGACAAGTA**gct**GACGAAGTTTT-3'	Loss of *Tat*I site
$MM_{296/297}$ fwd	5'-ATTAAATCCA**ryGryG**GAAGGCACcTTCTGGAG-3'	Addition of *Ban*I site
DelL GC fwd	5'-CCTATAAACACcGGG**tgtgga**ATTTCACAACC-3'	Addition of *Bcn*I site
HnSOR fwd	5'-ACTAGTTAACGAGGGCAAAAAATGTCGAATGAAA ATCCAATTATA-3'	*Bcu*I site
HnSOR rev	5'-GTGACGCCAAGCGCTTTGCTTAAGATGCTTACGCC-3'	*Eco47*III site
AqSOR fwd	5'-ACTAGTTAACGAGGGCAAAAAATGCTGACAGATA TTAAAAAAGGC-3'	*Bcu*I site
AqSOR rev	5'-GTGACGCCAAGCGCTAGGAAAGAGAATCAGATCCT-3'	*Eco*47III site
Sequencing Oligo fwd	5'-TAGAGTTATTTTACCACTCCCTATCAG-3'	
Sequencing Oligo rev	5'-GCAGTAGCGGTAAACGGCAGAC-3'	

2.1.6. Molecular weight standards

GeneRuler DNA Ladder Mix	Fermentas, St.Leon-Rot, Germany
Unstained Protein Molecular Weight Marker	Fermentas, St.Leon-Rot, Germany
PageRuler Unstained Protein Ladder	Fermentas, St.Leon-Rot, Germany

2.1.7. Media

2 x LB medium (per liter dH_2O)	20	g	Tryptone
	10	g	Yeast extract
	20	g	NaCl
	adjusted to pH 7.3 with NaOH		
	Ampicillin: 100 µg/ml		
	Chloramphenicol: 12.5 µg/ml		

For solid agar plates, 1 % Difco bacto agar was used.

M9 medium (per liter dH_2O)	1	x	M9 salts
	2	mM	$MgSO_4$
	0.1	mM	$CaCl_2$
	0.4	%	Glucose (sterile)
5 x M9 salts (per liter dH_2O)	64	g	Na_2HPO_4 x 7 H_2O
	15	g	KH_2PO_4
	2.5	g	NaCl
	5	g	NH_4Cl
SOB medium (per liter dH_2O)	20	g	Tryptone
	5	g	Yeast Extract
	0.5	g	NaCl
SOC medium (per liter dH_2O)	100	ml	SOB medium
	1	ml	1 M $MgSO_4$
	1	ml	1 M $MgCl_2$
	1	ml	2 M Glucose (sterile)

Halothiobacillus neapolitanus medium	4	g	KH_2PO_4
(DSMZ medium 68; per 0.9 l dH_2O)	4	g	K_2HPO_4
	0.8	g	$MgSO_4$ x 7 H_2O
	0.4	g	NH_4Cl
	10	ml	Trace element solution
	0.5	ml	Bromcresol purple (saturated aqueous solution)

Salts were dissolved in 900 ml dH_2O and autoclaved. 100 ml of an autoclaved 10 % (w/v) Na_2SO_3 x 5 H_2O solution were subsequently added to 900 ml of the media. Alternatively, 1 l medium was supplied with 10 g tyndalized elemental sulfur instead of thiosulfate.

For solid agar plates, 1.5 % Difco bacto agar was used.

Trace element solution	50.0	g	Na_2-EDTA
(DSMZ medium 69; per liter ddH_2O;	22.0	g	$ZnSO_4$
see also Vishniac and Santer, 1957)	5.54	g	$CaCl_2$ x 2 H_2O
	5.06	g	$MnCl_2$ x 4 H_2O
	5.00	g	$FeSO_4$ x 7 H_2O
	1.10	g	$(NH_4)_6Mo_7O_{24}$ x 4 H_2O
	1.57	g	$CuSO_4$ x 5 H_2O
	1.61	g	$CoCl_2$ x H_2O
	adjusted to pH 6.0 with KOH		

2.1.8. Buffers and solutions

TEN-buffer (per liter dH_2O)	20	mM	Tris-HCl pH 8.0
	1	mM	EDTA
	100	mM	NaCl
	adjusted with HCl		
TE-buffer (per liter dH_2O)	20	mM	Tris-HCl pH 8.0
	1	mM	EDTA
	adjusted with HCl		
TAE-buffer (per liter dH_2O)	40	mM	Tris-HCl pH 7.5
	2	mM	EDTA
	adjusted with acetic acid		

Inclusion Body washing buffer	100	mM	Tris-HCl pH 8.0
(per liter dH_2O)	1	%	Sodium Deoxycholate
	1	M	Urea
	10	%	Glycerol
	2	mM	EDTA
Bradford solution (per liter dH_2O)	0.01	%	Coomassie Brilliant Blue G250
	4.75	%	Ethanol (99.6 %)
	8.50	%	Phosphoric acid (85 %)
10 x DNA loading buffer	0.25	%	Bromphenol Blue
(per liter dH_2O)	50	%	Sucrose
	0.1	M	EDTA pH 8.0

2.2. Microbiological Methods

2.2.1. Growth of *Halothiobacillus neapolitanus* DSM 15147

Halothiobacillus neapolitanus strain DSM 15147 was purchased from DSMZ (Braunschweig, Germany). Growth of *H. neapolitanus* in liquid culture was started by inoculation of the appropriate medium and incubation at 28°C under vigorous shaking in 500 ml medium including 1 % (v/v) of a thiosulfate solution. Alternatively, the organism was incubated with 1 % (w/v) tyndalized elemental sulfur instead of thiosulfate. Cells were grown until the color of bromcresol purple shifted to yellow and were subsequently harvested by centrifugation.

2.3. Molecular Biological Methods

2.3.1. Genomic DNA extraction from *Halothiobacillus neapolitanus* DSM 15147

Isolation of chromosomal DNA of *H. neapolitanus* was carried out according to a modified protocol of *Sulfolobus solfataricus* DNA extraction by Albers (http://www.rug.nl/gbb/research/researchGroups/molecularMicrobiology/research/extremophiles/DNAsulf.pdf; July 2011). Sedimented *H. neapolitanus* cells (600 µg) were resuspended in 550 µl of TEN buffer. 50 µl of a 10 % SDS (w/v) solution were added to the suspension which was subsequently incubated for 45 min at room temperature.

An equal volume (600 µl) of a phenol:chloroform:isoamyl alcohol (25:24:1) solution was added, thoroughly mixed and centrifuged (15 min, 16,500 x g; A1420 rotor, Universal 320R, Hettich, Tuttlingen, Germany). To extract residual phenol from the aqueous phase, 600 µl of a chloroform:isoamyl alcohol (24:1) mixture were added, thoroughly mixed and centrifuged (15 min, 16,500 x g). The genomic DNA was precipitated by addition of 1/10 volume of a 3 M sodium acetate solution pH 5.2 and 0.8 volumes of 2-propanol. The mixture was incubated at -20°C for 2 h and subsequently centrifuged for 30 min at 16,500 x g. The pelleted DNA was washed once with 70 % ethanol, centrifuged for 5 min at 16,500 x g, dried at room temperature and eventually resuspended in 50 µl of TE buffer.

2.3.2. Amplification of *Halothiobacillus neapolitanus* and *Aquifex aeolicus sor* genes

The *sor*-ORF of *Halothiobacillus neapolitanus* (*Hneap_1222*) was amplified by polymerase chain reaction (PCR) using the oligonucleotides HnSOR fwd and HnSOR rev with genomic DNA as template in a 50 µl reaction mixture that included:

5 µl	10 x reaction buffer
4 µl	dNTPs (final conc. 0.2 mM)
1 µl	oligonucleotide mix (30 pmol primer each)
0.2 µl	Genomic DNA of *H. neapolitanus* (500 µg /µl)
0.6 µl	*Taq* / *Pfu* polymerase mix (20:1)
39.2 µl	HPLC-grade H_2O

Table 2.2 PCR conditions for *sor* gene amplification from *H. neapolitanus*

Number of cycles	Denaturation	Annealing	Polymerization
1 cycle	95°C, 5 min	50°C, 60 sec	72°C, 90 sec
3 cycles	95°C, 30 sec	50°C, 60 sec	72°C, 90 sec
27 cycles	95°C, 30 sec	60°C, 60 sec	72°C, 90 sec
1 cycle	95°C, 30 sec	60°C, 60 sec	72°C, 10 min

The *sor*-ORF of *Aquifex aeolicus* VF5 (*aq_455*) was amplified using the same PCR conditions with the oligonucleotides AqSOR fwd and AqSOR rev and a pET22b plasmid that harboured the corresponding gene (pETSOR, Pelletier *et al.*, 2008) as template.

2.3.3. Preparation of SOR amplification products and of the pASK-SOR.05 vector

The PCR products were purified using the Gen-Elute PCR Clean-Up kit according to the manufacturer's recommendations (Sigma-Aldrich, St. Louis, USA). The purified DNA fragments were subsequently cleaved in a 70 µl reaction mix including 15 µl PCR product, 7 µl 10 x reaction buffer, 25 U *Bcu*I, 50 U of *Eco47*III and 40.5 µl HPLC-grade H_2O. The reaction mix was incubated for 4 h at 37°C. The hydrolyzed DNA was purified using the same kit to remove short DNA fragments and restriction endonucleases. The original pASK-SOR.05 vector carrying the *Acidianus ambivalens sor* gene was restricted using a reaction mixture that included 30 µl plasmid DNA, 8 µl 10 x reaction buffer, 25 U *Xba*I, 50 U *Eco47*III and 34.5 µl HPLC-grade H_2O. The mixture was incubated for 3 h at 37°C and the restriction enzymes were inactivated by heating the reaction tube to 65°C for 20 min. A second cleavage step was carried out to impede re-ligation of the original pASK-SOR.05 plasmid by adding 25 U *Xmi*I, a restriction enzyme that solely cleaves within the *A. ambivalens sor* gene. The plasmid DNA was eventually treated with 1 µl antarctic phosphatase according the manufacturer's recommendations for 1 h and heat-inactivated by incubation at 65°C for 10 min.

2.3.4. DNA ligation and analysis of transformants

The prepared PCR fragments were inserted into the hydrolyzed pASK-SOR.05 plasmid via a ligation reaction that included 2 µl plasmid DNA (50 µg/µl), 8 µl PCR product (40 µg/µl), 2 µl 10 x reaction buffer, 1 µl T4 DNA ligase and 7 µl HPLC-grade H_2O with an overnight incubation at 4°C. The reaction was stopped by heating the reaction tube to 65°C for 5 min and *E. coli* TOP10' cells (Invitrogen) were transformed with 6 - 7 µl of the ligation product. Positive transformants that were carrying the plasmid were detected by colony PCR, using the same conditions as described in chapter 2.2.2 but applying a small amount of a single colony to the reaction tube instead of genomic DNA. Plasmid DNA of positive transformants was extracted by a plasmid mini prep kit (Omega Bio-Tek, Norcross, USA) and sequenced for validation (Sequencing Service, LMU, München, Germany).

2.3.5. Site directed-mutagenesis and analysis of transformants

The *sor* gene of *Acidianus ambivalens* (EMBL accession number X56616) was heterologously expressed using the pASK-SOR.05 plasmid (Skerra *et al.*, 1994; Urich *et al.*, 2004). Mutations were inserted using the Quikchange method (Stratagene, now Agilent Technologies; Böblingen, Germany) with pASK-SOR.05 as template. The mutagenic oligonucleotides also contained silent mutations that caused a loss or an addition of a restriction site for restriction analysis (see Table 2.1). The PCR reaction included 0.25 mM dNTPs, 1 U *Pfu*Ultra High-fidelity polymerase (2.5 U/µl), 20 - 50 pmol of each oligonucleotide and 100 ng of plasmid DNA.

Table 2.3 Standard PCR conditions for site-directed mutagenesis

Number of cycles	Denaturation	Annealing	Polymerization
1 cycle	95°C, 5 min	45-61°C, 60 sec	72°C, 5 min
3 cycles	95°C, 30 sec	45-61°C, 60 sec	72°C, 5 min
18 cycles	95°C, 30 sec	52-68°C, 60 sec	72°C, 5 min
1 cycle	95°C, 30 sec	52-68°C, 60 sec	72°C, 10 min

The PCR product was subsequently digested for 4 h with 10 U *Dpn*I (Fermentas) and purified via the Gen-Elute PCR Clean-Up kit according to the manufacturer's recommendations, eluted with 25 µl of elution buffer and stored at -20°C until usage. *E. coli* TOP10' cells (Invitrogen) were transformed with 5 µl of purified PCR product. 5 ml of 2 x LB medium were inoculated with a single transformant colony and incubated overnight at 37°C under vigorous shaking. Plasmid DNA was extracted using the QIAprep Spin Miniprep kit (Qiagen). The isolated DNA was cleaved with the respective restriction enzyme in a 20 µl reaction mixture that was incubated for 2 h at 37°C. The reaction mix typically contained 5 µl plasmid-DNA, 2 µl 10 x reaction buffer, 10 U of the restriction enzyme and 8 µl HPLC-grade H_2O. Results of restriction analyses were analyzed via agarose gel electrophoresis. Positive plasmids were sequenced to verify the introduced mutation (Sequencing Service, LMU, München, Germany).

2.3.6. Agarose gel electrophoresis

Agarose gel electrophoresis was performed for analytical separation of DNA fragments. All agarose gels were prepared with 1 % agarose dissolved in 0.5 x TAE buffer. The samples and a DNA size standard were mixed with an appropriate volume of DNA loading buffer and loaded onto the gel. Electrophoresis was carried out at a voltage of 100 V and stopped when the bromphenol blue band of the loading dye reached ¾ of the gel length. The gels were stained with an ethidium bromide-containing solution (1 µg/l in ddH_2O) and visualized via a gel documentation system.

2.3.7. Heterologous gene expression in *E. coli*

E. coli BL 21 Codon plus (DE3) RIL cells were transformed with the mutant plasmids, the original pASK-SOR.05, pASK_HnSOR or pASK_AqSOR. The expression of the *sor* genes was induced by addition of anhydrotetracycline (200 µg/l of culture) to either 0.5 or 15 l cultures growing at 37°C in 2 x LB medium at an OD_{600} between 0.6 - 0.8. The cultures were incubated for 20 h after induction with either vigorous shaking (0.5 l; 200 rpm) or with vigorous aeration and stirring (15 l; 350 rpm). In order to ensure sufficient iron incorporation, 100 µM ferric citrate was added to the media at the time of induction. A small volume (50 - 500 µl) of a silicone-based anti-foam solution (Roth, Karlsruhe, Germany) was also added to prevent foam formation. After incubation for 20 h, cells were harvested by centrifugation (10,000 x g, 10 min, 4˚C, Sorvall, SLA-3000, Thermo Fisher Scientific, Schwerte, Germany).

2.3.8. Constructs for heterologous gene expression

pASK-SOR.05 (Urich *et al.,* 2004) contains the *A. ambivalens sor* gene sequence (927 bp) followed by a 30 bp sequence coding for a ten amino acids long streptavidin tag. The amplified *sor* gene was digested with *Eco47*III and *Xba*I followed and inserted into the original pASK 75 plasmid, digested with the same restriction enzymes.

pASK_HnSOR (this work) contains the *H. neapolitanus sor* gene sequence (942 bp) followed by a 30 bp sequence coding for a ten amino acids long streptavidin tag. The amplified *sor* gene was digested with *Spe*I and *Eco47*III and inserted into an *Eco47*III and *Xba*I-cleaved pASK-SOR.05 plasmid.

pASK_AqSOR (this work) contains the *A. aeolicus sor* gene sequence (999 bp) followed by a 30 bp sequence coding for a ten amino acids long streptavidin tag. The amplified *sor* gene was digested with *Spe*I and *Eco47*III and inserted into an *Eco47*III and *Xba*I-cleaved pASK-SOR.05 plasmid.

2.4. Biochemical methods

2.4.1. Purification of recombinant SOR from *E. coli*

E. coli cells were harvested via centrifugation (10,000 x g, 10 min, Sorvall, SLA-3000; Thermo Fisher Scientific, Schwerte, Germany) and were washed once in approximately 10 volumes (v/w) of 100 mM Tris/HCl / 150 mM NaCl buffer pH 8 (buffer W). The cells were resuspended in 5 volumes of the same buffer after the washing step. The cells were subsequently disrupted with a water-cooled High Pressure Homogenizer (Constant Systems; 0.18 mm nozzle and 1.35 MPa pressure). After a first centrifugation step (10,000 x g for 30 min, Sorvall, SLA-3000; Thermo Fisher Scientific, Schwerte, Germany), the soluble protein-containing supernatant was centrifuged in an ultracentrifuge (100,000 x g for 45 min, 45Ti, Beckman Instruments). The soluble crude extract from 5 - 10 g cells (wet mass) was applied to Strep-Tactin gravity flow columns with a bed volume of 1 ml (IBA, Göttingen, Germany). Solube crude extract from 15 - 112 g cells (wet mass) was applied to an 8 - 10 ml Strep-Tactin super-flow column (IBA, Göttingen, Germany) connected to an ÄKTApurifier 10 (GE Healthcare Bio-Sciences AB, Uppsala, Sweden). This step was repeated, when the binding capacity of the column was exceeded. The column was equilibrated with 5 column volumes (cv) with buffer W prior to loading of the protein solution. The column was subsequently washed with 6 cv of the same buffer and the protein eluted by applying 3 cv of 100 mM Tris/HCl / 150 mM NaCl / 2.5 mM desthiobiotin buffer pH 8. The column was regenerated with 15 cv of 100 mM Tris/HCl / 150 mM NaCl / 1 mM hydroxyl-azophenyl benzoic acid (HABA) buffer pH 8.

Alternatively, the column was regenerated with 3 column volumes each of ddH_2O, 0.5 M NaOH, and ddH_2O instead of the regular HABA solution (IBA).

Buffer W: 100 mM Tris/HCl pH 8 / 150 mM NaCl
Buffer E: 100 mM Tris/HCl pH 8 / 150 mM NaCl / 2.5 mM desthiobiotin
Buffer R: 100 mM Tris/HCl pH 8 / 150 mM NaCl /
1 mM hydroxyl-azophenyl benzoic acid (HABA)

2.4.2. Unfolding and refolding of recombinant SOR from inclusion bodies

E. coli cell pellets of the first centrifugation step after cell disruption contained large amounts of misfolded protein aggregates (inclusion bodies). These pellets were resuspended in inclusion body washing buffer and dispersed by sonication for five minutes (Branson Sonifier II, Heinemann, Schwäbisch Gmünd, Germany). After centrifugation (10,000 x g for 5 min, Sorvall, SLA-3000; Thermo Fisher Scientific, Schwerte, Germany), the supernatant was discarded and the sediment treated repeatedly as described above. Washed inclusion bodies were dissolved in 10 volumes of 8 M Urea / 50 mM Tris/HCl buffer pH 7.2 with 2 mM 2-mercaptoethanol or 30 mM dithiotreitol (DTT). Heat-labile *E. coli* proteins were precipitated by heating the suspension to 60°C for 1 h and separated from heat-stable proteins by centrifugation (100,000 x g for 10 min, Beckman Instruments, 45Ti). For metal-substitution experiments, 2 mM EDTA pH 8 was added to the supernatant in order to chelate residual iron ions, and the solution was dialyzed twice against a 100-fold excess of 8 M Urea / 50 mM Tris/HCl buffer pH 7.2 to remove EDTA-iron complexes. Afterwards, the metal-free SOR solution was dialysed against a 8 M Urea / 50 mM Tris/HCl buffer pH 7.2 containing 100 µM of the corresponding metal (1:1000 dilution of 100 mM metal salt dissolved in 100 mM citrate) and 2 mM of 2-mercaptoethanol to keep the metal in the reduced state. Refolding was carried out in a two step-dialysis using the same buffer with decreasing urea concentrations starting from 8 M to 2 M and followed by an urea-free 50 mM Tris/HCl buffer pH 7.2. Residual metal was removed by a final dialysis against 100 volumes of a 50 mM Tris/HCl buffer pH 7.2. All dialysis steps were done overnight at 4°C. Refolded fractions were utilized for the SOR activity assay and EPR spectroscopy. Therefore the samples were concentrated to approximately 9 mg/ml per fraction.

2.5. Analytic procedures

2.5.1. SOR activity assay

The SOR activity assay was performed as previously described (Kletzin 1989, Urich *et al.*, 2004). Specific activities were determined after incubation of 2 - 5 µg purified enzyme at 85°C in 1 ml of 70 mM Tris/HCl buffer pH 7.2 containing 2 % sulfur (w/v) and 0.1 % Tween 20. Alternatively, a citrate-phosphate buffer (0.1 M sodium citrate/ 0.2 M Na_2HPO_4; McIlvaine, 1921) containing 2 % sulfur (w/v) and 0.1 % Tween 20 was used for enzyme activity measurements in a pH range from pH 5 - 8. Samples were taken at constant time points (usually after 0, 2, 4, 6, 8 and 10 minutes) and centrifuged briefly to sediment elemental sulfur that could interfere in the assay. The concentration of the reaction products hydrogen sulfide, sulfite and thiosulfate was determined colorimetrically and quantified with the help of respective calibration curves. The specific activities were calculated from the linear increase of the reaction products. One Unit (U) of enzyme activity was defined as 1 µmol of formed sulfite and thiosulfate (oxygenase) or hydrogen sulfide (reductase) per minute.

Hydrogen sulfide assay

Quantification of hydrogen sulfide is based on the formation of methylene blue from hydrogen sulfide and N,N-dimethyl-p-phenylenediamine catalyzed by ferric iron (King and Morris, 1967). Reagents were added in the following order:

250 µl 2.6 % (w/v) zinc acetate in ddH_2O and 0.1 % acetic acid (conc.)
350 µl sample
50 µl 6 % (w/v) NaOH in ddH_2O
125 µl 0.1 % (w/v) N,N-dimethyl-p-phenylene diammonium dichloride in 5 M HCl
50 µl 12.5 mM $FeCl_3$ in 0.6 M HCl

After 12 h - 24 h incubation at room temperature, samples were measured spectrophotometrically at 670 nm using ddH_2O as reference.

Thiosulfate assay

Quantification of thiosulfate is based on the decolorization of methylene blue by thiosulfate. 250 µl sample was thoroughly mixed with 750 µl of a methylene blue solution (24 mg/l methylene blue in 5 M HCl), incubated at room temperature for 30 min and subsequently measured spectrophotometrically at 670 nm against ddH_2O as reference.

Sulfite assay

Sulfite reduces fuchsine and the addition of formalin generates a purple-colored stable complex (Pachmayr, 1960). Reagents were added in the following order:

50 µl fuchsine solution
(40 mg fuchsine dissolved in 87.5 ml ddH_2O + 12.5 ml conc. H_2SO_4)
195 µl ddH_2O
250 µl sample

After 5 min incubation at room temperature, 5 µl of formalin were added and the sample was measured spectrophotometrically after 90 min at 570 nm using ddH_2O as reference.

2.5.2. Inhibitor studies

Different concentrations of a freshly prepared $ZnCl_2$ solution, ranging from 10 - 300 µM Zn^{2+}, were added to 1 ml of SOR activity assay buffer including Tris/HCl. The reaction mixture was kept on ice water for 30 min after 2 - 5 µg of enzyme had been added. The reaction was started by heating the samples to 85°C and specific SOR activity was measured as described above. An enzymatic reaction without $ZnCl_2$ and a non-enzymatic reaction with inhibitor but without SOR were used as controls. As a second control, 2 mM EDTA was applied to zinc-containing reaction samples, thus showing the reversibility of inhibition. The calculated specific activities were plotted against the applied Zn^{2+} concentration. The slope of the trendline was used for calculation of the appropriate K_i-values of SOR-wt and the mutants $H_{166}A$ and $H_{277}A$.

2.5.3. Protein quantification

The protein concentration was determined by the Coomassie Blue method (Bradford, 1976) with 20 µl protein sample added to 980 µl Bradford solution. The mixture was incubated for 5 min at room temperature and photometrically measured at 595 nm with ddH_2O as reference. The protein concentration was calculated with help of a standard curve, resulting from a calibration series with different BSA concentrations (0 - 1000 µg). The BCA Protein Assay Kit (Novagen /Merck, Darmstadt, Germany) was alternatively used according to the manufacturer's instructions.

2.5.4. Iron quantification

Iron quantification was performed with pure protein preparations using the 2,4,6-tripyridyl-1,3,5-triazine method (TPTZ; Fischer and Price, 1964). TPTZ and ferrous iron form a blue complex that can be quantified at 593 nm. A protein solution of desired concentration was filled to 800 µl with ddH_2O and 100 µl 8 M HCl were added in order to extract iron. After 10 min of incubation at room temperature, the protein was precipitated by addition of 100 µl 80 % trichloroacetic acid (w/v) and sedimented by centrifugation (30 min, 15,000 x g, 4°C). 250 µl of 75 % (w/v) ammonium acetate were added to 800 µl of the supernatant for neutralization. Ferric iron was reduced to Fe^{2+} by adding 100 µl of a 10 % (w/v) hydroxylamine hydrochloride solution. After the addition of 100 µl of a 4 mM TPTZ solution, the adsorption was measured immediately at 593 nm with ddH_2O as reference.

2.5.5. SDS–PAGE

Denaturing sodium dodecyl sulfate gel electrophoresis (SDS-PAGE; Schägger and von Jagow, 1987) was performed for visualization of protein purity. The following buffers were used:

3 x Schägger gel buffer: 3 M Tris/HCl, 0.3 % SDS pH 8.45

10 x Cathode buffer: 0.2 M Tris/HCl pH 8.9

10 x Anode buffer: 0.1 M Tris/HCl, 0.1 M Tricine, 0.1 % SDS pH 8.45

3 x Loading buffer: 125 mM Tris/HCl, 20 % Glycerol, 4 % SDS, 0.2 % Bromthymol Blue, 10 % 2-Mercaptoethanol pH 6.8

Table 2.4 Standard SDS-gel composition

	Stacking gel (4 %)	**Seperation gel (10 %)**
Acrylamide (30:0.8)	3.9 ml	16.6 ml
Schägger Gel buffer	7.5 ml	16.6 ml
Glycerol	-	5.4 ml
ddH_2O	18 ml	11.4 ml
TEMED	40 µl	40 µl
APS (10 %)	200 µl	200 µl

10 % gels were cast and run in a self-built vertical chamber or in a Mini-PROTEAN Tetra Cell (Bio-Rad Laboratories Inc., Hercules, USA). The protein samples were provided with an appropriate volume of loading buffer, denatured for 5 min at 95°C, briefly centrifuged and loaded into the gel wells. Electrophoresis was started with an initial voltage of 50 V until the samples had completely entered the seperation gel, and the voltage was shifted to 100 - 120 V. The run was usually stopped, when the bromthymol blue band reached the end of the gel. The gels were stained with a colloidal Coomassie Blue staining solution (Roth, Karlsruhe, Germany) for at least 4 hours and were destained with ddH_2O.

2.5.6. BN–PAGE

Non-denaturing Blue Native polyacrylamide gel electrophoresis (BN-PAGE; Reisinger and Eichacker, 2006) was used for a following In-gel enzyme activity assay. Following buffers were used:

6 x BN-Gel buffer:	3 M ε-aminocaproic acid, 0.3 M Tris/HCl buffer pH 7.0
10 x Cathode buffer:	500 mM Tricine, 150 mM Bis / Tris/HCl buffer pH 7.0, 0.2 % (w/v) Coomassie G250
10 x Anode buffer:	500 mM Bis / Tris/HCl buffer pH 7.0
Loading buffer:	750 mM ε-aminocaproic acid, 5 % (w/v) Coomassie G 250

Table 2.5 Standard BN-gel composition

	Stacking gel (4 %)	**Seperation gel (6 %)**
Acrylamide (30:0.8)	1.35 ml	2.3 ml
BN Gel buffer	1.67 ml	1.92 ml
ddH_2O	6.98 ml	7.28 ml
TEMED	10 µl	20 µl
APS (10 %)	100 µl	200 µl

The gels were prepared and run in a Mini-PROTEAN Tetra Cell (Bio-Rad Laboratories Inc.). Usually, 70 µg of recombinant *A. ambivalens* SOR-wt were mixed with 100 µl of loading buffer and this mixture was applied to the sample wells of the stacking gel. The gel run was started and the voltage set to 100 V. As soon as the blue Coomassie dye front reached half of the separating gel, the electrophoretic run was stopped and the blue cathode buffer was replaced with a cathode buffer without Coomassie dye. Electrophoresis was continued and eventually stopped after 6 h. Afterwards, the gel was separated in two halves and one half stained with colloidal Coomassie Blue staining solution. The second half was used for the In-gel enzyme activity assay.

2.5.7. In-gel enyzme activity assay

The SOR enzyme activity was assessed by the consumption of polysulfide substrate as previously described (Pelletier *et al.*, 2008). Therefore, 500 mM Na_2S and 500 mM elemental S^0 were soluted in degassed ddH_2O. This mixture resulted in an orange-colored 500 mM polysulfide solution that was stored under N_2 atmosphere. The gel of the BN-PAGE was incubated in a 2 mM polysulfide solution that was freshly prepared by diluting the 500 mM polysulfide solution in 50 mM Tris/HCl buffer pH 8.3. The gel was incubated in the freshly prepared 2 mM polysulfide solution for 3 h at room temperature and then washed twice in ddH_2O to remove residual polysulfide. The wet gel was kept in a small volume of ddH_2O in a plastic box and heated in a waterbath to 80°C for 2 h. The gel was subsequently transferred to a 10 mM 2,3,5-triphenyl tetrazolium chloride (TTC) solution (10 mM TTC in 50 mM Tris/HCl pH 7.4). TTC is a redox indicator that is colorless after oxidation and forms purple-red complexes (1,3,5-triphenylformazan) under reductive conditions. A 2 mM polysulfide solution was again successively added to the TTC solution, until the gel was stained gel purple-red. Oxygenase activity was indicated by distinct colorless SOR bands, thus showing polysulfide consumption by the enzyme.

2.6. Spectroscopic Methods

2.6.1. UV/Visible spectroscopy

UV/Vis-Spectra were recorded at room temperature using a spectrophotometer (Beckman DU 640).

2.6.2. CD spectroscopy

Circular Dichroism (CD) spectroscopy was used to analyze secondary structure of recombinant *A. ambivalens* SOR and recombinant *H. neapolitanus* SOR. Spectra were measured using a JASCO J-815 spectropolarimeter with Peltier temperature control. Typically, 10 accumulations were recorded in the far-UV region (180 - 260 nm) at 20°C with a data pitch of 0.2 nm using a 0.1 cm path length-polarized quartz cuvette. A bandwidth of 2 nm was used with a detector response of 1 sec and a scanning speed of 200 nm/min.

Spectra were obtained with 0.1 mg/ml SOR protein in 20 mM Tris/HCl buffer pH 7.5 and afterwards corrected by subtracting the spectrum of the buffer solution. CD units are expressed as mean residue extinction coefficient [$\Delta\varepsilon_{mrw}$] in m^{-1}, cm^{-1}, which was calculated from the relationship $\Delta\varepsilon_{mrw}$ = S x mrw / (M x c x d), where S represents the measured CD signal in millidegrees, M the molar mass of the protein, c the protein concentration in mg/ml, d the path length of the cuvette in cm, and mrw the mean residue weight of the corresponding protein.

2.6.3. EPR spectroscopy

EPR (Electron Paramagnetic Resonance) spectroscopy was carried out to detect unpaired (paramagnetic) electrons before and after the SOR reaction with several metal-substituted SOR derivatives. The protein samples were assayed in 20 mM Tris/HCl buffer pH 7.5 and were concentrated to a final concentration ranging from 187 - 250 µM. EPR spectra of refolded metal-substituted SOR fractions were aquired using a Bruker EMX spectrometer equipped with an ESR 900 continuous-flow helium cryostat at 8.4 K, 9.38 GHz microwave frequency, 2.0 mW microwave power and 1 mT modulation amplitude. Small amounts of elemental sulfur were added to the protein and the mixture was incubated for 15 min at 80°C in order to start the SOR reaction. The samples were subsequently measured using the same parameters.

2.6.4. DLS analysis

DLS (Dynamic Light Scattering) is a method to determine particle distribution or particle size in solution. When a monochromatic light beam is applied to a solution with spherical particles in motion and hits these particles, light is scattered. Fluctuations of the scattered light are detected by a photon detector. Those fluctuations are a measure of the diffusion constant (Brownian motion) of the molecules and are related to the hydrodynamic radius of a molecule. Analysis of the intensity fluctuations enables determination of the average particle size and polydispersity of the particle in solution. DLS analyses were performed on a Zetasizer Nano apparatus (Malvern Instruments, Worcestershire, UK) at 25°C. Samples were assayed at 0.3 mg/ml in 20 mM Tris/HCl buffer pH 7.5. The protein sample was inserted into a 45 µl glass cuvette and measured at least three times with ten acquisitions

each. The hydrodynamic diameters of recombinant *A. ambivalens* and *H. neapolitanus* SORs were calculated using the corresponding Zetasizer software (Malvern Instruments).

2.6.5. TXRF analysis

TXRF (Total Reflection X-Ray Fluorescence) is a method used for multi elemental analysis. It is based on the principle that individual atoms, when excited by an X-ray beam, emit X-ray photons of a characteristic energy or wavelength. In case of TXRF, the sample is prepared as a very thin solid layer on a flat and polished sample slide usually made of quartz glass. When an X-ray beam impinges upon the sample slide in very small angles (< 0.1 °), it will be totally reflected. Due to the total reflection of the incident photons only a very small part of the primary beam penetrates into the sample carrier which leads to a drastically minimized X-ray background emission. All elements within the prepared sample are excited by the incoming X-ray beam and emit specific X-ray photons that are detected by an energy-dispersive detector. By counting the number of photons of each energy-emission from the sample, the elements present may be identified and quantitated. Inclusion bodies of SOR-wt were unfolded and refolded as described in chapter 2.4.6. Each sample was concentrated to 20 - 25 µM after a final dialysis against 20 mM Tris/acetate buffer pH 7.5. All TXRF measurements and sample preparation were carried out in the laboratory of Prof. B.O. Kolbesen (Institut für Anorganische/Analytische Chemie, Johann-Wolfgang-Goethe-Universität, Frankfurt, Germany) by Claudia Rittmeyer (now in the working group of Prof. A. Terfort, Institut für Anorganische/Analytische Chemie, Johann-Wolfgang-Goethe-Universität, Frankfurt, Germany). 45 µl sample were mixed with 5 µl of a Rb-standard solution (10 mg/l) that was used as an internal standard. 5 µl of that mixture was applied onto a quartz slide and subsequently measured five times using an EXTRAIIA (Atomika Instruments) apparatus with a 17.5 keV Mo-anode X-ray tube.

2.7. Sequence Analysis

2.7.1. Phylogenetic analysis

SOR homologues from other organisms were detected by different BLASTp analyses of the *Acidianus ambivalens* SOR amino acid sequence (NCBI accession number CAA39952.1) against the public database at NCBI (http://www.ncbi.nlm.nih.gov).

The *Sulfobacillus acidophilus* and the *Sulfobacillus thermosulfidooxidans* SOR sequences were identified via tBLASTn analyses against the corresponding genomes, obtained from the DOE Joint Genome Institute (http://www.jgi.doe.gov). All SOR sequences obtained from sequenced genomes or isolated proteins were aligned using ClustalX 2.1 (Larkin *et al.*, 2007). The alignment was manually refined by Arnulf Kletzin using eBioX (http://www.ebioinformatics.org/ebiox/). The alignment figure in chapter 1 (Figure 1.9) was generated using Jalview (Waterhouse *et al.*, 2009) and the dendrogram was constructed with Archaeopteryx (Han and Zmasek, 2009).

2.7.2. Homology modeling

Modeling of SOR mutants was performed with *Acidianus ambivalens* SOR-wt as template (**P**rotein **D**ata **B**ank [PDB; http://www.pdb.org; Berman *et al.*, 2000] id: 2cb2; Urich *et al.*, 2006) using the SWISS-Model server (http://swissmodel.expasy.org/; Arnold *et al.*, 2006) and the PHYRE server (**P**rotein**H**omology/analog**Y** Recognition **E**ngine, http://www.sbg.bio.ic.ac.uk/~phyre/; Kelley and Sternberg, 2009).

2.8. Crystallization

Crystallization attempts were performed in order to crystallize the recombinant *A. ambivalens* SOR-wt (*Aa*SOR), selected SOR mutants, a cobalt-substituted *Aa*SOR (Co-SOR) and the recombinant *H. neapolitanus* SOR-wt (*Hn*SOR). All protein samples were dialysed against 50 mM Tris/HCl buffer pH 7.5 and concentrated using Amicon Ultra-15 centrifugal filter units (Millipore, Schwalbach, Germany) to the concentration shown below prior to crystallization:

Sample name	Abbreviation	Final protein concentration
recombinant *A. ambivalens* SOR-wt	*Aa*SOR	12.9 mg/ml
recombinant *A. ambivalens* $E_{87}D$ SOR mutant	$E_{87}D$	13.8 mg/ml
recombinant *A. ambivalens* $H_{277}A$ SOR mutant	$H_{277}A$	12.8 mg/ml
recombinant *A. ambivalens* Co-derivative	Co-SOR	14.9 mg/ml
recombinant *H. neapolitanus* SOR-wt	*Hn*SOR	13.1 mg/ml

2.8.1. Crystallization of SOR-wt, SOR mutants and SOR derivatives

The initial crystallization screening was carried out at 22°C with sitting-drop vapour diffusion in 96-well plates (Greiner, Frickenhausen, Germany) using a 'Minibee' Microsys 4000 XL Cartesian Dispensing Systems robot (Genomic Solutions, Ann Arbor, USA) and the MbClass Suite (96 conditions; Qiagen, Hilden, Germany). 0.1 µl of crystallization solution was added to 0.1 µl of protein solution, equilibrated against 10 µl of crystallization solution in the reservoir and incubated at 22°C. The different protein samples crystallized in several conditions and the most promising conditions were refined individually using 24-well plates (Greiner) with sitting-drop vapour diffusion. The volume ratio between protein solution and crystallization solution usually ranged between 0.5 µl**:**1.5 µl and 1.5 µl**:**0.5 µl. The drops that contained protein and crystallization solution were equilibrated against 500 µl of crystallization solution in the reservoir. Final crystallization conditions are shown in Table 2.6:

Table 2.6: Crystallization conditions and cryoprotectant solution of the different SOR proteins

Protein name	Crystallization condition	Cryoprotectant solution
***Aa*SOR**	0.1 M Tris/HCl pH 8.5/ 0.5 M $NH_4(SO_4)_2$	0.1 M Tris/HCl pH 8.5/ 0.7 M $NH_4(SO_4)_2$/ 25 % Glycerol
E_{87}D	0.2 M ADA pH 6/ 5 % Glycerol	0.5 M ADA pH 6/ 25 % Glycerol
H_{277}A	0.1 M Tris/HCl pH 8.5/ 0.7 M $NH_4(SO_4)_2$	0.1 M Tris/HCl pH 8.5/ 0.9 M $NH_4(SO_4)_2$/ 25 % Glycerol
Co-SOR	0.1 M NaAc pH 4.5/ 0.1 M NaCl/ 8-12 % MPD	0.1 M NaAc pH 4.5/ 0.1 M NaCl/ 20 % MPD/ 25 % Glycerol
***Hn*SOR**	0.1 M ADA pH 6.5-7/ 0.8-1 M $NH_4(SO_4)_2$	0.1 M ADA pH 6.2-7/ 0.8-1 M $NH_4(SO_4)_2$ / 25 % Glycerol

2.8.2. X-Ray diffraction data collection

X-Ray diffraction data sets were collected with synchrotron radiation at ESRF (European Synchrotron Radiation Facility, Grenoble, France) and at SLS (Swiss Light Source, Paul Scherrer-Institut, Villingen, Switzerland). The diffraction data sets of the *Hn*SOR and of the *Aa*SOR were measured in-house by Carlos Frazão (ITQB, Oeiras, Portugal) using a Microstar rotating-anode X-rays generator and a Proteum Pt135 diffractometer (Bruker AXS, Karlsruhe Germany) at the Cu K-edge (1.5418 Å).

The diffraction data sets for the *A. ambivalens* $E_{87}D$ SOR mutant ($E_{87}D$) and the cobalt-containing *Aa*SOR (Co-SOR) were all collected at SLS beam line X06DA with a wavelength of 0.9779 Å. To collect anomalous data, the K-absorption edge of cobalt was experimentally determined by Pedro Matias (ITQB, Oeiras, Portugal) using the CHOOCH software (Evans and Pettifer, 2001). Anomalous scattering describes the retarded scattering of a photon, which occurs for energies of the incident X-ray that are above the absorption edge of the respective element. It means in effect, when X-rays of a certain wavelength are above the metal's absorption edge, some photons are scattered with an altered phase, which can be usually used to solve the phase problem. Wavelengths of 1.5841 Å and 1.6257 Å, respectively, were chosen for data collection, since 1.5841 Å is close to the K-absorption edge of iron and 1.6257 Å close to the K-absorption edge of cobalt. The diffraction sets for the *Aa*SOR co-crystallized with thiosulfate and polysulfide were all collected at ESRF beamline id23-1 with a wavelength of 1.9300 Å. The dataset for the *A. ambivalens* SOR $H_{277}A$ mutant ($H_{277}A$) was collected at ESRF beam line id14-2 with a wavelength of 1.9300 Å.

2.8.3. Data processing and refinement of SOR models

Diffractions images were processed using MOSFLM and scaled together with SCALA, both programs from the CCP4 program suite version 6.1 (**C**ollaborative **C**omputation **P**rogram Nr.**4**; Winn *et al.*, 2011). TRUNCATE, also from CCP4, was used to convert SCALA intensities output into structure factor amplitudes. A rigid body refinement was carried out using the PHENIX (**P**ython-based **H**ierarchical **EN**vironment for **I**ntegrated **X**tallography; Adams *et al.*, 2010) software suite version 1.5 to adjust cell dimensions in case of crystals isomorphous to the original *Acidianus ambivalens* SOR-wt structure (PDB id: 2cb2; Urich *et al.*, 2006). When datasets differed from the tetragonal space group I4 crystal symmetry, the phase problem was solved via molecular replacement, using PHASER from the PHENIX software suite. All models were refined using the phenix.refine module of the PHENIX package and manually analyzed and optimized by COOT (**C**rystallographic **O**bject-**O**riented **T**oolkit; Emsley *et al.*, 2010). Data processing of the *Hn*SOR dataset was carried out by Carlos Frazão. This data set was processed and scaled with the program SADABS as part of the Bruker AXS PROTEUM software suite. The merging of the data and the calculation of the quality indicators were produced with

XPREP (Bruker AXS). The *Hn*SOR model was refined using the phenix.refine module of the PHENIX package.

2.8.4. Model analysis

The secondary structure composition of the *Hn*SOR was analyzed from the corresponding 3D structure by Carlos Frazão using PROMOTIF (Hutchinson and Thornton, 1996). The RMSD (**R**oot **m**ean **s**quare **d**eviation) between two structures was calculated using the program PDBeFOLD (http://www.ebi.ac.uk/msd-srv/ssm; Krissinel and Henrick, 2004) or by Carlos Frazão using MODELLER6v2 (Eswar *et al.,* 2006). In case of MODELLER, the α-carbon main chain atoms were automatically fitted with a cutoff distance of 3.5 Å, while default values were used for PDBeFOLD. All figures were prepared using Pymol (DeLano, 2002; Schrödinger LCC, 2010).

Abbreviations

°	degree
Å	Angström
°C	degrees Celsius
*Aa*SOR	*Acidianus ambivalens* SOR wild type
ad	filled up
adp	atomic displacement parameter
ADA	N-(2-Acetamido)iminodiacetic acid
AHT	Anhydrotetracycline
Amp	Ampicillin
APS	Ammonium persulfate
*Aq*SOR	*Aquifex aeolicus* SOR wild type
*At*SOR	*Acidianus tengchongensis* SOR wild type
BCA	Bicinchoninic acid
BLAST	Basic Local Alignment Search Tool
BN	Blue native
bp	Base pairs
C-terminus	Carboxy-terminus
CD	Circular Dichroism
Da	Dalton
dH_2O	deionized water
ddH_2O	double deionized water
DLS	Dynamic Light Scattering
DNA	Deoxyribonucleic acid
dNTP	Deoxynucleotide triphosphate
DSMZ	Deutsche Sammlung für Mikroorganismen und Zellkulturen
e.g.	*exempli gratiā* (for example)
EDTA	Ethylene-diamine-tetra acetic acid
EPR	Electron Paramagnetic Resonance
ESRF	European Synchrotron Radiation Facility
et al.	*et alii* (and others)
F_c	calculated structure factor
F_o	observed structure factor
FPLC	Fast Performance Liquid Chromatography
g	gram
h	hour
H-bond	Hydrogen bond
HABA	Hydroxy-azophenyl-benzoic acid
HCl	Hydrochloric acid
*Hn*SOR	*Halothiobacillus neapolitanus* SOR wild type
HPLC	High-performance Liquid Chromatography
I	intensity
i.e.	*id est* (that is)
K	Kelvin
kb	kilo bases
kDa	kilo dalton
l	liter
m	meter
M	molar
min	minute

MPD	2-Methyl-2,4-pentanediol
N-terminus	Amino-terminus
NCS	non-crystallographic symmetry
nt	Nucleotide
OD_{600}	optical density at 600 nm
PAGE	Polyacrylamide gel electrophoresis
PCR	Polymerase chain reaction
PEG	Polyethyleneglycol
RMSD	Root mean square deviation
RNA	Ribonucleic acid
rpm	rounds per minute
S^0	elemental sulfur
SDS	Sodium dodecyl sulfate
sec	second
SLS	Swiss Light Source
SOR	Sulfur oxygenase reductase
TCA	Trichloro acetic acid
TEMED	Tetramethylethylendiamine
TPTZ	2,4,6-Tripyridyl-s-1,3,5-triazine
Tris	Tris(hydroxymethyl)-aminomethane
Tween20	PEG(20) Sorbitan monolaurate
TXRF	Total Reflection X-Ray Fluorescence
U	Unit
UV	Ultra-violet
UV/Vis	Ultra-violet/visible
V	Volt
v/v	volume per volume
v/w	volume per weight
w/v	weight per volume
wt	wild type

Metals

Co	Cobalt
Cu	Copper
Fe	Iron
Ga	Gallium
Mg	Magnesium
Mn	Manganese
Ni	Nickel
Ru	Ruthenium
V	Vanadium
Zn	Zinc

Amino acid code

A	Ala	Alanine
C	Cys	Cysteine
Css	Css	Cysteine persulfide
D	Asp	Aspartic acid
E	Glu	Glutamic acid
F	Phe	Phenylalanine
G	Gly	Glycine
H	His	Histidine
I	Ile	Isoleucine
K	Lys	Lysine
L	Leu	Leucine
M	Met	Methionine
N	Asn	Asparagine
P	Pro	Proline
Q	Gln	Glutamine
R	Arg	Arginine
S	Ser	Serine
T	Thr	Threonine
V	Val	Valine
W	Trp	Tryptophane
Y	Tyr	Tyrosine

3. Sulfur pathway and zinc inhibition of the *A. ambivalens* SOR

3.1. Introduction

The SOR catalyzes the disproportionation of elemental sulfur to sulfide, sulfite and thiosulfate. Despite detailed knowledge of structural and biochemical properties of the spherical enzyme, the detailed pathways of the sulfur substrate and of the corresponding reaction products have not been resolved yet. The present chapter focuses on investigations on the sulfur pathway route of the *Acidianus ambivalens* SOR wild type (*Aa*SOR). Two different types of channels are located at the outer shell of the icosatetrameric enzyme. Six chimney-like protrusions at the non-crystallographic fourfold symmetry axes open to a hydrophobic channel that is hypothesized to be the substrate entrance point to the inner cavity (Urich *et al.,* 2006). The hydrophobic inner surface of these channels includes two phenylalanine rings restricting the diameter size of the entry pore, which allows only linear sulfur species to enter the inner cavity of the protein. The second type of channels is located at the non-crystallographic threefold symmetry axes. These structures, also referred to as trimer channels, were proposed to be the exit channels of the SOR reaction products hydrogen sulfide, sulfite and thiosulfate (Li *et al.,* 2008). The pore opening of the trimer channels is defined by a serine (S_{226} in *A. ambivalens* SOR numbering) and an arginine (R_{99}). The active site of the protein, comprising a mononuclear iron center and three conserved cysteine residues, is located in a separate pocket buried within a cavity of each monomer. It can be accessed through a narrow and hydrophobic pore formed by two adjacent methionines (M_{296} and M_{297}) and one phenylalanine (F_{23}). The current hypothesis of the substrate pathway of the SOR assumes that a linear sulfur substrate (*e.g.* linearized elemental sulfur or polysulfide) must pass the outer shell of the protein to enter the holoenzyme cavity where the active site pocket pores are located. Deletions or substitutions, achieved by site-directed mutagenesis, were introduced at the tetramer and trimer channels and at the active site pore in order to investigate the function of these pores. Furthermore, the question was addressed how enzyme activity is interfered with zinc, which is a strong SOR inhibitor (Kletzin, 1989; Chen *et al.,* 2005). Therefore, mutagenesis studies and crystallographic studies of a Zn-derivative were analyzed to indicate the binding position and the inhibition mechanism of the Zn^{2+} ion.

3.2. Results

3.2.1. Polysulfide can serve as SOR substrate

A linear sulfur species like polysulfide had already been proposed as the initial substrate for the SOR shown by *in silico* analyses or by in-gel activity experiments (Urich *et al.*, 2006; Pelletier *et al.*, 2008). In this work, an in-gel activity assay with the *Aa*SOR was performed to investigate whether polysulfide is a potential substrate. Therefore, 2 µg of purified and recombinant *Aa*SOR were applied to each well of a 6 % non-denaturing polyacrylamide gel. After several hours of electrophoresis, the protein entered the gel matrix only minimally. The electrophoretic run was stopped and the gel was cut into two halves. One half was stained using a colloidal Coomassie Blue staining solution. One single protein band was observed, indicating that only one oligomeric form of the *Aa*SOR is present (Figure 3.1). To demonstrate polysulfide consumption, the second half of the gel was soaked with a freshly prepared polysulfide solution (10 mM Na_2S + 10 mM sulfur powder dissolved in 50 mM Tris/HCl buffer pH 8.3) and subsequently incubated at 80°C. The gel was washed twice in 50 mM Tris/HCl buffer pH 8.3. A 10 mM triphenyltetrazolium chloride solution (TTC) was successively added to the buffer. While TTC is colorless in the oxidized state, it forms a red-colored complex (1,3,5-triphenylformazan) in the reduced state. The polysulfide solution was successively added until the gel color turned purple-red due to the reducing action of polysulfide. Clear white bands appeared at the height of the *Aa*SOR oligomer (Figure 3.1), demonstrating the polysulfide-oxidizing activity of the enzyme.

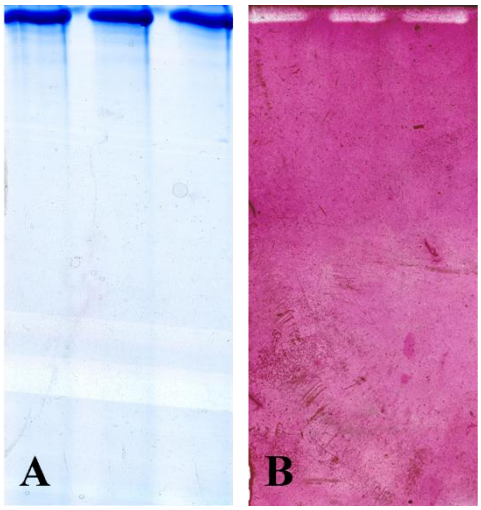

Figure 3.1 Detection of SOR and SOR activity in a Blue Native-Gel with 2 µg *Aa*SOR per lane. (**A**) Coomassie-stained gel half with *Aa*SOR. (**B**) TTC-treated gel half with *Aa*SOR after incubation with polysulfide at 80°C.

3.2.2. Properties of the SOR mutants

The mutated *sor* genes were generated via site-directed mutagenesis using the respective oligonucleotides (Table 2.1) and the *Aa*SOR-harboring plasmid pASK-SOR.05 as template (see chapter 2 for details). The cultures were inoculated with a single *E. coli* colony carrying the desired mutation and induced with anhydrotetracycline (AHT). After 16 h, the cells were harvested and mechanically disrupted. Approximately 10 - 30 % of the SOR protein was present in soluble form while ≥ 70 % precipitated in inclusion bodies as observed previously (Urich *et al.*, 2004). The recombinant *Aa*SOR and the mutant SOR proteins were purified from the soluble *E. coli* fractions in a one-step procedure using the attached Strep-tag and Strep-Tactin columns. The yields of purified protein ranged, depending on the mutant, from 0.5 - 1.2 mg/l 2x LB medium. Each protein preparation showed one larger band with a molecular mass of 70 kDa and several smaller protein bands representing degradation products of the SOR (Figure 3.2; Urich *et al.*, 2004). Wild type and mutant proteins were analyzed for specific enzyme activity and iron content in order to verify that altered enzyme activity is not a result of reduced iron incorporation into the active site. The iron content of the purified proteins was in the range of 1 - 3 Fe/subunit The average values of specific wild type SOR activities were 3.03 ± 0.31 U/mg (oxygenase) and 1.69 ± 0.44 U/mg (reductase; Figure 3.4).

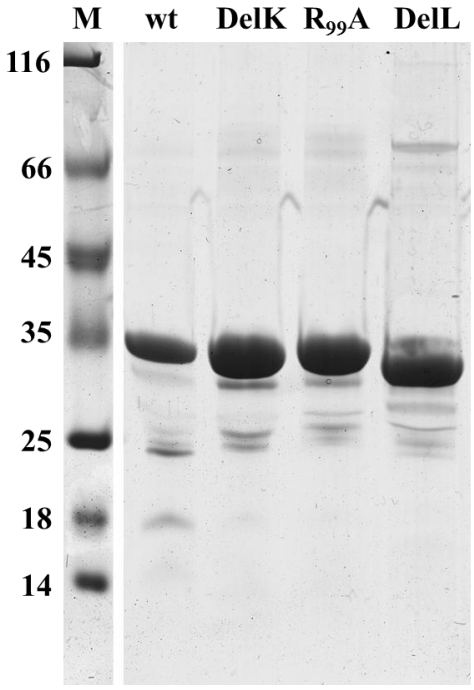

Figure 3.2 Coomassie-stained 10 % SDS gel of *Aa*SOR and three SOR sulfur pathway mutants DelK, $R_{99}A$ and DelL with 5 µg protein per lane. (**M**) Marker proteins with corresponding band sizes depicted here in kDa.

Table 3.1 Protein yield and iron content of SOR mutants

	Protein yield (mg per l 2x LB medium)	Absolute Fe content (nmol Fe)	Relative Fe content (nmol protein/ nmol Fe)
Tetramer channel mutants			
DelL	1.2	3.0	1.1
DelK	0.85	3.1	1.1
$F_{133}A$	n.r.*	n.d.†	n.d.†
$F_{141}A$	n.r.*	4.3	1.6
$F_{133}A/F_{141}A$	n.r.*	4.8	1.7
$M_{130}A$	0.55	3.2	1.2
Trimer channel mutants			
$R_{99}A$	0.87	4.0	1.4
$R_{99}I$	0.56	2.9	1
$S_{226}A$	0.66	3.4	1.2
$S_{226}T$	0.95	3.4	1.2
$S_{226}I$	0.89	3.1	1.1
$S_{226}L$	0.72	2.9	1
Active site pore mutants			
$M_{296}V$	0.71	3.9	1.4
$M_{297}A$	0.58	4.3	1.5
$MM_{296/297}VT$	0.71	4.0	1.4
$MM_{296/297}TT$	0.83	4.4	1.6
Zinc coordination site mutants			
$H_{166}A$	0.78	6.9	2.4
$H_{277}A$	0.54	3.3	1.2

*Not reported
†Not determined

3.2.3. Mutations at the tetramer channel

Two SOR mutants were constructed, featuring truncated versions of the chimney-like protrusions located at the fourfold symmetry axes (Seyfarth, 2006). The DelL mutant (deletion, L = long) lacks 23 amino acids that form the chimney-like protrusions including both phenylalanine rings. As a linker, three glycines were introduced. In comparison to the SOR-wt, the pore of the DelL mutant opened to a diameter of 9 - 10 Å, as calculated from the corresponding homology model obtained from the SwissModel server (Arnold *et al.*, 2006; Figure 3.3). In the DelK derivative (deletion, K = kurz; German for short) 10 residues including the outer phenylalanine ring were replaced by two glycines. The atomic distances of the inner phenylalanine ring did not change significantly in a homology model of the DelK mutant (from 5.0 Å in the wild type protein to 5.4 Å in the mutant; Figure 3.3). The apparent molecular masses of the DelL and DelK mutants were slightly smaller in SDS gels, when compared to the wild type enzyme (Figure 3.2).

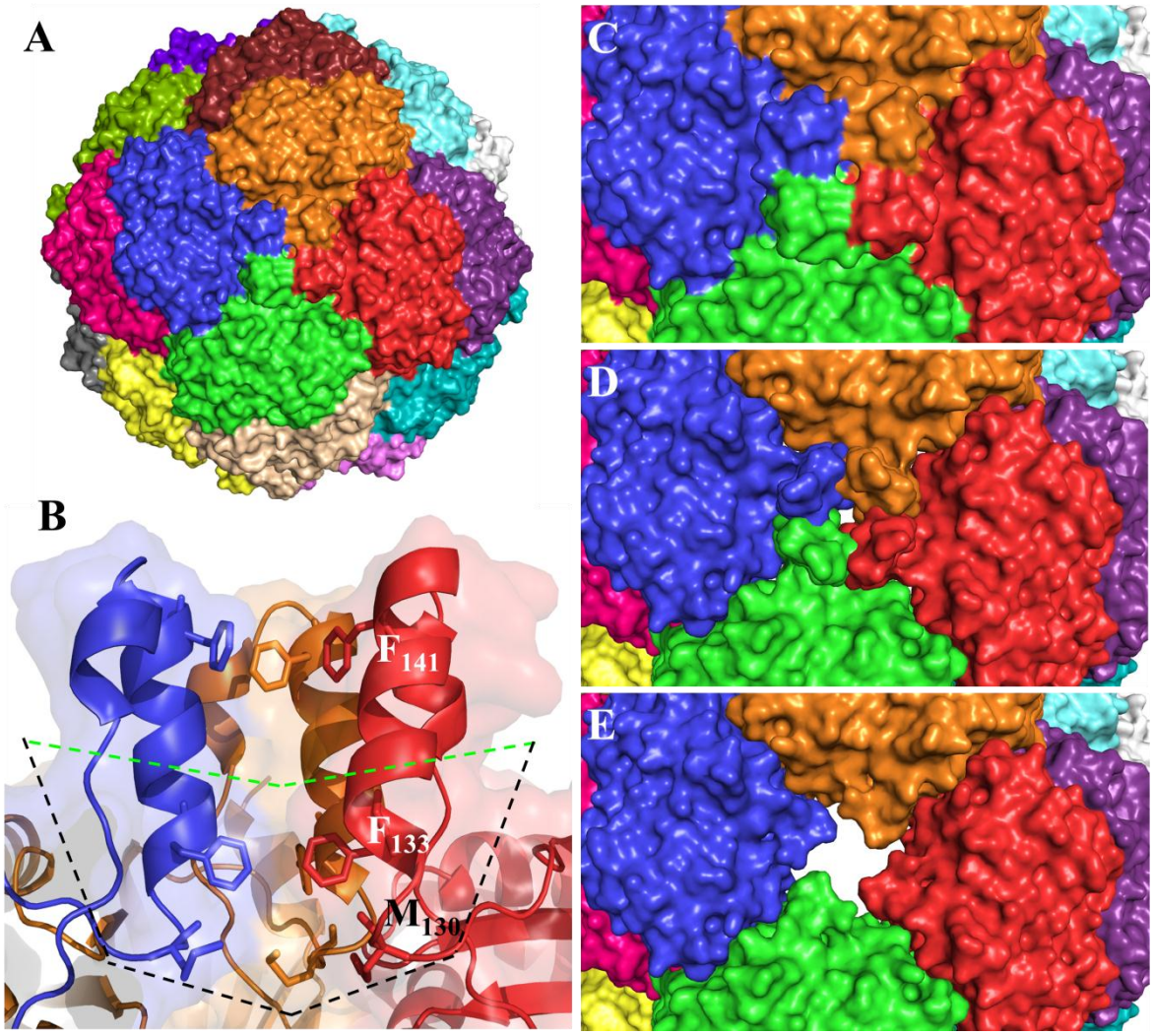

Figure 3.3 Structural representation of the SOR holoenzyme and DelK and DelL mutants viewed from the non-crystallographic fourfold symmetry axis. Mutant proteins were modeled at the SwissModel server (Arnold *et al.*, 2006) based on the *Aa*SOR structure. (**A**) *Aa*SOR holoenzyme with subunit representation. (**B**) Side view of the chimney channel at the fourfold symmetry axis with both phenylalanine rings (F_{141} and F_{133}; three subunits displayed) and the methionine ring at the base of the channel. The dashed green line represents the approximate position of the DelK mutation and the black dashed line the approximate position of the DelL mutant. (**C-E**) Subunit representations of the *Aa*SOR wild type (**C**), the DelK (**D**) and the DelL (**E**) mutants at the non-crystallographic fourfold symmetry axis.

A highly increased enzyme activity was observed for both mutant proteins: DelL showed 420 % of the oxygenase and up to 771 % of the reductase activity, while DelK showed an increase up to 326 % (oxygenase) and 476 % (reductase), respectively. In addition, the pore-restricting phenylalanine residues were mutated into alanine independently ($F_{133}A$, $F_{141}A$; Seyfarth, 2006) and also as a double mutant ($F_{133}A/F_{141}A$; Seyfarth, 2006). All three mutants showed increased activities with the double mutant displaying the highest activities (194 % of the oxygenase and 347 % of the reductase). Mutation of $M_{130}A$ located at the base of the channel did not alter the catalytic properties of the enzyme (Figure 3.4).

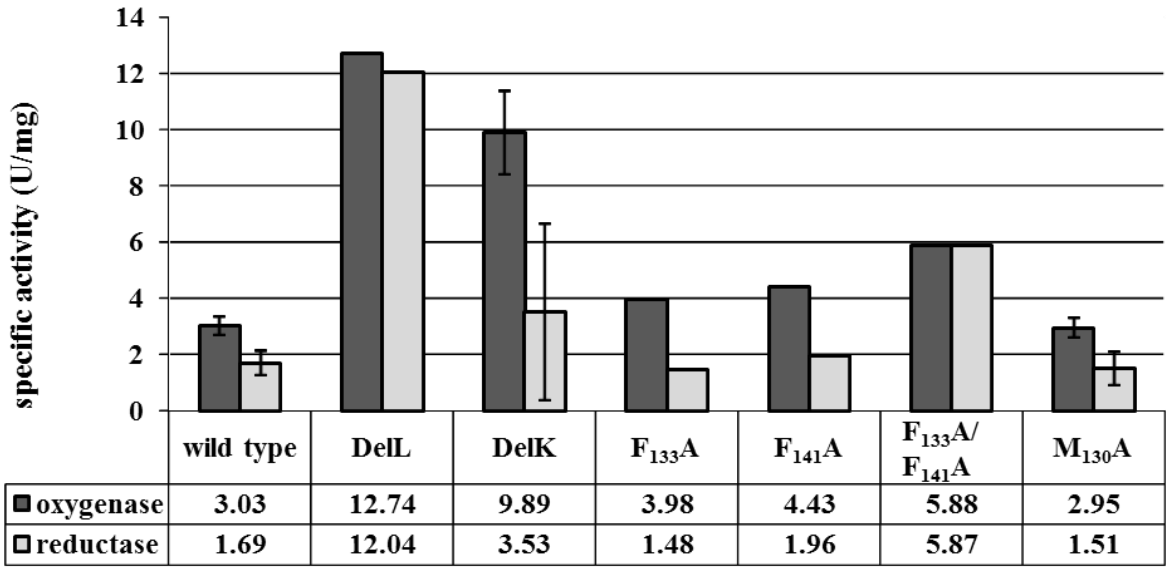

	wild type	DelL	DelK	$F_{133}A$	$F_{141}A$	$F_{133}A$/ $F_{141}A$	$M_{130}A$
oxygenase	3.03	12.74	9.89	3.98	4.43	5.88	2.95
reductase	1.69	12.04	3.53	1.48	1.96	5.87	1.51

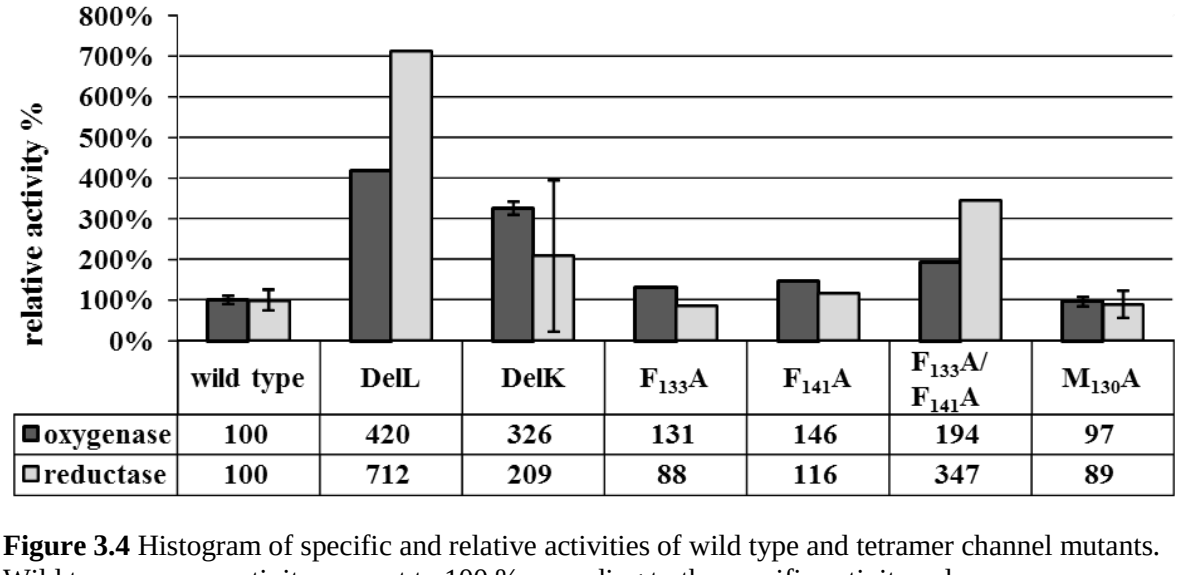

	wild type	DelL	DelK	$F_{133}A$	$F_{141}A$	$F_{133}A$/ $F_{141}A$	$M_{130}A$
oxygenase	100	420	326	131	146	194	97
reductase	100	712	209	88	116	347	89

Figure 3.4 Histogram of specific and relative activities of wild type and tetramer channel mutants. Wild type enzyme activity was set to 100 % according to the specific activity values.

3.2.4. Mutations at the trimer channel

R_{99} and S_{226}, both located at the postulated channel outlet of the product exit at the threefold symmetry axis (Figure 3.5), were substituted for alanines independently. Together with an $S_{226}T$ variant, all three mutants showed elevated enzyme activities. $R_{99}A$ and $S_{226}T$ were comparable having both about 182 % oxygenase and 156 % reductase activities. Isoleucine and leucine variants of the pore-forming channel outlet residues were comparable to the wild type in oxygenase activity but showed a significantly increased reductase activity of up to 496 % in case of $S_{226}L$ (Figure 3.6).

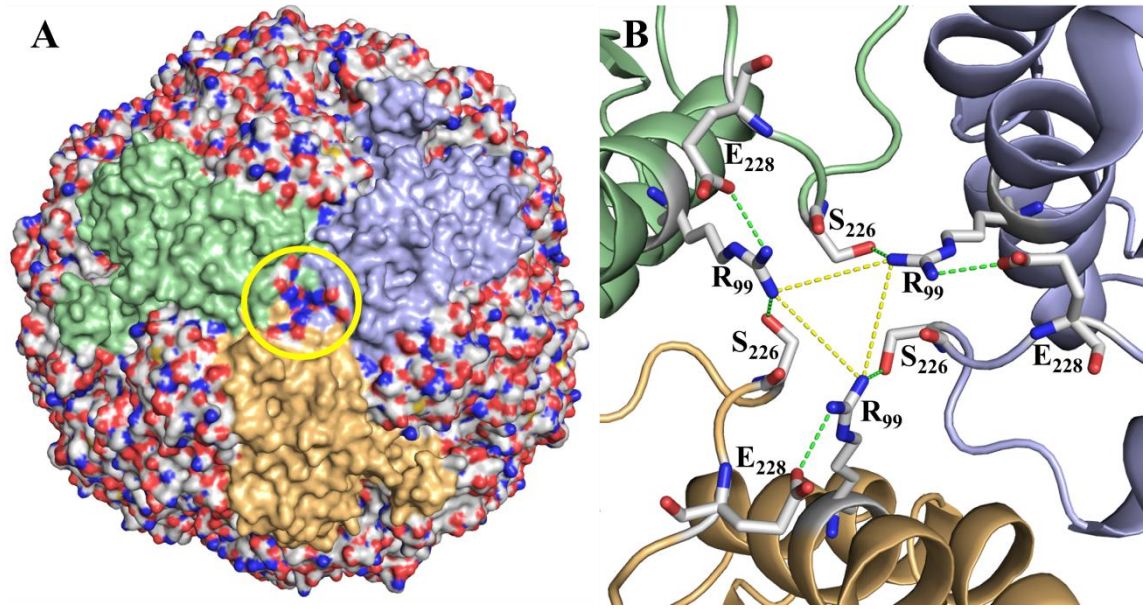

Figure 3.5 (A) Surface representation of the *Aa*SOR holoenzyme with the trimer channel-forming subunits colored in green, blue and ochre and the trimer channel outlet encircled in yellow. (**B**) Ribbon and stick representation of the trimer channel pore formed by R_{99} and S_{226}. Yellow dashed lines indicate the distances between each arginine residue. Green dashed lines represent salt bridges between R_{99} and E_{228} or S_{226}.

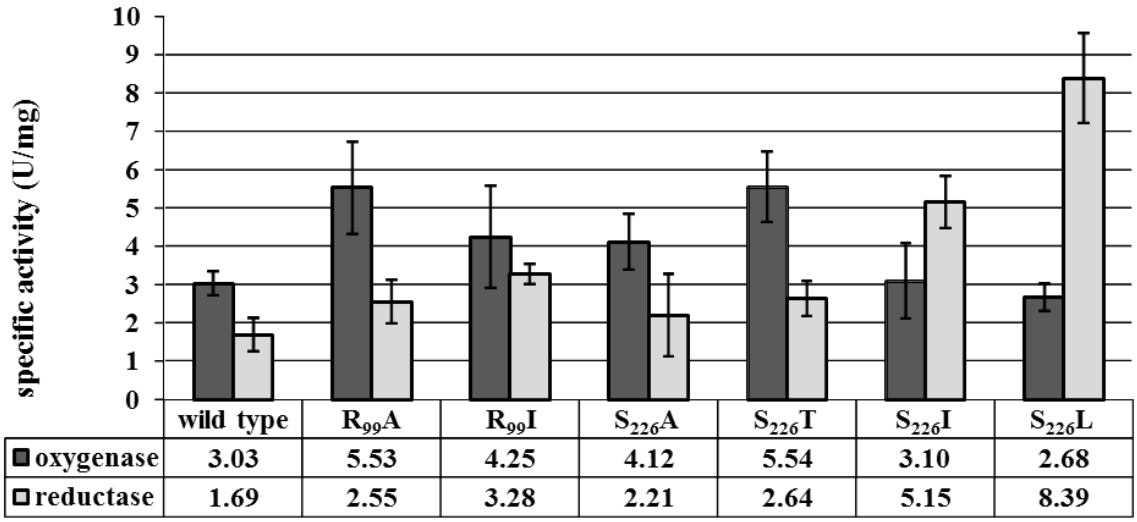

	wild type	R_{99}A	R_{99}I	S_{226}A	S_{226}T	S_{226}I	S_{226}L
oxygenase	3.03	5.53	4.25	4.12	5.54	3.10	2.68
reductase	1.69	2.55	3.28	2.21	2.64	5.15	8.39

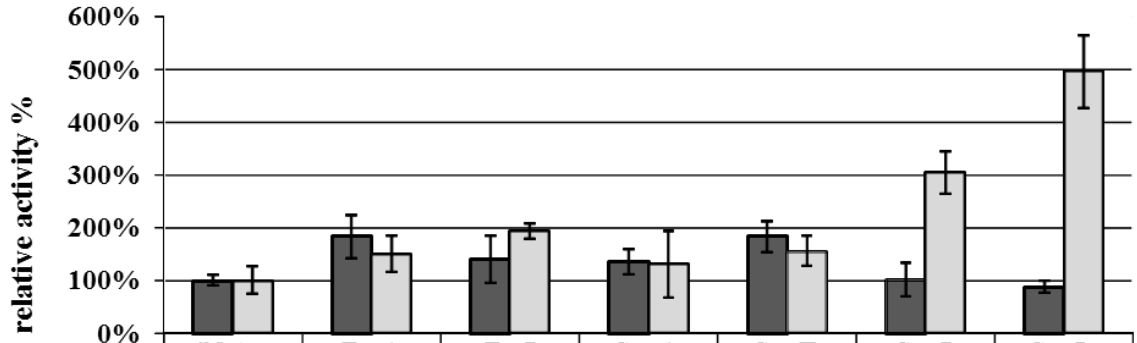

	wild type	R_{99}A	R_{99}I	S_{226}A	S_{226}T	S_{226}I	S_{226}L
oxygenase	100	183	140	136	183	102	88
reductase	100	151	194	131	156	305	496

Figure 3.6 Histogram of specific and relative activities of wild type and trimer channel mutants. Wild type enzyme activity was set to 100 % according to the specific activity values.

3.2.5. Mutations at the active site pore

The active site pore, which provides access to the reaction center from the inner cavity, is formed by two adjacent methionines (M_{296}/M_{297}) and one phenylalanine F_{23} (Figure 3.7). Both methionines were mutated via site-directed mutagenesis using degenerated primers that allow for 16 possible variations. Twenty-five different plasmids were screened and four different mutants were obtained including two double mutants ($MM_{296}/_{297}VT$ and $MM_{296}/_{297}TT$) and two single mutants ($M_{297}A$ and $M_{296}V$). The mutagenesis supposedly led to an opening of the active site pore as compared to the wild type with the exception of the $M_{296}V$ mutant (Figure 3.7). Both double mutants $MM_{296}/_{297}VT$, $MM_{296}/_{297}TT$ and the single mutant $M_{297}A$ showed a decrease of approximately 50 % of wild type activity. The $M_{296}V$ mutant showed an increase in reductase activity (162 %) but not in oxygenase activity (Figure 3.8). The latter residue is also present in several of the naturally occurring SORs from other species (Figure 1.10).

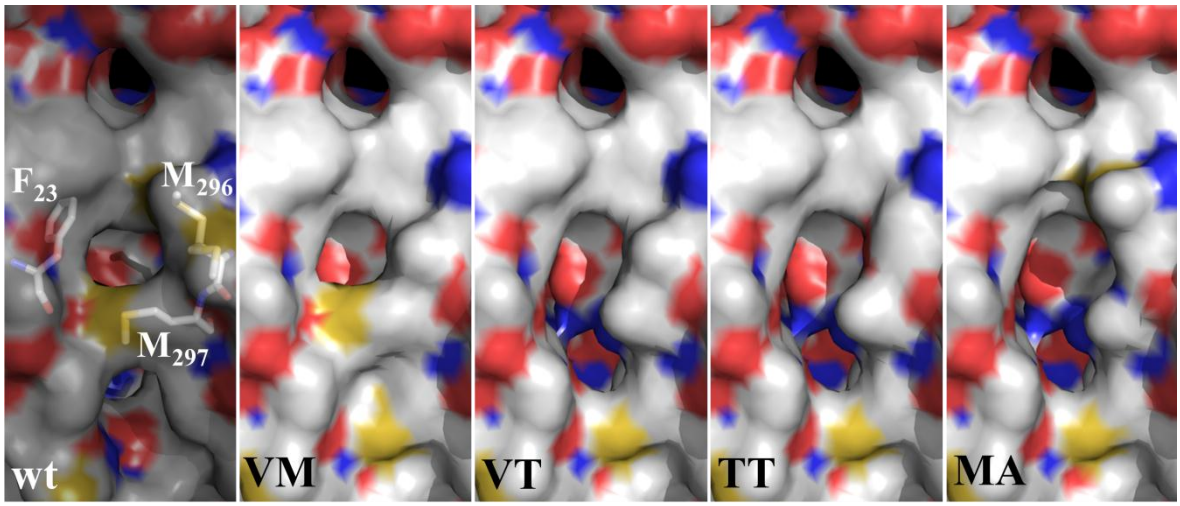

Figure 3.7 Modeling of active site pore mutants based on the *Aa*SOR structure at the SwissModel server (Arnold *et al.*, 2006). Abbreviations: **wt** - *Aa*SOR; **VM** - $M_{296}V$ mutant; **VT** - $MM_{296/297}VT$ mutant; **TT** - $MM_{296/297}TT$ mutant; **MA** - $M_{297}A$ mutant.

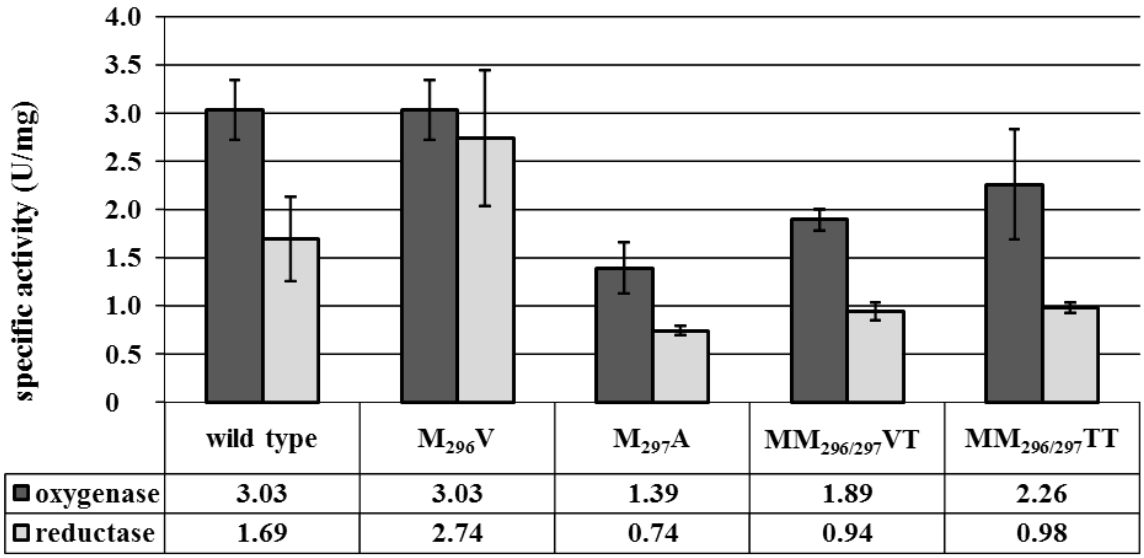

	wild type	$M_{296}V$	$M_{297}A$	$MM_{296/297}VT$	$MM_{296/297}TT$
oxygenase	3.03	3.03	1.39	1.89	2.26
reductase	1.69	2.74	0.74	0.94	0.98

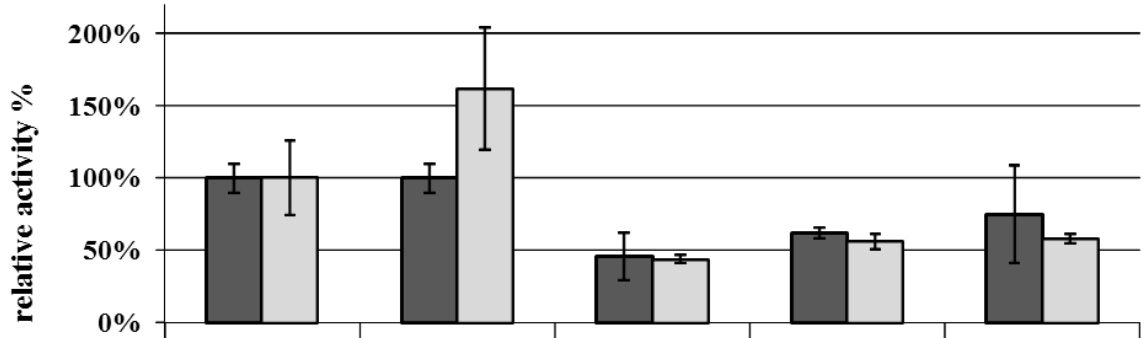

	wild type	$M_{296}V$	$M_{297}A$	$MM_{296/297}VT$	$MM_{296/297T}T$
oxygenase	100	100	46	62	75
reductase	100	162	44	56	58

Figure 3.8 Histogram of specific and relative activities of wild type and active site pore mutants. Wild type enzyme activity was set to 100 % according to the specific activity values.

3.2.6. Zinc-mediated inhibition of the SOR

Zn^{2+} had been shown to be a potent inhibitor of SOR activity as long as it is free in solution and not complexed by ligands such as EDTA (Kletzin, 1989; Urich *et al.*, 2004; Chen *et al.*, 2005). Crystals were soaked with Zn^{2+} in order to determine its binding site within the SOR (Urich, 2005c). One Zn^{2+} ion was detected in the zinc-complexed structure (with 0.8 occupancy) and refined at 1.7 Å resolution (Table 3.5). It was located on the opposite side of the beta barrel core of the monomer (not shown; see Urich *et al.*, 2006) but not in close vicinity to the active site (Figure 3.10). The refinement and reevaluation of the crystallographic dataset identified an acetate molecule and a chloride ion that, together with two water molecules, complete the coordination sphere of Zn^{2+}.

The zinc ion was bound in a distance of 2.1 Å to the H_{277} imidazole (interatomic distances are averages over of the six crystallographically independent monomers). H_{166}, which constitutes a conserved 2-His motif together with H_{277}, had its Nε2 in hydrogen-bonding distance to the two water molecules that coordinate the zinc ion (Figure 3.9).

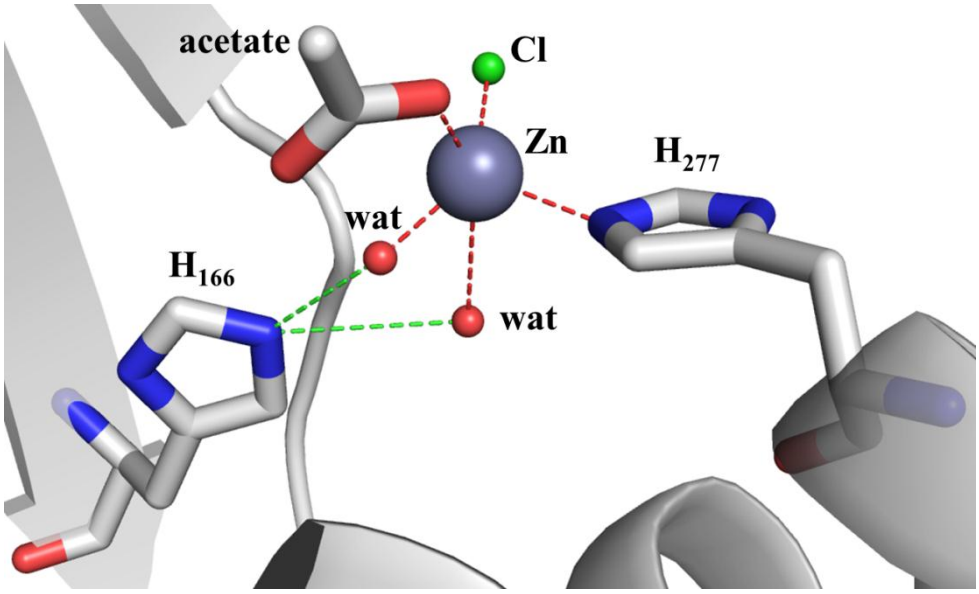

Figure 3.9 The Zn^{2+} binding site of the SOR. Zinc (grey sphere) is coordinated by one acetate molecule, two water molecues (red spheres), one chloride (green sphere) and by H_{277}. Zinc coordination is shown as red dashed lines. Hydrogen-bonding between H_{166} and the zinc-coordinating water molecules is represented by green dashed lines.

Both histidines are located at the bottom of a dead-ending channel that opens to the inner cavity of the holoenzyme next to the active site entrance of a neighboring monomer. The Fe - Zn distances were approximately 27 Å, both within the same and the neighboring subunits (Figure 3.10). The side chains of Css_{31} and M_{297} separate the entrances to the active site pocket and the zinc-binding channel. It was postulated that Css_{31} is the sulfur-binding residue in the active site pocket (Urich *et al.*, 2006). The distance between Zn^{2+} and the S-δ atom of the cysteine persulfide Css_{31} was 18 Å. Hence, direct interference of Zn^{2+} in the catalysis is unlikely. Both histidine residues were substituted for an alanine independently and the specific activities were similar to the wild type enzyme (Figure 3.11). K_i-values (half-maximal inhibitory concentration) of the wild type enzyme were 45 µM zinc chloride for the oxygenase activity and 39 µM for the reductase activity. K_i-values for H_{166}A were 121 µM (oxygenase) and 150 µM (reductase). The H_{277}A mutant showed slightly different K_i-values of 157 µM (oxygenase) and 144 µM (reductase). The latter mutant was chosen for crystallization to investigate the binding site of Zn^{2+} ions in absence of the histidine ligand.

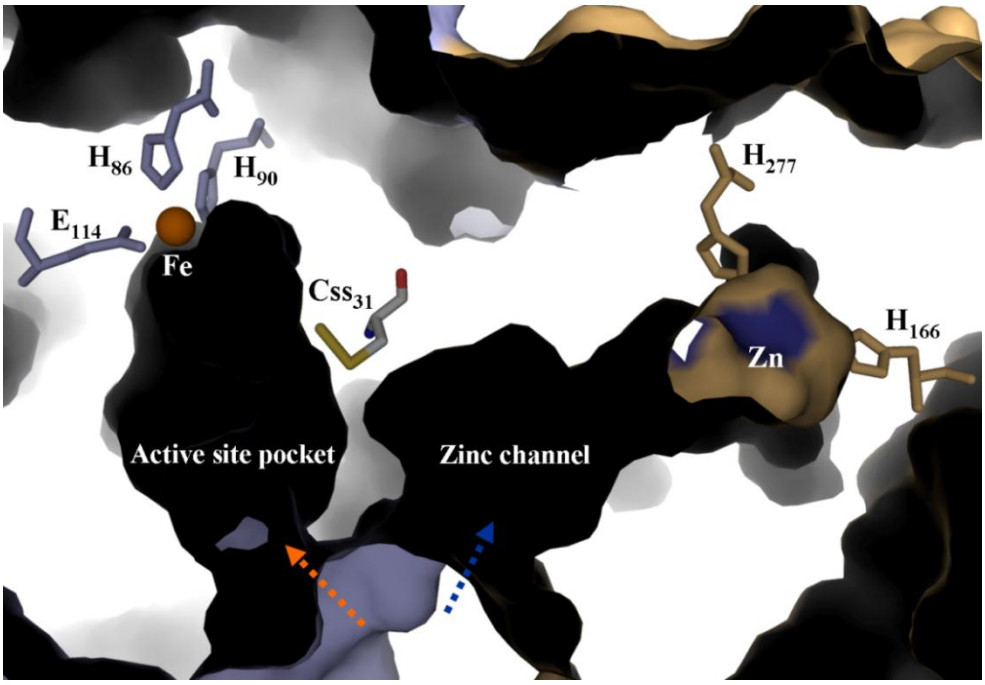

Figure 3.10 Surface representation of two neighboring subunits (light blue and ochre) highlighting the positions of the Zn and Fe sites with their respective ligands and channels and the bridging cysteine persulfide. The zinc site is located at the end of a tunnel leading to the active site Css_{31} of the neighboring monomer.

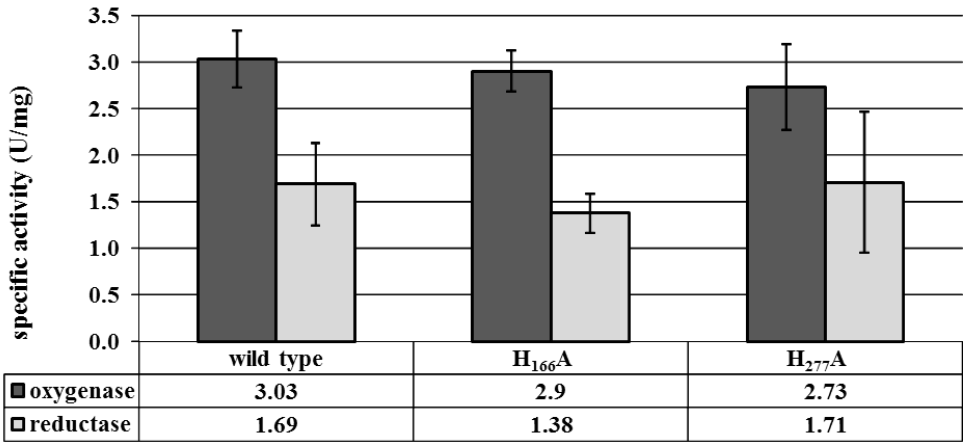

	wild type	$H_{166}A$	$H_{277}A$
oxygenase	3.03	2.9	2.73
reductase	1.69	1.38	1.71

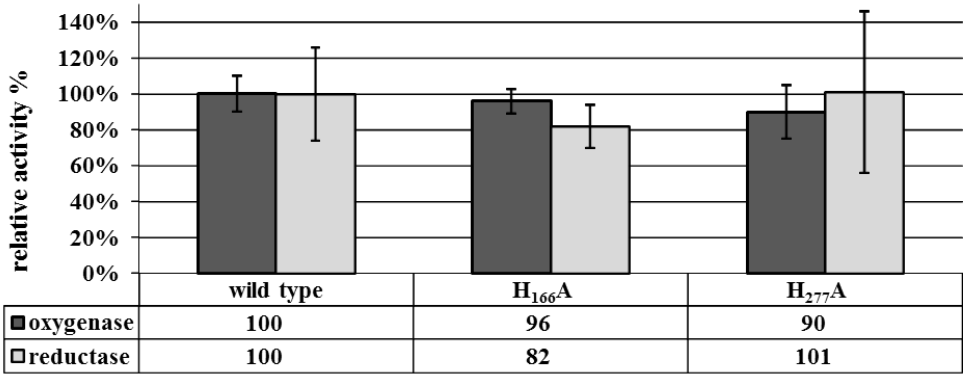

	wild type	$H_{166}A$	$H_{277}A$
oxygenase	100	96	90
reductase	100	82	101

Figure 3.11 Histogram of specific and relative activities of *Aa*SOR and Zn - channel mutants. Wild type enzyme activity was set to 100 % according to the specific activity values.

Purified recombinant $H_{277}A$ SOR was dialyzed against 50 mM Tris/HCl buffer pH 7.5 and concentrated up to 12.77 mg/ml. First crystallization screenings were carried out using 96 different crystallization conditions of the MbClassSuite (Qiagen) at 22°C. This kit was chosen, as it contained similar conditions as used previously for the crystallization of recombinant *Aa*SOR (Urich *et al.*, 2005a). $H_{277}A$ SOR crystallized in five different conditions displaying small crystals within 24 h. Most promising was condition 7 (0.1 M Tris/HCl pH 8.5, 1.2 M ammonium sulfate) that resulted in the formation of polyhedral crystals. Crystallization conditions were refined with 0.1 M Tris/HCl pH 8.5, 0.7 M ammonium sulfate. Only one single crystal was observed with a reasonable size. It was transferred to a cryoprotectant solution (0.1 M Tris/HCl pH 8.5, 0.9 M ammonium sulfate and 25 % glycerol) and flash-cooled in liquid nitrogen. Despite intense crystallization attempts, additional crystals were not obtained in either of the crystallization conditions, so that further zinc-soaking experiments could not be performed. X-ray diffraction data was collected at the ESRF beam line id14-2. The $H_{277}A$ SOR crystal diffracted to 2.08 Å resolution with the hexagonal space group I4 (International Tables for Crystallography number: 79; Hahn, 2002) with unit cell dimensions $a = b = 162.11$ Å and $c = 154.41$ Å (Table 3.5). The asymmetric unit comprised six independent monomers. Because of identical space groups of the $H_{277}A$ SOR crystal and the original *Aa*SOR dataset (Urich *et al.*, 2005a), a preliminary rigid body refinement was carried out using the PHENIX software suite (Adams *et al.*, 2010) and the original *Aa*SOR-dataset as template (PDB id: 2cb2; Urich *et al.*, 2006). Manual adjustments using the program COOT (Emsley *et al.*, 2010) were performed to improve the final model, which showed the successful mutation of H_{277} to A_{277} (Figure 3.14).

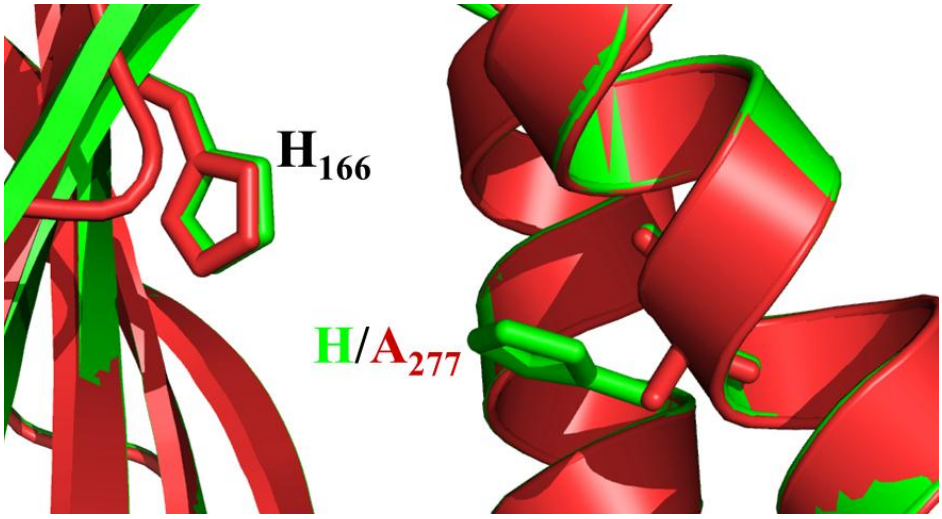

Figure 3.12 Cartoon and stick presentation of the 2-His motif. Overlay of the original *Aa*SOR structure (green) and $H_{277}A$ SOR (red).

Table 3.5 Diffraction data processing and model refinement statistics of SOR crystal derivatives

SOR derivative	**Zn^{2+} SOR**	**$H_{227}A$ SOR**
Source	ESRF ID14-3	ESRF ID14-2
Space group	I4 (79)	I4 (79)
Unit cell parameters (Å)	$a = b$ = 162.07	$a = b$ = 162.11
	c = 154.24	c = 154.41
Wavelength	0.9330	0.9330
Number of unique intensities	213,677	117,685
Redundancy	1.9	4.1
Resolution (outer shell) (Å)	38.20–1.70	55.92-2.08
	(1.76–1.70)	(2.19-2.08)
Completeness (outer shell) (%)	98.3 (94.1)	98.8 (96.9)
R_{merge}*(outer shell) (%)	6.4 (45.9)	11.4 (53.2)
I / σ (I) (outer shell)	12.0 (1.8)	8.8 (1.9)
Wilson B ($Å^2$)	19	24
Refinement		
Refined structure	1842 aa	1842 aa
	1382 waters	1288 waters
R_{work} (%)	16.3	16.7
R_{free} (%)	19.3	19.2
R (%)	16.2	16.7
Average ADP ($Å^2$)	21	24
Bonds RMSD (Å)	0.017	0.009
Angles RMSD (°)	1.220	1.125

*$R_{merge} = \Sigma|I_o - <I>| / \Sigma I_o$, where $<I>$ is the average of symmetry equivalent reflections and the summation extends over all observations I_o for all unique reflections.

3.3. Discussion

3.3.1. Polysulfide is a SOR substrate

Narrow pores with an apolar interior are localized at the chimney-like structures at the fourfold symmetry axes. They were already considered to be the substrate entrance points to the inner cavity of SOR (Urich *et al.,* 2006; Li *et al.,* 2008). The chimney pore diameter of the *Aa*SOR structure raised the question, whether elemental S_8-sulfur or a more favorable linear sulfur molecule such as polysulfide is the initial substrate for the SOR. The diameter of the tetramer channel pore is restricted to a diameter size of approximately 5 Å by both phenylalanine rings. A cyclo-octa sulfur molecule and a linear polysulfide molecule had both been modeled into the tetramer channel (Urich *et al.,* 2006), showing that the entry pore is too narrow for a cyclic S_8-sulfur molecule. An in-gel enzyme activity assay with the *Aquifex aeolicus* SOR-wt (*Aq*SOR) already demonstrated that the enzyme is active with polysulfide. Oxygenase activity of the *Aq*SOR was observed by colorless bands in the gel, indicating that polysulfide is used as substrate (Pelletier *et al.,* 2008). In the present work, the same assay was used for the *Aa*SOR. Oxygenase activity could be observed and was indicated by colorless protein bands in the non-denaturing gel, when the enzyme was incubated with a polysulfide solution (Figure 3.1). These observations suggest that the linear polysulfide molecule might be the substrate, even though the high instability of polysulfide at low pH values combined with high temperatures has to be considered. Polysulfide is unstable at acidic conditions (pH 1 - 3) and hydrolyzes into elemental sulfur and sulfide. Such an acidic environment can usually be found outside of the *Acidianus* cells. In contrast, the inner pH of the cell is almost neutral (~ pH 6.5; Moll and Schäfer, 1988) and polysulfide remains stable at neutral pH values. It remains unclear how polysulfide is formed and/or transferred into the cell. One option would include the transfer of cyclo-octa sulfur to the cytoplasm. A nucleophilic attack of the sulfur ring by a strong reductant such as H_2S could occur, thereby forming polysulfide. Another option would suggest the transfer of a stable polysulfide form from the pseudo-periplasmic space into the cell via a yet unknown enzyme. In both cases, the linear molecule could enter the inner SOR compartment through the tetramer channels at the fourfold symmetry axes.

3.3.2. Fourfold symmetry axis pores restrict SOR enzyme activity

The tetramer channels at the outer shell represent the entrance point to the inner cavity. An in-gel enzyme assay showed that linear sulfur molecules like polysulfides can serve as SOR substrate. It is consistent with a previous *in silico* model that only allowed linear sulfur molecules to enter the inner cavity (Urich *et al.*, 2006). Two rings of four phenylalanine side chains each define the tetramer channel pores in the present 3D model. Mutations of the phenylalanine residues into alanines enlarged the corresponding pores, leading to a moderate, less than twofold increase in specific enzyme activity (Figure 3.4). A full deletion of the chimney-forming loop structure resulted in a more than sevenfold increase in enzyme activity (Figure 3.4). Thus, substrate access to the active site and/or product exit is indeed limited by the outer shell of the protein. Therefore, it can be concluded that the specific activity of the wild type SOR is curbed to a lower level than optimally possible. The reasons for making the enzyme slow might be speculated upon. One option (among others) would predict that the reactive reaction products are not released uncontrollably into the cytoplasm but that they are delivered directly to the downstream oxidoreductases (Kletzin, 2008). One experimental indication for this interpretation in the absence of known interaction partners came from antibody/immunogold electron microscopy results of the *A. tengchongensis* SOR: the enzyme seemed to be attached to the inside of the cytoplasmic membrane (Chen *et al.*, 2005). In addition, these pores might provide highly controlled access points to the active sites, preventing the oxidation of "unwanted substrates"

3.3.3. Mutagenesis at the threefold symmetry axis elevates SOR activity

The amino acids R_{99} and S_{226} are central components of the subunit interface at the threefold symmetry axis. R_{99} forms an intra-subunit salt bridge to E_{228} (Figure 3.5). The other η-nitrogen atom is in hydrogen-bonding distance (2.8 Å) to the Oγ of S_{226} of the neighboring subunit. Alternative hydrogen-bonding networks are also possible: R_{99} might link to the α-carbonyl oxygen atoms of S_{226} of two subunits. In addition, a hypothetical salt bridge between the ε-nitrogen of the R_{99} and E_{228} is possible, provided that an extensive charge delocalization exists in the guanidinium group. Even though *E. coli* cells were transformed with a plasmid that harboured an E_{228}A mutation, no protein was obtained and consequently no analysis of its effects on salt bridge formation could be carried out (data not shown).

The mutation of R_{99} and S_{226} into an alanine gave a modest, less than 1.5-fold increase in specific activity (Figure 3.6). Mutation into more hydrophobic residues changed the ratio between oxidized and reduced reaction products in favor of sulfide (Figure 3.6). A similar situation but with a less pronounced increase of reductase activity was observed for the chimney mutant DelL, suggesting that opening of the closed reaction chamber in the interior of the protein changes the ratio between the oxygenase and disproportionase partial reactions. The interpretation of the activity data is complicated by non-enzymatic reactions occurring with sulfur and inorganic sulfur compounds in aqueous solutions, which depend on the incubation temperature and the pH of the buffer. Sulfite reacts rapidly with excess sulfur to thiosulfate at pH ≥ 5 and 85°C so that it is still unclear whether thiosulfate is a primary or secondary reaction product of the SOR (Kletzin, 1989). The sulfur disproportionation with H_2S, polysulfides and thiosulfate (instead of sulfite) as products occurs non-enzymatically at alkaline pH (detectable above pH 7.5 at 75°C; Roy and Trudinger, 1970; Kletzin, 1989). It was concluded from previous activity assays in the presence of chemically complexed zinc (to overcome zinc inhibition and to precipitate sulfide *in situ*) that an approximate 1:1 ratio between oxidized and reduced reaction products is maintained as opposed to the 1:2 ratio for the oxygen-independent disproportionation. Further, it was assumed that the sub-stoichiometric hydrogen sulfide detection in the standard assay is due to the rapid non-enzymatic re-oxidation under the aerobic assay conditions (see wild type enzyme activity for all histograms; Kletzin, 1989; Kletzin, 2008; Kletzin *et al.,* 2004; Urich *et al.,* 2004). This picture however changes with the channel mutants, which prove that the ratio between oxidized and reduced reaction products is not constant and that it depends on the integrity of the protein shell.

3.3.4. The integrity of the active site pore is important

The active site pore is constituted by two adjacent methionines (M_{296}/M_{297}) and a phenylalanine (F_{23}). M_{297} is conserved in all SORs, while M_{296} is exchanged for another hydrophobic amino acid in several naturally occurring SOR sequences (see SOR alignment, Figure 1.10). F_{23} is conserved in Archaea while Bacteria mostly use a methionine at this position. The pore most likely represents the entrance of the sulfur substrate, but no exit pore in the active site pocket of the *A. ambivalens* SOR was found, as suggested for the *A. tengchongensis* counterpart (Li *et al.,* 2008). This might be the result of alternating side chain conformations of amino acids involved in such an exit in the

*Aa*SOR. Expansion of the active site pore did not increase the enzyme activity, which is in contrast to the results of the tetramer and trimer channels (Figures 3.4 and 3.6). Replacement of the hydrophobic methionines with the smaller and in the case of the threonine more hydrophilic residues diminished the specific activity by half, suggesting that the hydrophobic barrier and/or at least one of the methionines are essential. It can be hypothesized that non-covalent nucleophilic interaction between the atoms of the sulfur substrate and the S-δ atom of the gate-keeping methionine residues could direct the sulfur substrate towards the active site cavity.

3.3.5. Inhibition mechanism of Zinc

It was previously shown that zinc is a potent SOR inhibitor (Kletzin, 1989). In presence of 1 mM Zn^{2+} ions, a complete loss of SOR activity was observed, whereas 0.1 mM resulted in 37 % residual residual oxygenase activity (Kletzin, 1989). Zinc inhibition could be neutralized by addition of at least equimolar concentrations of EDTA (Urich *et al.*, 2004). Zn^{2+} ions can theoretically bind to sulfur atoms of cysteine(s), to histidine and/or carboxylate ligands. In order to determine the mechanism of inhibition, the 3D structure of *Aa*SOR-crystals soaked in Zn^{2+} was resolved. The zinc ion was found in a dead-ending channel, which opens next to the active site pore of the contiguous subunit. The active site Css_{31} separates the lumina of both channels. The question arises how zinc is able to inhibit SOR activity over a distance of approximately 27 Å to the next iron. The zinc ion is coordinated by histidine residue H_{277}, one acetate, one chloride and two water molecules that in turn are hydrogen-bonding to H_{166}. This 2-His motif is conserved among all SOR sequences. Mutations of both histidines into alanine did not change enzyme activity significantly. However, the mutants K_i-values for Zn^{2+} increased two- to threefold, compared to the wild type. It cannot be answered at present which role the obviously conserved zinc channel plays. In contrast, several options exist about the inhibition mechanism. The Zn^{2+} ion might reduce the flexibility of the SOR thus block the substrate entry from the active site. In addition, it might block the important Css_{31} residue, which is located at the interface of both channels, in its movements during the catalytic cycle. Stiffening of the protein seems to be the most probable mechanism of inhibition because no further connection between the zinc channel and the active site pocket is present in the enzyme.

4. Active site and reaction mechanism of the *A. ambivalens* SOR

4.1. Introduction

The active site of the *Aa*SOR comprises a mononuclear iron center and a conserved cysteine persulfide. The iron atom is coordinated in a 2-His-1-carboxylate motif, a structural feature often found among non-heme iron enzymes. Typically, the side chains of two histidines and one aspartate or glutamate coordinate the catalytic metal, leaving up to three remaining sites for other ligands such as water molecules or other solvents (Hegg and Que, 1997; Bruijnincx *et al.*, 2008). In the *Aa*SOR structure, iron is coordinated by two histidines (H_{86} and H_{90}) and one glutamate (E_{114}), which serves as a bidentate ligand (Urich *et al.*, 2006). Two water molecules complete the slightly distorted octahedral coordination sphere (Figure 4.1).

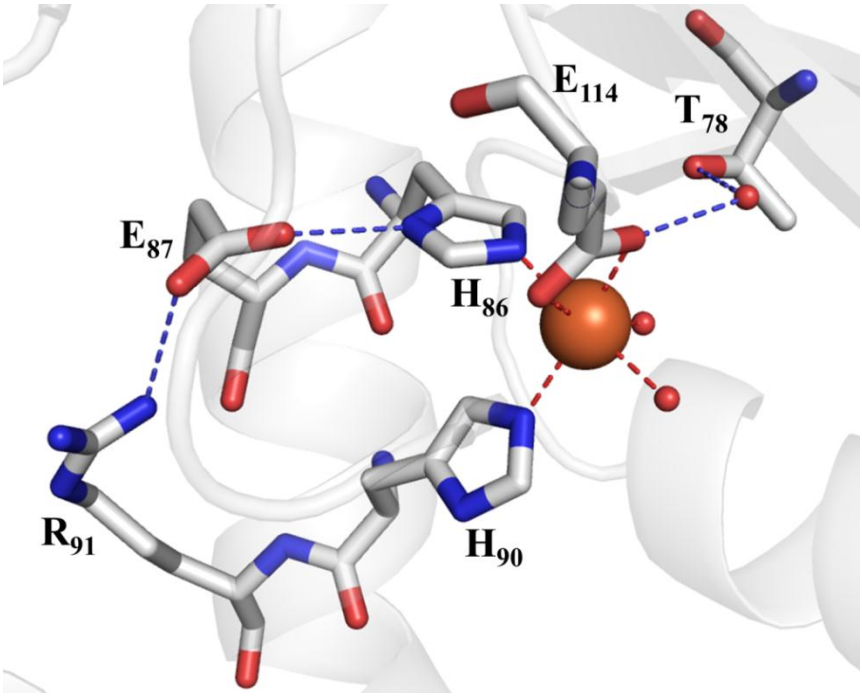

Figure 4.1 Stick and cartoon representation of the mononuclear iron center of the *Aa*SOR; color representation: red - oxygen, blue - nitrogen and white - carbon; water molecules are depicted by small red spheres and the Fe atom is depicted as an orange sphere. Red dashed lines represent iron atom coordination; blue dashed lines represent hydrogen bonds.

Amino acids of the second coordination sphere (*i.e.* amino acids or water molecules that are non-covalently attached via hydrogen bonds to the iron ligands that occupy the first coordination sphere) were assumed to contribute to the reduction potential of the enzyme (Seyfarth, 2006; Kletzin, 2008). Amino acids potentially involved in such an H-bond

network were mutated previously and tested for enzyme activity (Seyfarth, 2006). Two residues (T_{78} and E_{87}) appeared to be essential for catalysis. T_{78} is located in hydrogen-bonding distance to a water molecule that in turn is in hydrogen-bonding distance to the Fe-ligating E_{114} (Figure 4.1). The threonine was substituted for an alanine and the mutant showed a complete loss of SOR activity. The second amino acid, E_{87}, is located in hydrogen-bonding distance to the Fe-ligand H_{86} (Figure 4.1). An alanine variant of E_{87} caused an almost complete loss of activity while an aspartate variant increased enzyme activity up to 3.5-fold with a shift of the reaction products ratio towards sulfide (Seyfarth, 2006). These mutant proteins were reproduced in the course of this work to verify the previous results. Moreover, both E_{87} mutants were prepared for crystallization to investigate structural rearrangements at the active site caused by the mutations. Additionally, further putative members of the hydrogen bond network were replaced for other amino acids using site-directed mutagenesis, and the corresponding mutants were tested for SOR activity.

The second component of the active site center is a conserved cysteine persulfide. It also occurs as an unmodified cysteine, which was previously demonstrated for the recombinant *Acidianus tengchongensis* SOR (*At*SOR). It was stated that both cysteine forms probably represent different stages of the catalytic reaction cycle (Li *et al.*, 2008). In order to investigate the sulfuration process of the cysteine, the recombinant *Aa*SOR was crystallized and also co-crystallized in presence of different sulfur compounds, which could give new insights into the SOR reaction cycle. The present chapter includes the results of these experiments.

Previous EPR spectroscopy experiments of the "as isolated" *Aa*SOR revealed that the active site iron is reduced upon incubation with sulfur at high temperatures. The uncommonly low reduction potential was determined at E_0' = - 268 mV (Urich *et al.*, 2004), which is unusually low for this type of iron center but sufficient to reduce elemental sulfur to H_2S (S^0/HS^-; E_0' = - 270mV; Thauer *et al.*, 1977). The reduction of Fe^{3+} to Fe^{2+} upon sulfur incubation gave rise to the question, if this redox change is obligatory for SOR activity and whether oxygen is activated by the metal center or by the sulfur substrate. To address this question, inclusion bodies of *Aa*SOR were un- and refolded in presence of non-iron metals and analyzed for enzyme activity in this work. Electron paramagnetic resonance (EPR) spectroscopy was performed subsequently with biochemically active derivatized metal-SORs before and after incubation with sulfur and discussed in context of the reaction mechanism.

4.2. Results

4.2.1. Crystallization of recombinant *Aa*SOR

The recombinant *Aa*SOR was crystallized to address the question, whether the C_{31} residue is synthesized in persulfurated form by *E. coli* cells. The protein was purified in a one-step Strep-tag chromatography (see chapter 2 for details), dialysed against 50 mM Tris/HCl buffer pH 7.5 and subsequently concentrated to a final concentration of 12.90 mg/ml. The protein formed small crystals below 0.05 mm in size after 7 days of incubation at 32°C in the previously described conditions that were used to crystallized the original *Aa*SOR (Urich *et al.*, 2005a). A crystallization screening was started at the same time using the MbClass Suite (Qiagen) that contained 96 different conditions, which were similar to those used for the original *Aa*SOR screening (Urich *et al.*, 2005a; see chapter 3). Crystal formation was observed in 14 different conditions within 24 hours when incubated at 22°C. Condition number 4 (0.5 M ammonium sulfate / 0.1 M Tris/HCl pH 8.5) delivered reproducibly hexagonal-shaped crystals with a size between 0.1 and 0.15 mm. The incubation temperature was elevated to 32°C, which increased crystal size. After the ratio between crystallization buffer volume and protein amount had been optimized, crystals with a size of 0.35 and 0.1 mm were obtained within 5 - 7 days (Figure 4.2). They were subsequently soaked in a cryoprotectant-solution containing 0.7 M ammonium sulfate, 0.1 M Tris/HCl buffer pH 8.5 and 25 % glycerol before flash-cooling in liquid nitrogen.

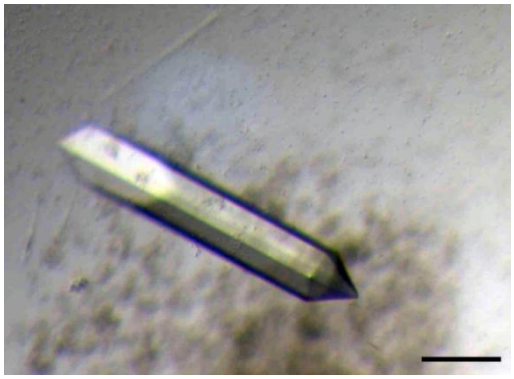

Figure 4.2 *Aa*SOR crystal grown in 0.5 M ammonium sulfate and 0.1 M Tris/HCl buffer pH 8.5. Black bar represents 0.1 mm.

X-ray diffraction data were collected by Carlos Frazão (ITQB, Oeiras, Portugal) in-house at the Cu K-α wavelength (1.5418 Å) from a cryo-protected crystal. A first batch of *Aa*SOR crystals diffracted to 2.50 Å resolution with the hexagonal space group $P6_322$

(International Tables for Crystallography number: 182; Hahn, 2002) and with the unit cell dimensions $a = b = 159.04$ Å and $c = 228.26$ Å. The asymmetric unit comprised four independent monomers. The structure was solved by molecular replacement using PHASER (McCoy *et al.*, 2007) from the PHENIX software Suite (Adams *et al.*, 2010) and the original *Aa*SOR model as template (PDB id: 2cb2; Urich *et al.*, 2006). The new *Aa*SOR crystal form showed different cell dimensions from those of the original *Aa*SOR deposited at the PDB. Thus, molecular replacement was used to obtain an initial set of phases by localizing the four *Aa*SOR monomers in the asymmetric unit which were used for the structural refinement. Another *Aa*SOR crystal was obtained with the hexagonal space group $P6_322$ (International Tables for Crystallography number: 182) and the unit cell dimensions $a = b = 158.71$ Å and $c = 228.09$ Å, which diffracted up to 2.40 Å resolution. The 2.40 Å resolution dataset had cell dimensions that differed within 2.2 % from those of the 2.50 Å dataset. Therefore, PHENIX was used with the previously obtained structure solution for an initial rigid body refinement, followed by positional, a.d.p.s and TLS standard refinements. Density maps were inspected at a graphics workstation and the model was improved manually with COOT (Emsley *et al.*, 2010). The same crystallization conditions (0.5 M ammonium sulfate / 0.1 M Tris/HCl pH 8.5) were used to co-crystallize the *Aa*SOR in presence of thiosulfate, polysulfide, sodium sulfide and elemental sulfur in order to investigate modifications of the protein caused by the sulfur compounds. Crystal formation was observed in all co-crystallization attempts but hexagonal-shaped crystals of a size of at least 0.1 mm were only observed for the tries using thiosulfate (SOR_TS; not shown) and polysulfide (SOR_PS; not shown). Those crystals were cryo-protected with the same stabilizing solution, flash-cooled in liquid nitrogen and sent to the ESRF (European Synchrotron Radiation Facility, Grenoble, France) for data collection. These crystals diffracted to 2.83 Å (SOR_TS) and 3.76 Å (SOR_PS) resolution, respectively. Both crystals were isomorphous with the previous ones and the working models SOR_TS and SOR_PS were refined using rigid body refinement prior to the standard PHENIX refinement procedure. Analyses of the lower resolution models SOR_TS and SOR_PS did not give any hint of modifications in the SOR structures, even taking into consideration the low resolution of the refined datasets. Superposition of the newly obtained and the original *Aa*SOR structure showed a virtually identical overall protein architecture with an RMSD of 0.23 Å. The RMSD value (**R**oot **M**ean **S**quare **D**eviation from standard geometry) is the measure of similarity of C-α atomic coordinates between two 3D structures, which was calculated using PDBeFold (http://www.ebi.ac.uk/msd-srv/ssm/; Krissinel and Henrick,

2004). However, some differences were observed within the active site pocket. The Fe coordination is completed by two water molecules in the original *Aa*SOR. In the newly obtained *Aa*SOR, only one water molecule was identified in binding distance to Fe, leaving the metal in a fivefold-coordination state. The slightly distorted octahedral geometry of the metal center was maintained with one vacant ligand position (Figure 4.3 a + b). The coordination distances between Fe and its ligands changed slightly between 0.09 Å and 0.38 Å. Additional 2 F_o-F_c electron density at the S-γ atom of C_{31} was not detected (Figure 4.3), indicating an unmodified cysteine at this position as already demonstrated for the *At*SOR (PDB id: 3bxv; Li *et al.*, 2008; Figure 4.3 c).

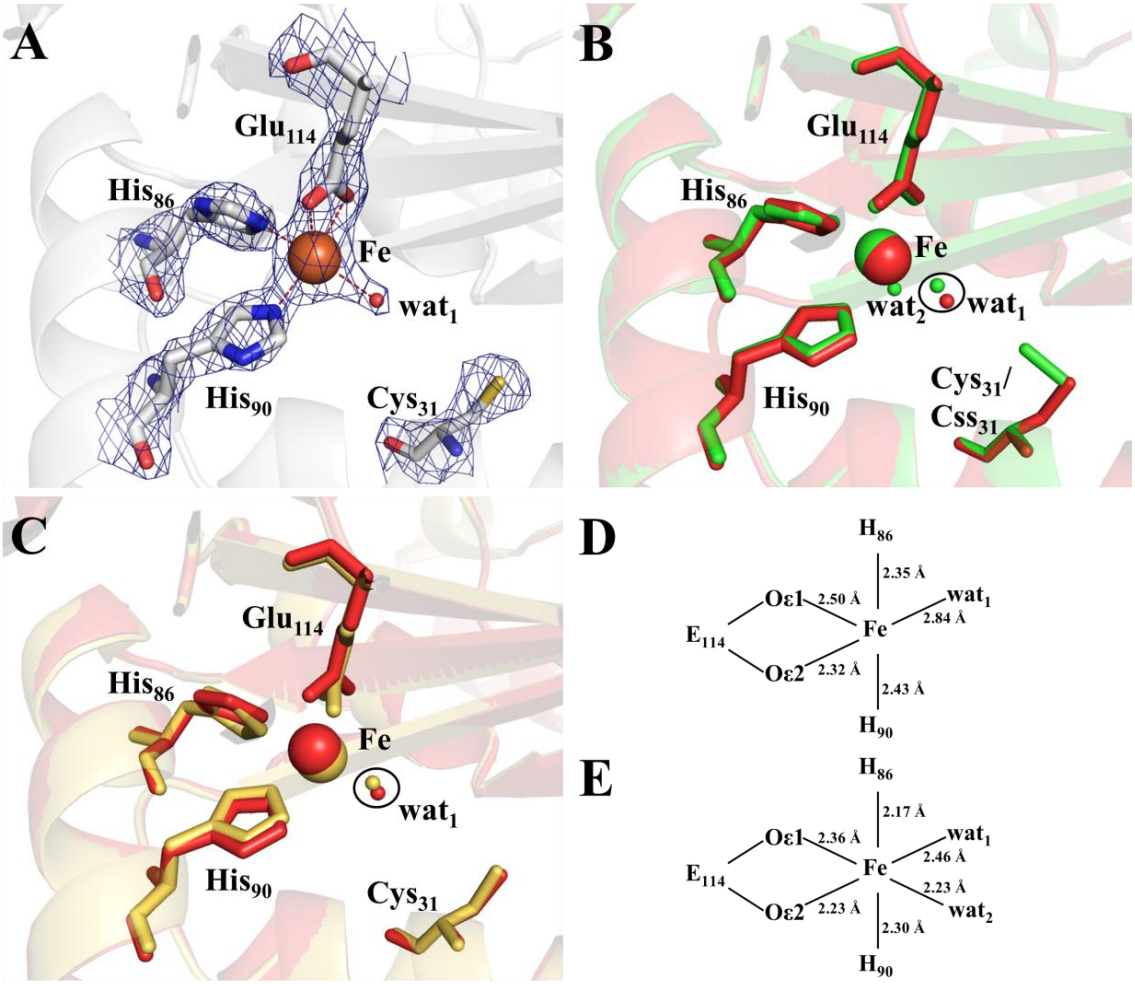

Figure 4.3 Stick and cartoon representation of the active site pocket of *Aa*SOR. (**A**) Active site of the newly crystallized *Aa*SOR (space group $P6_322$); color representation: red - oxygen, blue - nitrogen, sulfur - yellow and white - carbon. The iron atom is depicted as orange sphere and the water molecule as a small red sphere. 2 F_o-F_c electron density map contoured at 1.5 σ is shown in blue mesh; red dashed lines indicate iron coordination (**B + C**) Superposition of the newly crystalllized *Aa*SOR (red) with the original *Aa*SOR (green) or with the *At*SOR (yellow). (**D + E)** Schematic representation of the Fe center and the fivefold-coordinated octahedral geometry of the crystallized *Aa*SOR with one water ligand missing (**D**) and the sixfold-coordinated octahedral geometry of the original *Aa*SOR (**E**). Black solid lines represent the coordination distances (average values for 4 (**D**) and 6 (**E**) crystallographically independent monomers).

4.2.2. Properties of active site mutants

E_{87} and T_{78} were assumed to be involved in the formation of an H-bond network that putatively contributes to the low reduction potential of the SOR (Figure 4.4).

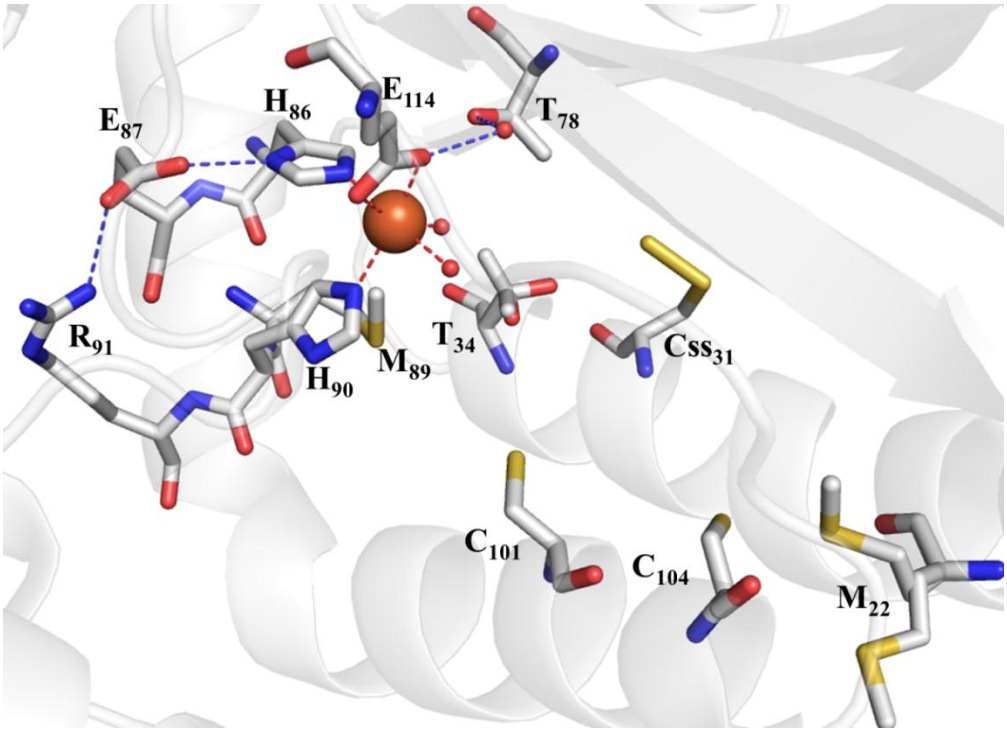

Figure 4.4 Stick and cartoon representation of the active site pocket of the *Aa*SOR (Urich *et al.*, 2006); color representation: red - oxygen, blue - nitrogen, sulfur - yellow and white - carbon; water molecules are depicted by small red spheres and the Fe atom is depicted as an orange sphere. Red dashed lines represent iron atom coordination; blue dashed lines represent putative hydrogen-bonds.

The δ2-oxygen of E_{87} is in hydrogen-bonding distance (2.78 Å; average distance of six crystallographically independent monomers) to the δ1-nitrogen of H_{86}, while the δ1-oxygen is in hydrogen-bonding distance to the η1-nitrogen of R_{91}. T_{78} is in hydrogen-bonding distance to a water molecule (2.76 Å; average distance of six crystallographically independent monomers) that in turn is in hydrogen-bonding distance to a carboxylate oxygen of E_{114} that coordinates iron. It is also feasible that an H-bond is directly formed between T_{78} and one of the Fe-coordinating water molecules (3.35 Å; average distance of six crystallographically independent monomers). Apart from that, three other residues including $M_{22,}$ T_{34} and M_{89} are involved in the formation of the active site pocket of the *Aa*SOR. T_{34} is located in the proximity of the essential cysteine persulfide with an average distance of 3.84 Å or 4.84 Å between the S-δ and the hydroxyl-group of the threonine. The distance depends of the position of the threonine, since two alternating side chain conformations exist. M_{22} is close to the S-γ atom of the active site cysteine C_{104}.

The average distance is either 2.93 Å or 4.93 Å, as two alternating side chain conformations exist as well (Figure 4.4). M_{89} is around 5 Å away from the iron-coordinating H_{90} and 4.3 Å away from T_{34}. In order to investigate the role of these active site pocket-forming and hydrogen-bonding residues, several mutants were constructed via site-directed mutagenesis (Table 4.1). The properties of the heterologously produced proteins were tested with standard procedures (see chapter 2 for details). The *Aa*SOR mutants $E_{87}A$, $E_{87}D$ and $T_{78}A$ mutants were originally produced by K. Seyfarth (Seyfarth, 2006). The mutants $R_{91}A$, $M_{89}A$, $M_{22}L$, $M_{22}C$ and $T_{34}S$ were constructed in the course of this work via site-directed mutagenesis using the original pASK-SOR.05 vector and the respective oligonucleotides (see Table 2.1 in chapter 2). No protein was detected in *E. coli* after overexpression of the $M_{89}A$ mutant gene. All other SOR proteins were prepared independently at least twice and purified via Strep-tag chromatography. The yields of the purified SOR proteins ranged from 0.14 - 0.80 mg/l 2x LB medium, depending on the mutant. All proteins were analyzed for SOR activity and iron content to verify that changes in enzyme activity are not a result of insufficient iron incorporation at the catalytic site. Iron incorporation was in the range of 1.0 - 2.1 Fe atoms per subunit (Table 4.1).

Table 4.1: Protein yield and iron content of the SOR mutants.

	Protein yield (mg per l 2x LB medium)	**Absolute Fe content (nmol Fe)**	**Relative Fe content (nmol protein/ nmol Fe)**
Hydrogen bond network mutants			
$T_{78}A$	0.30	3.30	1.2
$E_{87}A$	0.14	3.00	1.1
$E_{87}D$	0.80	2.98	1.1
$R_{91}A$	0.33	2.86	1.0
Active site pocket mutants			
$M_{22}C$	0.32	5.86	2.1
$M_{22}L$	0.35	2.79	1.0
$T_{34}S$	0.53	3.11	1.1

A highly decreased enzyme activity was observed for the alanine variants of E_{87} and $R_{91.}$ $E_{87}A$ and $R_{91}A$ showed comparable oxygenase activities with 12 % and 18 % of the wild-type enzyme. No reductase activity was detected in case of $E_{87}A$, while 3 % remained in case of $R_{91}A$ (Figure 4.5). The highly diminished SOR activity of $E_{87}A$ was in good agreement with previous results that showed a residual enzyme activity of 7 % (Seyfarth, 2006). A different situation was obtained for the $E_{87}D$ variant.

The previously determined enzyme activity showed an increase of more than 300 % with a strong product stoichiometry bias towards H_2S (Seyfarth, 2006). These results could not be reproduced despite several independent measurements of different protein preparations. Instead, a decrease of oxygenase (61 % residual activity) and reductase activity (27 %) was observed. Previous analysis of the $T_{78}A$ mutant revealed a very low residual SOR activity with 6 % oxygenase and a complete loss of reductase activity (Seyfarth, 2006). The $T_{78}A$ mutant analyzed in the present work was active, yielding 54 % oxygenase and 23 % reductase activity instead. The active site pocket-forming T_{34} was substituted for a serine. This mutant only affected reductase activity, lowering it to 69 %. M_{22} was changed into a leucine and a cysteine, respectively. The leucine variant decreased both SOR activities around 50 %, while the cysteine mutant showed a residual activity of 72 % (oxygenase) and 41 % (reductase), respectively (Figure 4.5).

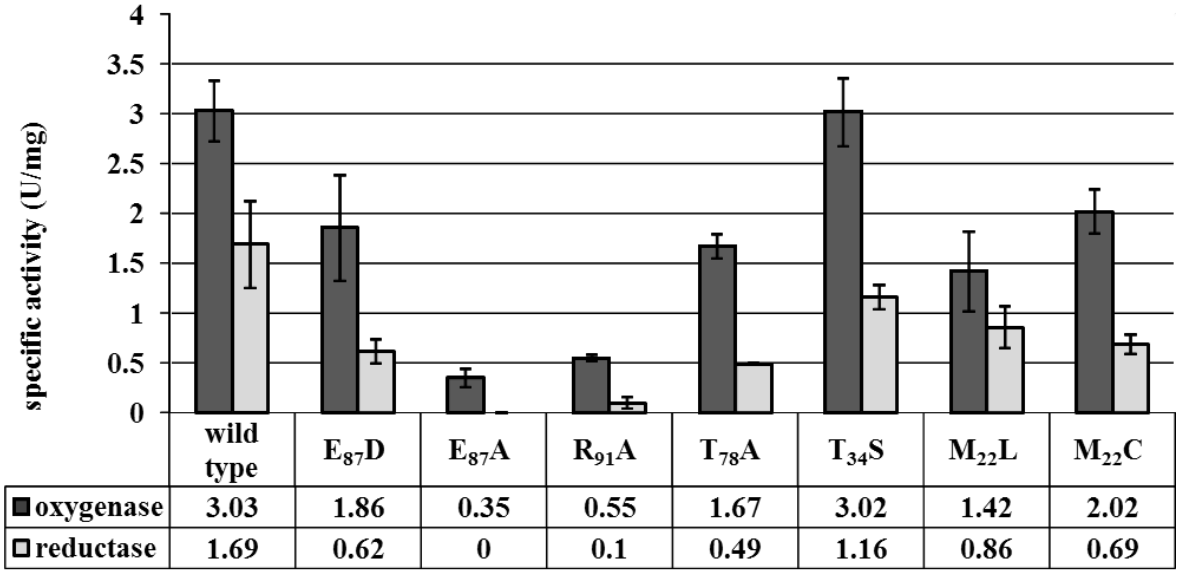

	wild type	$E_{87}D$	$E_{87}A$	$R_{91}A$	$T_{78}A$	$T_{34}S$	$M_{22}L$	$M_{22}C$
oxygenase	3.03	1.86	0.35	0.55	1.67	3.02	1.42	2.02
reductase	1.69	0.62	0	0.1	0.49	1.16	0.86	0.69

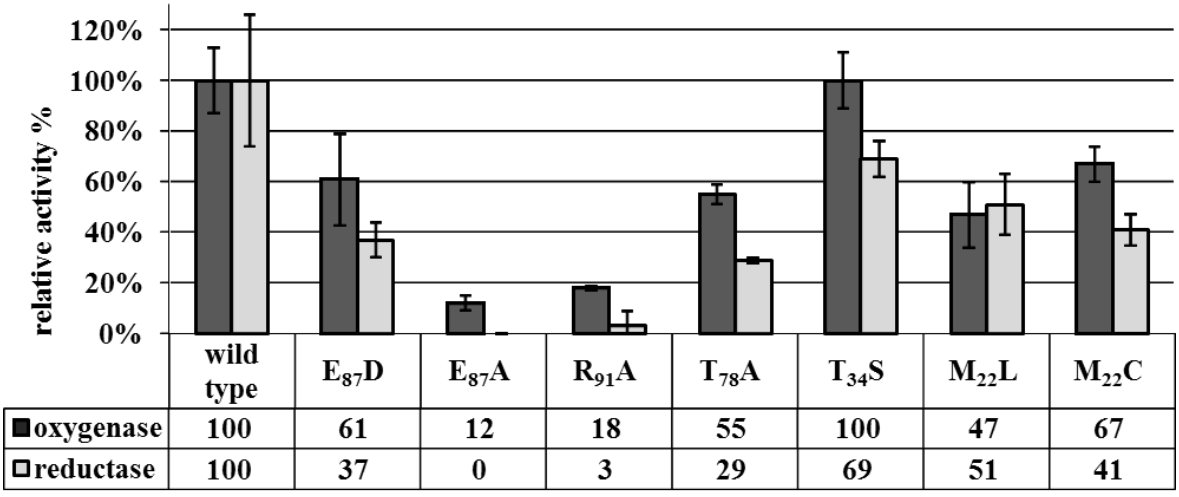

	wild type	$E_{87}D$	$E_{87}A$	$R_{91}A$	$T_{78}A$	$T_{34}S$	$M_{22}L$	$M_{22}C$
oxygenase	100	61	12	18	55	100	47	67
reductase	100	37	0	3	29	69	51	41

Figure 4.5 Specific activities and relative activities of *Aa*SOR and mutants. *Aa*SOR activity was set to 100 %. Black columns, oxygenase activity; gray columns, reductase activity.

Several preparations of $E_{87}A$ and $E_{87}D$, respectively, were each combined to crystallize the proteins. The 3D structure should then be investigated for structural rearrangements or delocalizations at the active site center, which might also influence neighboring residues.

4.2.3. Crystallization of the *Aa*SOR mutants $E_{87}A$ and $E_{87}D$

Both protein samples were dialysed against 50 mM Tris/HCl buffer pH 7.5 and concentrated to 11.83 U/mg ($E_{87}A$) and 13.82 U/mg ($E_{87}D$), respectively. The initial crystallization screen was the same as used for the *Aa*SOR screening (MbClass Suite; Qiagen). The $E_{87}D$ mutant crystallized under numerous buffer conditions, while only one condition (0.05 M sodium phosphate pH 6.7 / 5 % [w/v] PEG 4000) delivered recognizable crystals for $E_{87}A$. It was not possible to reproduce $E_{87}A$ crystals, although the crystallization buffer was refined extensively and an additional "additives" screening (Hampton Research, Aliso Viejo, USA) was performed. In contrast, $E_{87}D$ crystals were observed in more than 15 different crystallization conditions. Consequently, a simple screen was initiated at 32°C that solely contained the buffer substances Tris/HCl, sodium acetate or ADA (N-[2-acetamido]-iminodiacetic acid) at various pH values. Crystal formation was observed within few minutes of incubation at 32°C using 0.1 M ADA buffer pH 6 and crystals of reasonable sizes were obtained after 24 - 48 h. Different ADA concentrations between 0.1 M and 0.5 M slightly changed the crystal sizes with 0.2 M and 0.3 M ADA appearing to be optimal. Additionally, 1 - 5 % glycerol was added to the crystallization buffer in order to lower the number of nucleations and thus to increase the crystal size. Optimal conditions were found at 0.2 M ADA pH 6 including 3 % and 5 % glycerol, respectively with crystal dimensions of 0.3 and 0.1 mm (Figure 4.6). The crystals were transferred to a cryoprotectant solution containing 0.5 M ADA and 25 % glycerol. They were subsequently flash-cooled in liquid nitrogen and stored for synchrotron radiation experiments.

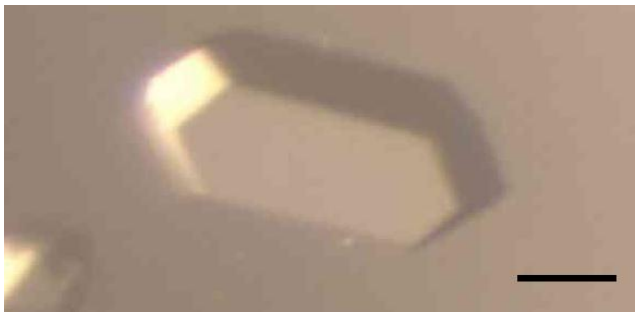

Figure 4.6 $E_{87}D$ crystal grown in 0.2 M ADA buffer pH 6 and 3 % glycerol. The black bar represents 0.1 mm.

The $E_{87}D$ crystals were measured at SLS (Swiss Light Source, Paul Scherrer Institut, Villingen, Switzerland) beam line X06DA. They diffracted to 1.75 Å resolution with the tetragonal space group I4 (International Tables for Crystallography number: 79) and unit cell dimensions $a = b = 161.92$ Å and $c = 154.25$ Å with six monomers in the asymmetric unit. Because of identical space groups of the $E_{87}D$ crystal and the original *Aa*SOR dataset (PDB id: 2cb2), a preliminary rigid body refinement was carried out using PHENIX. Manual adjustments using COOT were performed to improve the final model. Analysis of its structure showed that the aspartate mutation was present in all six monomers. Additional electron density at the S-γ atom of C_{31} was not detected, similar to the observations for the newly crystallized *Aa*SOR (Figure 4.3). The binding distance between δ1-nitrogen of H_{86} and δ2-oxygen of $E_{87}D$ changed minimally from 2.77 Å to 2.75 Å (average distance of six crystallographically independent monomers) but the binding distance of δ1-oxygen of $E_{87}D$ to η1-nitrogen of R_{91} increased from 3.00 Å to 4.24 Å. Both water molecules, which complete the Fe coordination at the original *Aa*SOR were clearly visible, but no iron atom was detected in any of the six monomers (Figure 4.7).

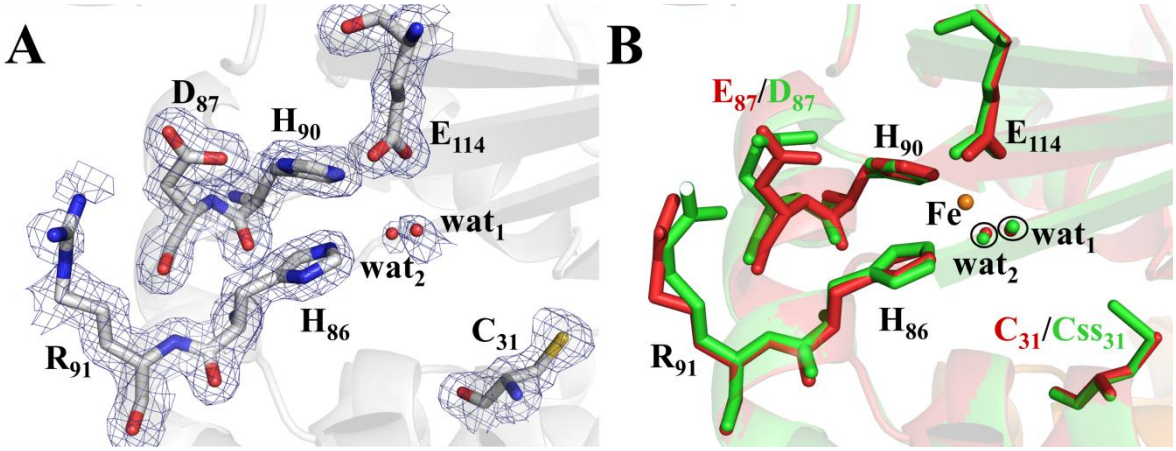

Figure 4.7 (**A**) Stick and ribbon representation of the $E_{87}D$ active site; color representation: red - oxygen, blue - nitrogen, sulfur - yellow and white - carbon. Water molecules are indicated as red spheres. The 2 F_o-F_c electron density map contoured at 2.0 σ is shown in blue mesh. (**B**) Superposition of the original *Aa*SOR (green) and the $E_{87}D$ mutant (red). The iron atom was only visible in the *Aa*SOR (orange sphere).

4.2.4. Generation of metal-substituted SOR derivatives

Metal-substituted SOR derivatives were generated to investigate whether alternative metal ions can replace iron in the active site. *Aa*SOR inclusion bodies were extensively washed using the corresponding washing buffer (see chapter 2 for details). About 5 - 10 g of inclusion bodies were resuspended in the tenfold volume of 50 mM Tris/HCl buffer pH 7.2 containing 8 M urea to unfold the precipitated SOR proteins. Dithiotreitol (DTT) or alternatively 2-mercaptoethanol were used as reductants and added to the suspension before the mixture was heated to 60°C for 1 h to dissolve the inclusion bodies. Heat-labile *E. coli* proteins precipitated and were separated by a short centrifugation step. Subsequently, the supernatant was used for refolding (see chapter 2). During the refolding process, 100 µM of the corresponding metal salt were added to the dialysis tube and to the dialysis buffer to ensure adequate metal incorporation. Metal-salts used during the refolding process included Fe^{II}-chloride, Co^{II}-sulfate, Mn^{II}-chloride, Ni^{II}-sulfate, Ga^{III}-nitrate, Ru^{III}-chloride, Cu^{II}-sulfate, V^{IV}-sulfate or Mg^{II}-sulfate. Transition metals of the fourth period (Mn, Co, Ni) were chosen as they share similar characteristics with iron. Together was iron, ruthenium belongs to the same period in the periodic table, so that Ru^{3+} was selected as well. Mg^{2+}, V^{4+} and Cu^{2+} were selected because of their biological relevance in other metal-containing enzymes. Gallium, a post-transition metal, was chosen as it is often used as a non-redox-active Fe^{3+} substitute for studying metal complexation in proteins because of a similar ion radius and charge as Fe^{3+} (Merkx and Averill, 1998). An inactive "metal-free" SOR was obtained by refolding inclusion bodies in the absence of metal ions. All metal-containing samples were dialysed twice against 50 mM Tris/HCl buffer pH 7.2 to eliminate residual dissolved metal ions, and they were subsequently purified via Strep-tag chromatography. Protein purity was visualized by SDS-PAGE using 10 % gels followed by Coomassie staining (Figure 4.8). Apart from the major protein band at 36 kDa, protein bands of approximately 30 kDa and 25 kDa were observed and interpreted as proteolysis products (Urich *et al.,* 2004; see also chapter 3). Faint bands of approximately 50 kDa and 60 kDa were observed for some of the derivatives, probably arising from residual *E. coli* proteins.

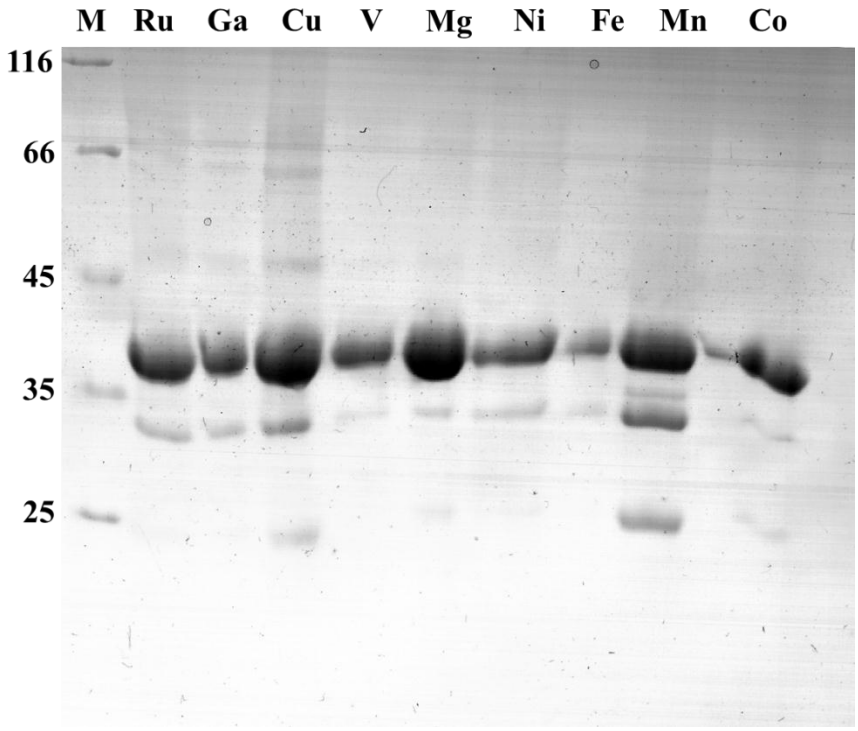

Figure 4.8 Coomassie-stained 10 % SDS gel with purified SOR metal-derivatives. **M**, marker proteins with the corresponding band sizes in kDa. SOR protein preparations derivatized with the following metals: **Ru**, ruthenium; **Ga**, gallium; **Cu**, copper; **V**, vanadium; **Mg**, magnesium; **Ni**, nickel; **Fe**, iron; **Mn**, manganese; **Co**, cobalt.

Alternatively, *E. coli* BL21 Codon Plus cells containing the pASK.05-SOR plasmid that was used to produce recombinant *Aa*SOR (Urich *et al.*, 2004) were grown in M9 minimal medium (Sambrook and Russell, 2001). The cells were induced with anhydrotetracycline at an OD_{600nm} of 0.5 and 10 µM of the corresponding transition metal salt ($CoSO_4$, $MnCl_2$ or $NiSO_4$) were added. Bacterial growth was observed in presence of $MnCl_2$, but not with $CoSO_4$ or $NiSO_4$. The cells were harvested by centrifugation after 5 days of incubation with a yield of 3 g/l wet cell mass. They were eventually disrupted as described in chapter 2, and the recombinant protein was purified via Strep-tag chromatography.

4.2.5. Characterization of metal derivatives of the *Aa*SOR

Metal-substituted SORs and a metal-free sample were analyzed for SOR activity using standard procedures (see chapter 2) and using the corresponding metal-containing buffers as negative control. The reaction was stopped by transferring the reaction tubes at appropriate time points (0, 4, 8, 16, 24, 32 min) to ice water. These time intervals were chosen due to the comparably low activity of the metal-substituted SOR fractions.

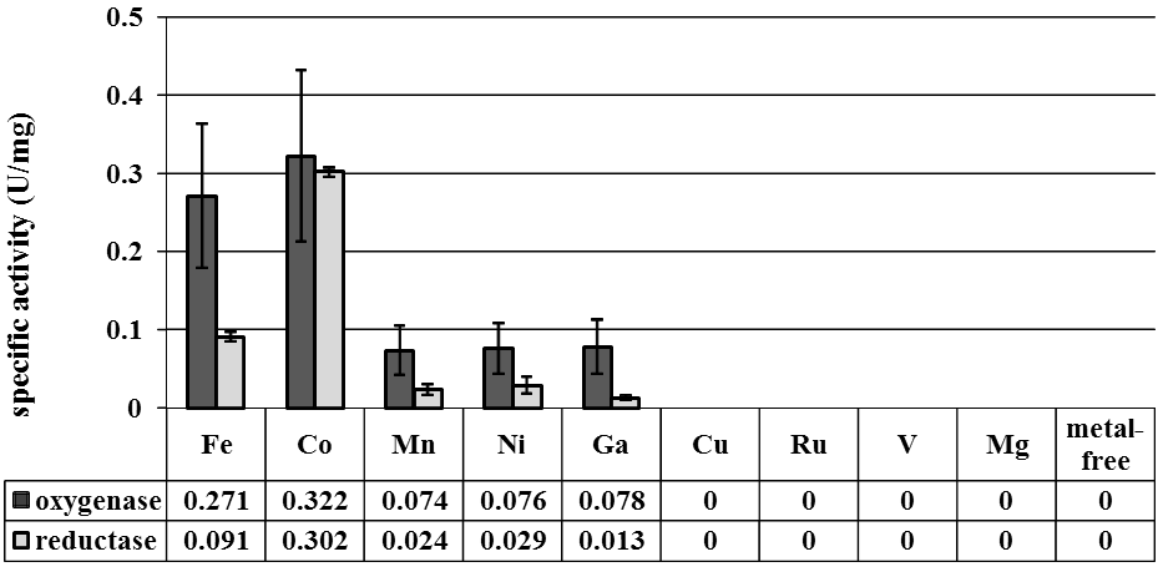

	Fe	Co	Mn	Ni	Ga	Cu	Ru	V	Mg	metal-free
oxygenase	0.271	0.322	0.074	0.076	0.078	0	0	0	0	0
reductase	0.091	0.302	0.024	0.029	0.013	0	0	0	0	0

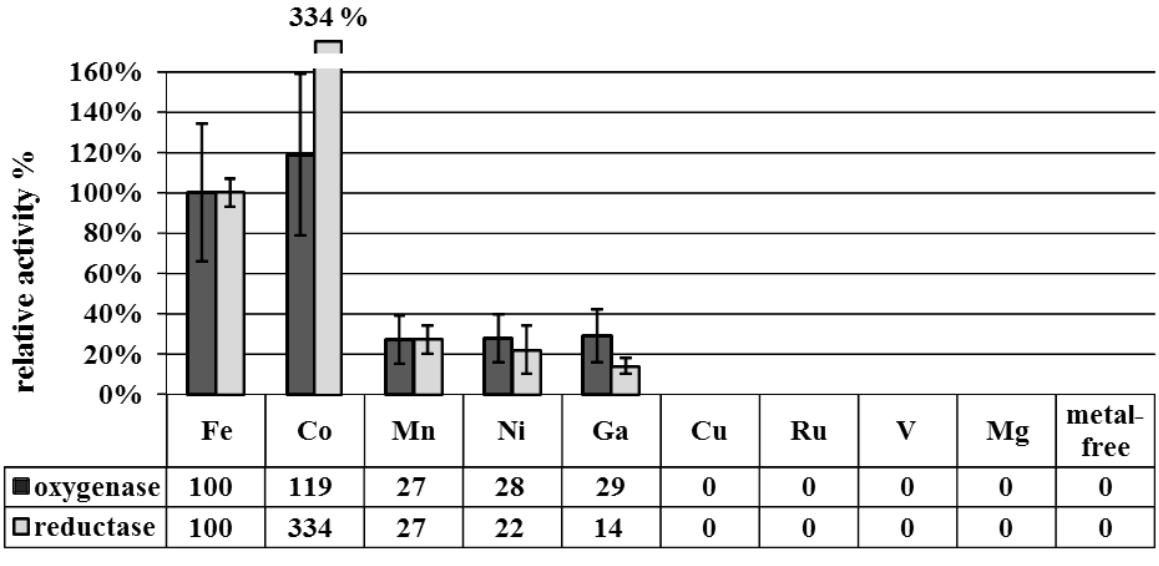

	Fe	Co	Mn	Ni	Ga	Cu	Ru	V	Mg	metal-free
oxygenase	100	119	27	28	29	0	0	0	0	0
reductase	100	334	27	22	14	0	0	0	0	0

Figure 4.9 Specific activities and relative activities of refolded SOR metal derivatives. Black columns: oxygenase activity, gray columns: reductase activity. Specific activities are average values of three measurements from three independent preparations.

A very low specific SOR activity was observed in case of every refolded and metal-derivatized SOR protein (also with Fe). As a consequence, high amounts of protein (50 µg) were used for each measurement. Activity of the refolded Fe-containing SOR was set to 100 % and the different samples were compared to the Fe enzyme. SOR activity was observed for the cobalt-, manganese-, nickel- and gallium-containing derivatives, while the copper-, ruthenium-, vanadium- and magnesium-containing derivatives were enzymatically inactive (Figure 4.9). The oxygenase activity of the cobalt-containing SOR (Co-SOR) was comparable to the Fe enzyme. In contrast, the Co-SOR showed a more than threefold higher reductase activity. Residual enzyme activity of approximately 30 % was observed for the Mn^{2+}-, Ni^{2+}- and Ga^{3+}-derivatives.

The metal content of each active metal-derivative was determined via TXRF (Total Reflection X-Ray Fluorescence) analysis to verify that SOR activity is reflected by the corresponding metal and not by residual iron or other contaminants. All samples were dialysed against 10 mM Tris/acetate buffer pH 7.2 to reduce high chloride background emission during the TXRF analysis. The SOR derivatives were subsequently concentrated using a vacuum centrifuge to a final concentration of about 20 µM and stored at -20°C. All measurements were performed and analyzed by Claudia Rittmeyer (AG Kolbesen, now AG Terfort, Goethe-Universität, Frankfurt, Germany). Each sample was measured five times, while data for the metal-free SOR could not be obtained due to technical problems of the instrument. Results for the TXRF analysis are summarized in Table 4.2.

Table 4.2 Metal and protein concentrations measured by TXRF analysis with calculated values of metal occupancy of the metal center within the active site.

Concentration	**Fe-SOR**	**Co-SOR**	**Mn-SOR**	**Ni-SOR**	**Ga-SOR**
SOR (µM)	21	20	20	24	20.66
Metal	9 µM Fe	41 µM Co	3 µM Mn	11 µM Ni	0.2 µM Ga
Occupancy	43 %	205 %	15 %	46 %	1 %
Fe (µM)	9	1.4	0	0.6	0.6
Cu (µM)	0.5	0.4	0.3	1	4
Other contaminants					4 µM Ni

The metal content measurements indicated that the respective metals were present substoichiometrically in the corresponding samples. The Co-derivative was the exception with two cobalt atoms determined per monomer. The relative iron and copper background values ranged from 2 - 7 % in almost all samples. The situation was more complicated for the gallium-containing protein (Ga-SOR). Only 1 % gallium occupancy was observed, while the relative content of iron was around 3 %. The relative copper content was around 19 % and additionally 19 % Ni atoms were detected, suggesting that the Ga-SOR activity might not be the result of gallium within the active site.

Electron paramagnetic resonance (EPR) spectroscopy was performed with biochemical active metal-derivatized SORs to investigate whether the oxidation state of the respective metal changes, when the protein is incubated with sulfur at high temperatures, as already demonstrated for the "as isolated" *Aa*SOR (Urich *et al.*, 2004). In those experiments, the Fe^{3+} signal disappeared in EPR spectra upon incubation with sulfur or after addition of dithionite due to its reduction to the EPR-silent Fe^{2+} species. The EPR spectra of the

original *Aa*SOR showed an isotropic resonance at g = 4.3, which is consistent with the presence of a mononuclear non-heme iron center in the ferric high-spin state (Urich *et al.*, 2004). Even though the oxidation state of iron changed upon catalysis, it remained unclear, whether such a valence change is mandatory for SOR activity. The refolded SOR derivatives were concentrated to a final concentration ranging between 187 - 250 µM. A small amount of ascorbic acid (10 µM) was added to each sample in order to minimize the background signal of ferric iron found in every sample. The SOR proteins were flash-cooled in liquid nitrogen and stored until usage. All EPR spectroscopy experiments were performed by Miguel Teixeira (ITQB, Oeiras, Portugal). Besides the expected iron signal at g = 4.3, every spectra contained a minor signal at g ~ 2.0 that had its source from residual Cu^{2+} in the protein preparations. The EPR spectra of the refolded Fe-containing protein showed the expected Fe^{3+} signal at g = 4.3 and a small copper peak (Cu^{2+}) at g ~ 2.0. Both signals decreased after incubation with sulfur at 80°C (Figure 4.11).

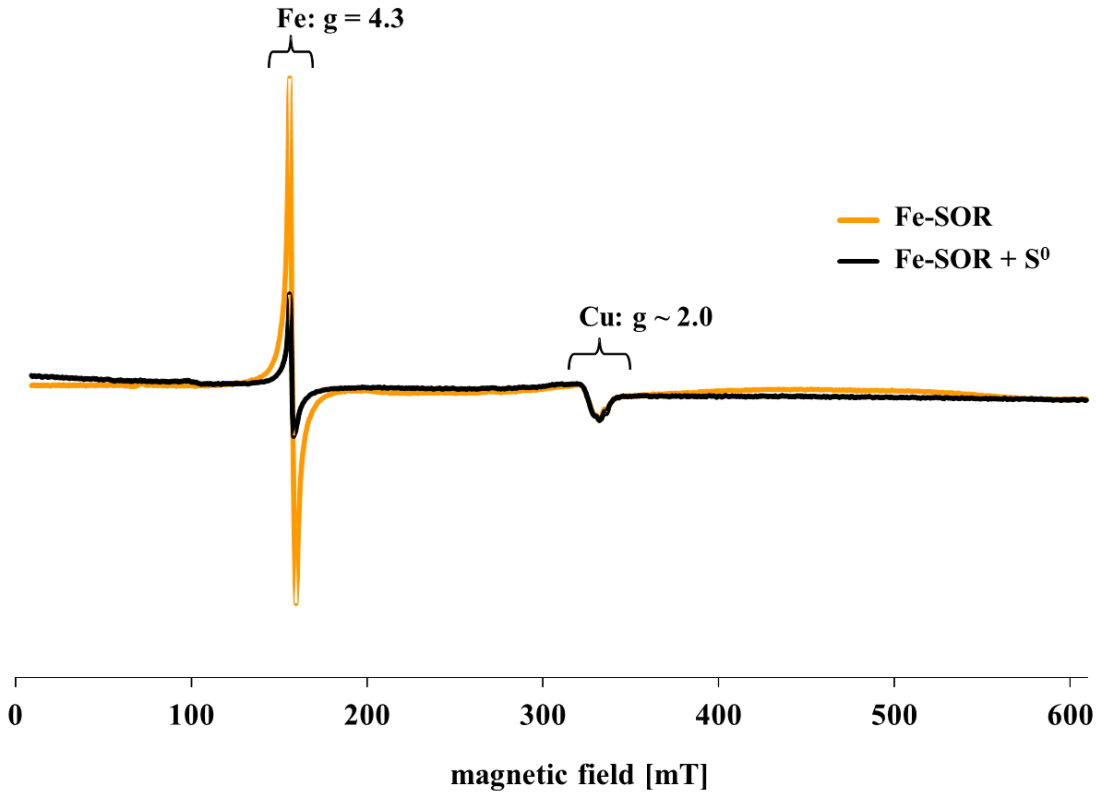

Figure 4.11 EPR spectrum of refolded Fe-SOR. Temperature 8.4 K, 2.0 mW microwave power and 193 µM protein. Fe-SOR is depicted before (yellow) and after incubation with elemental sulfur (dark blue).

No signals except those originating from residual iron or copper were expected for the Ga-substituted SOR (Ga-SOR), because of the diamagnetic nature of the redox-inactive Ga^{3+}. Residual iron and copper peaks were comparable to the signal intensity of the metal-free SOR (Figure 4.12), suggesting that the SOR activity cannot be attributed to residual iron but rather to the metal incorporated.

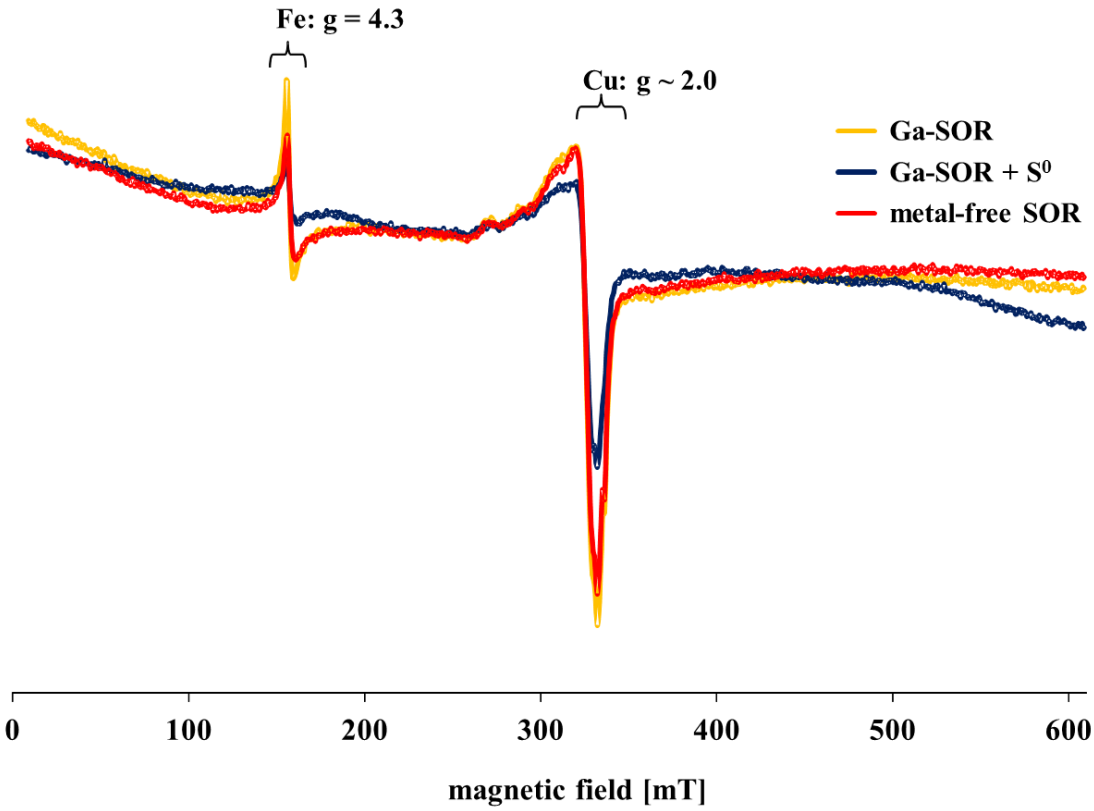

Figure 4.12 EPR spectra of refolded Ga-SOR in comparison with metal-free SOR. Temperature 8.4 K; protein concentration 187 µM; microwave power 2.0 mW. Ga-SOR is depicted before (yellow) and after incubation with elemental sulfur (dark blue); metal-free SOR before incubation with sulfur is depicted in red.

EPR spectra of the Fe-containing SOR and of the Ga-SOR were compared to each other in order to examine the signal intensity of the Fe-signal at g = 4.3. It was shown that the iron signal intensity of the Ga-SOR was 12-fold lower than the iron signal of the Fe-containing SOR (Figure 4.12).

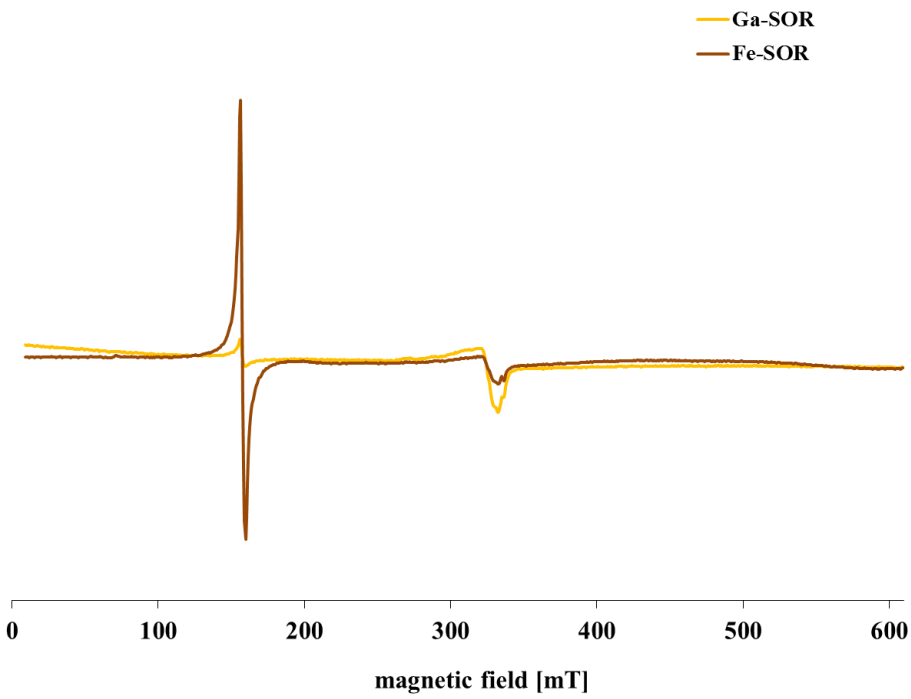

Figure 4.13 Comparison of EPR spectra of refolded Ga-SOR and Fe-SOR. Ga-SOR is depicted in yellow, Fe-SOR is shown in brown.

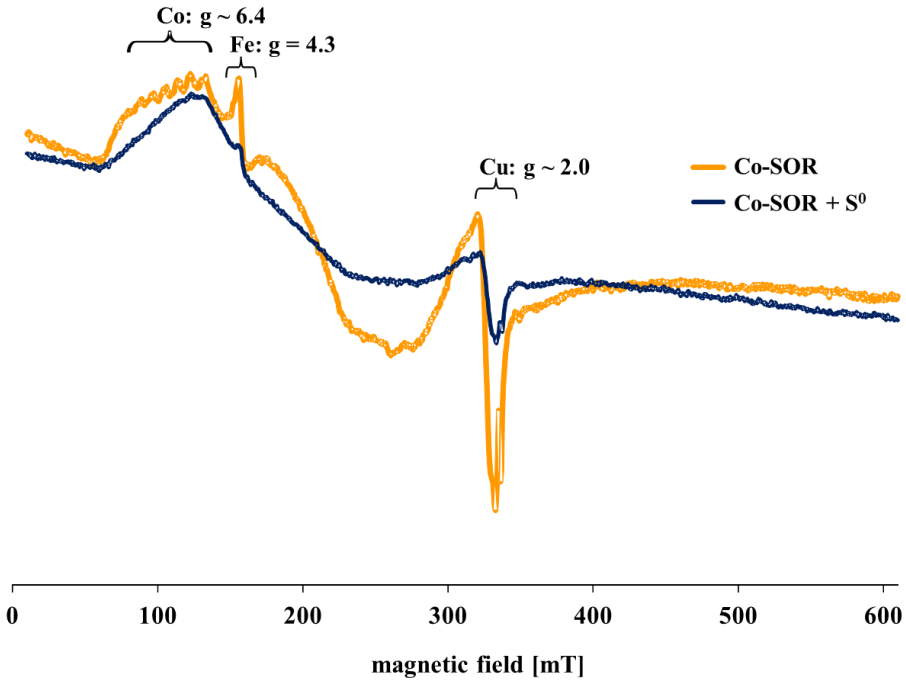

Figure 4.14 EPR spectra of Co-SOR. Temperature 8.4 K; protein concentration 250 µM; microwave power 2.0 mW. Co-SOR is depicted before (yellow) and after incubation with elemental sulfur (dark blue).

The Co-substituted SOR derivative showed a distinct signal indicative for a high spin Co^{2+} species (S = 3/2) with a barely resolved hyperfine splitting interaction pattern (nuclear spin I = 7/2) at g ~ 6.4, which vanished after incubation with sulfur (Figure 4.14). Iron and copper signals were observed and both signals decreased after sulfur incubation.

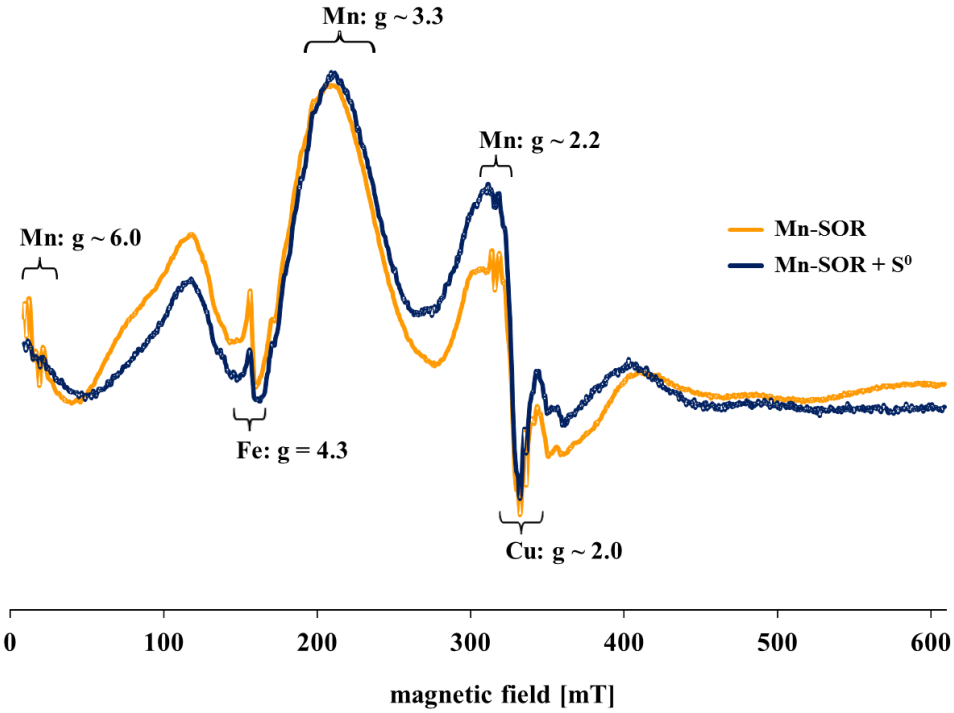

Figure 4.15 EPR spectra of Mn-SOR. Temperature 8.4 K; protein concentration 232 µM; microwave power 2.0 mW. Mn-SOR is depicted before (yellow) and after incubation with elemental sulfur (dark blue).

The Mn-SOR EPR spectra showed minor signals at g = 4.3 and g ~ 2.0, both indicative for residual Fe and Cu. Characteristic signals for a Mn^{2+} species at g ~ 2.2 (near the Cu signal), a broad signal at g ~ 3.3 (near the Fe signal) and a small signal at g ~ 6 were observed before and after sulfur incubation, even though the signal intensities changed slightly (Figure 4.15). The Ni-SOR derivative did not exhibit any signals except the iron and copper background, which was expected from EPR-silent Ni^{2+} species (not shown).

4.2.6. Crystallization of the Co-SOR

The Co-derivatized protein was crystallized in order to investigate potential changes of the metal coordination site and to examine the presence of the second cobalt atom detected by the TXRF measurement. Furthermore, a wavelength scan of the crystal combined with analyses of anomalous scattering data would provide information, whether the activity of the Co-SOR can be attributed to incorporated cobalt or to residual iron. The Co-SOR was retained after EPR spectroscopy and concentrated to 14.90 mg/ml. The first crystallization trials were carried out using the same conditions that were originally used to crystallize the original *Aa*SOR (Urich *et al.*, 2005a).

Crystal formation was observed at 32°C after few hours of incubation in 0.1 M NaCl / 0.1 M sodium acetate buffer pH 4.5 including 8 % MPD (2-Methyl-2,4-pentanediol). The concentration of the precipitant MPD was slightly increased from 8 % to 12 % in order to control crystal formation. Two different crystal forms were obtained, hexagonal- and prism-shaped (Figure 4.16). The latter crystal form had dimensions up to 0.25 mm and 0.1 mm. The Co-SOR containing protein solution featured a reddish-brown color, even though UV/Vis spectra of the Co-SOR did not show any signals indicative for cobalt (not shown). In contrast, all crystals were colorless, independent of the buffer condition. Reddish-brown precipitate formed in every crystallization trial of the Co-SOR, most likely resulting from adventitious Co. The hexagonal-shaped crystal was deeply buried within the precipitate, which impeded measurements of the crystal dimensions and the photographic documentation. However, all Co-SOR crystals were transferred to a cryoprotectant solution containing 0.1 M NaCl / 0.1 M sodium acetate buffer pH 4.5 with 20 % MPD and 25 % glycerol. The crystals were flash-cooled in liquid nitrogen and stored for synchrotron radiation experiments.

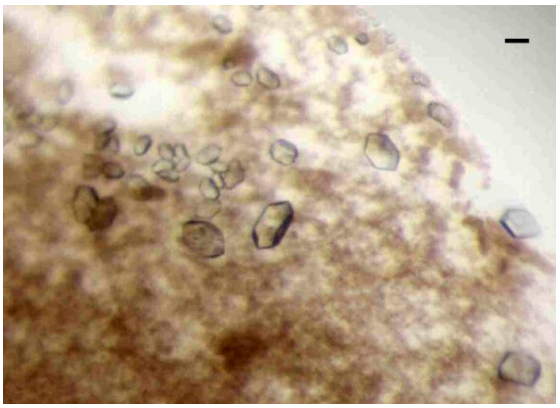

Figure 4.16 Mix of prism-shaped Co-SOR crystals grown in 0.1 M NaCl / 0.1 M sodium acetate buffer pH 4.5 and 12 % MPD. The black bar represents 0.1 mm.

Anomalous scattering data was collected at different wavelengths in order to verify whether cobalt or iron or even a cobalt/iron mixture is present at the active site (see chapter 2 for details). "Heavy" elements such as cobalt or iron usually exhibit anomalous scattering, when the wavelength of the incident X-ray beam is above the element's absorption edge. A fluorescence scan of the prism-shaped crystal gave a first hint that both metals might be present at the active site of the Co-SOR (Figure 4.17). Subsequently, the absorption K-edge of cobalt was determined by Pedro Matias (ITQB, Oeiras, Portugal) at the ESRF using the CHOOCH software (Evans and Pettifer, 2001), since theoretical values may differ from those determined experimentally, depending on spin and charge of the respective metal.

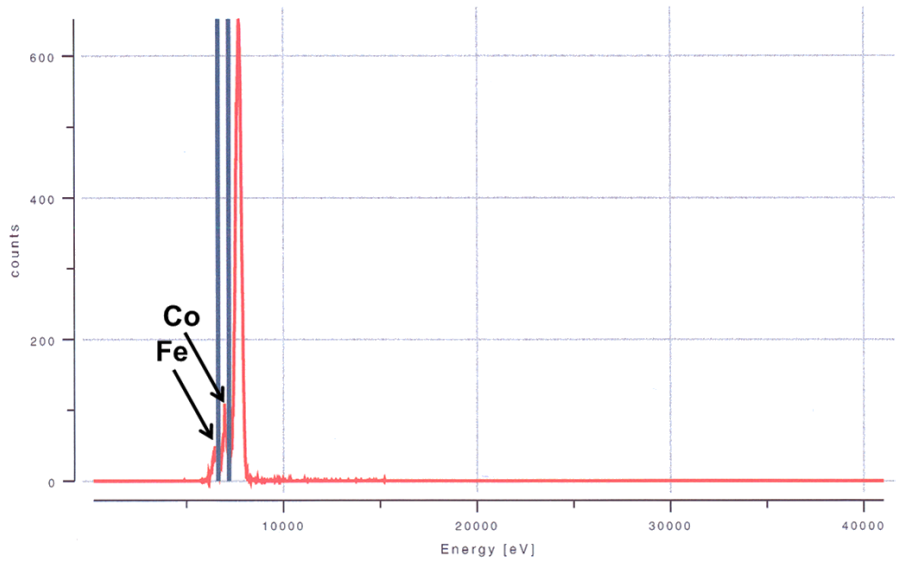

Figure 4.17 Fluorescence scan of the prism-shaped Co-SOR crystal with Fe and Co signals indicated by black arrows. X-axis, energy of the incident X-ray beam; Y-axis (counts) represents the intensity of the fluorescence signal.

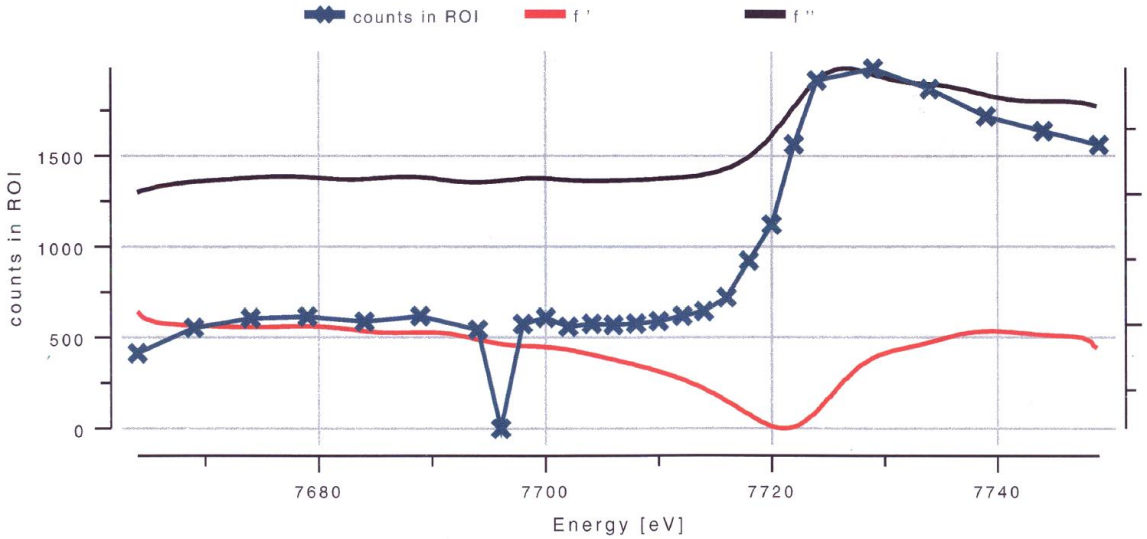

Fig 4.18 Experimental determination of the Co absorption K-edge using a prism-shaped crystal. X-axis, energy of the incident X-ray beam; Y-axis, signal intensity. Both components of the anomalous scattering signal are depicted with f' (red line) and f'' (black line). The experimental fluorescence signal intensities are represented by blues crosses, and their interpolation shown by the blue line.

According to the previous fluorescence scan, the region of interest (ROI) for the determination of the cobalt absorption K-edge was selected between 7650 and 7750 eV. The theoretically calculated absorption K-edge for cobalt is at 7709 eV (http://csrri.iit.edu/cgi-bin/period-form?ener=&name=Co), corresponding to a wavelength of 1.61 Å. The data differed slightly from the experimentally value identified at 7727 eV, which corresponds to a wavelength of 1.60 Å (Figure 4.18). Anomalous data was collected from the high and low energy sides of the Co K-absorption edge to determine whether iron or cobalt is coordinated at the active site.

Two datasets were collected at a wavelength of 1.5841 Å (corresponds to 7827 eV) and 1.6257 Å (corresponds to 7627 eV), respectively. The anomalous signal of iron but not of cobalt can be detected at an energy state lower than the Co absorption edge, whereas anomalous scattering of both metals can be observed at higher energy levels. The very high energy remote dataset was measured at 0.9779 Å to optimize the highest possible resolution, since absorptions errors are minimized at lower wavelengths. Prism-shaped crystals diffracted to 1.98 Å resolution with the tetragonal space group I4 (International Tables for Crystallography number: 79) and unit cell dimensions $a = b = 161.64$ Å and $c = 153.97$ Å with six monomers in the asymmetric unit. Hexagonal-shaped crystals also diffracted to 1.98 Å resolution with the cubic space group I432 (International Tables for Crystallography number: 211) and unit cell dimensions $a = b = c = 159.1$ Å, containing one monomer in the asymmetric unit (Table 4.3). A rigid body refinement was carried out for the Co-SOR that crystallized in space group I4. Molecular replacement was performed for the Co-SOR that crystallized in space group I432 to solve the phase problem. Rigid body refinement and molecular replacement were carried out using the PHENIX software suite and the original *Aa*SOR as template. Both datasets were manually improved using COOT and refined using PHENIX to obtain the best phases for the anomalous difference map. The anomalous difference maps were created for the low and high energy dataset of both crystals using PHASER from the PHENIX software suite.

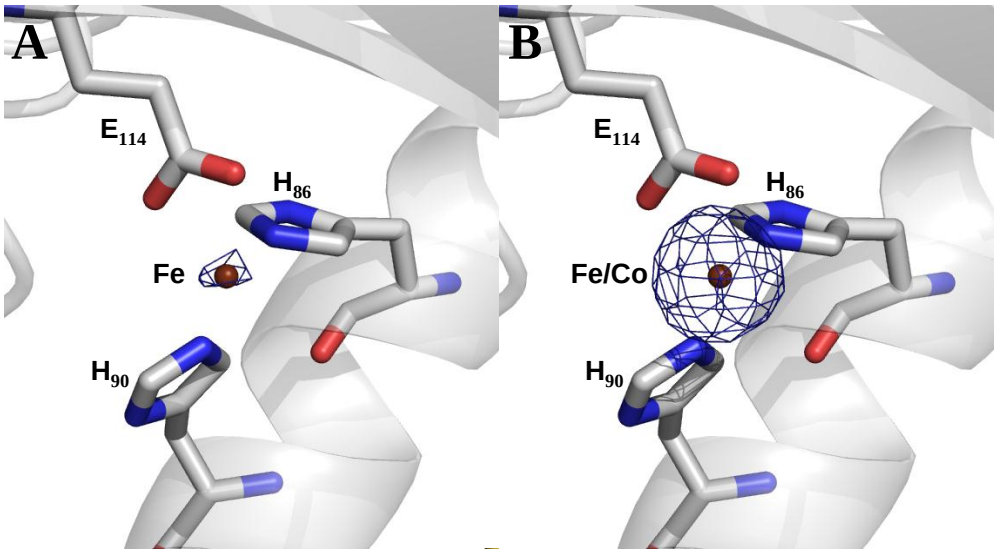

Figure 4.19 Stick and ribbon representation of the Co-SOR (space group I4) metal center; color representation: red - oxygen, blue - nitrogen, and white - carbon. (**A**) Anomalous difference electron density map of iron anomalous scattering, derived from the low energy dataset and contoured at 8.0 σ is shown in blue mesh. The iron atom is represented by the orange sphere. (**B**) Anomalous difference electron density map of iron and cobalt anomalous scattering, derived from the high energy dataset and contoured at 8.0 σ is shown in blue mesh. The iron /cobalt mixture in the active site is represented by the orange sphere.

The low energy dataset (1.6257 Å) of the Co-SOR crystallized in space group I4 showed an anomalous signal for iron at the metal center (Figure 4.19). In contrast, the high energy dataset (1.5841 Å) showed anomalous signals for both cobalt and iron, suggesting that both metals are featured at the catalytic center. At 1.6257 Å, only Fe contributes to the anomalous signal (3.5 electrons). At 1.5841 Å, Co has a slightly more intensive anomalous signal (3.89 electrons) than Fe (3.30 electrons), suggesting that more Co than iron is present at the catalytic center. Support comes from observations when the anomalous difference electron density maps of the low and high energy dataset were contoured at the same level and compared to each other (Figure 4.16). Examination of the datasets of the second Co-SOR structure (space group I432) led to similar conclusions (not shown). Analyses of the high energy remote datasets of both crystals, measured at 0.9779 Å, did not show any indication for a second cobalt atom within the Co-SOR structure, as suggested by TXRF measurements. The coordination distances between the metal (Co/Fe) and the corresponding ligands changed slightly between 0.01 - 0.28 Å (space group I4) or 0.02 - 0.43 Å (space group I432), respectively. Even though, the slightly distorted octahedral geometry of the metal center did not change. Additional electron density was refined at the S-γ atom of Cys_{31} for both datasets, clearly indicating the presence of a cysteine persulfide. Both metal-coordinating water molecules were visible, resembling the situation for the original *Aa*SOR (Urich *et al.*, 2006; Figure 4.20).

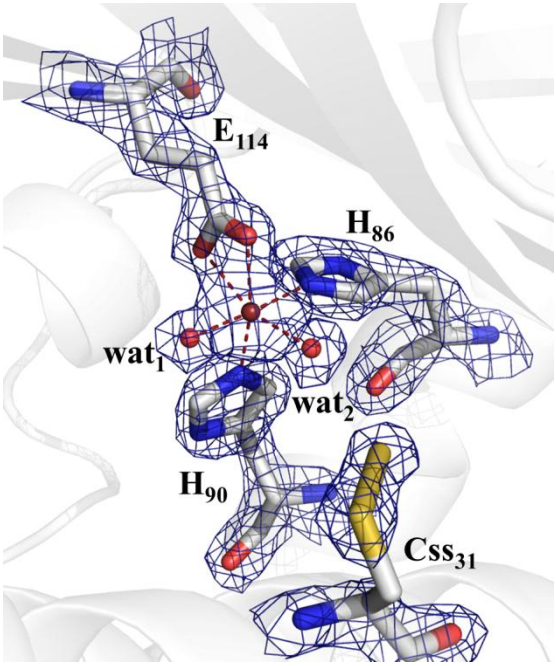

Figure 4.20 Stick and ribbon representation of the Co-SOR active site (space group I4); color representation: red - oxygen, blue - nitrogen, sulfur - yellow and white - carbon. Water molecules are indicated as red spheres and the iron / cobalt mixture is represented by a dark orange sphere. The 2 F_o-F_c electron density map contoured at 2.0 σ is shown in blue mesh.

Table 4.3 Diffraction data processing and refinement statistics of the different SOR structures.

	Co-SOR (tetra)	Co-SOR (cubic)	*Aa*SOR	*Aa*SOR + PS	*Aa*SOR + TS	*Aa*SOR $E_{87}D$
Source	SLS X06DA	SLS X06DA	In-house	ESRF id23-1	ESRF id23-1	SLS X06DA
Space group	I4	I432	$P6_322$	$P6_322$	$P6_322$	I4
Unit cell parameters (Å)	$a = b = 161.79$, $c = 154.07$	$a = b = c = 158.97$	$a = b = 158.71$, $c = 228.09$	$a = b = 161.74$, $c = 230.41$	$a = b = 161.02$, $c = 229.49$	$a = b = 161.71$, $c = 154.12$
Wavelength	0.9779	0.9779	1.5418	1.9000	1.9000	0.9779
Number of unique intensities	137,323	24,145	66,735	17,290	42,555	198,904
Redundancy	3.8	11.3	5.27	7.2	22.0	4.0
Resolution (outer shell) (Å)	40.45 – 1.98 (2.09 – 1.98)	39.47 – 1.98 (2.09 – 1.98)	58.86 – 2.40 (2.45 – 2.40)	51.76 – 3.67 (3.87 – 3.67)	59.59 - 2.98 (3.14 – 2.98)	34.78 – 1.75 (1.84 – 1.75)
Completeness (outer shell) (%)	100 (100)	100 (100)	99.8 (99.2)	86.8 (86.8)	100 (99.6)	100 (100)
R_{merge*} (outer shell) (%)	10.5 (55.8)	8.5 (30.5)	7.16 (25.18)	43.5 (75.0)	46.2 (220.6)	9.7 (67.7)
I / σ (I) (outer shell)	4.4 (1.6)	22.4 (6.5)	16.44 (3.78)	3.3 (2.1)	7.3 (2.7)	10.1
Wilson B (Å²)	19	15	34	0	83	19
Refinement						
Refined structure	1842 aa 1026 waters	307 aa 146 waters	1228 aa 451 waters	1228 aa 12 waters	1228 aa 115 waters	1842 aa 2086 waters
R_{work} (%)	16.79	17.08	16.96	16.78	16.67	16.63
R_{free} (%)	20.01	22.1	21.64	21.06	19.77	19.87
R (%)	16.95	17.48	17.20	17.21	16.84	16.66
Average ADP (Å²)	26.28	16.42	23.29	70.84	44.28	20.79
Bonds RMSD (Å)	0.008	0.014	0.016	0.012	0.013	0.008
Angles RMSD (°)	1.11	1.5	1.54	1.123	1.156	1.168

*$R_{merge} = \Sigma|I_o - \langle I \rangle| / \Sigma I_o$, where $\langle I \rangle$ is the average of symmetry equivalent reflections and the summation extends over all observations I_o for all unique reflections.

4.3. Discussion

4.3.1. Different *Acidianus* SOR structures represent different stages of catalysis

The superposition of the *Aa*SOR and *At*SOR (*A. tengchongensis* SOR-wt; PDB id: 3bxv) structures showed a high structural similarity between both proteins (Li *et al.,* 2008) however, significant differences were observed within the active site pocket. Whereas a persulfurated cysteine was refined for the original *Aa*SOR (Urich *et al.,* 2006), an unmodified cysteine was observed for the *At*SOR (Li *et al.,* 2008). The iron atom is sixfold coordinated at the *Aa*SOR structure, while it is fivefold coordinated in the *At*SOR structure, lacking one water ligand. It was assumed that these differences probably represent the SOR enzyme in different stages of the catalytic cycle (Li *et al.,* 2008). The *Aa*SOR was crystallized in order to clarify these differences. The protein formed crystals in buffer conditions that differed from the original *Aa*SOR crystallization conditions (Urich *et al.,* 2005a). The newly obtained crystals diffracted to 2.40 Å resolution with the hexagonal space group $P6_322$. The refined "new" *Aa*SOR dataset displayed the Fe atom in a fivefold coordination state, similar to the *At*SOR structure (Figure 4.3). It was previously discussed that the lack of the second water ligand might represent the SOR in a different reaction stage (Li *et al.,* 2008). In the case of the newly crystallized *Aa*SOR, the absence of the second Fe-coordinating water molecule most likely results from the comparably low resolution of the dataset (2.40 Å), since distinct water molecules become visible and reliable only at higher resolutions (Carugo and Bordo, 1999). It has to be taken into consideration that the original *Aa*SOR structure (PDB id: 2cb2; Urich *et al.,* 2005a; Urich *et al.,* 2006) was refined at 1.7 Å resolution. The absence of the second Fe-liganding water molecule caused by low resolution can also be applied to the *At*SOR structure, which was refined at 2.7 Å resolution (PDB id: 3bxv; Li *et al.,* 2008), suggesting that the *At*SOR does not represent a different reaction stage. Besides that, additional electron density at the S-γ atom of C_{31} was neither detected in the *At*SOR (Li *et al.,* 2008) nor in the newly crystallized *Aa*SOR structure, indicating an unmodified cysteine at this position. It was speculated that the absence of a cysteine persulfide might result from different purification methods used for both proteins (Carlos Frazão, personal communication). Prior to chromatography, the soluble *E. coli* extract containing the original recombinant *Aa*SOR was heat-treated in order to precipitate heat-labile *E. coli* proteins. This heating step was omitted during the purification of the newly crystallized *Aa*SOR, since considerable

amounts of the SOR protein precipitate as well. It is plausible that C_{31} becomes sulfurated during that heat treatment, while the additional sulfur atom most likely originates from the *E. coli* extract. The presence of an unmodified or a persulfurated cysteine may thus rather represent different activation states of the SOR.

4.3.2. A hydrogen bond network is present at the active site

The active site of the *Aa*SOR comprises the modifiable C_{31} and the mononuclear Fe center with its unusually low reduction potential. It was hypothesized that the reduction potential probably results from an H-bond network around the metal site, which might also influence SOR activity (Kletzin, 2008; Seyfarth, 2006). Site-directed mutagenesis was performed with members of such a network in order to investigate changes of enzyme activity. The mutants were originally constructed by K. Seyfarth (Seyfarth, 2006) or in the course of this work. T_{78}, R_{91} and E_{87} were changed into an alanine each, while the latter residue was also mutated into an aspartate. $E_{87}A$ and $R_{91}A$ both showed a high decrease of activity, consistent with previous observations of the $E_{87}A$ mutant (Seyfarth 2006). Contrarily, $E_{87}D$ yielded enzyme activity that was more than fourfold lower than the previously observed activity (Seyfarth, 2006). Although the $T_{78}A$ mutant was previously inactive (Seyfarth, 2006), new protein preparations showed half of the wild type activity. Those differences are most likely the result of different protein preparations, showing that distinct fluctuations can occur between different samples and enzyme activity assays. The highly diminished SOR activity in case of the $E_{87}A$ and the $R_{91}A$ mutant clearly indicates that an H-bond interaction between E_{87} and H_{86} or R_{91} is crucial for the enzyme. In contrast, the $T_{78}A$ mutant maintained around 50 % of the wild type activity, suggesting that amino acids interacting with Fe-coordinating water molecules are less important for the SOR activity. Substitutions of active site pocket-forming amino acids showed less pronounced effects in regard to enzyme activity. Both mutant proteins $M_{22}L$ and $M_{22}C$ did not change enzyme activity significantly. It could be assumed that these residues may play a role in the formation of the active site pocket without being essential for catalysis. Support comes from sequence alignments (Figure 1.9), showing that M_{22} is not conserved. In contrast, a highly conserved region is found around the essential C_{31} residue, including T_{34}. However, a $T_{34}S$ mutant was active, suggesting that the hydroxyl moiety of the side chain is important at that position and which could interact with other amino acids or water molecules at the active site.

Both mutant proteins $E_{87}A$ and $E_{87}D$ were prepared for crystallization to investigate structural changes within the active site pocket. $E_{87}D$ did form crystals, while it was not possible to crystallize the alanine counterpart. Analysis of the $E_{87}D$ protein structure demonstrated the successful mutation of the glutamate into an aspartate (Figure 4.7). Surprisingly, no Fe atoms were identified at the metal center, which contradicts the results of previous iron content measurements, where one iron atom per subunit had been detected (Table 4.1). A substoichiometric load of the metal centers may explain the low SOR activity of this mutant, which was expected to be more than fourfold higher than wild type activity (Seyfarth, 2006). However, a total absence of iron usually results in a completely inactive enzyme, which was apparently not the case for the $E_{87}D$ mutant. It can only be speculated upon for what reason iron was completely absent at the metal center. It is rather unlikely that the metal was lost during the crystallization process, so that the reasons remain unclear. Analysis of the second coordination sphere of the aspartate mutant revealed a hydrogen-bonding distance between D_{87} and H_{86} of 2.75 Å, which differed only by 0.02 Å from the wild-type enzyme. It has to be noticed that E_{87} is also replaced for an aspartate in some of the naturally occurring SOR sequences (see Figure 1.10), suggesting that the length of the side chain is less important than the presence of a negatively charged carboxylate. The binding distance between D_{87} and R_{91} expanded from 3.0 to 4.2 Å, making an interaction between both residues rather unlikely. If the enzyme activity of $E_{87}D$ is taken into account, it appears that a hydrogen bond to R_{91} is not essential for enzyme activity, which contradicts the highly diminished enzyme activity of the $R_{91}A$ mutant. Support comes from the 3D structure of the *Halothiobacillus neapolitanus* SOR, where a tyrosine residue represents the second coordination sphere. This tyrosine residue adopts the role of E_{87} by interacting with one of the iron ligands, but it is located distant from the R_{91} homolog (chapter 5). Apparently, the arginine rather interacts with other neighboring residues or water molecules to influence the SOR activity in a greater extent.

4.3.3. Redox change of the metal center is not strictly required for SOR catalysis

Inclusion bodies of *Aa*SOR were un- and refolded in presence of various metals such as Fe, Co, Mn, Ni, Ga, Cu, Mg or V to introduce the respective metal into the active site. The metal derivatives were measured for activity to demonstrate that Fe can be replaced by another metal, while SOR activity is maintained. The Cu-, Mg- and V-containing SOR-derivatives were completely inactive.

All other metal-derivatives showed a very low specific enzyme activity, which was the result of insufficient metal incorporation into the active site. The Co-SOR demonstrated an oxygenase activity that was comparable to the Fe enzyme but the reductase activity was elevated up to threefold. Mn-, Ni-, and Ga-containing SORs showed a residual activity around 30 %. Biochemically active Ni- and Co-SOR derivatives were not surprising: both transition metals share, together with iron, similar chemical properties and are often grouped together to the so-called "iron triad". Metal content measurements using TXRF indicated that the respective metals were substoichiometrically present in the corresponding samples with the exception of the Co-SOR. Two cobalt atoms per monomer were determined for the Co-derivative. The iron and copper background was around 5 % in all measured samples. The situation was ambiguous for the Ga-SOR. While the gallium occupancy was very low, higher amounts of iron, copper and nickel were determined (Table 4.2), suggesting that SOR activity might rather result from residual iron and nickel at the active site. All enzymatically active SOR derivatives were studied via EPR spectroscopy to investigate potential changes of the metal's oxidation state. The ferric iron of the wild-type SOR was reduced to Fe^{2+} after incubation with sulfur, resulting in a concomitant decrease of the isotropic signal at g = 4.3 (Figure 4.11), similar to the results previously obtained for the same protein (Urich *et al.*, 2004). Co^{2+} in the high spin state showed a characteristic hyperfine splitting signal in case of the Co-SOR (Figure 4.14). Similar signals had also been observed for a Co-containing quercertinase (Merkens *et al*., 2008). Hyperfine interactions (also termed as hyperfine coupling) occur, when the unpaired electron interacts with neighboring nuclei, which may "split" the EPR signal (hyperfine splitting). The hyperfine splitting vanished and the signal intensity decreased but the cobalt ion remained in the same oxidation state after incubation with sulfur. In contrast, a reduced Co^{1+} species would be "EPR-silent", since no unpaired electron would be present that could be influenced by a magnetic field. The disappearance of the hyperfine interaction signal might result from small modifications such as structural rearrangements that occur during catalysis at the cobalt site (Miguel Teixeira, personal communication). The Mn-derivative showed several signals which were indicative for manganese in a +2 oxidation state (Figure 4.15; see also Gaffney *et al.,* 2001). The signal intensity decreased marginally without changing the oxidation state of manganese, since a Mn^{1+} species would be "EPR-silent" as well. Because of its diamagnetic nature, gallium did not show any other signals than the iron and copper background (Figure 4.12). The intensity of the iron signal was comparable to the same signal from a "metal-free" SOR, suggesting that the Ga-SOR

activity might not result from residual iron but from Ni contaminations at the active site. Since Ni^{2+} species are "EPR-silent" no signal was observed for the Ni-SOR before incubation with sulfur, suggesting that Ni remains in an "EPR-silent" Ni^{2+} oxidation state. The missing change of the oxidation state in the Co- and Mn-SOR gave a first hint that the SOR reaction might not require a redox change for catalytic activity. Instead, little structural changes may occur at the metal center during catalysis, as indicated by small changes in the signal intensity of the Mn- and Co-SOR EPR spectra. The Co-derivatized SOR was subsequently crystallized in order to examine those changes and to locate the second cobalt atom, which was indicated by TXRF measurements.

4.3.4. Co-derivatized SOR is highly similar to the Fe-containing wild-type enzyme

Crystallization of the Co-SOR gave rise to hexagonal-shaped and prism-shaped crystal forms resulting from slight modifications of the crystallization buffer. Prior to data collection, a fluorescence scan was performed and the cobalt absorption K-edge was experimentally determined from the crystals (Figure 4.17 + 4.18). The fluorescence scan demonstrated the presence of cobalt and iron presumably at the active site. Anomalous data were collected from both energy sides of the cobalt absorption edge. Analyses of the data verified the presence of both cobalt and iron at the active site with a higher amount of cobalt in both crystals, so that enzyme activity likely derives from both transition metals. A second cobalt atom was not detected in either of the two different crystal datasets, suggesting that it probably had been unspecifically attached to the outer shell of the protein. This is supported by the observation that colorless crystals formed from the reddish-brown colored Co-SOR protein solution, while brownish precipitate formed outside the crystals during the crystallization process. If the additional cobalt atom was loosely attached to the outer sphere of the protein, it is conceivable that it might have precipitated, forming a red-colored precipitate. Further investigations of the very high energy remote datasets measured at 0.9779 Å did not show any structural changes within the metal site as proposed by EPR spectroscopy (Figure 4.20). Both water ligands were visible at the metal center of both Co-SOR datasets as already observed for other high resolution SOR datasets (*e.g.* $E_{87}D$ and the original *Aa*SOR). The coordination distances between the ligands and the Fe/Co atoms at the active site varied slightly but the distorted octahedral geometry of the coordination sphere was maintained (Figure 4.20).

It is likely that structural changes at the active site might have occurred within a very short time period during catalysis and that the original state was restored. Additional electron density was refined at the S-δ atom of Cys_{31} in both Co-SOR structures, indicating a cysteine persulfide. The heat treatment of the protein sample is probably responsible to give rise to the cysteine persulfide. In case of the Co-SOR, the heating step occurred during inclusion body purification, when unfolded inclusion bodies were heated to 60°C in order to dissolve SOR inclusion bodies. The results from the present chapter demonstrate that the second coordination sphere of the enzyme is essential for catalysis although it is unknown to which extent it influences the low redox potential of the SOR. Moreover it was shown that Fe can be replaced by other transition metals without losing enzyme activity. EPR experiments with biochemically active non-iron SOR proteins suggested that a redox change of the metal is not necessarily required for catalysis, pointing to a non-redox reaction.

5. Characterization of the *Halothiobacillus neapolitanus* SOR

5.1. Introduction

The sulfur oxygenase reductase of the hyperthermophilic archaeon *Acidianus ambivalens* represents the best-studied member of the SOR protein family. The enzyme can be found among a variety of thermoacidophilic sulfur-oxidizing archaea and bacteria. The recently sequenced genomes of the mesophilic bacteria *Desulfomicrobium baculatum* and *Halothiobacillus neapolitanus* revealed that SORs are not restricted to thermophilic microorganisms. *Halothiobacillus neapolitanus* DSMZ 15147 was first isolated from corroded concrete sewers in Australia (Parker, 1947) and described as *Thiobacillus* X (Parker and Prisk, 1953). It is an obligately chemolithoautotrophic mesophile growing optimally at 28 - 32˚C at neutral pH and with sulfur, thiosulfate or tetrathionate as electron donors (Kelly and Wood, 2000). Although structural and biochemical information of different SORs from (hyper-) thermophilic microorganisms is accessible, the question arose, whether these findings can be applied to a SOR derived from a mesophile. Moreover, numerous *Acidianus ambivalens* SOR variants were generated via site-directed mutagenesis and analyzed in order to shed light on the SOR reaction mechanism. Few of these mutants showed a significantly altered enzyme activity (see chapter 3 and 4; Urich *et al.*, 2005b). Therefore, the attention was turned to naturally occurring SOR variants from mesophilic microorganisms in order to reveal further residues, which are essential for the reaction mechanism of the enzyme. The following chapter focuses on the characterization of the recombinantly produced *Halothiobacillus neapolitanus* SOR (*Hn*SOR) and its similarities and differences with respect to the *Acidianus ambivalens* SOR wild-type (*Aa*SOR). The heterologous expression and purification system used for overproduction and purification of *Aa*SOR was set up for the *sor* gene of *H. neapolitanus* in order to yield high amounts of protein for biochemical purposes. Optimal conditions of the recombinant *Hn*SOR were determined by measuring enzyme activity at different temperatures and pH values. For further biochemical characterizations, the iron content of the protein was quantified and K_i values for zinc chloride were determined. Structural properties like secondary structure composition were investigated using CD spectroscopy and the particle size of the holoenzyme was estimated via Dynamic Light Scattering. Finally, the protein was crystallized to compare the structural architecture with the *Aa*SOR.

5.2. Results

5.2.1. Generation of a pASK_HnSOR plasmid

A BLAST analysis of the *Aa*SOR amino acid sequence revealed a homolog with a sequence identity of 40 % in the genome of the mesophilic bacterium *Halothiobacillus neapolitanus* c2 (ATCC 23641). A detailed examination confirmed a *sor*-encoding open reading frame (ORF) (locus tag: *Hneap_1222*), flanked by a putative ribonuclease H ORF and a putative FAD-dependent pyridine nucleotide-disulphide oxidoreductase ORF. Oligonucleotides were designed (HnSOR fwd and HnSOR rev, see Table 2.1 chapter 2) and the *sor*-encoding ORF was PCR-amplified using genomic *Halothiobacillus neapolitanus* DSM 15147 DNA as template. The PCR product was hydrolyzed with *Spe*I and *Eco*47III, purified and subsequently inserted into an *Xba*I/*Eco*47III cleaved pASK-SOR.05 expression vector that was originally used to produce recombinant *Aa*SOR (Urich *et al.*, 2004). The 3' end of the *sor* gene was fused to a sequence coding for a Strep-tag, a short peptide, which binds with high affinity to streptavidin and that can be used for purification by affinity chromatography (Skerra, 1994). After transformation of *E. coli* TOP10' cells with the ligation product, approximately 100 colonies were analyzed by colony-PCR that identified > 90 % as positive transformants. Plasmid DNA was extracted using a miniprep kit. When sequenced for validation, the *sor* genes of *H. neapolitanus* DSMZ 15147 and ATCC23641 were identical. The resulting plasmid pASK_HnSOR was then introduced into *E. coli* BL21-CodonPlus cells.

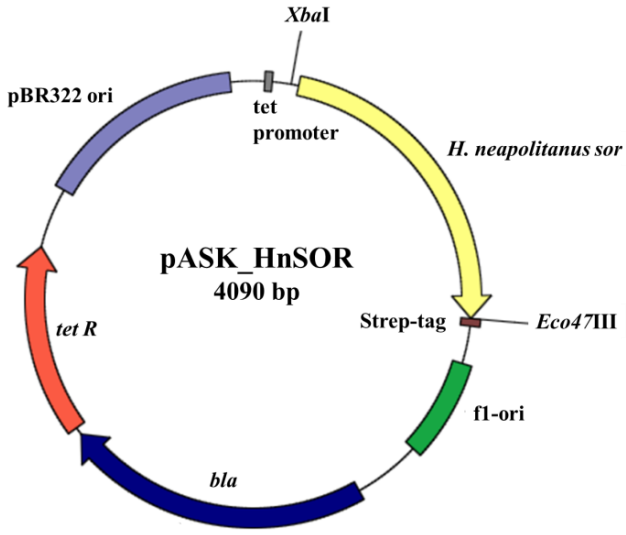

Figure 5.1 Map of pASK_HnSOR plasmid used for heterologous expression of the *H. neapolitanus sor* gene. The gene is expressed under control of a tetracycline promoter that is repressed by a TetR repressor and which can be induced by anhydrotetracycline (AHT). The *bla* gene encodes for a ß-lactamase that is used as selection marker.

5.2.2. Overproduction and purification of recombinant *Hn*SOR

After transformation of *E. coli* BL21-CodonPlus cells with pASK_HnSOR, protein overproduction was induced with anhydrotetracycline (AHT) after the addition of iron citrate to the growth medium. After 16 hours, the cells were harvested and disrupted using a high pressure homogenizer apparatus (see chapter 2 for details). Approximately 20 - 30 % of protein was present in soluble form, while about 70 % precipitated as inclusion bodies, similar to the observations for the *Aa*SOR. The soluble supernatant was either applied to Strep-tag gravity flow columns with 1 ml bed volume or to a Strep-tag column with a bed volume of 8 ml that was connected to an ÄKTA purifier system. Purification of the recombinant SOR was carried out according to the manufacturer's recommendations, yielding 11 - 18 mg of soluble recombinant *Hn*SOR protein per liter 2 x LB medium. Protein purity of *Hn*SOR was visualized by SDS-PAGE using 10 % SDS gels followed by Coomassie staining (Figure 5.2). Apart from the major SOR band corresponding to 36 kDa, smaller bands at approximately 25 kDa and at 30 kDa were observed and interpreted as proteolysis products of the SOR (see *Urich et al.*, 2004 and chapter 3). A small amount of purified *Hn*SOR protein was stored at –20°C, but enzymatic activity was completely lost after thawing. Therefore, *Hn*SOR preparations were kept mostly at 4°C or stored at -20°C after addition of 50 % glycerol, which prevented loss of activity.

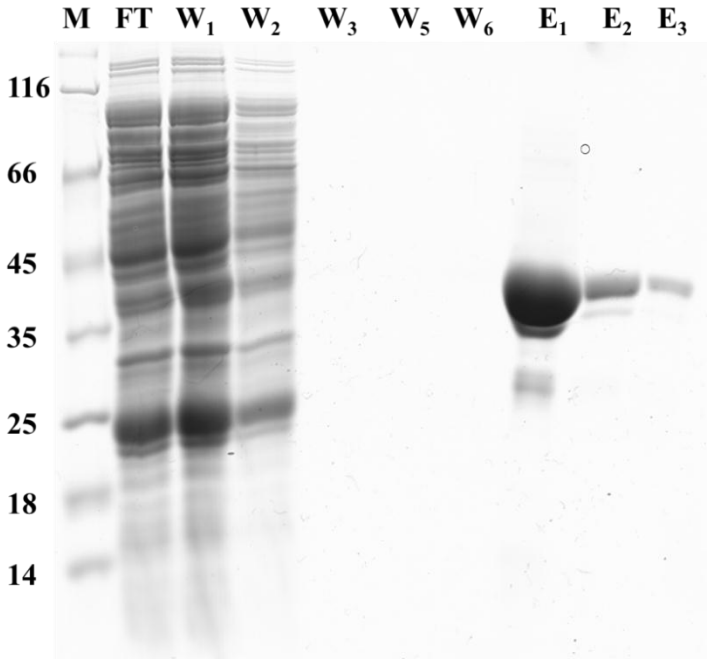

Figure 5.2 Coomassie-stained 10 % SDS-gel of purified *H. neapolitanus* SOR. (**M**) Protein size standard with the corresponding band sizes in kDa; (**FT**) flow-through of the column; (**W**) column wash steps (1, 2, 3, 5, 6); (**E**) elution fractions 1 - 3.

5.2.3. Biochemical characterization of the recombinant *Hn*SOR

Prior to enzyme activity measurements, the iron content of the protein was measured using the TPTZ-based method to determine the iron incorporation into each monomer. The average ratio was 1.64 Fe ± 0.33 atoms per protein monomer. The optimal pH and temperature of *Hn*SOR activity were determined using the SOR activity assay (Kletzin, 1989; Urich *et al.*, 2004) with different buffer systems. When *Hn*SOR was assayed in the standard Tris/HCl-containing buffer at 80°C and pH 7.2, an oxygenase activity of 4.1 U/mg and a reductase activity of 2.3 U/mg were obtained (not shown). A similar Tris/citrate buffer showed slightly higher oxygenase (6.1 U/mg) and reductase (2.8 U/mg) activities. Highly elevated SOR activity was observed by using a citrate/phosphate-based buffer that resulted in an oxygenase activity of 42.4 U/mg and in a reductase activity of 4.1 U/mg. Consequently, a citrate/phosphate buffer (0.1 M sodium citrate/ 0.2 M Na_2HPO_4; McIlvaine, 1921) including 2 % (w/v) elemental sulfur and 0.1 % Tween 20 was used to determine the pH optimum of the protein in a pH range from pH 5 - 8. For pH values exceeding pH 8, 0.2 M Na_2HPO_4 was titrated with a 0.1 M Na_3PO_4 solution to the desired pH. The SOR activity assay was carried out at 50°C due to extensive non-enzymatic sulfur disproportionation observed at high temperatures combined with high pH values (Kletzin, 1989; Steudel, 2003). Usually, 0.75 - 2.65 µg of purified HnSOR were added to 1 ml of ice cold assay buffer. The reaction was started by incubation of the reaction tubes in a heating block at 50°C. Amount of reaction products and specific activities were both determined colorimetrically as described in chapter 2. Oxygenase and reductase activity were observed between pH 5.4 and pH 11 with an optimal pH at 8.4 (Figure 5.3). At pH 12, it was no longer possible to distinguish between non-enzymatic sulfur disproportionation and enzymatic reaction. At slightly acidic conditions (pH 5.4 - pH 6.4), reductase and oxygenase activities were at comparable levels (Figure 5.3 and Table 5.1). Oxygenase activity significantly increased at neutral and especially at alkaline conditions: at pH 8.4, oxygenase activity peaked at 15.9 U/mg, which resulted in a fivefold excess to the reductase activity of 3.27 U/mg.

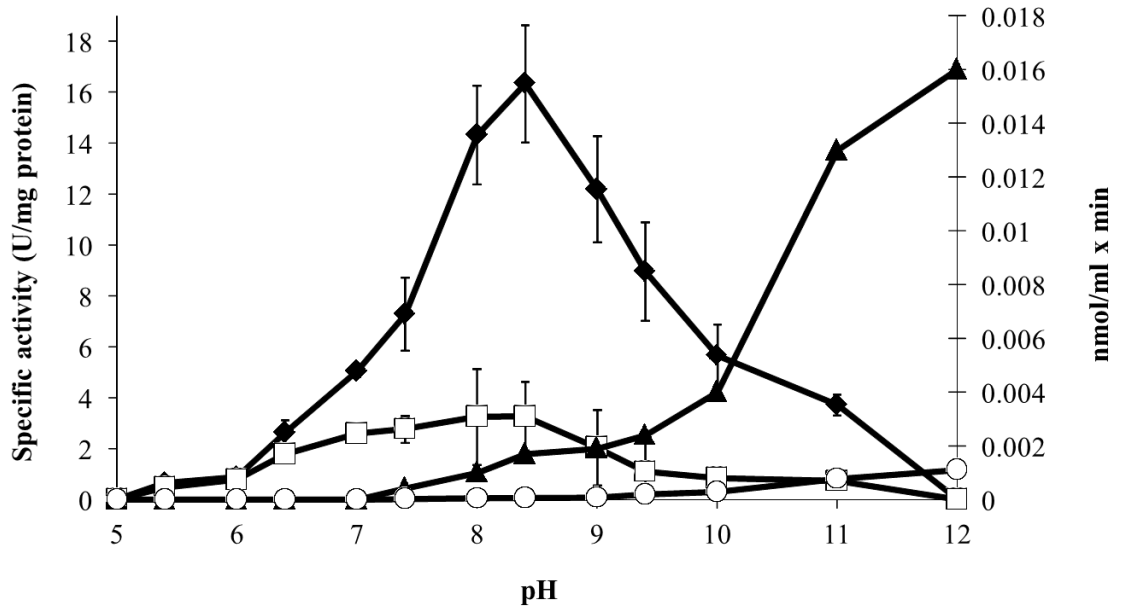

Figure 5.3 pH-dependence of *Hn*SOR activity at 50°C. Left y-axis: specific enzyme activity; (◆) = sulfite plus thiosulfate production; (□) = H_2S production. Right y-axis: non-enzymatic sulfur disproportionation; (▲) = sulfite plus thiosulfate; (○) = H_2S.

Table 5.1 Specific enzyme activities of the *Hn*SOR at different pH values and at 50°C.

pH	**5.4**	**6**	**6.4**	**7**	**7.4**	**8**
Oxygenase activity in U/mg (Thiosulfate)	0.06	0.23	1.21	3.36	4.71	11.09
Oxygenase activity in U/mg (Sulfite)	0.59	0.65	1.41	1.68	2.56	3.23
Oxygenase activity in U/mg (Thiosulfate and sulfite)	0.65	0.88	2.62	5.04	7.27	14.32
Reductase activity in U/mg (Sulfide)	0.47	0.78	1.78	2.59	2.77	3.25
pH	**8.4**	**9**	**9.4**	**10**	**11**	**12**
Oxygenase activity in U/mg (Thiosulfate)	11.59	9.23	6.17	4.89	3.15	-
Oxygenase activity in U/mg (Sulfite)	4.31	2.95	2.79	0.76	0.56	-
Oxygenase activity in U/mg (Thiosulfate and sulfite)	16.34	12.18	8.96	5.65	3.71	-
Reductase activity in U/mg (Sulfide)	3.27	2.04	1.1	0.84	0.73	-

Both products of the oxygenase reaction, sulfite and thiosulfate, were detected between pH 5.4 and pH 11 (Figure 5.4). However, at slightly acidic conditions (pH 5.4 - pH 6.4), sulfite was the major product with a tenfold excess of sulfite formation at pH 5.4. At neutral and at alkaline conditions, the bias changed towards thiosulfate formation: at pH 8, thiosulfate production was more than threefold higher than sulfite formation (Table 5.1).

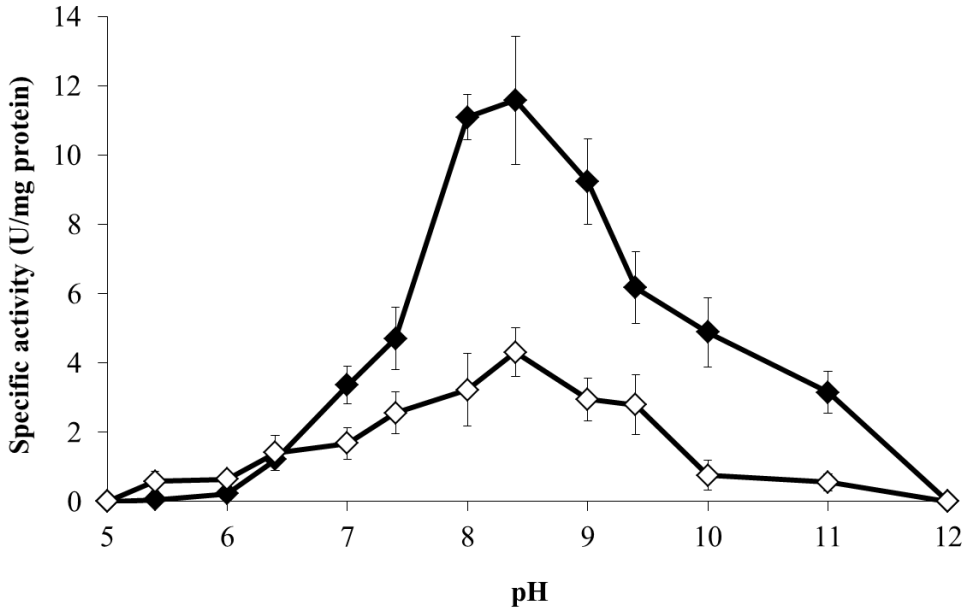

Figure 5.4 pH-dependence of enzymatic thiosulfate (◆) and sulfite (◇) production by the *Hn*SOR oxygenase reaction at 50°C.

The temperature-dependence of *Hn*SOR is shown in Figure 5.5. Oxygenase and reductase activity were both detected between 10 and 95°C using a citrate/phosphate buffer pH 8 with optimal enzyme activity at 80°C. At moderate temperatures (*i.e.* 10 - 40°C), both enzyme activities were at equal levels. At temperatures higher than 40°C, oxygenase activity was up to tenfold higher than reductase activity, which was already observed for the *Aquifex aeolicus* SOR (Pelletier *et al.*, 2008).

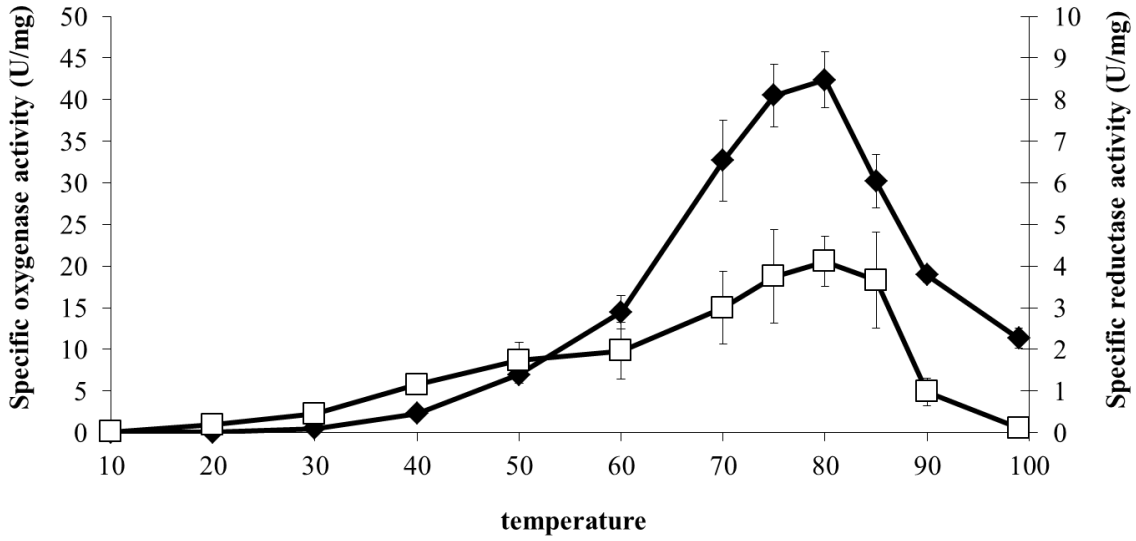

Figure 5.5 Temperature-dependence of *Hn*SOR activity at pH 8. Left y-axis (◆): specific oxygenase activity (sulfite and thiosulfate); right y-axis (□): specific reductase activity (H_2S).

Table 5.2 Specific enzyme activities of *Hn*SOR at different temperatures and at pH 8.

Temp	**10°C**	**20°C**	**30°C**	**40°C**	**50°C**	**60°C**
Oxygenase activity in U/mg (Thiosulfate)	0.0225	0	0.106	1.3	3.93	11.62
Oxygenase activity in U/mg (Sulfite)	0.01	0.042	0.40	1.00	3.00	2.84
Oxygenase activity in U/mg (Thiosulfate and sulfite)	0.033	0.042	0.506	2.3	6.93	14.46
Reductase activity in U/mg (Sulfide)	0.0205	0.19	0.45	1.15	1.73	1.96
Temp	**70°C**	**75°C**	**80°C**	**85°C**	**90°C**	**99°C**
Oxygenase activity in U/mg (Thiosulfate)	27.54	35.07	36.26	26.99	18.87	11.32
Oxygenase activity in U/mg (Sulfite)	5.14	5.45	6.12	3.2	0.083	0
Oxygenase activity in U/mg (Thiosulfate and sulfite)	32.68	40.52	42.38	30.19	18.95	11.32
Reductase activity in U/mg (Sulfide)	3.00	3.75	4.11	3.66	0.98	0.11

An equal ratio between both oxygenase products (sulfite and thiosulfate) was observed at moderate temperatures (10 - 40°C). The ratio changed drastically when temperatures exceeded 50°C, resulting in an up to sixfold higher amount of thiosulfate at 75°C (Figure 5.6).

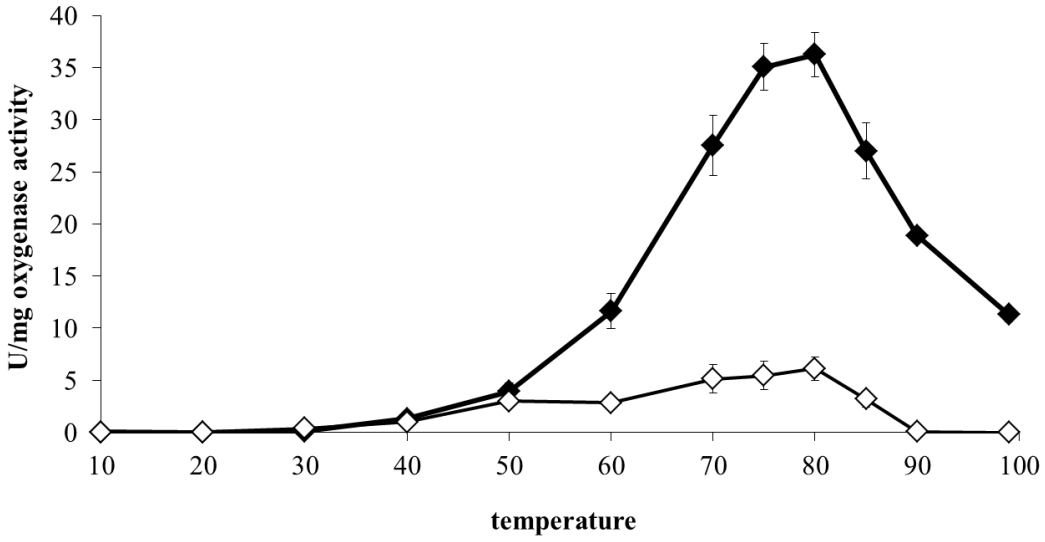

Figure 5.6 Temperature-dependence of enzymatic thiosulfate (◆) and sulfite (◇) production by the *Hn*SOR oxygenase reaction at pH 8.

Inhibition studies of the *Hn*SOR were carried out using zinc chloride. Zn^{2+} is a potent inhibitor for SORs, which had already been demonstrated for the *A. ambivalens* (Kletzin, 1989; see also chapter 3) and the *A. tengchongensis* SORs (Chen *et al.,* 2005). K_i-values of *Hn*SOR with zinc chloride at pH 8 and at 80°C were 46 µM zinc chloride for the oxygenase and 36 µM for the reductase activity, which is in good agreement with the K_i-values determined for the *Aa*SOR (45 µM for oxygenase and 39 µM for reductase activity, see also chapter 3).

5.2.4. Structural properties of the recombinant *Hn*SOR

The hydrodynamic protein diameter of different SOR proteins was determined experimentally using Dynamic Light Scattering (DLS) analysis with protein samples (0.3 mg/ml in 20 mM Tris/HCl buffer pH 7.5) on a Zetasizer Nano apparatus at 25°C. Size distribution and diameter values of the corresponding samples were calculated using the corresponding Zetasizer software. The calculated average values of the particle size were 18.0 nm for the *Aa*SOR, 17.8 nm for the *Aa*SOR $R_{99}A$ (*A. ambivalens* $R_{99}A$ SOR mutant; see chapter 3) and 17.3 nm for the *Hn*SOR. Besides the major peak, 200 nm aggregates were observed for the *Hn*SOR and 4000 nm particles for the $R_{99}A$ mutant (Figure 5.7), but both signals disappeared after volume normalization.

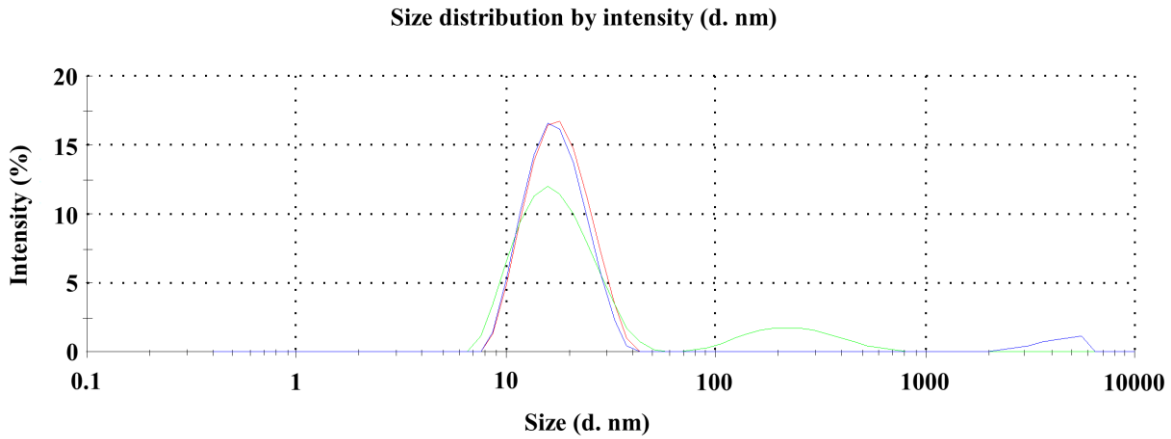

Figure 5.7 Calculated size distribution from DLS measurements of different SOR samples; Red line = *Aa*SOR; blue line = *Aa*SOR $R_{99}A$ mutant; green line = *Hn*SOR.

Table 5.3 Calculated hydrodynamic diameter sizes of different SOR proteins.

Sample name	Calculated hydrodynamic diameter
*Aa*SOR	18.0 ± 0.8 nm
*Aa*SOR $R_{99}A$	17.8 ± 0.1 nm
*Hn*SOR	17.3 ± 1.0 nm

The secondary structure of each SOR sample was analyzed by circular dichroism (CD) spectroscopy. Samples were assayed at 0.1 mg/ml in 20 mM Tris/HCl buffer pH 7.5 each and measured at 25°C. The program CDNN (Böhm *et al.,* 1992) was used for deconvolution of the CD spectra data to estimate proportions of the different secondary structures. The CD spectra of both *A. ambivalens* SOR proteins (*Aa*SOR and *Aa*SOR $R_{99}A$) were rather similar, with minima around 220 nm and a maximum between 195 and 200 nm. The CD spectrum of the *Halothiobacillus* enzyme was rather similar, showing a minimum around 220 nm. The low wavelength maximum of *Hn*SOR was not identifiable in the accessible spectral window.

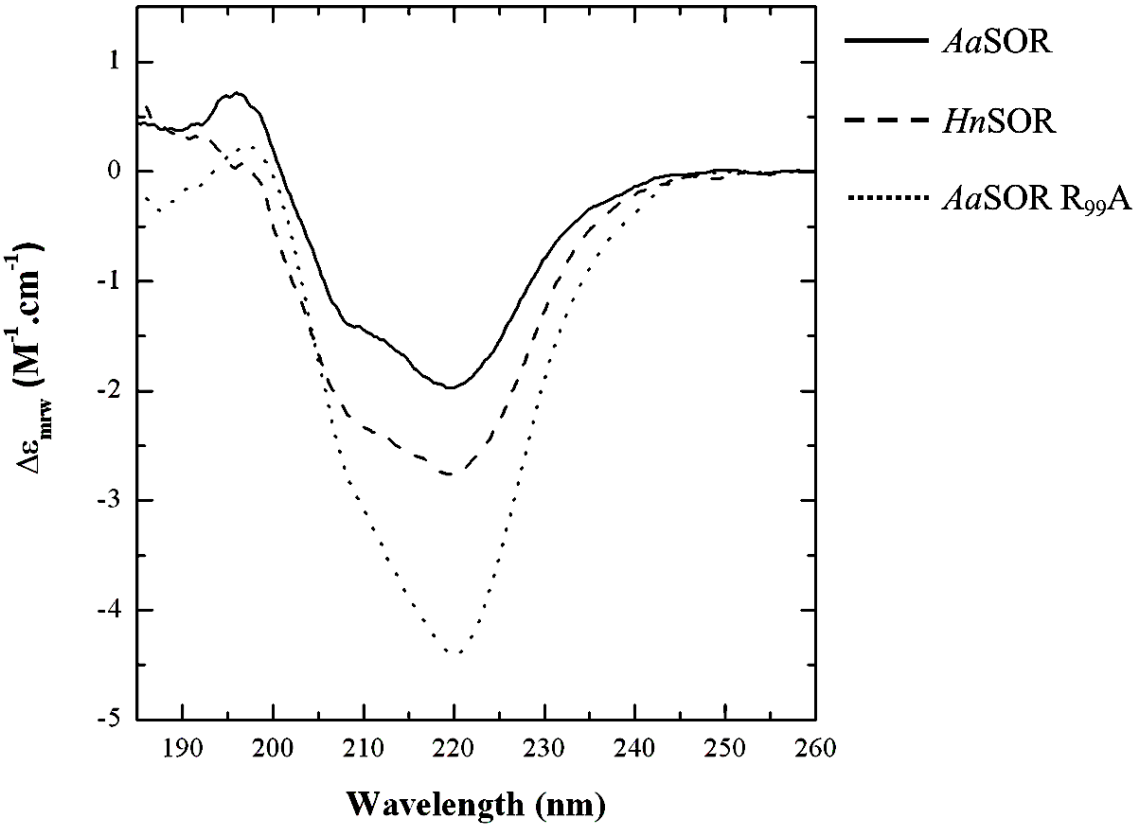

Figure 5.8 Circular dichroism spectra of *Aa*SOR (black solid line), *Aa*SOR $R_{99}A$ mutant (black dotted line) and *Hn*SOR (black dashed line). The y-axis represents delta epsilon, mean residue weight (mrw) divided by the protein concentration (M) and the path length (cm).

Table 5.5 Secondary structure estimation of different SOR proteins

Experimental CDNN Deconvolution	***Aa*SOR**	***Aa*SOR $R_{99}A$**	***Hn*SOR**
α-Helix	17.4 % /23.8 %[1]	23.0 %	19.6 %
β-sheets	32.8 % / 23.4 %[1]	28.2 %	32.7 %
β -Turn	16.3 % / n.r.[1]	17.5 %	16.9 %
Random Coil	33.5 % / n.r.[1]	31.3 %	30.8 %
GOR Prediction Server*	***Aa*SOR**	***Aa*SOR $R_{99}A$**	***Hn*SOR**
α-Helix	19.1 %	19.1 %	20.7 %
β-sheets	30.7 %	30.4 %	32.1 %
Random Coil	50.2 %	50.5 %	47.1 %

[1] Estimated secondary structure content analysis of *Aa*SOR by T. Urich (Urich *et al.*, 2004).
* GOR secondary structure prediction server based on the GOR (Garnier-Osguthorpe-Robson)-method for secondary structure prediction (Garnier *et al.*, 1996).

Secondary structure quantification of the *Hn*SOR spectrum resulted in a structural composition of 19.6 % α-helices, 32.7 % β-sheets, 16.9 % β-turn and 30.8 % random coil which corresponds well to the secondary structure prediction values of 20.7 % α-helices, 32.1 % β-sheets and 47.1 % random coil (GOR IV secondary structure prediction method; http://npsa-pbil.ibcp.fr/cgi-bin/npsa_automat.pl?page=npsa_gor4.html; Garnier *et al.*, 1996). The estimated secondary structure composition obtained for the *Aa*SOR varied from the values previously determined for the same protein (Urich *et al.*, 2004; Table 5.5). The amount α-helices decreased to 17.4 % (previously 23.8 %), while the amount of β-strands increased to 32.8 % (previously 23.4 %).

5.2.5. Crystallization of the recombinant *Hn*SOR and data collection

Recombinant *Hn*SOR was dialysed twice against 50 mM Tris/HCl buffer pH 7.5 and concentrated up to 13.1 mg/ml. First crystallization screenings were carried out using 96 different crystallization conditions of the MbClassSuite (Qiagen) at 22°C. This kit was chosen, as it was previously used for the crystallization of the *Aa*SOR and the *Aa*SOR mutants (see chapter 4). Small crystals of *Hn*SOR were obtained within 24 h in 12 different conditions. Most promising was condition 6 (0.1 M ADA [N-[2-Acetamido]-iminodiacetic acid] pH 6.5, 1 M ammonium sulfate) that resulted in cubic-shaped and needle-like crystals (Figure 5.9). Both crystal forms were reproducibly obtained, however the cubic ones lost their crystal shape shortly after appearing. The formation of the needle-like crystals was further optimized by Ricardo Coelho (ITQB, Oeiras, Portugal) using slightly different conditions ranging from 0.1 M ADA pH 6.4 - 7.0 and 0.8 - 1.0 M ammonium sulfate with

different ratios between applied protein solution and crystallization buffer (0.7 µl**:**1.3 µl to 1.5 µl**:**0.5 µl). The crystals were transferred to a cryoprotection solution supplemented with glycerol (0.1 M ADA pH 6.4, 1.3 M ammonium sulfate and 25 % glycerol) and flash-cooled in liquid nitrogen and stored until data collection.

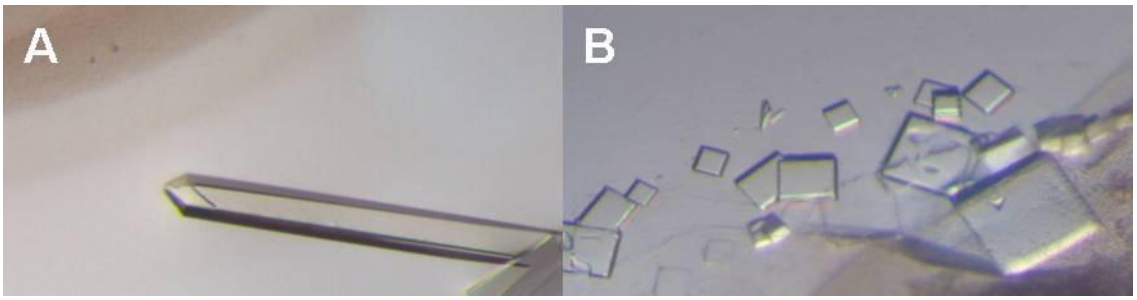

Figure 5.9 SOR crystals grown in 0.1 M ADA pH 6.5, 1 M ammonium sulfate.
(**A**) Needle-like crystals; (**B**) Cubic-shaped crystals.

X-ray diffraction data were collected up to a resolution of 2.9 Å by Carlos Frazão (ITQB, Oeiras, Portugal) in-house at the Cu K-α wavelength (1.5418 Å) from a cryo-protected crystal. *Hn*SOR crystallized in space-group $P2_12_12_1$ (International Tables for Crystallography number: 19) with cell dimensions a = 200.89 Å, b = 212.71 Å and c = 216.85 Å. The resolution-dependent probability distribution of the Matthews coefficient for the *Hn*SOR crystal showed a relatively flat distribution with the maximum (with 10 % probability only) corresponding to 27 monomers in the asymmetric unit and 48 % of calculated solvent content, while 24 monomers (with 8 % probability) would correspond to 54 % solvent content and a Matthews coefficient Dm of 2.67 A^3/Da. It was previously shown that SOR dimers are the building blocks of the *Acidianus ambivalens* SOR holoenzyme, forming the icosatetramer (Urich *et al.*, 2006). As the crystal asymmetric unit seemed to contain one icosatetramer, molecular replacement was performed with the refinement module of PHENIX using the *Aa*SOR (40 % amino acid sequence identity) dimer as search template instead of the monomer, which reduced the number of search fragments to be localized in the asymmetric unit to 12 (instead of 24). The phase problem was solved with PHENIX using PHASER and the quaternary structure of *Hn*SOR displayed the 432 point group symmetry arrangement, as found in the previously obtained SOR structures thus corroborating the structure solution (Table 5.6).

Table 5.6 Diffraction data processing and refinement statistics of *Hn*SOR structure

	***Hn*SOR**
Source	in-house
Space Group	$P2_12_12_1$ (19)
Unit cell parameters (Å)	a = 200.89, b = 212.71, c = 216.85
Wavelength	1.5418 Å
Number of unique intensities	205,792
Redundancy	11.0 (5.2)
Resolution (outer shell) (Å)	66.86 - 2.90 (3.00 - 2.90)
Completeness (outer shell) (%)	99.8 (98.3)
R_{merge}*(outer shell) (%)	11.11 (42.49)
I / σ (I)	17.87 (2.95)
Wilson B ($Å^2$)	46
Refinement	
Refined structure	7440 aa 949 waters 48 sulfate molecules
R_{work} (%)	18.03
R_{free} (%)	19.90
R (%)	18.09
Average ADP ($Å^2$)	32
Bonds RMSD (Å)	0.020
Angles RMSD (°)	0.885

*$R_{merge} = \Sigma|I_o - \langle I \rangle| / \Sigma I_o$, where $\langle I \rangle$ is the average of symmetry equivalent reflections and the summation extends over all observations I_o for all unique reflections.

5.2.6. Analysis of the *Hn*SOR structure

Careful examination of the recombinant *Hn*SOR protein structure showed that the first three amino acids at the N-terminus and the last amino acid at the C-terminus were missing in the final model. A similar situation was observed for the *Aa*SOR structure lacking the N-terminal methionine and the last amino acid of the C-terminus. The N-terminal methionine is post-translationally cleaved off in the *Aa*SOR and the missing C-terminal residue results from the high structural flexibility of this region (Urich, 2005c). The α-carbon main chain atoms of the *Hn*SOR structure were superimposed to the corresponding atoms of the *Aa*SOR structure (Figure 5.10), showing that the *Hn*SOR monomer consists of a central β-barrel surrounded by α-helices, as already demonstrated for the *Aa*SOR (Urich *et al.*, 2006). Minor deviations were observed in the coiled and loop regions, while three α-helical domains of the *Aa*SOR structure were not present in the *Hn*SOR model. The RMSD (Root mean square deviation) was calculated by Carlos Frazão using MODELLER (Eswar *et al.*, 2001). Therefore, the *Hn*SOR model was superimposed to the *Aa*SOR or to the *At*SOR structure. The low values of 1.03 Å (*Hn*SOR vs. *Aa*SOR) and 1.00 Å (*Hn*SOR vs. *At*SOR) gave a first hint that the SOR structures of mesophilic and thermophilic organisms share a highly similar protein architecture (Figure 5.10 and 5.11).

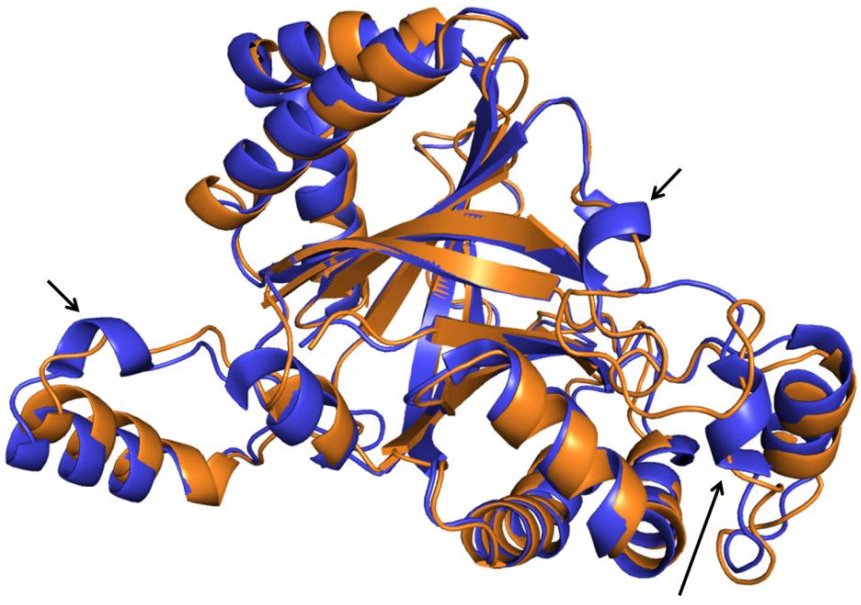

Figure 5.10 Superposition of the *Hn*SOR monomer (orange) and *Aa*SOR monomer (blue). Black arrows indicate the helical regions of the *Aa*SOR that are not present in the *Hn*SOR structure.

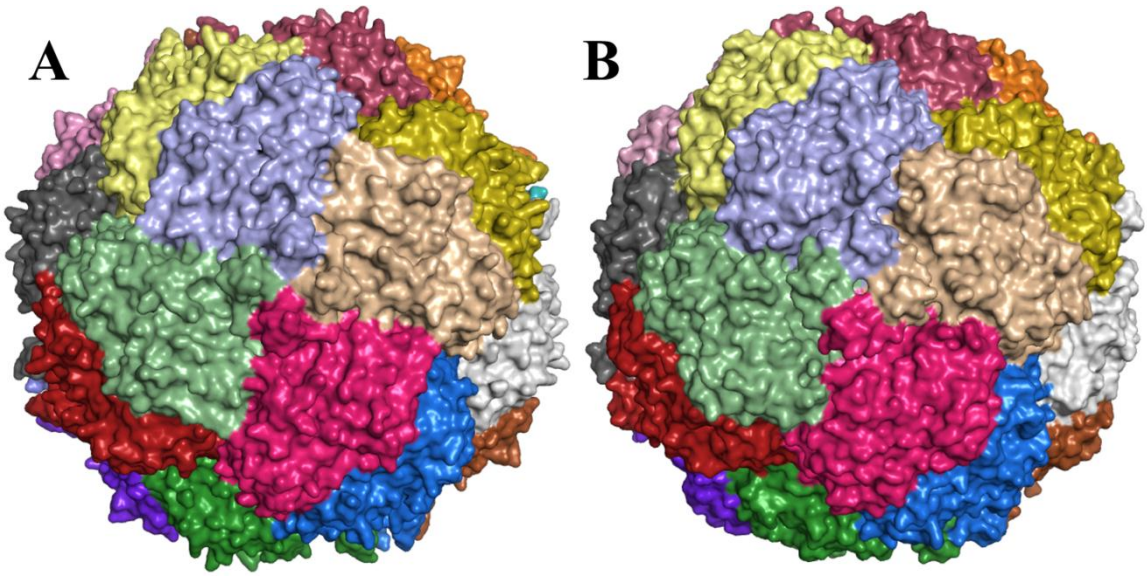

Figure 5.11 Structural models of the *Hn*SOR (**A**) and *Aa*SOR (**B**) holoenzymes viewed from the non-crystallographic fourfold rotational symmetry axis with subunit coloring.

The secondary structure composition of the *Hn*SOR 3D structure was analyzed using the PROMOTIF software (Hutchinson and Thornton, 1996). The results were compared to the values obtained through CD spectroscopy (Table 5.7). Both data sets showed a similar β-sheet content of *Hn*SOR, while the α-helical content of the CD spectroscopy data was 8 % lower than the value obtained through PROMOTIF.

Table 5.7 Secondary structure composition of the *Hn*SOR obtained via CD spectroscopy and through analysis of the corresponding 3D structure.

Secondary structure content	α-Helix	β-sheets
CD spectroscopy (CDNN)	19.6 %	32.7 %
3D structure (PROMOTIF)	27.5 %	31.4 %
GOR IV Prediction server	19.1 %	30.7 %

Due to the high structural similarities between the *Aa*SOR and the *Hn*SOR, it is most likely that the sulfur substrate follows the same pathway as described in chapter 3. The linear sulfur molecule passes through chimney-like structures at the rotational fourfold symmetry axes that give access to the inner hollow. The inner surface of these chimney-like structures, which are composed by the residues 132 to 154 (*Hn*SOR numbering), is mainly hydrophobic. The interior includes an inner valine (V_{135}), a middle leucine (L_{139}) and an outer phenylalanine (F_{143}) ring, which restrict the pore opening (Fig 5.12). The C-C distances of the phenylalanine side chains are 4.9 Å, while the C-C distances of the leucine side chains are 5.4 Å. The C-C distances of the valine ring, which is homologous to the inner phenylalanine ring of the *Aa*SOR, are 11.3 Å. A conserved methionine ring (M_{132}) is located at the base of the chimney, providing the transition to the inner hollow with side chain distances of nearly 20 Å.

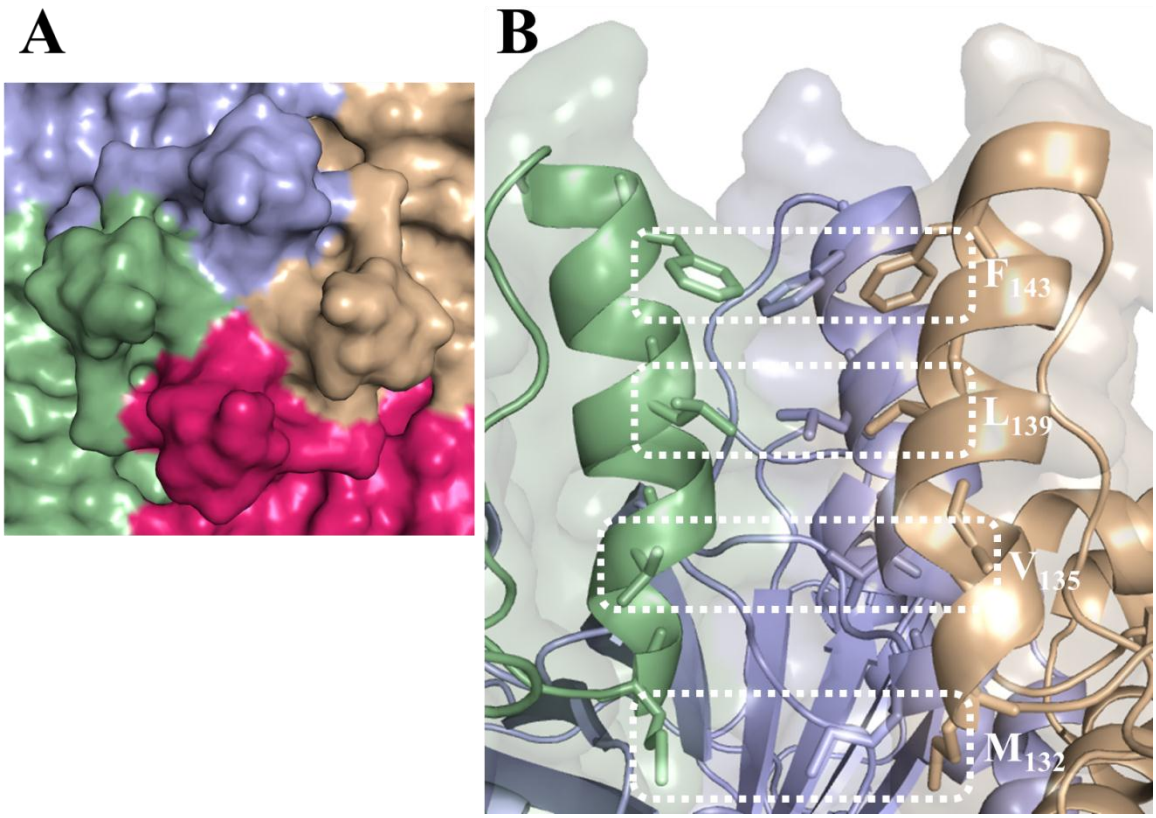

Figure 5.12 Top and side views of the channel at the fourfold symmetry axis of *Hn*SOR. (**A**) Top view from the rotational fourfold symmetry axis with surface representation of the four channel-forming subunits. (**B**) Side view with three subunits displayed with the outer (F_{143}) phenylalanine, the middle leucine (L_{139}), the inner valine (V_{135}) and the methionine ring at its base (M_{132}). The corresponding amino acids are framed by white dashed lines.

The second opening at the outer shell of the *Hn*SOR is located at each of the rotational threefold symmetry axes, which is referred to as the trimer channel (see chapter 3). The pore is mainly composed of an alanine (A_{226}) and a glutamate (E_{101}; Figure 5.13), whereas the latter is homologous to the pore-forming arginine of the *Aa*SOR structure (see chapter 3). Both oxygen atoms of the carboxyl group of E_{101} are in hydrogen-bonding distance of 3.0 Å to the α-amino group nitrogen of A_{226} and 2.9 Å away from the δ2-nitrogen of a neighboring asparagine (N_{227}), which is homologous to the glutamate in the *Aa*SOR structure (see chapter 3). The C-C distances between the methyl groups of alanine, which presumably restrict the pore opening, are 3.9 Å.

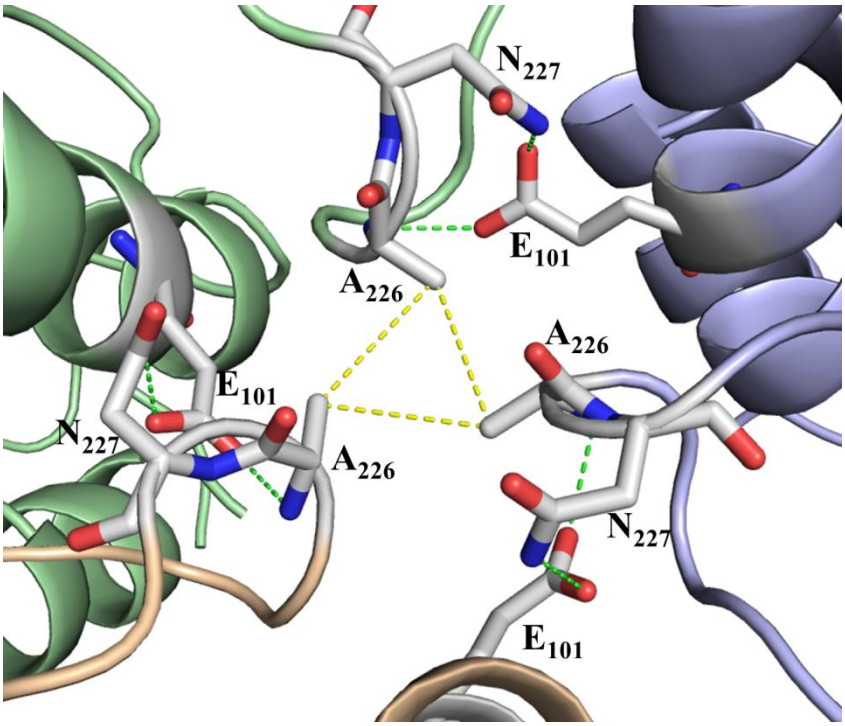

Figure 5.13 Structure of the trimer channel-forming subunits colored in green, blue and ochre. E_{101} and A_{226} form the opening of the channel. Yellow dashed lines indicate the distances between each alanine residue. Green dashed lines represent potential salt bridges between E_{101} and N_{227} or A_{226}, respectively.

The narrow pore giving access to the active site pocket is shaped by three methionines in the *Hn*SOR structure (M_{25}, M_{302} and M_{303}; Figure 5.14). A glutamine (Q_{47}) at the active site pore entrance causes the pore to appear in a closed state. In contrast to the *Aa*SOR structure, a second opening of the active site pocket was observed at its opposite side. This "back exit" is formed by two phenylalanines (F_{210}, F_{100}), one leucine (L_{107}) and one serine (Ser_{104}) and presumably provides a direct connection of the active site pocket with the product exit at the threefold symmetry axes, as already suggested for the *A. tengchongensis* SOR (Li *et al.*, 2008).

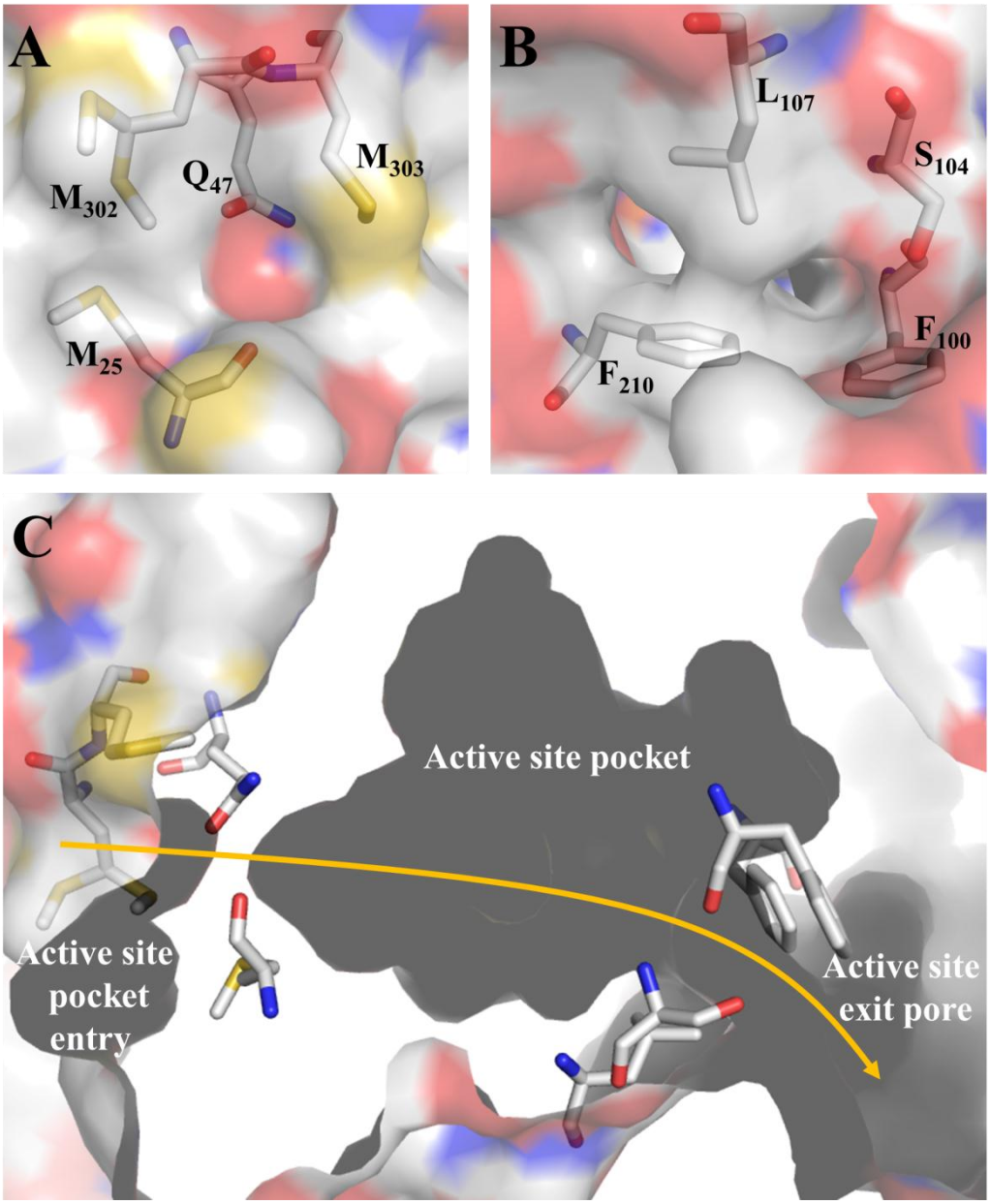

Figure 5.14 Surface representation and active site cavity of the *Hn*SOR monomer. (**A**) Active site pocket entry shaped by M_{25}, M_{302} and M_{303}. (**B**) Active site pocket exit pore located at the opposite side of the entry pore and formed by F_{100}, S_{104}, L_{107} and L_{210}. (**C**) Surface representation of the active site pocket with the corresponding entry and exit pore. The pathway of the sulfur substrate is depicted as an orange arrow.

The catalytic center architecture of the *Hn*SOR showed many similarities but also marked differences with respect to the available 3D structures from *Acidianus ambivalens* and *Acidianus tengchongensis*: the active site core comprises a mononuclear iron center and three conserved cysteine residues (C_{33}, C_{103} and C_{106}). Additional electron density was observed at the S-γ atom of C_{33}, indicating the presence of a cysteine persulfide at this position (Figure 5.15). The persulfurated residue corresponds to the modified Css_{31} of the original *Aa*SOR. The first coordination sphere ligating the iron atom at the active site consists of two histidines (H_{88} and H_{92}) and one glutamate. One single water molecule was observed in coordination distance to the Fe, but only in 7 of 24 crystallographically independent monomers. A second iron-coordinating water molecule was not detected, leaving the metal in a fivefold-coordination state, as already demonstrated for the *At*SOR (Li *et al.*, 2008). The coordination distances between Fe and the corresponding ligands increased slightly (0.21 Å - 0.38 Å) in comparison to the original *Aa*SOR (Figure 5.15).

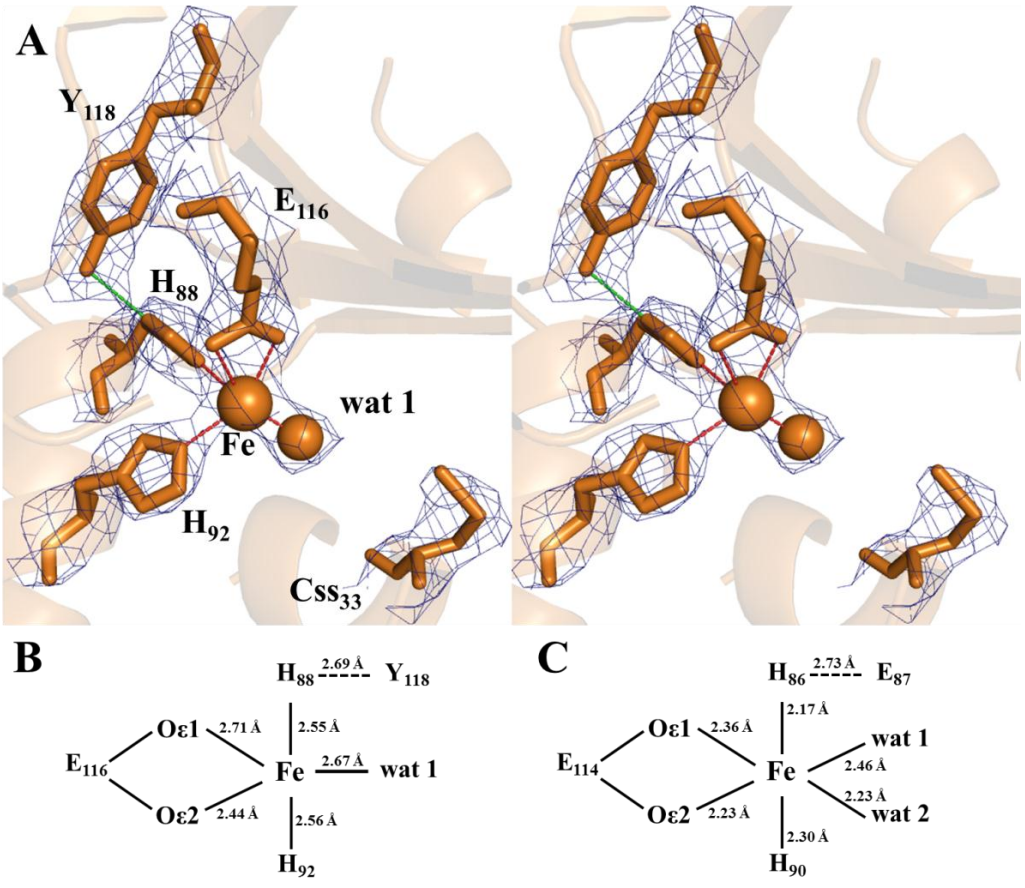

Figure 5.15 (**A**) Stick and ribbon representation of active site residues of the *Hn*SOR in cross-eye stereo view. The 2 F_o-F_c electron density map, contoured at 1.0 σ is shown in blue mesh. Fe and the water molecule are depicted as spheres. Red dashed lines represent Fe-coordination and green dashed lines represent H-bond distances between Y_{118} and H_{88}. (**B + C**) Schematic representation of the Fe center and the (**B**) fivefold-coordination in the *Hn*SOR and the (**C**) sixfold-coordination of the *Aa*SOR. Black solid lines represent the coordination distances (average values of 24 (*Hn*SOR) or 6 (*Aa*SOR) crystallographically independent monomers); black dashed lines represent H-bond distances.

The second coordination sphere describes residues that are non-covalently bond to the iron ligands through hydrogen bonds (see also chapter 4). In the *Hn*SOR structure, the second coordination sphere comprises a single tyrosine residue, Y_{118}. Its distance to the δ1-nitrogen of the iron-coordinating H_{88} is 2.69 Å (average value of 24 crystallographically independent monomers). In the *Aa*SOR structure, the role of Y_{118} is adopted by the glutamate residue E_{87}, while the homologous E_{89} in the *Hn*SOR points away from the carboxylate oxygen of H_{88} (Figure 5.16). The resulting distance between E_{89} and H_{88} ranges between 4.2 - 4.3 Å, making a hydrogen-bonding interaction between these residues improbable.

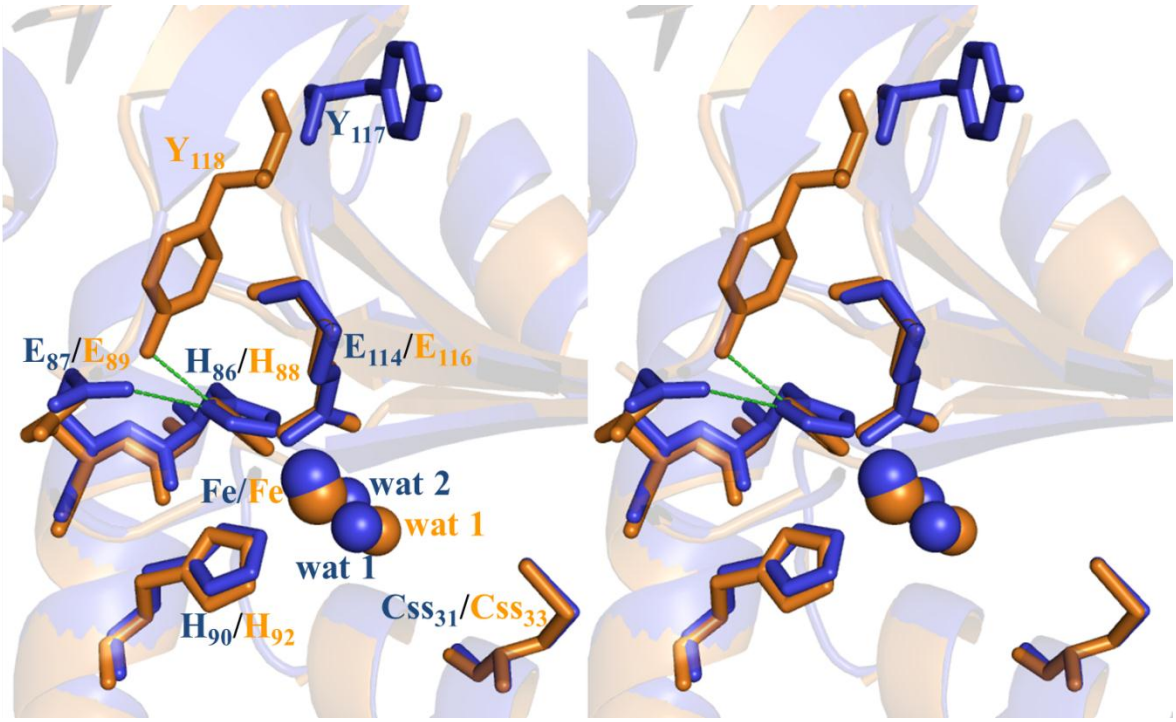

Figure 5.16 Overlay ribbon and stick representation of active site residues of *Hn*SOR and *Aa*SOR in cross-eye stereo view. The water molecules and the Fe atom are depicted as spheres. *Hn*SOR is displayed in orange, *Aa*SOR is displayed in blue. H-bonds between Y_{118} and H_{88} (*Hn*SOR) and between E_{87} and H_{86} (*Aa*SOR) are depicted as green dashed lines.

5.3. Discussion

Sulfur oxygenase reductases were detected predominantly in thermoacidophilic microorganisms but the encoding genes were also identified recently in genomes of mesophilic bacteria such as *Halothiobacillus neapolitanus* or *Desulfomicrobium baculatum*. This chapter focuses on the characterization of the *H. neapolitanus* SOR. Therefore, the recombinant *H. neapolitanus sor* gene was amplified from genomic DNA and heterologously expressed in *E. coli*. The resulting protein was biochemically and structurally characterized.

5.3.1. *Hn*SOR exhibits a broad temperature and pH range

The *sor* gene of *H. neapolianus* was PCR-amplified, inserted into a plasmid and heterologously expressed in *E. coli*. The yield of recombinant *Hn*SOR was up to tenfold higher than protein yields for recombinant *Aa*SOR or *Aa*SOR mutants (see chapter 3 and 4). When the *Hn*SOR activity was measured using a modified SOR activity assay, it became apparent that a citrate/phosphate buffer is more suitable for *Hn*SOR than a Tris/HCl-containing buffer, indicated by an up to tenfold increase of enzyme activity. These results suggest that a Tris-based buffer developed for the *Aa*SOR is suboptimal for *Hn*SOR activity, although a similar Tris/HCl buffer had been used for the *Aquifex aoelicus* SOR activity assay yielding a very high enzyme activity of 78.8 U/mg oxygenase and 3.05 U/mg for reductase activity, respectively (Pelletier *et al.,* 2008). It is feasible that citrate and/or phosphate might chelate small amounts of metal ions that usually inhibit the enzyme such as Cu^{2+} and Zn^{2+} (Kletzin, 1989; Chen *et al.,* 2005) and hence reduce the inhibitory effects of residual impurities in the buffer.

K_i values for zinc chloride were determined for both *Hn*SOR activities (46 µM for oxygenase and 36 µM for reductase activity) using a Tris/HCl-based buffer since citrate and/or phosphate would precipitate zinc chloride. Both K_i values were almost identical to those determined for *Aa*SOR, giving a first hint that both proteins might be highly similar on the biochemical level.

*Hn*SOR displayed a broad pH range when measured at 50°C, showing activity between pH 5.4 and pH 11 (Figure 5.3). At pH 12 it was no longer possible to distinguish between enzymatic reaction and non-enzymatic sulfur disproportionation. This pH range extends further into the alkaline region of activity than for any of the SORs characterized so far (Kletzin, 1989; Sun *et al.*, 2003; Chen *et al.*, 2007; Pelletier *et al.*, 2008). A direct pH-dependent comparison with *Aa*SOR activity was not possible because of the high rate of non-enzymatic sulfur disproportionation at pH 8.5 and above combined with the optimal temperature for *Aa*SOR catalysis (85°C). Lowering of the reaction temperature to 50°C allowed activity measurements at alkaline pH values. It was shown that the *Halothiobacillus* enzyme has an optimum at pH 8.4 so that it proved to be slightly alkaliphilic. The determined pH optimum correlates with the slightly alkaline internal pH of *H. neapolitanus* (~ 7.8; Tsai *et al.*, 2007). Both oxygenase reaction products thiosulfate and sulfite were produced in significantly higher amounts than sulfide, resulting in an up to tenfold excess of oxygenase activity at pH 8.4. At acidic pH values, the stoichiometries were more or less equal, while the disequilibrium at alkaline pH is contrary to the proposed 1:1 stoichiometry for the *Aa*SOR (Kletzin, 1989). This might be the result from quick evaporation of H_2S. Rapid oxidation of sulfide to thiosulfate might also lead to the unequal distribution of products, as already discussed for trimer channel- and tetramer channel-opening mutants of *Aa*SOR (see chapter 3). As a second striking feature, *Hn*SOR activity covered a temperature span of nearly 90°C (Figure 5.5). Enzyme activity was detected from 10°C to at least 99°C, whereas temperatures above 100°C could not be measured due to technical restrictions. Even though the recombinant *Hn*SOR originates from a mesophilic microorganism with an optimal growth temperature around 30°C (maximum 42°C; Kelly and Wood, 2005), both enzyme activities peaked at 80°C. At optimal temperature, *Hn*SOR oxygenase activity (42.38 U/mg) was more than tenfold and reductase activity (4.01 U/mg) was more than twofold higher than the corresponding activities of the *Aa*SOR enzyme (average value: 3.03 U/mg oxygenase and 1.68 U/mg reductase activity). Similar observations had already been made for the *Aquifex aeolicus* protein (78.8 U/mg oxygenase activity and 3.05 U/mg reductase activity). The high activity of the *Aquifex aeolicus* SOR was interpreted as a result of amino acid substitutions in the tetramer channel pore, causing a higher accessibility of the sulfur substrate into the catalytic center (Pelletier *et al.*, 2008). It is arguable whether or not this can be applied to the *Hn*SOR, since different buffer systems were used raising enzyme activities up to tenfold.

A surprising result was the detection of both oxygenase products at any temperature point (Figure 5.6), since thiosulfate had been considered as a secondary reaction product resulting from non-enzymatic sulfite condensation occurring at high temperatures (Kletzin, 1989). This reaction may explain the disequlibrium between both oxygenase products with a bias towards thiosulfate at temperatures higher than 50°C. The same process also explains the bias towards sulfite at low temperatures. However, it was unusual to detect thiosulfate at low temperatures (10 - 40°C) and sulfite at higher temperatures (60 - 90°C). The appearance of thiosulfate at low temperatures led to the conclusion that it may also represent a primary oxidation product of the *Hn*SOR. The result would be a yet unknown product stoichiometry that differs significantly from the *Aa*SOR.

After analysis of the biochemical data, the question remained, why the optimal enzyme activity of the *Hn*SOR was detected around 80°C, which exceeds the optimal growth temperature of the microorganism by 50°C. Since elemental sulfur had been described to be up to 25-fold more soluble at 80°C than at room temperature (Kamyshny, 2009), the high activity may result from the elevated availability of the sulfur substrate. Apart from that, it is still unclear why the enzyme remains active and stable at conditions far from optimal growth temperature of *H. neapolitanus.* The *Aquifex aeolicus* SOR had been demonstrated to be active from 20°C on with 3.6 % residual activity relative to maximal activity at 80°C (Pelletier *et al.*, 2008). That is comparable to the *Hn*SOR with 1 % (oxygenase) and 4.6 % (reductase) residual activity relative to maximal activity at 80°C. The *Aa*SOR had also been shown to be active from 50°C to 108°C (Kletzin, 1989), suggesting that enzyme activity over a broad temperature range is a common feature of SOR proteins. It is most likely that *H. neapolitanus* could have adopted a *sor* gene from an environment that includes thermophilic or at least moderate thermophilic microorganisms. The type strain was isolated from corroded concrete sewers in Australia and described as *Thiobacillus* X (Parker, 1947) but it is probable that *H. neapolitanus* was first isolated from sea water in Naples by Nathansohn in 1902. It was thus named "pertaining to the sea water at Naples from which this species was probably first isolated" (Kelly and Wood, 2000). *Halothiobacillus* also seems to be present in sulfide-rich spas (Wood *et al.*, 2005), and it can also be found among microbial leaching communities (Brandl, 2001). In other respects, nearly all SOR-containing microorganisms are usually found in sulfide-/sulfur-rich springs or solfatares and are also involved in microbial leaching. It is plausible that the *sor* gene was adopted from the environment via horizontal gene transfer between the different sulfur-oxidizing species.

Apart from the *sor* gene, *H. neapolitanus* is also equipped with genes encoding a complete SOX complex. The SOX system is a multiple sulfur substrate oxidation complex restricted to Bacteria (Friedrich *et al.,* 2005). A similar situation was observed for *Acidithiobacillus caldus,* a moderately thermophilic and acidophilic bacterium. It was speculated that two different sulfur oxidation pathways might exist with the utilization of SOR at elevated growing temperatures of 65°C (Mangold *et al.,* 2011). Even though *H. neapolitanus* is not able to grow at conditions exceeding 42°C (Kelly and Wood, 2000), it is likely that both sulfur-oxidizing systems might be used during sulfur oxidation in a temperature-regulated way with the SOR utilized at higher temperatures.

5.3.2. Architecture of different SORs is highly similar

It had already been shown by electron microscopy and X-ray crystallography that the *Aa*SOR diameter size varies between 15 - 15.5 nm (Kletzin, 1989; Urich *et al.,* 2004). In this work, the hydrodynamic diameters of the *Aa*SOR, the *Aa*SOR R_{99}A mutant and of the *Hn*SOR were determined by Dynamic Light Scattering (DLS) analyses (Figure 5.7). The particle sizes of both *Acidianus* SORs were comparable with 18.0 and 17.8 nm, representing an increase of about 15 % over the values determined by other techniques. The calculated hydrodynamic diameter of *Hn*SOR was slightly smaller with 17.3 nm. These values showed that the *Halothiobacillus* holoenzyme does not differ significantly in size from the other enzymes. It has to be noted that the diameters obtained via DLS are the hydrodynamic diameters. They refer to the translational diffusion coefficients that in turn are dependent of surface structures and the concentration and types of ions in the solvent. The diameter size can thus be larger than measured by electron microscopy, so that the actual particle size could match the previously obtained diameter sizes. The values thus suggest that the quarternary structure of the *Hn*SOR is similar to both *Acidianus* enzymes. In addition, it was demonstrated that SOR proteins from *Acidianus ambivalens, Acidianus tengchongensis* and *Aquifex aoelicus* all share similar secondary structures (Urich *et al.,* 2004; Chen *et al.,* 2005; Pelletier *et al.,* 2008). The CD spectra of *Hn*SOR and *Aa*SOR were rather similar (Figure 5.8), while the different signal intensities likely resulted from quantification errors. The spectrum intensity of the *Aa*SOR R_{99} mutant differed significantly. This might be due to different protein concentrations, although all samples were concentrated to 0.1 mg/ml, and the protein concentration was determined prior to CD spectroscopy. Moreover, it cannot be excluded that partial unfolding of the protein may

have occurred, even though all protein samples were active when incubated with sulfur at high temperatures prior to CD spectroscopy.

The secondary structure composition of the *Hn*SOR calculated from CD spectroscopy showed an α-helical content of 19.56 % and 32.7 % β-sheets, which matched the secondary structure prediction values obtained from the GOR IV secondary structure prediction server (with 20.7 % α-helices and 32.17 % β-sheets content; Garnier *et al.,* 1996). Different secondary structure prediction servers were used in this work and the values obtained from the GOR IV server gave the best consensus to the experimentally determined values. The secondary structure composition that was extracted from the 3D structure showed indeed a higher amount of α-helices with 27.5 % but a similiar amount of β-sheets with 31.4 %. However, the values of the *Aa*SOR differed from those derived from the first CD spectroscopy analyses of the same protein (Urich *et al.,* 2004), which had indicated 24 - 27 % α-helix and 24 - 29 % β-sheet content. These differences can be attributed to different *Aa*SOR preparations that had not been treated equally and analyzed at a different time.

5.3.3. Two different channels in the outer shell of the *Hn*SOR

The present X-ray crystallography data showed that, in consistence with both *Acidianus* SORs, *Hn*SOR crystallizes as an icosatetramer. The same pathways for the sulfur substrate and a similarly structured active site center can therefore be proposed. The sulfur pathway includes both tetramer and trimer channels in the outer shell and the entry and exit sites of the active site pocket that are together discussed below. The hydrophobic tetramer channel is formed predominantly by hydrophobic residues including a phenylalanine (F_{143}) ring, a leucine (L_{139}) ring and a valine (V_{135}) ring (Figure 5.12). The outer phenylalanine ring restricts the tetramer channel pore to a size of 4.9 Å, which is comparable with the pore size of the *Aa*SOR protein (~ 5 Å; see chapter 3). The C-C distances of the leucines are 5.4 Å and of the valines 11.3 Å. While the inner phenylalanine ring restricts the pore opening in the *Aa*SOR structure, the outer phenylalanine ring restricts it in the *Hn*SOR. This might also explain the observation that the tetramer channel pore appears to be in a closed state in the *Hn*SOR structure. The trimer channel opening at the threefold symmetry axes represents the product exit for sulfite, thiosulfate and H_2S. It is defined by the methyl groups of three alanines (A_{226}) to a size of 3.9 Å (Figure 5.13), which is comparable to the *Aa*SOR structure (~ 4 Å). Salt bridges between R_{99} and E_{228} in the *Aa*SOR stabilize the

subunit contact (see chapter 3), which is not possible in the *Hn*SOR structure. Instead, hydrogen bonds can be formed between N_{227} and E_{101} and/or E_{101} and A_{226}. The salt bridges in the *Aa*SOR keep the pore opening in a rigid conformation, while the H-bond interactions in the *Hn*SOR might allow a more flexible channel opening that could ultimately lead to an increased pores size and also to an increase of SOR activity at low temperatures.

5.3.4. Entrance and exit channels of the catalytic center

The active site pocket is deeply buried in each of the 24 subunits and can be accessed from the inner hollow of the SOR. It is highly similar to the equivalent pocket of the *Aa*SOR. The entrance to the active site pocket is provided by a hydrophobic pore formed by three methionine residues (M_{25}, M_{302} and M_{303}; Figure 5.14). M_{303} is conserved among all available SOR sequences. M_{25} and M_{302} are mostly conserved but replaced in some of the proteins with different hydrophobic residues such as phenylalanine, isoleucine or leucine. A "back exit" at the opposite site of the reaction center, as already suggested for the *A. tengchongensis s*tructure (Li *et al.*, 2008), was found in the *Hn*SOR as well (Figure 5.14). This exit pore is also formed by mainly hydrophobic residues (F_{210}, F_{100}, L_{107} and S_{104}). The phenylalanines are mostly conserved in other SOR sequences but replaced in some proteins with other hydrophobic residues such as leucine and methionine and in both *Acidithiobacillus* species with a tyrosine instead of F_{100}. Alanine, methionine or phenylalanine can be found in other SOR proteins instead of the $L_{107,}$ while S_{104} is not conserved at all. The opening establishes a direct link to the trimer channel where H_2S, sulfite and thiosulfate supposedly exit the SOR. Such a connection would also prevent the exit of reaction products through the active site entry pore, which could interfere with the sulfur substrate pathway. These results indicate that the pathway of sulfur substrate and of the corresponding reaction products follow similar routes as observed in *A. ambivalens* with the exception of the putative "back exit" (see chapter 3).

5.3.5. Active site architecture

The active site core of the *Hn*SOR comprises the mononuclear Fe center, which is coordinated in a 2-His-1-carboxylate motif (H-X_3-H-X_{23}-E). It is highly conserved among all available SOR sequences and includes two histidines (H_{88} and H_{92}) and one glutamate (E_{116}), which provides a bidentate Fe ligand in the 3D structure (Figure 5.15). While two water molecules complete the sixfold coordination of the iron atom in the *Aa*SOR structure, only one water molecule was observed in the *Hn*SOR. It could only be identified in 7 of the 24 different subunits in the asymmetric unit. It has to be noted that the missing water molecules in the other 17 subunits did appear, when the 2 F_o-F_c electron density map of the corresponding map was decreased to 0.5 σ. The absence of a second water molecule most probably results from the low resolution of the *Hn*SOR dataset (2.9 Å), since similar observations were made for low resolution datasets of the *Aa*SOR (see chapter 4). Analysis of the coordination distances between Fe and the ligands showed a slight increase of the bond lengths between 0.12 and 0.48 Å, which might be caused by a comparably high B-factor (~ 90 $Å^2$) of the Fe atom (The B-factor indicates the mobility of each atom in the structure). The corresponding ligand atoms showed a lower B-factor around 20 - 45 $Å^2$. This high B-factor of Fe probably results from partial iron occupancy at the metal site, which is contradictory to the overstoichiometric load of the respective Fe centers that was determined biochemically for the *Hn*SOR. However, the initial cause for the apparent substoichiometric iron load remains unclear.

The second coordination sphere of the *Hn*SOR is constituted by a single tyrosine residue (Y_{118}) that lies in hydrogen-bonding distance to the iron-ligating H_{88} (Figure 5.16). The sole second coordination sphere residue in *A. ambivalens* is E_{87} that corresponds to E_{89} in the *Hn*SOR structure. E_{89} points away from H_{88} in the *Hn*SOR, resulting in a distance of more than 4 Å, which is too far for a hydrogen-bonding interaction. Y_{118} appears to be the sole second coordination sphere residue in the *Hn*SOR structure that directly interacts with the Fe ligands. Both, E_{87} of *A. ambivalens* and Y_{118} of *H. neapolitanus* share the same function in the respective SOR proteins, even though they are located on different secondary structure segments. E_{89} (E_{87} in *A. ambivalens* numbering) is located in the same α-helix as the Fe-coordinating histidines, while Y_{118} (Y_{117} in *A. ambivalens* numbering) is positioned in the same β-sheet as the bidentate glutamate ligand. It had been described for non-heme iron proteins that aromatic residues such as tyrosine and tryptophane are usually

preferred to other amino acids such as glutamate in the second coordination sphere (Andreini *et al.,* 2009), which could explain the use of tyrosine instead of glutamate. It can also be speculated that different compositions of the second coordination sphere might contribute to the corresponding enzyme activity. Besides the mononuclear iron center, three conserved cysteines were present at the active site. Additional electron density was refined at the S-γ of $C_{33,}$ pointing to the presence of a cysteine persulfide, which was also detected in the *Aa*SOR. The *Acidianus ambivalens* enzyme requires a heating step to modify the respective cysteine, while the HnSOR seems to auto-sulfurate Cys33 to Css33 at moderate temperatures. It is feasible that this sulfurization process of the recombinant *Hn*SOR occurs at room temperature or during heterologous gene expression at 37°C. All results taken together clearly indicate that the biochemical and structural properties of SOR proteins are highly similar although small modifications might be present with respect to the growth conditions of the corresponding microorganism.

6. General Discussion

Sulfur is an integral part in numerous biogeochemical and biochemical processes. Despite its significance in habitats of chemolithotrophic bacteria and archaea, detailed knowledge of the dissimilatory oxidation of reduced inorganic sulfur compounds (RISCs) is limited to a few examples (Kletzin *et al.*, 2004; Friedrich *et al.*, 2005; Frigaard and Dahl, 2009; Sakurai *et al.*, 2010; Kappler, 2011). The multienzyme sulfur oxidation (SOX) complex, which catalyzes the oxidation of various different RISCs in neutrophilic bacteria is biochemically well characterized (Friedrich *et al.*, 2005; Friedrich *et al.*, 2001; Dambe *et al.*, 2005; Sauvé *et al.*, 2007; Sauvé *et al.*, 2009; Zander *et al.*, 2011). Beyond that, progress was made in the understanding of single steps of sulfur oxidation in the thermoacidophilic archaeon *A. ambivalens* (Kletzin *et al.*, 2004; Müller *et al.*, 2004; Brito *et al.*, 2009; Protze *et al.*, 2011). The sulfur oxygenase reductase, representing the initial enzyme of the sulfur oxidation pathway in *A. ambivalens*, is biochemically and structurally well-characterized, but details of the reaction mechanism remain to be shown (Urich *et al.*, 2006). The unraveling of the sulfur substrate route and the structures involved are presented in this work as well as new insights into processes occurring at the metal center during catalysis. Furthermore, a SOR originating from a mesophilic bacterium is described and characterized in detail for the first time.

6.1. The distribution of *sor* genes and SOR proteins

In the past, the SOR was regarded as a sulfur-disproportionating enzyme restricted exclusively to thermophilic bacteria and archaea (Liu, 2008). The recent availability of genomes of sulfur-metabolizing microorganisms made it possible to identify the *sor* gene also in neutrophilic and mesophilic bacteria such as *Halothiobacillus neapolitanus* or *Desulfomicrobium baculatum*. This was surprising, since the SOX system had been considered as the prevalent sulfur-oxidizing apparatus in neutrophilic and/or anaerobic bacteria (Friedrich *et al.*, 2005; Ghosh and Dam, 2009). However, a complete SOX system and a SOR were identified in the *H. neapolitanus* genome. A similar situation was observed for the moderately thermophilic bacterium *Acidithiobacillus caldus*, suggesting that these microorganisms use both systems under different conditions (Mangold *et al.*, 2011). The identification of a *sor* gene in *Desulfomicrobium baculatum* was rather unexpected, as the bacterium had been described as a strictly anaerobic sulfate-reducer

(Rozanova and Razina, 1976; Copeland *et al.,* 2009). It is unknown, whether the *sor* gene is transcribed and the corresponding RNA translated to synthesize a SOR protein requiring dioxygen for activity. It is feasible that *D. baculatum* might tolerate microaerobic conditions like several other members of the sulfate-reducing *Desulfovibrionales* (Cypionka, 2000), which would allow the utilization of a functional SOR. In another case, the archaeon *Picrophilus torridus*, which had been described as an obligatory heterotrophic microorganism (Schleper *et al.,* 1995; Futterer *et al.,* 2004) is equipped with a *sor* gene as well. Apart from that it is conspicuous that *sor* genes are often identified in microorganisms that can be found in bioleaching habitats (Chen *et al.,* 2007; Brandl, 2001). The presence of heterogeneous microbial communities in such an environment easily allows a horizontal gene transfer between those species (Valdés *et al.,* 2010) and probably forces the distribution of *sor* genes to other microorganisms.

6.2. Phylogenetic origin of the SOR

Within the Archaea, SORs and/or *sor* genes can be found exclusively in some thermoacidophilic members of the order *Sulfolobales* (*Sulfolobus* and *Acidianus*) and *Thermoplasmatales* (*Picrophilus* and *Ferroplasma*). Within the Bacteria, SOR and/or *sor* genes are present in thermophilic *Sulfobacillus* species, in a limited number of δ- and γ-proteobacteria (*Halothiobacillus, Acidithiobacillus* and *Desulfomicrobium)* and in the hyperthermophilic bacterium *Aquifex aeolicus*. The dendrogram calculated from the alignment (Figure 1.10) reflects a clear grouping of the enzymes according to phylogenetic relationship (Figure 1.5). Interestingly, the *Aquifex aeolicus* SOR is the enzyme with the lowest similarity in comparison to all other SOR proteins with a sequence identity of 33 - 40 %, although catalytic important regions are highly conserved among all SOR sequences. The amino acid sequence of the *Aq*SOR features a length of 333 aa, which is around 15 - 25 aa longer than any other SOR and which is caused by additional insertions. Nevertheless, it remains unclear, whether the SOR has an archaeal or bacterial origin. The high temperature optima of the biochemically characterized SOR proteins (chapter 5 and Table 1.1) however suggest that the SOR originally derives from a thermophilic microorganism.

6.3. General properties of the *Hn*SOR and its relevance for the SOR protein family

Apparently, the SOR is an oxygen-dependent sulfur-disproportionating enzyme, which is found mostly in microbial sulfur oxidizers. In the course of this work, detailed biochemical and structural data were acquired for the recombinant *H. neapolitanus* SOR. Optimal conditions for the enzyme were demonstrated at 80°C and at a slightly alkaline pH of 8.4 (Figure 5.3 and 5.5). The pH optimum was not surprising with respect to the internal moderately alkaline pH of *H. neapolitanus* (Tsai *et al.*, 2007), while the optima of other SORs varied between pH 5 and 7.5 (see Table 1.1 for details). Those pH optima can be explained by the cytoplasmic location of the SOR. In contrast, other sulfur-oxidizing enzymes of acidophilic microorganisms mostly reside in the periplasm at acidic conditions of pH 1 - 3 (Rohwerder and Sand, 2003). The *Hn*SOR activity covers a temperature span of nearly 90°C with an activity peak that is far from the physiological conditions of *H. neapolitanus*. Similar observations were made for SOR proteins deriving from *Acidithiobacillus caldus*-like strains. Optimal enzyme activity was observed at 65°C, which is around 20°C higher than the optimal growth temperature of *A. caldus* (Janosch *et al.*, 2009). Enzyme activity over a large temperature range combined with a high thermostability appears to be common features of the SOR protein family, which was also demonstrated for the SOR proteins of *A. ambivalens* (Kletzin, 1989), *Aquifex aeolicus* (Pelletier *et al.*, 2008) and *Acidithiobacillus caldus*-like strains (Janosch *et al.* 2009). Although these proteins feature different catalytic properties such as pH and temperature optima (Table 1.1), the secondary and quarternary structures of SOR proteins from mesophilic and thermophilic microorganisms are highly similar as judged from CD spectroscopy and crystallographic datasets (Figure 5.8 and 5.10). However, an indispensable requirement for enzymes covering such a broad temperature range is a significant structural rigidity (Jaenicke, 2000; Trivedi *et al.*, 2006; Vieille and Zeikus, 2001; Radestock and Gohlke, 2011). In accordance, the *Hn*SOR 3D structure shows comparably low B-factors around the outer shell, giving a first hint that the framework is in a rigid condition (Figure 6.1). The B-factor, also known as atomic displacement parameters (ADP), indicates the mobility of each atom in the structure. Interestingly, the B-factors of all pore-forming residues are higher than those from residues constituting the SOR framework, suggesting an increased flexibility of the pores.

This might expand the actual pore size and could result in an elevated enzyme activity as already observed for deletion mutants of the *Aa*SOR (chapter 3). Taking into account that the *Hn*SOR activity is tenfold higher at 80°C than at 30°C, it is plausible that the entry and exit pores are significantly enlarged at elevated temperatures allowing a high influx of substrate and an increased exit rate of reaction products.

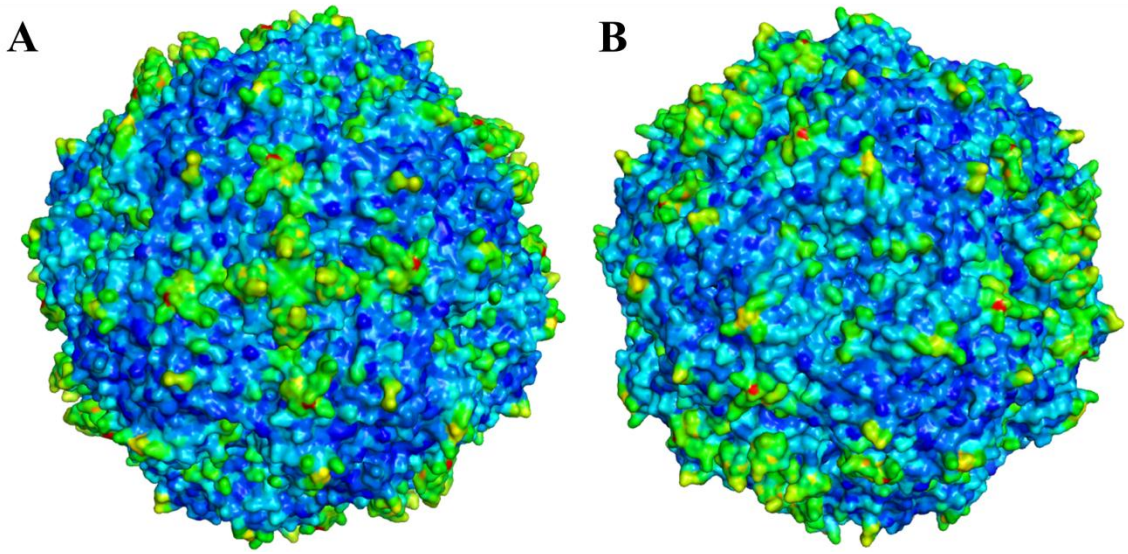

Figure 6.1 Surface representation of *Hn*SOR viewed from the non-crystallographic fourfold symmetry axis (**A**) and from the threefold symmetry axis (**B**). Atoms with B-factor coloring; dark blue - low B-factor; red - high B-factor.

6.4. Transport of sulfur substrate into the microbial cell

Even though elemental sulfur is used for the SOR assay *in vitro*, the initial substrate of the enzyme has to be a linear sulfur molecule such as polysulfide as already demonstrated by *in silico* analyses (Urich *et al.*, 2006). Polysulfide has a much higher solubility in aqueous solutions at neutral and alkaline conditions and its consumption by the SOR was shown with an in-gel enzyme activity assay for the *A. aeolicus* protein (Pelletier *et al.*, 2008) and for the *Aa*SOR in this work (chapter 3). Nevertheless, the sulfur substrate has to cross the cytoplasmic membrane to reach the SOR within the microbial cell. The transport of sulfur substrate, either polysulfide or elemental sulfur, across the membrane is barely understood in sulfur-metabolizing bacteria and archaea, although different studies were carried out for the purple sulfur bacterium *Allochromatium vinosum* to unravel this type of transport mechanism (Franz *et al.*, 2007; Franz *et al.*, 2009; Franz *et al.*, 2010).

A sulfur transport system was not identified, but it was shown that cell surface-sulfur contact was necessary for the uptake of elemental sulfur, while polymeric sulfur chains were strongly preferred over thermodynamically stable cyclic octasulfur molecules. It has to be noted that elemental sulfur always contains small amounts of polymeric sulfur (Franz *et al.,* 2007). Different enzymes such as rhodaneses, rhodanese-like proteins or cysteine desulfurases were described to be capable to catalyze the transfer of sulfur, thereby converting it into its activated form also termed as "persulfidic sulfur" (Kessler, 2006). An example for a rhodanese-like protein is the periplasmatic sulfur-transporting enzyme named Sud. It was originally isolated as a sulfide dehydrogenase from the proteobacterium *Wolinella succinogenes*, which can grow anaerobically with polysulfide as electron acceptor. Sud mediates the polysulfide transport to the active site of a membrane-bond polysulfide reductase in the periplasm (Klimmek *et al.,* 1998). More recently, a thermostable rhodanese from *A. aeolicus* has been described catalyzing the transfer of thiosulfate, tetrathionate and polysulfide *in vitro* (Giuliani *et al.,* 2007). A similar enzyme could mediate the transfer of the sulfur substrate but it remains unclear, whether the transport can be mediated across the cytoplasmic membrane.

6.5. The sulfur substrate pathway

Although the uptake and transport of the sulfur substrate is unknown in the microbial cell, a detailed picture of the hypothetical substrate route in the SOR could be drawn from the observations and results of the corresponding sulfur pathway mutants in the *Acidianus ambivalens* enzyme (chapter 3):

(1) The linear sulfur molecule, most probably polysulfide, enters the inner cavity of the holoenzyme through chimney-like structures at the fourfold symmetry axes in the outer shell (Figure 3.3 and 5.12). Those structures are defined by four adjacent subunits and form a hydrophobic pore that is restricted to approximately 5 Å in size in the *Aa*SOR and in the *Hn*SOR (Table 6.1). A deletion of the chimney-like structures enlarges the entry pores in the *Aa*SOR up to 10 Å and elevates enzyme activity up to the eightfold, indicating that these structures are not essential for the SOR *in vitro.* The boost of enzyme activity however suggests that these pores must be the entry point for the substrate.

(2) Access from the inner hollow to the active site, which is buried in a pocket at each monomer, is gained via a narrow pore that is formed by three hydrophobic residues (Figure 3.7 and 5.14a).

The integrity of this entry pore appears to be crucial for enzyme activity, since substitutions for hydrophilic residues decrease enzyme activity (chapter 3). It can be speculated, whether the negatively charged polysulfide substrate molecule is guided to the active site pocket entry by the attraction to positive surface charges in the interior. This is supported by conserved positively charged amino acids that are located halfway between tetramer channel and active site pocket pore.

(3) After catalysis, the reaction products exit the active site pocket through a second narrow opening (Fig 5.14b). It is formed by four mainly hydrophobic residues that are located at the opposite side of the pocket entry. Interestingly, this "back exit" appears to be in a closed state in the *Aa*SOR structure, probably resulting from alternative conformations of the respective residues.

(4) The active site exit pore opens to a short passage that leads to a second type of pore openings at the outer shell. These apertures are located at the threefold symmetry axes and are defined by three adjacent subunits (Fig 3.5 and 5.13). The pore opening is formed by three polar residues that can interact with the corresponding residues of the adjacent monomers via hydrogen-bonding or salt bridges. In the *Aa*SOR, the pore with a size of 5 Å is thus kept in a less flexible conformation. The enlargement of this exit pore elevated enzyme activity up to the threefold (chapter 3). In contrast, the pore size in the *Hn*SOR structure is reduced to 3.9 Å, while the pore-forming residues provide an H-bond network centered at E_{101}. The salt bridges, which confer rigidity to the threefold axis of the *Aa*SOR, are substituted for hydrogen-bonding interactions, keeping the *Hn*SOR opening more flexible.

In combination with the observations at the tetramer channel it can be concluded that an enlarged pore size in the outer shell is generally accompanied by a higher SOR activity. The pathways for substrate entry and product exit, originally described from crystallography data for the *A. ambivalens* and the *A. tengchongensis* protein (Li *et al.*, 2008; chapter 3), were also found in the *Hn*SOR structure. The substrate entry pores of the *Aa*SOR and the *Hn*SOR structures were highly similar in structure and pores sizes, while the product exit pores differed slightly in flexibility and in opening size (Table 6.1). The structural composition of the active site pocket pores was similar as well, even though an exit opening was only observed in the *Hn*SOR and in the *At*SOR (Table 6.1).Therefore, the proposed substrate pathway seems to be universally valid for all SOR proteins (Figure 6.2).

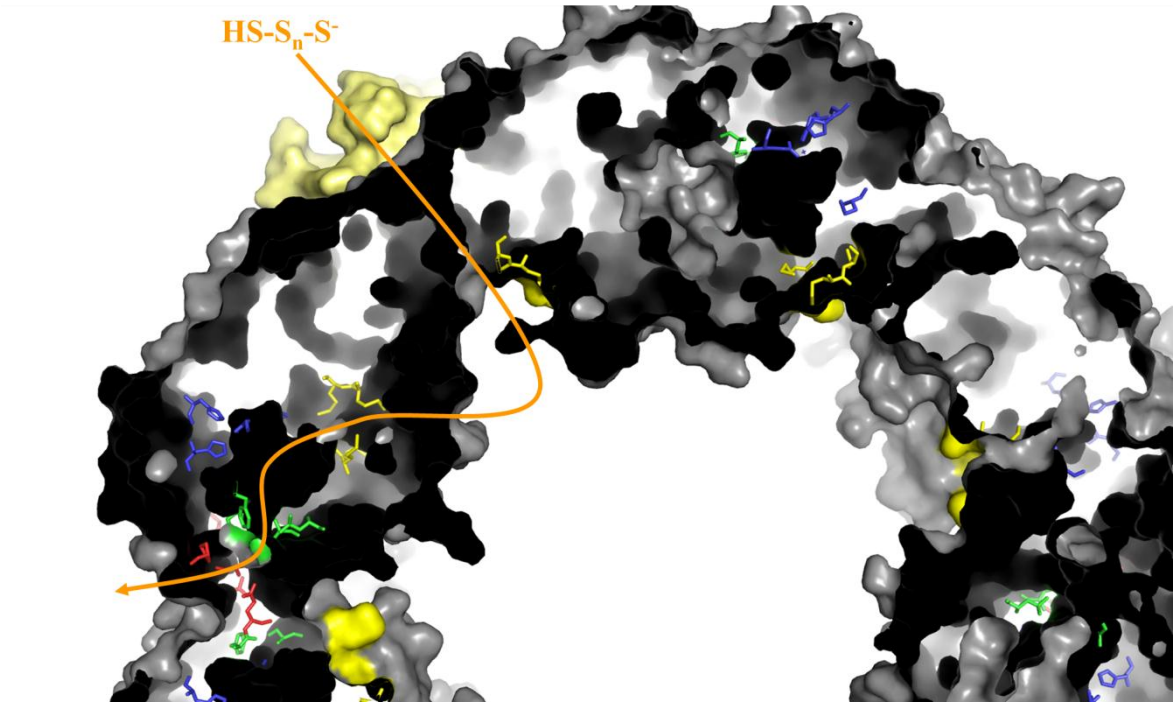

Figure 6.2 Cross section of the *Hn*SOR holoenzyme showing the cavities (white) and the pathway of the substrate and products (orange arrow). The chimney-like structure at the fourfold symmetry axis is shown in pale yellow. Yellow sticks represent the active site pore-forming residues M_{25}, M_{302} and M_{303}. Blue sticks represent the iron-coordinating amino acids H_{88}, H_{92} and E_{116}. Green sticks represent the active site exit pore, shaped by F_{100}, F_{210}, L_{107} and $S_{104.}$ Red sticks represent the trimer channel opening, framed by A_{226} and E_{101}.

Although the catalytic efficiency of SOR proteins is elevated significantly at higher temperatures, the role of the activity-limiting tetramer and trimer pores remains to be investigated. A strictly regulated SOR activity appears to be essential for the microbial cell *in vivo*. It is plausible that the reaction products are delivered directly and in a regulated way to the downstream and membrane-associated thiosulfate:quinone oxidoreductase (TQO) and sulfide:quinone oxidoreductase (SQR), thereby preventing the excessive accumulation of highly reactive sulfur species in the cytoplasm. Support for an interaction with those enzymes comes from antibody/immunogold electron microscopy experiments with the *At*SOR, indicating that the protein is mainly attached to the cytoplasmic membrane (Chen *et al.*, 2005).

Table 6.1 Structural differences and similarities between both *Aa*SOR proteins and *Hn*SOR

	***Aa*SOR (Urich *et al.*, 2006)**	***Aa*SOR (this work)**	***Hn*SOR (this work)**
Space group	I4	$P6_322$	$P2_12_12_1$
Monomers in the asymmetric unit	6	4	24
Monomer topology	central β-barrel surrounded by α-helices		
Tetramer channel pore size and features	5.0 Å, restricted by two phenylalanine rings (F_{133}/F_{141})		4.9 Å, restricted by one phenylalanine ring (F_{143})
Trimer channel pore size	4.0 Å		3.9 Å
Trimer channel pore-forming residues	R_{99}, S_{226}, E_{228}		$E_{101,}$ A_{226}, N_{227}
Active site pocket pore-forming residues	F_{23}, M_{296}, M_{297}		M_{25}, M_{302}, M_{303}
Active site pocket exit	not identified; pore appears to be in a closed state		open pore formed by F_{210}, F_{100}, L_{107}, S_{104}
Cysteine persulfuration	yes (Css_{31})[1]	no (Cys_{31})[2]	yes (Css_{33})
Fe coordination sphere residues	H_{86}, H_{90}, E_{114}		H_{88}, H_{92}, E_{116}
Second coordination sphere residues	E_{87}		Y_{118}

[1]with heat treatment
[2] without heat treatment

6.6. The active site of the SOR

6.6.1. Temperature-induced persulfuration of the cysteine

The active site of the SOR comprises a mononuclear iron center and the three cysteines of the enzyme, located in a spacious pocket deeply buried in each monomer. One of these cysteines, namely C_{31} (*A. ambivalens* numbering) or C_{33} (*H. neapolitanus* numbering), can contain an additional sulfur atom at the S-γ atom in the originally resolved recombinant *Aa*SOR structure and in the recombinant *Hn*SOR structure. The additional sulfur atom makes it an ideal candidate to be the actual binding site of the sulfur substrate. Support comes from previous mutation analyses performed for the three conserved cysteine residues at the active site pocket (Urich *et al.*, 2005b). The mutation of C_{31} resulted in a completely inactive enzyme, while C_{101} and C_{104} mutants (*A. ambivalens* numbering) showed residual SOR activity. An unmodified cysteine was present at the same position in the newly crystallized recombinant *Aa*SOR (Figure 4.3; Table 6.1) and in the recombinant *At*SOR structure (Li *et al.*, 2008), suggesting that this residue may not be modified *ab*

initio. A comparison of the different purification processes of the *Aa*SOR proteins showed that a heating step is required to modify the residue in an auto-sulfuration process (chapter 4) without the involvement of other proteins (Figure 6.3).

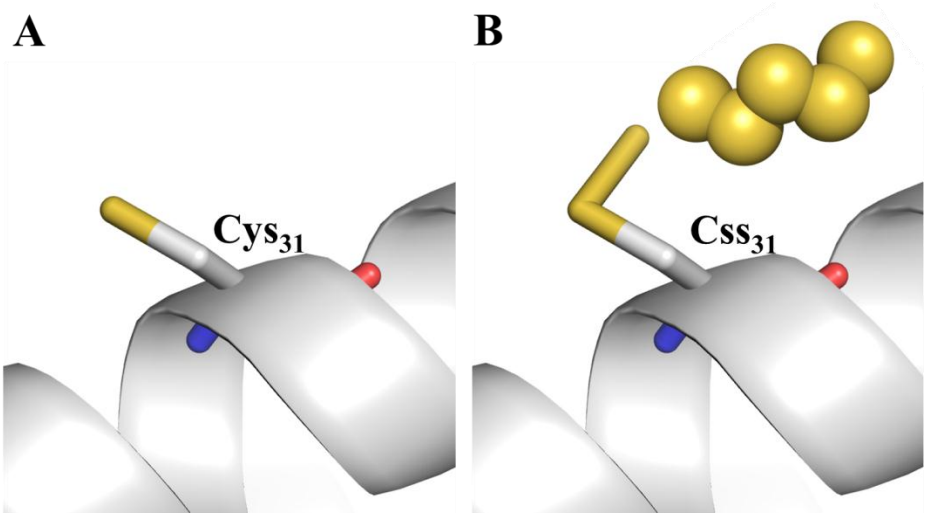

Figure 6.3 Ribbon and stick view from the essential active site cysteine in (**A**) unmodified state as observed in the recrystallized *Aa*SOR and (**B**) in the persulfurated state with an additional S-δ atom. Color representation: red - oxygen, blue - nitrogen, and white - carbon. The polysulfide substrate is represented by yellow spheres.

In contrast, the persulfuration of the *Hn*SOR cysteine did not require an additional heating step. It is feasible that 37°C, the temperature at which heterologous gene expression was carried out, is sufficient to induce the auto-sulfuration of the respective cysteine, since *Hn*SOR is biochemically active at these temperatures. The additional sulfur atom most probably derives from soluble *E. coli* extract although it is unknown which sulfur-containing molecule serves as sulfur donor. In addition, it was demonstrated that the auto-sulfuration is not essential for enzyme activity, since the unmodified *Aa*SOR was biochemically active without additional heat treatment. It is likely, that the modified SOR already underwent the catalytic cycle and that the persulfide represents the residual sulfur substrate chain attached to the respective cysteine.

6.6.2. Hydrogen bond network and the metal's redox state

The second central component of the active site is the mononuclear iron center with its first and second coordination spheres. The first coordination sphere of the *Aa*SOR comprises two conserved histidines (H_{86} and H_{90}), one conserved glutamate (E_{114}) and two water molecules, which all coordinate the Fe atom in a distorted octahedral geometry (Urich *et al.*, 2006). The second water ligand is missing in the *At*SOR and *Hn*SOR structure as a

result of the lower resolution of the crystallography datasets. The second coordination sphere in the three available SOR 3D structures consists of a single amino acid, either Y_{118} (*Hn*SOR) or E_{87} (*Aa*SOR and *At*SOR). The latter is conserved among all SOR proteins, while the tyrosine is replaced for a phenylalanine in several other SORs (Fig 1.10). Analysis of an *Aa*SOR E_{87}A mutant showed a strong decrease of enzyme activity with a complete loss of reductase activity (Seyfarth, 2006; chapter 4), indicating the crucial role of the second coordination sphere. It is feasible that E_{87} or Y_{118}, respectively, stabilizes the position of the Fe-liganding histidine, thereby keeping the iron in a sixfold-coordination state. It is unknown, whether E_{87} is directly involved in the catalytic cycle. Nevertheless, the intramolecular hydrogen bond to one of the Fe-coordinating amino acid ligands seems to be essential for SOR activity. The importance of hydrogen bond networks at the active site had already been described for a number of different enzymes. Mutations in the second coordination sphere for instance caused a decreased catalytic efficiency of a soybean lipooxygenase (Schenk *et al.*, 2003) or a strong shift in the redox potential of a superoxide dismutase from *E. coli* (Yikilimaz *et al.*, 2007). The reduction potential of the iron center of the *Aa*SOR was determined to be unusually low for non-heme mononuclear enzymes with E_0' = - 268 mV, which is low enough to allow the reduction of sulfur to sulfide (Urich *et al.*, 2004). Moreover, it was shown via EPR spectroscopy that both native and recombinant "as isolated" *Aa*SOR proteins contain ferric iron, which becomes reduced upon sulfur incubation (Urich *et al.*, 2004). The question, whether this redox change is mandatory for SOR activity was addressed in this work by refolding and derivatizing *Aa*SOR inclusion bodies with different metal ions. SOR derivatives containing iron, cobalt, manganese or nickel were enzymatically active. EPR spectra of the refolded Fe-containing protein showed the expected change of oxidation state of iron (Figure 4.11). The respective metals in the cobalt-, nickel- and manganese-derivatized SORs were detected in the 2+ oxidation state. Neither a Co-containing nor a Mn-containing SOR were reduced upon sulfur incubation and both metals remained in the same oxidation state. The hyperfine splitting signal of cobalt disappeared (Figure 4.14), while slightly decreased signal intensities of cobalt and manganese pointed to small structural rearrangements occurring at the metal site during catalysis (Figure 4.15). In contrast, the 3D structure of the cobalt-derivative did not show significant differences within the active site and especially the positions of the second or first coordination sphere residues did not change (Figure 4.20).

6.7. Catalytic mechanism of the SOR

Non-heme mononuclear iron oxygenases are very diverse in sequence and structure, although they have one problem in common: the activation of dioxygen. Most of these enzymes contain a common structural motif for iron-coordination, referred to as the "2-His-1-carboxylate facial triad" (Hegg and Que, 1997; Bruijnincx *et al.*, 2008). The protein family carrying such a motif catalyzes a wide range of different oxidations and/or transformations, so that different O_2 activation strategies had developed (Kovaleva and Lipscomb, 2008). However, a general pattern was recognized (Figure 6.4; Koehntop *et al.*, 2005). The iron center is sixfold-coordinated at the start of the catalytic cycle (**A**). Binding of the substrate to the metal center is caused by ligands that open the sixfold coordination state (**B**). Dioxygen binds to the Fe center (**C**), thereby generating different short-lived Fe/peroxo/oxo intermediates (**D/E**) with Fe(III), Fe(IV) or even Fe(V) (Kovaleva and Lipscomb, 2008; Bruijnincx *et al.*, 2008; Koehntop *et al.*, 2005).

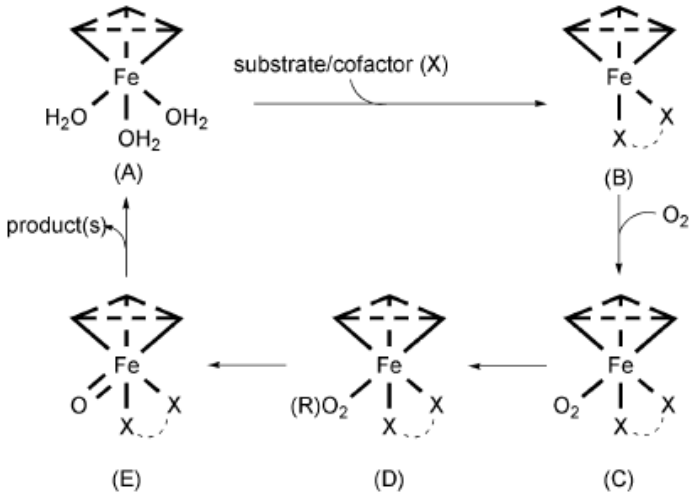

Figure 6.4 General mechanistic pathway proposed for oxygenases with a 2-His-1-carboxylate facial triad (from Bruijnincx *et al.*, 2008).

In contrast, metal-substituted homoprotocatechuate dioxygenases, also members of the non-heme oxygenase protein family, have been recently shown to activate dioxygen without a change of the metal's redox state. Electrons are directly transferred from the substrate to dioxygen via the metal center, while both substrate and dioxygen are bound to the metal site (*Emerson et al.*, 2008; Fielding *et al.*, 2011). It is feasible that a similar situation could be valid for the SOR reaction cycle. With respect to the reaction mechanism of the SOR, different scenarios are possible (Figure 6.5).

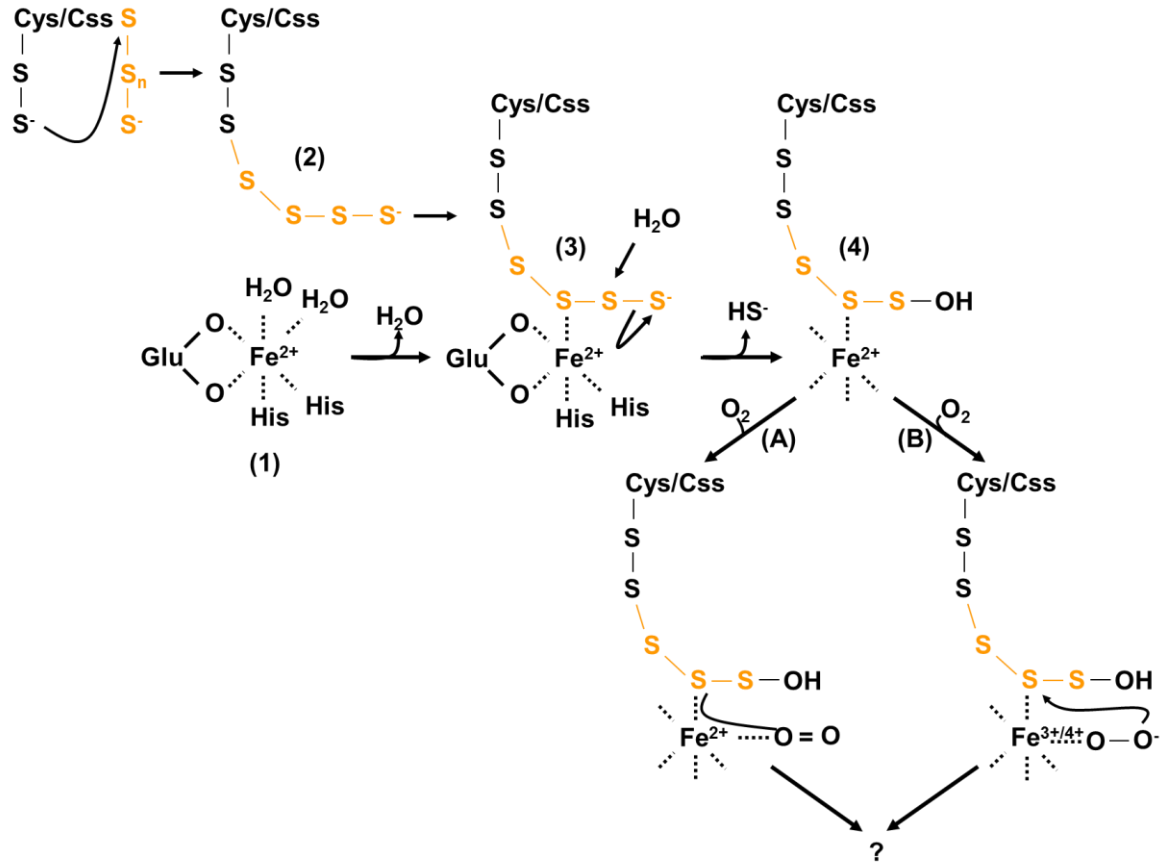

Figure 6.5 Hypothetical model of the initial steps of the SOR reaction mechanism.

The resting state of the SOR includes the metal center in the Fe(II) state. This is contrary to EPR spectra of the "as isolated" protein, but ferrous iron is the common theme among all other mononuclear non-heme iron oxygenases (Koehntop *et al.*, 2005). Moreover, it is difficult to imagine that the iron becomes oxidized in a surplus of reductants such as sulfide (E_0' = - 270 mV) and/or sulfite (E_0' = - 516 mV). The iron atom is centered in the 2-His-1-carboxylate motif including two water molecules that occupy the two vacant coordination sites (1). The auto-sulfurization of the cysteine is not essential but its thiol group has to be in an activated state to bind the sulfur substrate (2). After covalent binding to the persulfurated/non-persulfurated cysteine, the sulfur chain becomes aligned to the metal center (3). Consequently, at least one of the solvent ligands leaves the coordination sphere and binding of the enzyme-substrate complex primes the iron to activate dioxygen.

The following series of reactions is unclear, although the present hypothesis predicts a nucleophilic attack on the sulfur chain, most probably by a hydroxyl ion formed by deprotonation of the second water ligand (Kletzin, 2008). The metal would thus act as a Lewis acid in this reaction. Sulfide is abstracted while the cysteine-bound substrate is

converted into an unstable and reactive cysteine-polysulfenic acid (4) (Kettenhofen and Wood, 2010; Reddie and Carroll, 2008). In the next step, dioxygen binds to the vacant position of the unsaturated Fe(II) center. The following steps are rather unknown, since O_2 can either be activated by the substrate or by the metal center. The first scenario (A) includes the parallel binding of substrate and dioxygen to the metal center, whereas electrons are directly transferred to O_2 without a change of the redox state of the iron. The second scenario (B) provides dioxygen-binding to the metal site with the formation of transient Fe intermediates that can either be Fe(III), Fe(IV) or even Fe(V). Usually, Fe-superoxo intermediates are formed, followed by cleavage of the O-O bond. The remaining Fe-hydroperoxo species forms a high-valent Fe-oxo (Fe(IV)/Fe(V)) state, which eventually oxidizes the substrate (Nam, 2007). Further steps are unknown and it is still unclear, how sulfite and or thiosulfate are generated during the catalytic cycle.

6.8. Conclusions and perspectives

The present work showed new details of the SOR reaction mechanism including a description of the structure-function relationship of the sulfur substrate pathway. In addition, the first biochemical characterization of a SOR originating from a mesophilic microorganism showed that this protein family not only shares a similar monomer and holoenzyme structure but also a distinct thermostability and a broad temperature and pH range of enzyme activity. EPR spectroscopy of metal-substituted SOR enzymes and numerous active site mutants gave new insights in regard to the protein's reaction mechanism. Future studies should aim to unravel the catalytic process completely. The *Hn*SOR represents a great starting point for future experiments, as it covers a broader range of activity with respect to temperature and pH in comparison to the *Aa*SOR. Randomized mutants could by analyzed more easily because of the high activity exhibited by the enzyme. In contrast, enzyme activity at 30°C also enables monitoring of the catalytic cycle at moderate temperatures. Therefore, it is essential to focus on spectroscopical methods such as stopped-flow transient kinetics experiments, Mössbauer spectroscopy and EPR spectroscopy of the *Hn*SOR to detect transient Fe-intermediates at the active site during catalysis. X-ray crystallography of *Hn*SOR in presence of polysulfide could also reveal intermediate stages of the enzyme's catalytic cycle. Those methods are protein- and time-consuming, but the heterologous gene expression system of the *Hn*SOR, which was adapted from the *Aa*SOR, was established in the course of this work. It

provided around tenfold higher protein amounts in comparison to the *Aa*SOR. Another important prerequisite is to establish a sensitive HPLC-based activity assay to detect both substrate and reaction products in parallel. It also would be of interest to investigate the role of the SOR in *Halothiobacillus neapolitanus* with respect to the presence of a complete SOX multienzyme system. *H. neapolitanus* is genetically accessible and a knockout mutant could not only deliver details about the regulation of sulfur oxidation in this bacterium but also about the potential interaction of the SOR with other enzymes. In addition, the SOR can serve as a future model system for thermostability, which might also be used as a nanocontainer for biological or technological applications at different conditions.

Literature

(1994) The CCP4 suite: programs for protein crystallography. *Acta Crystallogr D Biol Crystallogr* **50**: 760-763.

Adams, P. D., Afonine, P. V., Bunkoczi, G., Chen, V. B., Davis, I. W., Echols, N., Headd, J. J., Hung, L. W., Kapral, G. J., Grosse-Kunstleve, R. W., McCoy, A. J., Moriarty, N. W., Oeffner, R., Read, R. J., Richardson, D. C., Richardson, J. S., Terwilliger, T. C. and Zwart, P. H. (2010). PHENIX: a comprehensive Python-based system for macromolecular structure solution. *Acta Crystallogr D* **66**: 213-221.

Andreini, C., Bertini, I., Cavallaro, G., Najmanovich, R. J. and Thornton, J. M. (2009). Structural Analysis of Metal Sites in Proteins: Non-heme Iron Sites as a Case Study. *J Mol Biol* **388**: 356-380.

Arnold, K., Bordoli, L., Kopp, J. and Schwede, T. (2006). The SWISS-MODEL workspace: a web-based environment for protein structure homology modelling. *Bioinformatics* **22**: 195-201.

Beard, S., Paradela, A., Albar, J. P. and Jerez, C. A. (2011). Growth of *Acidithiobacillus ferrooxidans* ATCC 23270 in thiosulfate under oxygen-limiting conditions generates extracellular sulfur globules by means of a secreted tetrathionate hydrolase. *Front Microbio* **2:**79 doi: 10.3389/fmicb.2011.00079.

Bencini, A., Bertini, I., Canti, G., Gatteschi, D. and Luchinat, C. (1981). The epr Spectra of the Inhibitor Derivatives of Cobalt Carbonic Anhydrase. *J Inorg Biochem* **14**: 81-93.

Berman, H. M., Westbrook, J., Feng, Z., Gilliland, G., Bhat, T. N., Weissig, H., Shindyalov, I. N. and Bourne, P. E. (2000). The Protein Data Bank. *Nucleic Acids Res* **28**: 235-242.

Böhm, G., Muhr, R. and Jaenicke, R. (1992). Quantitative Analysis of Protein Far UV Circular Dichroism Spectra by Neural Networks. *Protein Eng* **5**: 191-195.

Boulegue, J. (1978). Solubility of elemental sulfur in water at 298 K *Phosphorus Sulfur Silicon Relat. Elem* **5**: 127-128.

Bradford, M. M. (1976). A rapid and sensitive method for the quantitation of microgram quantities of protein utilizing the principle of protein-dye binding. *Anal Biochem* **72**: 248-254.

Brandl, H. (2001). Microbial leaching of metals. In: Biotechnology: Vol. 10 - Special Processes (Rehm, H. J. [ed.]). Wiley-VCH Verlag GmbH, Weinheim, Germany, pp. 191-224.

Brasseur, G., Levican, G., Bonnefoy, V., Holmes, D., Jedlicki, E. and Lemesle-Meunier, D. (2004). Apparent redundancy of electron transfer pathways via bc(1) complexes and terminal oxidases in the extremophilic chemolithoautotrophic *Acidithiobacillus ferrooxidans*. *Biochim biophys acta* **1656**: 114-126.

Brito, J. A., Sousa, F. L., Stelter, M., Bandeiras, T. M., Vonrhein, C., Teixeira, M., Pereira, M. M. and Archer, M. (2009). Structural and functional insights into sulfide:quinone oxidoreductase. *Biochemistry* **48**: 5613-5622.

Bruijnincx, P. C., van Koten, G. and Klein Gebbink, R. J. (2008). Mononuclear non-heme iron enzymes with the 2-His-1-carboxylate facial triad: recent developments in enzymology and modeling studies. *Chem Soc Rev* **37**: 2716-2744.

Bugaytsova, Z. and Lindstrom, E. B. (2004). Localization, purification and properties of a tetrathionate hydrolase from Acidithiobacillus caldus. *Eur J Biochem* **271**: 272-280.

Carugo, O. and Bordo, D. (1999) How many water molecules can be detected by protein crystallography? *Acta Crystallogra D* **55**: 479-483.

Chen, Z. W., Jiang, C. Y., She, Q. X., Liu, S. J. and Zhou, P. J. (2005). Key role of cysteine residues in catalysis and subcellular localization of sulfur oxygenase-reductase of *Acidianus tenghongensis*. *Appl Environ Microb* **71**: 621-628.

Chen, Z. W., Liu, Y. Y., Wu, J. F., She, Q., Jiang, C. Y. and Liu, S. J. (2007). Novel bacterial sulfur oxygenase reductases from bioreactors treating gold-bearing concentrates. *Appl Microbiol Biotechnol* **74**: 688-698.

Chen, Z. W., Jiang, C. Y. and Liu, S. J. (2009). Site-directed mutagenesis reveals new and essential elements for iron-coordination of the sulfur oxygenase reductase from the acidothermophilic Acidianus tengchongensis. Chinese Sci Bull **54**: 652-657.

Copeland, A., Spring, S., Goker, M., Schneider, S., Lapidus, A., Del Rio, T. G., Tice, H., Cheng, J. F., Lucas, S., Chen, F., Nolan, M., Bruce, D., Goodwin, L., Pitluck, S., Ivanova, N., Mavromatis, K., Ovchinnikova, G., Pati, A., Chen, A., Palaniappan, K., Land, M., Hauser, L., Chang, Y. J., Jeffries, C. C., Meincke, L., Sims, D., Brettin, T., Detter, J. C., Han, C., Chain, P., Bristow, J., Eisen, J. A., Markowitz, V., Hugenholtz, P., Kyrpides, N. C. and Klenk, H. P. (2009). Complete genome sequence of *Desulfomicrobium baculatum* type strain (X-T). *Stand Genomic Sci* **1**: 29-37.

Costas, M., Mehn, M. P., Jensen, M. P. and Que, L. (2004). Dioxygen activation at mononuclear nonheme iron active sites: Enzymes, models, and intermediates. *Chem Rev* **104**: 939-986.

Cypionka, H. (2000). Oxygen respiration by *Desulfovibrio* species. *Annu Rev Microbiol* **54**: 827-848.

Dahl, C., Engels, S., Pott-Sperling, A. S., Schulte, A., Sander, J., Lubbe, Y., Deuster, O. and Brune, D. C. (2005). Novel Genes of the dsr Gene Cluster and Evidence for Close Interaction of Dsr Proteins during Sulfur Oxidation in the Phototrophic Sulfur Bacterium *Allochromatium vinosum*. *J Bacteriol* **187**: 1392-1404.

DeLano, W. L. (2002). The PyMOL Molecular Graphics System, 0.97 Edn. San Carlos, CA: DeLano Scientific.

Emerson, J. P., Kovaleva, E. G., Farquhar, E. R., Lipscomb, J. D. and Que, L. (2008). Swapping metals in Fe- and Mn-dependent dioxygenases: Evidence for oxygen activation without a change in metal redox state. *Proc Natl Acad Sci U S A* **105**: 7347-7352.

Emmel, T., Sand, W., König, W. A. and Bock, E. (1986). Evidence for the Existence of a Sulfur Oxygenase in *Sulfolobus brierleyi*. *J Gen Microbiol* **132**: 3415-3420.

Emsley, P., Lohkamp, B., Scott, W. G. and Cowtan, K. (2010). Features and development of Coot. *Acta Crystallogr D Biol Crystallogr* **66**: 486-501.

Eswar, N., Webb, B., Marti-Renom, M. A., Madhusudhan, M. S., Eramian, D., Shen, M.-y., Pieper, U. and Sali, A. (2001). Comparative Protein Structure Modeling Using MODELLER. In: *Current Protocols in Protein Science*, Johnn Wiley & Sons, Inc., Supplement 15, 5.6.1-5.6.30.

Evans, G. and Pettifer, R. F. (2001). CHOOCH: a program for deriving anomalous-scattering factors from X-ray fluorescence spectra. *J Appl Crystallogr* **34**: 82-86.

Fielding, A. J., Kovaleva, E. G., Farquhar, E. R., Lipscomb, J. D. and Que, L. (2011). A hyperactive cobalt-substituted extradiol-cleaving catechol dioxygenase. *J Biol Inorg Chem.* **16**: 341-355.

Fischer, D. S. and Price, D. C. (1964). A Simple Serum Iron Method Using the New Sensitive Chromogen Tripyridyl-s-triazine. *Clin Chem* **10**: 21-31.

Franz, B., Lichtenberg, H., Hormes, J., Dahl, C. and Prange, A. (2009). The speciation of soluble sulphur compounds in bacterial culture fluids by X-ray absorption near edge structure spectroscopy. *Environ Technol* **30**: 1281-1289.

Franz, B., Balkundi, S. S., Dahl, C., Lvov, Y. M. and Prange, A. (2010). Layer-by-Layer Nano-Encapsulation of Microbes: Controlled Cell Surface Modification and Investigation of Substrate Uptake in Bacteria. *Macromol Bios.* **10**: 164-172.

Franz, B., Lichtenberg, H., Hormes, J., Modrow, H., Dahl, C. and Prange, A. (2007). Utilization of solid 'elemental' sulfur by the phototrophic purple sulfur bacterium *Allochromatium vinosum*: a sulfur K-edge X-ray absorption spectroscopy study. *Microbiol-Sgm* **153**: 1268-1274.

Friedrich, C. G., Rother, D., Bardischewsky, F., Quentmeier, A. and Fischer, J. (2001). Oxidation of reduced inorganic sulfur compounds by bacteria: Emergence of a common mechanism? *Appl Environ Microb* **67**: 2873-2882.

Friedrich, C. G., Bardischewsky, F., Rother, D., Quentmeier, A. and Fischer, J. (2005). Prokaryotic sulfur oxidation. *Curr Opin Microbiol* **8**: 253-259.

Friedrich, C. G., Quentmeier, A., Bardischewsky, F., Rother, D., Orawski, G., Hellwig, P. and Fischer, J. (2008). Redox Control of Chemotrophic Sulfur Oxidation of *Paracoccus pantotrophus*. In: *Microbial Sulfur Metabolism* (Dahl, C. and Friedrich, C.G., [eds.]). Springer, Berlin, Germany, pp. 139-150.

Frigaard, N. U. and Dahl, C. (2009). Sulfur Metabolism in Phototrophic Sulfur Bacteria. In: *Advances in Microbial Physiology*, Vol 54. (Hell, R.; Dahl, C.; Knaff, D. B.; Leustek, T. [eds.]). Academic Press Ltd, London, UK, pp. 103-200.

Fuchs, T., Huber, H., Burggraf, S. and Stetter, K. O. (1996). 16S rDNA-based phylogeny of the archaeal order *Sulfolobales* and reclassification of *Desulfurolobus ambivalens* as *Acidianus ambivalens* comb. nov. *Syst Appl Microbiol* **19**: 56-60.

Futterer, O., Angelov, A., Liesegang, H., Gottschalk, G., Schleper, C., Schepers, B., Dock, C., Antranikian, G. and Liebl, W. (2004). Genome sequence of *Picrophilus torridus* and its implications for life around pH 0. *Proc Natl Acad Sci U S A* **101**: 9091-9096.

Gaffney, B. J., Su, C. and Oliw, E. H. (2001). Assignment of EPR transitions in a manganese-containing lipoxygenase and prediction of local structure. *Appl Magn Reson* **21**: 411-422.

Garnier, J., Gibrat, J. F. and Robson, B. (1996). GOR method for predicting protein secondary structure from amino acid sequence in *Computer Methods for Macromolecular Sequence Analysis* (Doolittle, R. F. [ed.]). *Methods Enzymol* **266**: 540-553.

Ghosh, W. and Dam, B. (2009). Biochemistry and molecular biology of lithotrophic sulfur oxidation by taxonomically and ecologically diverse bacteria and archaea. *FEMS Microbiol Rev* **33**: 999-1043.

Ghosh, W., Mallick, S. and DasGupta, S. K. (2009). Origin of the Sox multienzyme complex system in ancient thermophilic bacteria and coevolution of its constituent proteins. *Res Microbiol* **160**: 409-420.

Giuliani, M. C., Tron, P., Leroy, G., Aubert, C., Tauc, P. and Giudici-Orticoni, M. T. (2007). A new sulfurtransferase from the hyperthermophilic bacterium *Aquifex aeolicus* - Being single is not so simple when temperature gets high. *FEBS J* **274**: 4572-4587.

Grimm, F., Franz, B. and Dahl, C. (2008). Thiosulfate and Sulfur Oxidation in Purple Sulfur Bacteria. In: *Microbial Sulfur Metabolism* (Dahl, C. and Friedrich, C.G., [eds.]). Springer, Berlin, Germany, pp. 101-116.

Guiral, M., Tron, P., Aubert, C., Gloter, A., Iobbi-Nivol, C. and Giudici-Orticoni, M. T. (2005). A membrane-bound multienzyme, hydrogen-oxidizing, and sulfur-reducing complex from the hyperthermophilic bacterium *Aquifex aeolicus*. *J Biol Chem* **280**: 42004-42015.

Hahn, T. (2002). *International Tables for Crystallography*. Volume A: Space-group symmetry. Springer, Heidelberg, Germany.

Han, M. V., Zmasek, C. M. (2009). phyloXML: XML for evolutionary biology and comparative genomics. *BMC Bioinf*ormarics **10:**356 doi:10.1186/1471-2105-10-356

He, Z., Li, Y., Zhou, P. and Liu, S. (2000). Cloning and heterologous expression of a sulfur oxygenase/reductase gene from the thermoacidophilic archaeon *Acidianus* sp. S5 in *Escherichia coli*. *FEMS Microbiol Lett* **193**: 217-221.

Hegg, E. L. and Que, L., Jr. (1997). The 2-His-1-carboxylate facial triad--an emerging structural motif in mononuclear non-heme iron(II) enzymes. *Eur J Biochem* **250**: 625-629.

Hensen, D., Sperling, D., Trüper, H. G., Brune, D. C. and Dahl, C. (2006). Thiosulphate oxidation in the phototrophic sulphur bacterium *Allochromatium vinosum*. *Mol. Microbiol.* **62**: 794-810.

Hutchinson, E. G. and Thornton, J. M. (1996). PROMOTIF—A program to identify and analyze structural motifs in proteins. *Protein Science* **5**: 212-220.

Jaenicke, R. (2000). Stability and stabilization of globular proteins in solution. *J Biotechnol* **79**: 193-203.

Janner, A., (2008a) Comparative architecture of octahedral protein cages. I. Indexed enclosing forms. *Acta Crystallogr A* 64: 494-502.

Janner, A., (2008b) Comparative architecture of octahedral protein cages. II. Interplay between structural elements. *Acta Crystallogr A* 64: 503-512.

Janosch, C., Thyssen, C., Vera, M., Bonnefoy, V., Rohwerder, T. and Sand, W. (2009). Sulfur oxygenase reductase in different *Acidithiobacillus caldu*s-like strains. *Adv Materials Res* **71-73**: 239-242.

Kamyshny, A., Jr. (2009). Solubility of cyclooctasulfur in pure water and sea water at different temperatures. *Geochim Cosmochim Acta* **73**: 6022-6028.

Kanao, T., Kamimura, K. and Sugio, T. (2007). Identification of a gene encoding a tetrathionate hydrolase in *Acidithiobacillus ferrooxidans*. *J Biotechnol* **132**: 16-22.

Kappler, U. (2011). Bacterial sulfite-oxidizing enzymes. *Biochim Biophys Acta-Bioenerg* **1807**: 1-10.

Kelley, L. A. and Sternberg, M. J. (2009). Protein structure prediction on the Web: a case study using the Phyre server. *Nat Protoc* **4**: 363-371.

Kelly, D. P. and Wood, A.P. (2000). Reclassification of some species of *Thiobacillus* to the newly designated genera *Acidithiobacillus* gen. nov., *Halothiobacillus* gen. nov. and *Thermithiobacillus* gen. nov. Int J Syst Evol Microbiol **50 Pt 2**: 511-516.

Kelly, D. P. and Wood, A. P. (2005). *Halothiobacillus.* In: *Bergey's Manual of Systematic Bacteriology* (Brenner, D.J., Krieg, N.R., Staley, J.T. and Garrity, G.M. [eds.]). Springer, New York, USA, pp. 58-59.

Kessler, D. (2006). Enzymatic activation of sulfur for incorporation into biomolecules in prokaryotes. *FEMS Microbiol Rev* **30**: 825-840.

Kettenhofen, N. J. and Wood, M. J. (2010). Formation, Reactivity, and Detection of Protein Sulfenic Acids. *Chem Res Toxicol* **23**: 1633-1646.

King, T. E. and Morris, R. O. (1967). Determination of acid-labile sulfide and sulfhydryl groups. (Ronald W. Estabrook, M.E.P. [eds.]) *Methods Enzymol* **10**: 634-641.

Kletzin, A. (1989). Coupled enzymatic production of sulfite, thiosulfate, and hydrogen sulfide from sulfur: purification and properties of a sulfur oxygenase reductase from the facultatively anaerobic archaebacterium *Desulfurolobus ambivalens*. *J Bacteriol* **171**: 1638-1643.

Kletzin, A. (1992). Molecular characterization of the *sor* gene, which encodes the sulfur oxygenase/reductase of the thermoacidophilic Archaeum *Desulfurolobus ambivalens*. *J Bacteriol* **174**: 5854-5859.

Kletzin, A. (1994). Sulfur Oxidation and Reduction in Archaea - Sulfur Oxygenase/Reductase and Hydrogenases from the Extremely Thermophilic and Facultatively Anaerobic Archaeon *Desulfurolobus ambivalens*. *Syst Appl Microbiol* **16**: 534-543.

Kletzin, A., Urich, T., Muller, F., Bandeiras, T. M. and Gomes, C. M. (2004). Dissimilatory oxidation and reduction of elemental sulfur in thermophilic archaea. *J Bioenerg Biomembr* **36**: 77-91.

Kletzin, A. (2008). Oxidation of Sulfur and Inorganic Sulfur Compounds in *Acidianus ambivalens*. In: *Microbial Sulfur Metabolism* (Dahl, C. and Friedrich, C.G., [eds.]). Springer, Berlin, Germany, pp. 184-201.

Klimmek, O., Kreis, V., Klein, C., Simon, J., Wittershagen, A. and Kroger, A. (1998). The function of the periplasmic Sud protein in polysulfide respiration of *Wolinella succinogenes*. *Eur J Biochem* **253**: 263-269.

Koehntop, K. D., Emerson, J. P. and Que, L. (2005). The 2-His-1-carboxylate facial triad: a versatile platform for dioxygen activation by mononuclear non-heme iron(II) enzymes. *J Biol Inorg Chem* **10**: 87-93.

Kovaleva, E. G. and Lipscomb, J. D. (2008). Versatility of biological non-heme Fe(II) centers in oxygen activation reactions. *Nat Chem Biol* **4**: 186-193.

Krissinel, E. and Henrick, K. (2004). Secondary-structure matching (SSM), a new tool for fast protein structure alignment in three dimensions. *Acta Crystallogr D* **60**: 2256-2268.

Larkin, M. A., Blackshields, G., Brown, N. P., Chenna, R., McGettigan, P. A., McWilliam, H., Valentin, F., Wallace, I. M., Wilm, A., Lopez, R., Thompson, J. D., Gibson, T. J. and Higgins, D. G. (2007). Clustal W and clustal X version 2.0. *Bioinformatics* **23**: 2947-2948.

Li, M., Chen, Z., Zhang, P., Pan, X., Jiang, C., An, X., Liu, S. and Chang, W. (2008). Crystal structure studies on sulfur oxygenase reductase from *Acidianus tengchongensis*. *Biochem Biophys Res Commun* **369**: 919-923.

Liu, S. J. (2008). Archaeal and Bacterial Sulfur Oxygenase-Reductases: Genetic Diversity and Physiological Function. In: *Microbial Sulfur Metabolism* (Dahl, C. and Friedrich, C.G., [eds.]). Springer, Berlin, Germany, pp. 217-224.

Madigan, M. T. (2003). Anoxygenic phototrophic bacteria from extreme environments. *Photosynth Res* **76**: 157-171.

Mangold, S., Valdés, J., Holmes, D. and Dopson, M. (2011). Sulfur metabolism in the extreme acidophile *Acidithiobacillus caldus*. *Front Microbio* **2:**17
doi: 10.3389/fmicb.2011.00017

McCampbell Hamilton, E. (1991). The chemistry of low valent sulfur compounds in the sulfur-water system. PhD thesis, University of Minnesota, Minneapolis/St. Paul, USA.

McCoy, A. J., Grosse-Kunstleve, R. W., Adams, P. D., Winn, M. D., Storoni, L. C. and Read, R. J. (2007). Phaser crystallographic software. *J Appl Crystallogr* **40**: 658-674.

McIlvaine, T. C. (1921). A buffer solution for colorimetric comparison.
J Biol Chem **49**: 183-186.

Merkens, H., Kappl, R., Jakob, R. P., Schmid, F. X. and Fetzner, S. (2008). Quercetinase QueD of *Streptomyces* sp. FLA, a Monocupin Dioxygenase with a Preference for Nickel and Cobalt. *Biochemistry* **47**: 12185-12196.

Merkx, M. and Averill, B. A. (1998). Ga^{3+} as a Functional Substitute for Fe^{3+}: Preparation and Characterization of the $Ga^{3+}Fe^{2+}$ and $Ga^{3+}Zn^{2+}$ forms of Bovine Spleen Purple Acid Phosphatase. *Biochemistry* **37**: 8490-8497.

Moll, R. and Schäfer, G. (1988). Chemiosmotic H^+ cycling across the plasma membrane of the thermoacidophilic archaebacterium *Sulfolobus acidocaldarius FEBS Lett* **232**: 359-363.

Müller, F. H., Bandeiras, T. M., Urich, T., Teixeira, M., Gomes, C. M. and Kletzin, A. (2004). Coupling of the pathway of sulphur oxidation to dioxygen reduction: characterization of a novel membrane-bound thiosulphate:quinone oxidoreductase. *Mol Microbiol* **53**: 1147-1160.

Nam, W. (2007). Dioxygen activation by metalloenzymes and models. *Accounts Che. Res* **40**: 465.

Pachmayr, F. (1960). Vorkommen und Bestimmung von Schwefelverbindungen in Mineralwasser. PhD thesis, Justus-Maximilian Universität, Munich, Germany.

Parker, C. D. (1947). Species of sulphur bacteria associated with the corrosion of concrete. *Nature* **159**: 439-440.

Parker, C. D. and Prisk, J. (1953). The oxidation of inorganic compounds of sulphur by various sulphur bacteria *J Gen Microbiol* **8**: 344-364.

Pau, M. Y. M., Lipscomb, J. D. and Solomon, E. (2007). Substrate activation for O_2 reactions by oxidized metal centers in biology. *Proc Natl Acad Sci U S A* **104**: 18355-18362.

Pelletier, N., Leroy, G., Guiral, M., Giudici-Orticoni, M. T. and Aubert, C. (2008) First characterisation of the active oligomer form of sulfur oxygenase reductase from the bacterium *Aquifex aeolicus*. *Extremophiles* **12**: 205-215.

Pott, A. S. and Dahl, C. (1998). Sirohaem sulfite reductase and other proteins encoded by genes at the dsr locus of *Chromatium vinosum* are involved in the oxidation of intracellular sulfur. *Microbiol-Sgm* **144**: 1881-1894.

Protze, J., Müller, F. H., Lauber, K., Naß, B., Mentele, R., Lottspeich, F. and Kletzin, A. (2011). An extracellular tetrathionate hydrolase from the thermoacidophilic archaeon *Acidianus ambivalens* with an activity optimum at pH 1. *Front Microbio.* **2**:68
doi: 10.3389/fmicb.2011.00068

Quatrini, R., Appia-Ayme, C., Denis, Y., Jedlicki, E., Holmes, D. S. and Bonnefoy, V. (2009). Extending the models for iron and sulfur oxidation in the extreme Acidophile *Acidithiobacillus ferrooxidans*. *BMC Genomics* **10:**394. doi:10.1186/1471-2164-10-394

Radestock, S. and Gohlke, H. (2011). Protein rigidity and thermophilic adaptation. *Proteins* **79**: 1089-1108.

Reddie, K. G. and Carroll, K. S. (2008). Expanding the functional diversity of proteins through cysteine oxidation. *Curr Opin Chem Biol* **12**: 746-754.

Reisinger, V. and Eichacker, L. A. (2006). Analysis of membrane protein complexes by blue native PAGE. *Proteomics* **6**:S2: 6-15.

Rohwerder, T. and Sand, W. (2003). The sulfane sulfur of persulfides is the actual substrate of the sulfur-oxidizing enzymes from *Acidithiobacillus* and *Acidiphilium* spp. *Microbiology* **149**: 1699-1710.

Rohwerder, T. and Sand, W. (2007). Oxidation of inorganic sulfur compounds in acidophilic prokaryotes. *Eng Life Sci* **7**: 301-309.

Rother, D., Henrich, H. J., Quentmeier, A., Bardischewsky, F. and Friedrich, C. G. (2001). Novel genes of the sox gene cluster, mutagenesis of the flavoprotein SoxF, and evidence for a general sulfur-oxidizing system in *Paracoccus pantotrophus* GB17. *J Bacteriol* **183**: 4499-4508.

Roy, A. B. and Trudinger, P. A. (1970). *The chemistry of some sulphur compounds*. Cambridge University, Cambridge, UK.

Rozanova, E. P. and Nazina, T. N. (1976). Mesophilic rod-*like* nonsporeforming bacterium reducing *sulfates Mikrobiologiia* **45**: 711-716.

Rzhepishevska, O. I., Valdes, J., Marcinkeviciene, L., Gallardo, C. A., Meskys, R., Bonnefoy, V., Holmes, D. S. and Dopson, M. (2007). Regulation of a novel *Acidithiobacillus caldus* gene cluster involved in metabolism of reduced inorganic sulfur compounds. *Appl Environ Microb* **73**: 7367-7372.

Sakurai, H., Ogawa, T., Shiga, M. and Inoue, K. (2010). Inorganic sulfur oxidizing system in green sulfur bacteria. *Photosynth Res* **104**: 163-176.

Sambrook, J. and Russell, D. W. (2001). Molecular Cloning: *A Laboratory Manual*. Cold Spring Harbor, Laboratory Press, New York. Third Edition.

Schägger, H. and von Jagow, G. (1987). Tricine-sodium dodecyl sulfate-polyacrylamide gel electrophoresis for the separation of proteins in the range from 1 to 100 kDa. *Anal Biochem* **166**: 368-379.

Schauder, R. and Kröger, A. (1993). Bacterial Sulfur Respiration. *Arch Microbiol* **159**: 491-497.

Schenk, G., Neidig, M. L., Zhou, J., Holman, T. R. and Solomon, E. I. (2003). Spectroscopic characterization of soybean lipoxygenase-1 mutants: the role of second coordination sphere residues in the regulation of enzyme activity. *Biochemistry* **42**: 7294-7302.

Schleper, C., Puehler, G., Holz, I., Gambacorta, A., Janekovic, D., Santarius, U., Klenk, H. P. and Zillig, W. (1995). *Picrophilus* gen. nov., fam. nov.: a Novel Aerobic, Heterotrophic, Thermoacidophilic Genus and Family Comprising Archaea Capable of Growth around pH 0. *J Bacteriol* **177**: 7050-7059.

Schrödinger, LLC (2010). The PyMOL Molecular Graphics System, Version 1.3r1.

Seyfarth, K. (2006). Gerichtete Mutagenese zur Funktionsbestimmung einzelner Aminosäuren aus der Schwefel Oxygenase- /Reduktase. Diploma Thesis, Technische Universität Darmstadt, Darmstadt, Germany.

Skerra, A. (1994). Use of the tetracycline promoter for the tightly regulated production of a murine antibody fragment in Escherichia coli. *Gene* **151**: 131-135.

Smith, P. K., Krohn, R. I., Hermanson, G. T., Mallia, A. K., Gartner, F. H., Provenzano, M. D., Fujimoto, E. K., Goeke, N. M., Olson, B. J. and Klenk, D. C. (1985). Measurement of protein using bicinchoninic acid. *Anal Biochem* **150**: 76-85.

Steudel, R. (2003). Inorganic polysulfanes H_2Sn with n > 1. *Top Curr Chem* **231**: 99-125.

Sun, C. W., Chen, Z. W., He, Z. G., Zhou, P. J. and Liu, S. J. (2003). Purification and properties of the sulfur oxygenase/reductase from the acidothermophilic archaeon, *Acidianus* strain S5. *Extremophiles* **7**: 131-134.

Thauer, R. K., Jungermann, K. and Decker, K. (1977). Energy conservation in chemotrophic anaerobic bacteria. *Bacteriol Rev* **41**: 100-180.

Trivedi, S., Gehlot, H. S. and Rao, S. R. (2006). Protein thermostability in Archaea and Eubacteria. *Genet Mol Res* **5**: 816-827.

Tsai, Y., Sawaya, M. R., Cannon, G. C., Cai, F., Williams, E. B., Heinhorst, S., Kerfeld, C. A. and Yeates, T. O. (2007). Structural analysis of CsoS1A and the protein shell of the *Halothiobacillus neapolitanus* carboxysome. *PLoS Biol* **5**: 1345-1354.

Urich, T., Bandeiras, T. M., Leal, S. S., Rachel, R., Albrecht, T., Zimmermann, P., Scholz, C., Teixeira, M., Gomes, C. M. and Kletzin, A. (2004). The sulphur oxygenase reductase from *Acidianus ambivalens* is a multimeric protein containing a low-potential mononuclear non-haem iron centre. *Biochem J* **381**: 137-146.

Urich, T., Coelho, R., Kletzin, A. and Frazao, C. (2005a). The sulfur oxygenase reductase from *Acidianus ambivalens* is an icosatetramer as shown by crystallization and Patterson analysis. *Biochim Biophys Acta* **1747**: 267-270.

Urich, T., Kroke, A., Bauer, C., Seyfarth, K., Reuff, M. and Kletzin, A. (2005b). Identification of core active site residues of the sulfur oxygenase reductase from *Acidianus ambivalens* by site-directed mutagenesis. *FEMS Microbiol Lett* **248**: 171-176.

Urich, T. (2005c). The sulfur oxygenase reductase from *Acidianus ambivalens* - Functional and structural characterization of a sulfur-disproportionating enzyme. PhD thesis, Technische Universität Darmstadt, Darmstadt, Germany.

Urich, T., Gomes, C. M., Kletzin, A. and Frazao, C. (2006). X-ray Structure of a self-compartmentalizing sulfur cycle metalloenzyme. *Science* **311**: 996-1000.

Valdes, J., Quatrini, R., Hallberg, K., Dopson, M., Valenzuela, P. D. T. and Holmes, D. S. (2009). Draft Genome Sequence of the Extremely Acidophilic Bacterium *Acidithiobacillus caldus* ATCC 51756 Reveals Metabolic Versatility in the Genus *Acidithiobacillus*. *J Bacteriol* **191**: 5877-5878.

Valdes, J., Cardenas, J. P., Quatrini, R., Esparza, M., Osorio, H., Duarte, F., Lefimil, C., Sepulveda, R., Jedlicki, E. and Holmes, D. S. (2010). Comparative genomics begins to unravel the ecophysiology of bioleaching. *Hydrometallurgy* **104**: 471-476.

Veith, A., Klingl, A., Zolghadr, B., Lauber, K., Mentele, R., Lottspeich, F., Rachel, R., Albers, S. V. and Kletzin, A. (2009). *Acidianus*, *Sulfolobus* and *Metallosphaera* surface layers: structure, composition and gene expression. *Mol Microbiol* **73**: 58-72.

Veith, A., Urich, T., Seyfarth, K., Protze, J., Frazão, C. and Kletzin, A. (2011) Substrate pathways and mechanisms of inhibition in the sulfur oxygenase reductase of *Acidianus ambivalens*. *Front Microbio* **2:**37. doi: 0.3389/fmicb.2011.00037

Vieille, C. and Zeikus, G. J. (2001). Hyperthermophilic enzymes: Sources, uses, and molecular mechanisms for thermostability. *Microbiol Mol Biol R* **65**: 1-43.

Vishniac, W. and Santer, M. (1957). The Thiobacilli. *Bacteriological Reviews* **21**: 195-213.

Wakai, S., Kikumoto, M., Kanao, T. and Kamimura, K. (2004). Involvement of Sulfide : Quinone oxidoreductase in sulfur oxidation of an acidophilic iron-oxidizing bacterium, *Acidithiobacillus ferrooxidans* NASF-1. *Biosci. Biotechnol. Biochem.* **68**: 2519-2528.

Waterhouse, A. M., Procter, J. B., Martin, D. M. A., Clamp, M. and Barton, G. J. (2009). Jalview Version 2 - a multiple sequence alignment editor and analysis workbench. *Bioinformatics* **25**: 1189-1191.

Winn, M. D., Ballard, C. C., Cowtan, K. D., Dodson, E. J., Emsley, P., Evans, P. R., Keegan, R. M., Krissinel, E. B., Leslie, A. G. W., McCoy, A., McNicholas, S. J., Murshudov, G. N., Pannu, N. S., Potterton, E. A., Powell, H. R., Read, R. J., Vagin, A. and Wilson, K. S. (2011). Overview of the CCP4 suite and current developments. *Acta Crystallogr D* **67**: 235-242.

Wood, A. P., Woodall, C. A. and Kelly, D. P. (2005). *Halothiobacillus neapolitanus* strain OSWA isolated from "The old sulphur well" at Harrogate (Yorkshire, England). *Syst Appl Microbiol* **28**: 746-748.

Yikilmaz, E., Porta, J., Grove, L. E., Vahedi-Faridi, A., Bronshteyn, Y., Brunold, T. C., Borgstahl, G. E. O. and Miller, A. F. (2007). How can a single second sphere amino acid substitution cause reduction midpoint potential changes of hundreds of millivolts? *J A. Chem Soc* **129**: 9927-9940.

Zillig, W., Yeats, S., Holz, I., Bock, A., Gropp, F., Rettenberger, M. and Lutz, S. (1985). Plasmid-related anaerobic autotrophy of the novel archaebacterium *Sulfolobus ambivalens*. *Nature* **313**: 789-791.

Zillig, W., Yeats, S., Holz, I., Bock, A., Rettenberger, M., Gropp, F. and Simon, G. (1986). *Desulfurolobus ambivalens*, gen.nov., sp.nov., an autotrophic archaebacterium facultatively oxidizing or reducing sulfur. *Syst Appl Microbiol* **8**: 197-203.

Zimmermann, P., Laska, S. and Kletzin, A. (1999). Two modes of sulfite oxidation in the extremely thermophilic and acidophilic archaeon *Acidianus ambivalens*. *Arch Microbiol* **172**: 76-82.

Experiments, data analyes and writing of the present thesis were all done by myself unless otherwise noted and with the exception of the following items:

Chapter 3: The *Aa*SOR-harboring plasmid pASK-SOR.05 was originally constructed by Peter Zimmermann (Urich *et al.*, 2004). The tetramer channel mutants Del L, Del K, $F_{141}A$, $F_{133}A$ and $F_{141}A$ /$F_{131}A$ and the active site mutants $E_{87}A$, $E_{87}D$ and $T_{78}A$ were originally constructed by Kerstin Seyfarth (Seyfarth, 2006). The active site pore mutants $M_{296}V$, $M_{297}A$ $MM_{296/297}VT$ and $MM_{296/297}TT$ as well as the pocket-forming mutants $T_{34}S$ and $M_{22}C$ were constructed by Jonas Protze under my supervision in the course of this work. The zinc-containing *Aa*SOR derivative was originally determined by Tim Urich (Urich, 2005).

Chapter 4: Metal content TXRF measurements were performed by Claudia Rittmeyer (Goethe Universität, Frankfurt, Germany) in the group of Prof. Kolbesen (now in the group of Prof. Terfort). All EPR spectroscopy measurements were performed by Miguel Teixeira (ITQB, Oeiras, Portugal). The K-absoprtion edge of cobalt was experimentally determined by Pedro Matias (ITQB, Oeiras, Portugal), who also performed the fluorescence scan of the corresponding crystal.

Chapter 5: Dynamic Light Scattering and Far UV/CD spectroscopy experiments were carried out under the guidance of Hugo Botelho (ITQB, Oeiras, Portugal) in the group of Cláudio M. Gomes (ITQB, Oeiras, Portugal). Preparation of protein crystals for X-ray diffraction was carried out with the help of Ricardo Coelho (ITQB, Oeiras, Portugal), who is also responsible for the preparation of *Hn*SOR crystals when I was absent. Analysis of X-ray diffraction data was analyzed under the guidance of Carlos Frazão (ITQB, Oeiras, Portugal), while the *Halothiobacillus neapolitanus* SOR-wt (*Hn*SOR) structure was determined by Carlos Frazão.

Appendix

The atomic coordinates of the SOR crystal structures mentioned in the previous chapters are not (yet) publicly available in the Protein Data Bank. The enclosed CD-ROM contains the the coordinate files in *.pdb format and the corresponding reflection data in *.mtz format.

AaSOR	*A. ambivalens* SOR
AaSOR_PS	*A. ambivalens* SOR co-crystallized with polysulfide
AaSOR_TS	*A. ambivalens* SOR co-crystallized with thiosulfate
$H_{277}A$	*A. ambivalens* SOR mutant $H_{277}A$
$E_{87}D$	*A. ambivalens* SOR mutant $E_{87}D$
Co-SOR_tetra	*A. ambivalens* SOR derivatized with cobalt; space group I4
Co-SOR_cubic	*A. ambivalens* SOR derivatized with cobalt; space group I432
HnSOR	*H. neapolitanus* SOR

The coordinate files can be visualized using programs such as Rasmol, Jmol, Pymol or COOT.

Curriculum Vitae

Personal information

Name: Andreas Veith
Date of birth: 22th March 1980
Place of birth: Seeheim-Jugenheim, Germany

University education:

2007 – 2011 PhD student at the Institute of Microbiology and Genetics, Technical University of Darmstadt

2006 Diploma Thesis in Microbiology
Title: "The S-layer proteins of *Acidianus ambivalens*: protein isolation, gene sequencing and heterologous gene expression

2000 - 2006 Studies of biology at the Technical University of Darmstadt
Major: Microbiology, Diploma Thesis in Microbiology
Advisors: Dr. Arnulf Kletzin, Prof. Felicitas Pfeifer
Degree earned: Diplom-Biologe

Research stays abroad:

2008 – 2009 Temporary visits at Instituto de Tecnologia Química e Biológica (ITQB), Universidade Nova de Lisboa, Oeiras, Portugal in 2008 (Oct – Dec) and 2009 (Oct – Dec) in the working groups of Dr. Carlos Frazão, Dr. Cláudio M. Gomes and Prof. Miguel Teixeira